Brunel University

School of Engineering & Design

Department of Electronic & Computer Engineering

Thesis submitted for the degree of Doctor of Philosophy

Analysis of signals related to the generation process of extreme events: towards a unified approach

by

George Minadakis

Supervisor: Prof. John Stonham

London, 2013

Contents

0.1 Abstract

In the last decades, although the scientific community has attempted to explain a series of complex phenomena, ranging from natural hazards to physical conditions and economic crises, aspects of their generation process still escape our full understanding. The present thesis intends to promote our understanding of the spatiotemporal behavior and the generation mechanisms that govern large and strong earthquakes, employing a broad multidisciplinary perspective for the interpretation of catastrophic events. Two main questions are debated. The first question concentrates on *"whether the generation process of an extreme event has more than one facets prior to its final appearance"*. In the scientific study of earthquakes, attention is drawn to the predictive capability and monitoring of different precursory observations. Among them preseismic electromagnetic emissions have been also observed indicating that the science of earthquake prediction should be from the start multidisciplinary. Drawing on recently introduced models for earthquake dynamics, that address issues such as long-range correlations, self-affinity, complexity-organization and fractal structures, the present work endeavors to further penetrate on the analysis of preseismic electromagnetic emissions and elucidate their link with the generation process of large and strong earthquakes. A second question deals with *"whether there is a unified approach for the study of catastrophic events"*. This question implies the possibility for common statistical behavior of diverse extreme events and the potential for transferability of methods from the study of earthquake dynamics across other fields. On these grounds, the present work extends the focus of inquiry to the analysis of electroencephalogram recordings related to epileptic seizures, in the prospect to identify common mechanisms that may explain the nature and the generation process of both phenomena, and to open up different directions for future research. Finally, with a view to consider alternative ways of studying key theoretical principles associated with the generation process of catastrophic phenomena, a relevant framework based on proposed algorithms is presented, focusing on parameters such as: the energy of earthquakes, the mean and maximum magnitude of the sample, the probability that two samples may come from the same population. Such an attempt aims to contribute to the knowledge of natural phenomena, by extending the existing theory and models and providing a few more ways for their interpretation.

0.2 Author's declaration

I hereby declare that I am the sole author of this thesis.

Signature

Date

0.3 Acknowledgements

I would like to acknowledge research funding received from the Greek State Scholarships Foundation (IKY), which has provided financial support throughout my studies for PhD and without which my work could not have been easily completed.

I would like to express my deep appreciation to my supervisor Prof. John Stonham, who offered guidance and significant insights throughout my PhD work, with his valuable knowledge and expertise. He has been a source of inspiration and support, giving me the courage to continue my research with passion and focus.

I would also like to express my appreciation to professor Konstantinos Nomicos, who has stood by me like a father for more than 10 years, ever since I started my higher education. He is the one who initially motivated me to proceed with doctoral research and has spent priceless time on discussions around issues related to my research, teaching me the value of being a good scientist with human integrity. On these grounds, I would also like to thank my close friend and mentor, in earlier years, professor Dionisis Cavouras, who introduced me to rigorous scientific analysis and taught me to never give up, no matter how hard things get.

My gracious acknowledgement and sincere gratitude also goes to Prof. Konstantinos Eftaxias, for his willingness to share his deep knowledge and experience in the field of preseismic electromagnetic emissions, which has been of great value and inspiration for me. His critical perspective and availability for theoretical debates have provided a solid background to the work undertaken in relation to the present thesis. I am extremely thankful for his encouragement to proceed with publications.

Finally, I would like to thank Dr. Gerassimos Papadopoulos, for the collaboration during the last decade and constructive discussions during the period of my doctoral studies, which promoted my knowledge on statistical seismology and informed my understanding of regional seismicity.

0.4 Dedication

This thesis is dedicated to my wonderful partner in life, Eirini Kampriani, who supported me all these years, in good and bad times. I simply thank you more than words can say.

0.5 Publications & Conferences

The following list concerns the publications since I started my PhD candidacy. Please note that the list also includes works that relate to my PhD project indirectly.

0.5.1 Publications in Scientific Journals with referees

1. G. Minadakis, E. Ventouras, S. D. Gatzonis, A. Siatouni, H. Tsekou, I. Kalatzis, D. E. Sakas, and J. Stonham, "Dynamics of regional brain activity in epilepsy: a cross-disciplinary study", Journal of Neural Engineering, 11 (2): 026012, 2014

2. K. Eftaxias, G. Minadakis, S. M. Potirakis, G. Balasis, "Dynamical analogy between epileptic seizures and seismogenic electromagnetic emissions by means of nonextensive statistical mechanics", Physica A, 392(3), 497-509, 2012

3. G. Minadakis, S. M. Potirakis, J. Stonham, C. Nomicos and K. Eftaxias. "The role of propagating stress waves in geophysical scale: evidence in terms of nonextensivity", Physica A, 391(22), 5648-5657, 2012

4. S. M. Potirakis, G. Minadakis, and K. Eftaxias, "Relation between seismicity and pre-earthquake electromagnetic emissions in terms of energy, information and entropy content", Nat. Hazards Earth Syst. Sci., 12, 1179-1183, 2012.

5. S. M. Potirakis, G. Minadakis, and K. Eftaxias, "Sudden drop of fractal dimension of electromagnetic emissions recorded prior to significant earthquake", Natural Hazards, 64(1), 641-650, 2012

6. G. Minadakis, S. M. Potirakis, C. Nomicos, K. Eftaxias, "Linking electromagnetic precursors with earthquake dynamics: an approach based on nonextensive fragment and self-affine asperity models", Physica A, 391(6), 2232-2244, 2012

7. S. M. Potirakis, G. Minadakis, and K. Eftaxias. "Analysis of electromagnetic pre-seismic emissions using Fisher Information and Tsallis entropy", Physica A, 391, 300-306, 2011

8. S. M. Potirakis, G. Minadakis, C. Nomicos, and K. Eftaxias., "A multidisciplinary justification for traces of the last state of earthquake generation in preseismic electromagnetic emissions", Nat. Hazards Earth Syst. Sci., 11, 2859-2879, 2011

9. G.A Papadopoulos, M. Charalampakis, A. Fokaefs, and G. Minadakis. "Strong foreshock signal preceding the L'Aquila (Italy) earthquake (Mw 6.3) of 6 April 2009". Natural Hazards

and Earth System Sciences, 10: 19-24, 2010

0.5.2 Papers & Abstracts in International Scientific Conferences

1. G. Minadakis and G. A Papadopoulos, "A strategy for the discrimination between different seismicity styles: implications for operational applications" European Geosciences Union (EGU) General Assembly 2014, Vienna, Austria, forthcoming April 2014

2. G. A Papadopoulos, E. Daskalaki, G. Minadakis and K. Orfanogiannaki, "Pre-earthquake foreshock activity and its discrimination from swarms" (invited), American Geophysical Union (AGU) Fall Meeting, San Francisco CA, USA, December 9-13, 2013

3. E. Daskalaki, G.A Papadopoulos, G. Minadakis, K. Spiliotis and C. Siettos, "Description of earthquake sequences using complex network theory: the cases of Italy (L'Aquila, 2009) and Southern California (Baja, 2010)", American Geophysical Union (AGU) Fall Meeting, San Francisco CA, USA, December 9-13, 2013

4. G. Minadakis, C. Nomicos, and J. Stonham, "Observing electromagnetic signals as earthquake precursors in terms of complexity", European Geosciences Union (EGU), Vienna, Austria, 02 - 07 May 2010

5. G. A. Papadopoulos, G. Minadakis, M. Charalampakis, , A. Fokaefs "A Strategy of Real-Time Seismicity Evaluation for Operationa l Earthquake Forecasting: Retrospective Application on the 6 April 2009 earthquake (Mw=6.3) in L'Aquila, Italy", Proc. of the 32nd General Assembly ESC2010, September 6-10, Montpellier, France, 71. 2010.

6. G. A. Papadopoulos, G. Minadakis, K. Orfanogiannaki, "A Review of Statistical Seismology Studies in Greece: Past Achievements and Current Trends", Proc. of the 32nd General Assembly ESC2010, September 6-10, Montpellier, France, 127. , 2010.

7. G. A. Papadopoulos, G. Minadakis, M. Charalampakis, A. Fokaefs, "Foreshocks and their value for the prediction of the mainshock: The case of the 6 April 2009 Earthquake (Mw=6.3) in L'Aquila, Italy", Proc. of the 32nd General Assembly ESC2010, September 6-10, Montpellier, France, 96., 2010.

8. G. A. Papadopoulos, B. Di Fiore and G. Minadakis," Towards CSEP Tests in Greece: Completeness of the Greek national catalogue", 7th International Workshop on Statistical Seismology, Greece - Thera (Santorini) , 25 - 27 May 2011

9. G. A. Papadopoulos, G. Minadakis and B. Di Fiore, "Was the big 2011 Tohoku earthquake preceded by a foreshock activity?", 7th International Workshop on Statistical Seismology, Greece - Thera (Santorini) , 25 - 27 May 2011

10. G. A. Papadopoulos, G. Minadakis and B. Di Fiore, "Foreshocks and short-term hazard evaluation: A Global Review", 7th International Workshop on Statistical Seismology, Greece - Thera (Santorini) , 25 - 27 May 2011

11. D. Cavouras, P. Georgiadis, K. Ninos, G. Minadakis, K. Sidiropoulos, and A. Kyriazopoulos, "Pattern recognition system for identifying the site of EM precursor signals preceding major seismic events", European Geosciences Union (EGU) General Assembly 2011, Vienna , Austria, 03 - 08 April 2011

12. M. Kefalas, J. Kopanas, G. Antonopoulos, G. Koulouras, D. Cavouras, C. Eftaxias, G. Minadakis, and C. Nomicos, "The Telemetric System of Zante station for measuring the Electromagnetic Variations", European Geosciences Union (EGU) General Assembly 2011, Vienna , Austria, 03 - 08 April 2011

13. K. Eftaxias, G. Minadakis, G. Kopanas, and G. Antonopoulos, "Approach of puzzling features in the study of pre-seismic electromagnetic Emissions", European Geosciences Union (EGU) General Assembly 2011, Vienna , Austria, 03 - 08 April 2011

14. G. Minadakis, C. Nomicos, J. Stonham, and K. Eftaxias, "Is the statistical analysis of regional seismicity a macroscopic reflection of the physical processes in the earthquake source?", European Geosciences Union (EGU) General Assembly 2011, Vienna , Austria, 03 - 08 April 2011

15. G. A. Papadopoulos, B. Di Fiore, and G. Minadakis, "Short-Term Foreshocks and the Prediction of Mainshock in the Aftermath of L' Aquila Earthquake: A Global Review", European Geosciences Union (EGU) General Assembly 2011, Vienna , Austria, 03 - 08 April 2011

16. G. A. Papadopoulos, B. Di Fiore, G. Minadakis, "Real-time seismicity evaluation: results from testing in Greece", European Seismological Commission 33-rd General Assembly, Moscow, Russia, 19-24 August 2012

17. G. A. Papadopoulos, M. Avlonitis, B. Di Fiore and G. Minadakis. "The Predictive Value of Foreshocks", European Geosciences Union (EGU), General Assembly 2012, Vienna, Austria, 22 - 27 April 2012

0.6 List of commonly used equations

0.6.1 The Gutenberg & Richter Law

In seismology, the scaling relation between magnitude and the number of EQs is given by the Gutenberg-Richter (G-R) relationship (described analytically in Sec. 2.1.3 [89]):

$$\log N(>M) = c - bm \tag{1}$$

where, $N(>M)$ is the cumulative number of EQs with a magnitude greater than M occurring in a specified area and time and b and c are constants.

0.6.2 A fragment-asperity model for earthquake dynamics coming from nonextensive statistical mechanics

Sotolongo-Costa and Posadas (SCP) [218] have developed a fragment-asperity (SCP) model for EQ dynamics that derives from the nonextensive Tsallis formalism. The model consists of two rough profiles interacting via fragments filling the gap between them. The latter model has been recently revised by Silva et al. [208] where their approach leads to the following G-R type law for the magnitude distribution of EQs:

$$G(>M) = \frac{N(>M)}{N} = \left(\frac{2-q}{1-q}\right) \times \log\left[1 - \left(\frac{1-q}{2-q}\right)\left(\frac{10^{2M}}{a^{2/3}}\right)\right] \tag{2}$$

where,

$$G(>M) = \frac{N(>M)}{N}$$

where, N is the total number of EQs, $N(>M)$ the number of EQs with magnitude larger than M, and $M \approx \log(\varepsilon)$. The parameter α is the constant of proportionality between the EQ energy, ε, and the size of fragment r. The q-parameter included in the non-extensive formula (Eq. (2)) is associated with the b parameter of Gutenberg & Richter formula (Eq. (1)), by the relation [202]:

$$b = 2 \times \left(\frac{2-q}{q-1}\right) \tag{3}$$

For further details about the model please refer to Sec. 2.1.3

0.7 Abbreviation List

Herein the list of abbreviations is presented in alphabetical order as follows:

B-G	Boltzmann-Gibbs
EEG	Electroencephalogram
EEG-EQ	Electroencephalogram Electric Earthquake
EL-EQ	Electric Earthquake
EM	Electromagnetic Emissions
EM-EQ	Fracto-Electromagnetic Earthquake
EQ	Earthquake
EW	East-West
G-R	Gutenberg & Richter
IC	Intermittent Criticality
LM	Levenberg-Marquardt
MLE	Maximum Likelihood Estimation
NS	North-South
SCP	Sotolongo-Costa and Posadas
SOC	Self Organized Criticality
ES	Epileptic Seizure
ULF	Ultra-Low-Frequency
SES	Seismic Electric Signals
TIR	Thermal Infrared Spectral Range
R/S	Rescaled Range Analysis
IDE	Integrated Development Environment

List of Figures

List of Tables

Chapter 1

Introduction: setting the research context

1.1 Aims and approach of this study

In the last decades, although the scientific community has attempted to explain a series of complex phenomena, ranging from natural hazards to physical conditions and economic crises, aspects of their generation process still escape our full understanding. Characteristically, Kossobokov [130], stated that *"No scientific prediction is possible without exact definition of the anticipated phenomenon and the rules, which define clearly in advance of it whether the prediction is confirmed or not"*. Such definition indicates that the degree to which we can predict an extreme phenomenon is often measured by how well we understand it [54] and how do we set the appropriate framework for the analysis of the separate regimes that might exist or even coexist during its generation process. Influenced by this concept, the present work comes to further penetrate and to elucidate a series of questions related to catastrophic events, from the perspective of the earthquake (EQ) dynamics.

Several methods have been performed and several fault-mechanisms have been suggested from studies in both laboratory and geophysical scale, in the prospect to identify and explain the preparation process of large and strong EQs [88, 120, 255, 47, 173, 174, and references therein]. In general, the crack propagation seems to be the basic mechanism of material failures, but the scientific community does not appear to be favorable in short-term EQ prediction since the exact seismogenic origin of EQs is still unknown. Characteristically, Geller et al. [79] suggested that EQs cannot be predicted and any precursory activity is impossible. Such negative views are not groundless considering the difficulties that scientists have faced due to the prediction of EQs, such as the complex nature, the rarity of large and strong EQs, the absence of foreshock activity observed in some cases. Nevertheless, it should be considered that the research towards

the possible prediction of catastrophic phenomena such as EQs is still a challenging field in the sense that science should have some predictive power to explain such physical phenomena by performing new ideas, and even more detailed numerical investigations on both laboratory and geophysical scale [54].

Under these circumstances, the first question that this work deals with is *"whether the generation process of an extreme event has more than one facets prior to its final appearance"*. This question implies the possibility that nature manifests itself in different ways from those the scientific community expects to see and analyse. Indeed, several precursory phenomena beyond the seismic activity have been observed prior to large EQs [261, 63, 71]. Among them preseismic electromagnetic (EM) emissions have been also observed indicating that the science of EQ prediction should be from the start multidisciplinary [123, 36, 55, 172]. However, the study of precursory phenomena in terms of preseismic EM precursors is still questionable, from the most part of the scientific community, rising several questions that contest their credibility, since they have not been adequately accepted as real physical quantities [259, 179]. A better understanding to whether an EM precursor is related to the physical process of EQ generation is an important issue for EQ prediction. In this direction, the main contribution of this work, in its most part, is to further penetrate on the analysis of preseismic EM emissions in the prospect to further elucidate their link with the generation process of large and strong EQs.

Such a multidisciplinary analysis could possibly answer a second question concerning the relation between diverse catastrophic events, which deals with *"whether there is a unified approach for the study of such phenomena?"*. Practically, this question implies the possibility for common statistical behavior in the study of diverse extreme events. The basic concept is that transferring ideas, methods and insights from investigations in hitherto disparate areas will cross-fertilize and lead to important new results rising up deep questions concerning the existence of common basic generation mechanisms. Such analysis could provide many similar features indicating that diverse phenomena could be analyzed within similar mathematical frameworks. On these grounds the present work extends the focus of inquiry to the analysis of two diverse extreme phenomena: (i) large catastrophic EQs and their relation with preseismic kHz EM emissions, and (ii) epileptic seizures (ESs), in the prospect to identify common mechanisms that may explain both the nature and the generation process of such phenomena.

In the following sections a critical review on literature related to the preseismic kHz - MHz EM emissions observed prior to large EQs is first provided. The main perspective is to give an overall understanding of the up to date analysis applied so far and to further apply arguments that contribute to the seismigenic origin of these precursors. Secondly, further discussion

on theoretical evidence concerning the unified approach of extreme phenomena will be also provided aiming to give an overall sense of the analysis that will follow in the next chapters. As concerns the individual theoretical background in which this work has been based, these issues will be briefly mentioned here and will be further discussed analytically in each chapter.

1.2 A critical review of the literature

There are several studies related to the seismogenic origin of preseismic EM emissions suggesting that micro-cracks in the earth's crust produce both acoustic and EM emissions. The most common theoretical approach states that when a heterogeneous material is strained, EM emissions in a wide frequency spectrum ranging from kHz to MHz are mainly produced by opening cracks, which can be considered as so-called "precursors of general fracture". These precursors have been detected on both laboratory and a geological scale [11, 66, 99, 98, 100, 259], providing an alternative tool for the monitoring of the micro-fractures, which possibly occur in the pre-focal area before the final break-up.

From experiments applied in many materials (deformation, wearing, peeling, e.t.c.), it has been observed that during the formation of new surface, emissions of photons, electrons, ions and neutral particles have been detected which are mainly refereed as *"fracto-emissions"* [138, 48, 84, 160, 224, 156, 270]. It has been stated that the crack propagation seems to be the basic mechanism of material's failure. Specifically, when a heterogeneous material is strained the local nucleation and coalescence of micro-cracks seem to be the basic features that characterize its evolution towards breaking [59]. Characteristically, Sharon and Fineberg [206] have provided experimental evidence showing that the instability mechanism is that of local branching. The authors mentioned that the motion of a crack in dynamics fracture has been shown to be governed by a dynamical instability causing oscillations in its velocity and structure on the fracture surface. A multi-crack state is formed by repetitive, frustrated micro-fracturing events [207]. It should also be noted that experiments in laboratory scale, have shown that more intense fracto-emissions have been observed during the unstable crack growth [84]. In addition, the rupture of inter-atomic (or ionic) bonds also leads to intense charge separation, forming the origin of the electric charge between the micro-crack faces. On the faces of a newly created micro-crack the electric charges constitute an electric dipole or a more complicated system. In the stage of the micro-branching instability, the crack strong wall vibration behaves as an efficient EM emitter [11, and references therein].

In the last two decades, more than 50 articles have been published providing strong evidence for the association of the detected pre-seismic EM emissions with the fracturing process in the

focal area of the impending EQ. Analysis applied so far in terms of: fault modeling [61], laboratory experiments [60], criticality [123, 38, 36], scaling similarities of multiple fracturing of solid material[121], fractal electrodynamics [58] and complexity [122, 117], has provided sufficient evidence that validate their association of these precursors with the fracturing process in the pre-focal area [45, 131, 55]. Nevertheless the most part of the scientific community is still suspicious with the aforementioned association [259, 179], implying that different approaches could provide additional evidence that would allow one to accept that these EM anomalies are related to the fracture process of an impeding EQ. The present study deals with this assumption focusing on a recently introduced two-stage model for the study of preseismic EM activity, described in the following section.

1.2.1 A two-stage model on preseismic EM activity

A two-stage model has been recently proposed [123, 36, 40, 172, 59, 65] suggesting that the MHz EM emission is due to the fracture of the highly heterogeneous system that surrounds the fault. More specifically, the MHz EM activity can be attributed to phase transition of second order [36], while a Levy walk type mechanism can explain the observed critical state [40]. The finally emerged kHz EM emission, usually observed from approximately one week up to a few hours before the main EQ, is rooted in the final stage of EQ generation, namely, the fracture of entities sustaining the system [123, 36, 117, 172, 55]. The basic ingredients of this model read as follows:

- *A backbone of strong and large asperities distributed along the fault that sustains the system.*
- *A strongly heterogeneous material that surrounds the family of asperities.*

The last two decades, several kHz-to-MHz EM anomalies have been detected prior large EQs, on which physicists have attempted to link the available EM observations to the processes occurring in the Earth's crust. Up to now analysis has revealed that these anomalies have been mainly and repeatedly detected in cases of EQs that: (i) have been occurred in land (or near coast-lines), (ii) were strong with magnitude $M \geq 6$, and (iii) were relative shallow. These conditions have provided the main framework for the retrospective detection and initial discrimination of these anomalies as seismogenic ones. Furthermore, multidisciplinary analysis applied on these preseismic MHz-kHz EM emissions, has mainly focused on two epochs characterized by the following ingredients:

(i) The first epoch, which includes the initially emerged MHz part, originates during cracking in the highly heterogeneous component of the focal area, while the underlying *fracto-*

electromagnetic mechanism can be described in terms of a generalized continuous second order phase transition [36].

(ii) The second epoch includes the abrupt emergence of strong impulsive kHz EM emission in the tail of the precursory activity. This activity is thought to be due to the fracture of the family of main asperities that are distributed along the activated fault sustain the system. The kHz EM radiation evolves as a phase transition far from equilibrium [123, 36, 40, 172, 59, 65].

Fig. 1.1, shows an indicative graphical representation of the focal area which the two-stage model has been based, namely a strongly heterogeneous material that surrounds the family of asperities (depicted with gray), and a backbone of strong and large asperities (like red one) distributed along the fault that sustains the system.

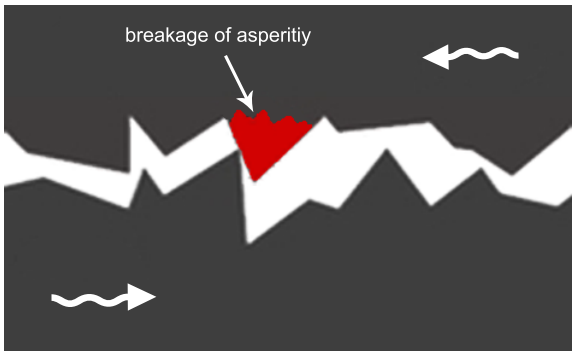

Figure 1.1: The model of focal area consisting of a strongly heterogeneous material that surrounds the family of asperities, and a backbone of strong and large asperities (like red one) distributed along the fault that sustains the system.

The aforementioned scenario has been further verified from studies related to Seismic Electric Signals (SES) [260], EM precursors rooted in Lithosphere - Atmosphere - Ionosphere (LAI) coupling [191], and precursors related with other disciplines such as: Seismology [173, 251], Infrared Remote Sensing [170], Synthetic Aperture Radars Interferometry [195], suggesting that the science of EQ prediction should, from the start, be multidisciplinary [54]. The latter evidence have provided a coherent framework of analysis which ties together the observed phenomenology of MHz and kHz EM precursors on one hand, and the precursory activity deriving from different disciplines on the other hand. In the following subsections, the theoretical framework of these two epochs is further presented separately for MHz and kHz EM emissions respectively.

1.2.1.1 The MHz EM activity as a second order phase transition phenomenon

Recent studies have shown that in heterogeneous materials the fracture process can be attributed to a second-order phase transition [104, 213, 38]. The MHz EM activity seems to be related to that process, revealing the transition from the phase from non-directional almost symmetrical cracking distribution to a directional localized cracking zone that includes the backbone of strong asperities [36, 40, 41]. This process has been defined as *Symmetry Breaking* [36]. The time interval related to the completion of this phenomenon indicates that the fracture of heterogeneous system in the focal area has been obstructed along the backbone of asperities that sustain the system. This means that the siege of strong asperities has started and the impeding EQ will occur only if and when the local stress exceeds fracture stresses-threshold of asperities [36].

This stage of fracturing is naturally related to rocks at large length scales where long-range anti-correlations exist. Such anti-correlations essentially characterize the existence of a *non-linear negative feedback mechanism*, where high value of a rock property (e.g. threshold for breaking) is followed by a low value and vice versa. Failure nucleation begins to occur at a region where the resistance to rupture growth has the minimum value. At this phase, the EM event is emitted and the fracture process continues in the same weak region until a much stronger region is encountered in its neighborhood area. When this happens, fracture stops, and thus the emitted EM emission ceases. The stresses are redistributed, while the applied stress in the focal area increases. A new population of cracks nucleates in the weaker of the unbroken regions, and thus a new EM event appears again, and so on.

It has been found that this critical signature which characterizes the interplay between the system heterogeneities and the field-stresses, is also hidden in the recorded MHz EM precursors [121, 36, 55, 56, 41], and such process should be placed in the category of critical phenomena. In this direction, a recently introduced Method of Critical Fluctuations (MCF), is analytically described in [37, 39]. Note that the appearance of MHz EM anomalies does not mean that the EQ will definitely occur and that is unavoidable. According to the aforementioned two-stage model, this footprint is rooted in the preseismic kHz EM anomalies related to the last-stage of the EQ preparation process, namely the breakage of asperities [37, 39, 54].

1.2.1.2 The kHz EM activity as the last stage of EQ generation

Based on the two-stage model described in Sec. 1.2.1, it has been found that the preseismic kHz EM precursors are actually refer to the last stage of the EQ generation process which involves the fracture of asperities that sustain the fault [121, 36, 117, 172, 55, 56]. Multi-

disciplinary statistical analysis applied so far has revealed that this process of fracturing has been characterized by a non-equilibrium instability, thus acquiring a self-regulating character and to a great degree the property of irreversibility. It has also been characterized as a phase transition far from equilibrium without any footprint of an equilibrium phase transition [54]. In the following sections, a short review of the symptoms that characterize these precursors and distinguish them from the MHz EM anomalies is presented.

1.2.2 The seismogenic origin of the detected kHz EM anomalies

It should be noticed that most of the methods that will be mentioned here have also been used in the present study and will be further analyzed in details individually in the chapters that follow along with the findings of this work.

It has been stated that the eligible seismogenic kHz EM time series, are considered those where the eligible signal deviates from the normal background-behaviour [117]. According to this framework of analysis, entropy techniques, such as: T-entropy [244], Approximate entropy [181, 55], Tsallis entropy [245], Correlation Dimension [86], Shannon n-block entropies: conditional entropy, entropy of the source, Kolmogorov-Sinai entropy [205, 51, 49, 52, 50], have revealed that these emissions are characterized by significant higher organization (or lower-low complexity) in respect to that of noise (or even background levels) [125, 124, 117, 55, 56].

In addition, analysis in terms of the Hurst exponent (Rescaled Range Analysis R/S [109, 110]), has revealed that these preseismic EM emissions are also characterized by strong persistent behaviour [123, 36], implying that the underlying fracture process is governed by a *"positive feedback mechanism"* which is consistent with an anomaly being a precursor of an ensuing catastrophic event [54]. This suggestion has been further supported in terms of fractal spectral analysis applied on the kHz EM precursors, offering additional information concerning the signal/noise discrimination of these signals. More specifically, spectra analysis by means of "morlet" wavelet has revealed that the candidate kHz precursor follows the fractional Brownian motion (fBm)-model as opposed to the background activity which follows the $1/f$-noise model [57]. Such analysis also implies that the candidate kHz precursor has persistent behaviour since the β-exponent that derives from the power-law form $S(f) \propto f^{-\beta}$ of the wavelet spectrogram is connected to the Hurst exponent (H) by the relation: $\beta = 2H + 1$ [102]. Moreover, the conclusion that the candidate kHz EM precursor follows the persistent fBm-model has been also verified by Detrended Fluctuation Analysis [55].

In the prospect to link the kHz EM precursors with the last stage of the EQ generation, the latter evidence have been further verified from the scientific community using methods

and laws that derive from statistical seismology. An important pursuit in this direction was to investigate whether universal features of fractures and faulting are included in the recorded kHz EM precursors. Thus in the following sections, a short review of these studies is presented.

1.2.2.1 Evidence in terms of the Gutenberg and Richter magnitude-frequency relation

Beginning with the definition, an earthquake (EQ) is essentially a large scale fracture which has heterogeneous structures. As with any physical phenomenon, it should have some predictive power regarding its future behaviour. Statistical seismology has become the most common field of research related to the EQ preparation process. A crucial contribution was first made by Richter in 1935 [194], suggesting that EQs are not uniformly distributed in time, space and magnitude but such distribution exhibits scale invariability, appears to be self-similar and obeys a power law or fractal scaling. In this framework, an empirical formula known in the east as Ishimoto and Iida (1939) [111] relation and in the west as the Gutenberg and Richter (1942) [91] relation, was proposed, which defines the distribution of earthquakes with respect to the magnitude, for a certain region of interest.

$$\log N(> M) = c - bm \tag{1.1}$$

where $N(> m)$ is the cumulative number of EQs with a magnitude greater than m occurring in a specified area and time. c and b are positive, real constants deriving from the least-squares fitting of the (log-log) representation of the cumulative number of EQs with magnitude larger than M. c describes the seismic activity and b indicates the level of accumulated stresses and/or material conditions in the focal region. This relation is usually referred to as the Gutenberg-Richter (G-R) magnitude-frequency relationship.

In the prospect to express the preseiemic kHz EM time-series under the magnitude-frequency relationship, the notion of "electromagnetic earthquake" has been recently introduced [121, 172], which reads as follows: The amplitude A of a candidate "fracto-EM fluctuation" is regarded as the difference $A_{fem}(t_i) = A(t_i) - A_{noise}$, where A_{noise} is the background (noise) level of the EM time series. The sequence of k successively emerged "fracto-EM fluctuations" $A_{fem}(t_i)$, $i = 1, \ldots, k$ represents the EM energy released, ε, during the damage of a fragment, in which the literature refers to that as an "electromagnetic earthquake" (EM-EQ). Since the squared amplitude of the fracto-EM emissions is proportional to their power, the magnitude m of the candidate "EM-EQ" is given by the following relation:

$$m = \log \varepsilon \sim \log \left(\sum \left[A_{fem}(t_i) \right]^2 \right) \tag{1.2}$$

It should be noted that studies on premonitory behaviour of the b-value, have reported that the foreshock sequences and main shocks are characterized by a much smaller b-exponent, compared to aftershocks [92, 185, 175]. Indicatively, Ponomarev et al. [185] have reported a significant fall of the observed b-values from $(0.6 \sim 1.0)$ just before the global rupture. The same behaviour has also been found form laboratory experiments related to acoustic emissions where a significant decrease of the b-values were observed immediately before the global fracture [123]. In addition, Lei and Satoh [141], who recorded acoustic emission events during the fracture of typical rock samples stressed under differential compression, have shown that the pre-failure damage evolution is characterized by a significant decrease in b-value, ranging from approximately $1.5 \sim 0.5$ for hard rocks.

Analysis of preseismic kHz EM emissions has shown that Eq. (1.2), has provided excellent fit to the sequence of kHz EM-EQs associated with the Athens EQ following the Gutenberg-Richter law with $b = 0.51$ indicating the consistency with the aforementioned results [172]. Moreover, Rabinovitch et al. [192] have studied the fractal nature of EM radiation emitted during the rock fracture, showed that the cumulative distribution of the amplitudes of the prefracture EM time series also follows a power law with exponent $b = 0.62$. Similar statistical analysis applied on kHz EM time series associated with the Athens EQ, has also revealed that the cumulative distribution of the amplitudes also follows the power law $N(> A) \sim A^{-b}$, where $b = 0.62$ [123]. On these grounds the activation of a single fault could be considered as a magnified self-affine image of both the regional and laboratory seismicity [54].

1.2.2.2 *The activation of a single fault as a self-affine image of both the regional and laboratory seismicity*

Sotolongo-Costa and Posadas [218], have recently introduced a model for EQ dynamics which is coming from a nonextensive Tsallis formulation [245, 246, 247]. According to this model, the authors stated that the mechanism of relative displacement of fault plates is the main cause of EQs. The main scenario concerns two rough profiles (fault planes) interacting via the fragments filling the gap between them. These fragments are mainly coming from the residues of the breakage of the tectonic plates, from where the faults have originated. The motion of the fault planes can be hindered not only by the overlapping of two irregularities of the profiles, but also by the eventual relative position of several fragments. The mechanism of triggering EQs is established through the combination of the irregularities of the fault planes on one hand and the fragments between them on the other hand. In this direction, the authors proposed a Gutenberg & Richter type formula which describes the EQ dynamics and includes

two parameters: the entropic index q, which describes the deviation of Tsallis entropy from the standard Boltzmann-Gibbs entropy, and the physical quantity α, which characterizes the energy density. The latter equation was later revised by Silva et al. [208], who made with two crucial updates in the context of Tsallis nonextensive statistics as proposed by Abe and Bagci [1]. Finally, their approach leads to the following G-R type law for the magnitude distribution of EQs:

$$G(>M) = \frac{N(>M)}{N} = \left(\frac{2-q}{1-q}\right) \times \log\left[1 - \left(\frac{1-q}{2-q}\right)\left(\frac{10^{2M}}{a^{2/3}}\right)\right] \tag{1.3}$$

where, N is the total number of EQs, $N(>M)$ the number of EQs with magnitude larger than M, and $M \approx \log(\varepsilon)$. The parameter α is the constant of proportionality between the EQ energy, ε, and the size of fragment.

Studies related to seismicities of various geological faults around the world have shown that values of $q \in [1.6 - 1.8]$ seem to be universal, in the sense that different data sets from different regions of the globe indicate a value for the nonextensive parameter lying in this interval [218, 208, 267, 229, 230]. Preliminary observations obtained from studies related to preseismic kHz EM time series, have shown that Eq. (1.3) provides an excellent fit to the preseismic kHz EM experimental data incorporating the characteristics of nonextensivity statistics into the distribution of the detected precursory "EM-EQs". Specifically, Papadimitriou et al. (2008) [172], who worked on the two strong EM bursts recorded a few hours prior to the Athens (Greece) catastrophic EQ (occurred on 09-Sep-1999, with magnitude $M = 5.9$), found a $q \sim 1.8$. Analogous results have been obtained from the analysis of kHz EM time series related to the L'Aquila (Italy) EQ (occurred on 06-Apr-2009, with magnitude $M = 6.4$). In addition, analysis in the context of Tsallis nonextensive entropic framework has also revealed the increased organization (low complexity) of the kHz EM bursts contained in those signals which have been characterized for their seismogenic origin [125, 124, 117, 55, 56].

It should be noted that, the magnitude-frequency relationship for EQs does not say anything about a specific activated fault (EQ). On the contrary the kHz EM precursors refer to the activation of a single specific fault. The similarity of q-parameters mentioned above indicates that the activation of a single fault could be considered as a reduced self-affine image of both the regional and laboratory seismicity [55, 56, 172]. Characteristically, Huang and Turcotte [108] suggested that *"the statistics of regional seismicity could be merely a macroscopic reflection of the physical processes in the EQ source"*. However, further consideration should be given in this direction in terms of nonextensivity.

1.2.3 The kHz EM activity from the perspective of Intermittent Criticality

The definition of Intermittent Criticality (IC) as suggested by the literature related to EQ dynamics, is a concept in which a region alternately approaches and retreats from a critical-point [27, and references therein]. More precisely, IC is based on the hypothesis that a large regional EQ is the end result of a process in which the stress field becomes correlated over increasingly long scale-lengths, which in turn set the size of the largest EQ that can be expected at any given time. The largest event on the fault network cannot occur until regional criticality has been achieved and stress is consequently correlated at all length scales up to the size of the region. It has been shown that the growth of the spatial correlation length obeys a power law with a singularity in the critical point [217, 29, 199, 216, 26, 114, 214, 213, 25, 27]. After the occurrence of this large event the criticality of its associated network is destroyed and a period of relative quiescence prevails. The process is repeated by rebuilding correlation lengths towards criticality until the next large event.

In recent years, many attempts have been made in the prospect to describe the physics of regional seismicity in the framework of self-organized criticality (SOC), which was originally defined on the basis of simple cellular automaton models [12, 209, 167]. However, since SOC models ideally contain no tuning parameters, when a system has achieved self-organized criticality it will remain in that state with constant power-law frequency-size statistics for as long as the external driving force remains constant. As opposed to SOC, intermittent criticality implies time-dependent variations in the activity during a seismic cycle. Before the large EQ event, the growing correlation length manifests itself as an increase in the frequency of intermediate-magnitude EQs. This is commonly referred by the literature as the "accelerating moment release model", and has been discussed by a number of authors [223, 29, 216, 26, 114].

Summarizing the above mentioned arguments, the basic features that characterize a system under IC are: the growing spatial correlation length, the accelerating energy release and self-organized criticality. Studies have shown that a preseismic kHz EM anomaly can be interpreted as an EM confirmation of the IC-hypothesis [54]. Indeed, studies on EM energy release have found a power-law type increase in the rate of EM energy release as the global instability approaches [62, 58, 123]. The recorded acceleration of the EM emission leading up to EM large event and "EM shadow" following this is in harmony with the IC-hypothesis [54]. In addition, it should be noted that the rate of seismic energy release computed around the epicenter of the EQ follows a similar power-law type behaviour (increase). This experimental evidence further supports the relation between the seismicity and the preseismic EM activity indicating that both are originated by the same underlying fracture mechanism. On the other

hand the increment of the correlation length has been supported by wavelet spectra analysis in which the correlation length r of the estimation of the β-exponent of the $S(f) \propto f^{-\beta}$ increases as the catastrophic event approaches. Consequently, although the two basic features have been predicted by the IC-model indicating its existence in the candidate kHz EM precursors, further analysis is needed in order to link this observation with a distinctive regime related to the last stage of fracture process.

1.2.4 The MHz-kHz EM precursors from the perspective of fractal electrodynamics

The theoretical framework of "fractal electrodynamics" is a relative new field of research, initially suggested by Jaggard (1990,2000) [112, 113]. It combines the fractal geometry with Maxwell's theory of electrodynamics suggesting that as the significant EQ approaches, a *Fractal EM Geo-Antenna* can be formed as an array of line elements having a fractal distribution on the ground surface. This is justified due to the fact that in both laboratory and geophysical scale, fault displacements, fault and fracture trace length, and fracture apertures follow a power-law distribution. In effect to this argument, a fault manifests a fractal pattern: a network of line elements having a fractal distribution in space is formed as the event approaches. Eftaxias et al. (2004) has tested this approach suggesting that the underlying MHz-kHz precursors are governed by characteristics that can predicted in the framework of fractal electrodynamics. These involve temporal evolution of the spectrum content, broad-band spectrum region, scaling laws and accelerating emission rate. Characteristically, the authors found that the fractal dimension of the fractal EM geo-antenna associated with the Athens (Greece) EQ is $D = 1.2$ which is consistent with the fractal dimension of a surface trace of a single major fault as has been suggested from seismological and theoretical studies [199, 211].

1.3 Setting the context for the analysis: perspectives and arguments

In recent years the scientific community has placed particular emphasis on the study of complex systems, in the prospect to provide a good definition of "what a complex system is". When someone suggests that a phenomenon or a system is "complex", this statement is indirectly interpreted with something that is hard to be analysed, separated or even hard to be solved. A common basis of the various catastrophic phenomena is that their generation is the result of a collective process with dynamical characteristics: the repeated interactions in many spatial scales progressively lead to the development of large-scale correlations between the entities and finally to the crisis. These dynamical characteristics include: self-organization, intermittent

criticality, simultaneous existence of many degrees of freedom, self-adaption, rugged energy landscapes, and scaling laws (e.g, power-law dependence). Several examples have been given in this direction providing evidence that support such definition [20, 180, 45, 131, 214, 2, 76, 176]. On these grounds, earthquakes, preseismic EM emissions and epileptic seizures, which are analysed in this study, seem to be complex phenomena since they have highly intricate cluster and hierarchical structures, they are governed by feedback mechanisms with spatial and temporal correlation and they provide footprints of self-organization and connection diversity [169, 54]. A promising and globally accepted way to investigate such transient phenomena is to analyze the experimental time-series as a sequence of distinct time windows of short duration or even in some cases as a sequence of separate epochs. Such an approach along with the appropriate methods of analysis, could clearly differentiate the possible dynamical characteristics, as the catastrophic event is approaching, and furthermore to reveal-discover the basic mechanism that characterize such phenomena.

1.3.1 Are there preseismic kHz EM emissions?

Focusing on the seismogenic origin of preseismic kHz EM emissions, the theoretical ingredients of information theory (concepts of entropy) and the fractal-spectra analysis have provided a profit able framework for capturing such deviations. Specifically, the abrupt simultaneous appearance of both high organization and persistency observed in the kHz EM anomalies indicates that the underlying "*fracto-electromagnetic process*" is governed by a positive feedback mechanism which in turn designates these anomalies as possible candidate precursors. Characteristically, Sornette (2004) [213] suggested that "*since the seismicity is a critical phenomenon, it is expected that significant changes in the statistical pattern, can be considered as deviation from normal behaviour*". Furthermore, temporal analysis applied so far in terms of: fractal-spectra analysis, Hurt Exponent, power-law power-law dependence, the G-R formula and nonextensive dynamics, has revealed that universal features of fracture and faulting have also been observed in precursory kHz EM emissions [58, 123, 36, 124, 55, 56] verifying the validity of the two-stage model presented in Sec. 1.2.1. However, such analysis rises several arguments related to the generation mechanism of EQs subjected to the following criticisms:

1^{st} argument: The two-stage model does not say anything about the fragments involved between the two fault planes but only mentions the breakage of the asperities. In addition, EM emissions observed due to laboratory experiments are mainly refer to homogeneous or even brittle materials such as rocks [74, 11, 165, 166, 144, 171, 74, 156, 77, 135, 10] indicating this absence of fragments. It is reasonable to assume that due to the slipping of the two

fault planes there is also interaction between fragments or even fragment-asperity interactions. These fragments may come from previous fractures comprising the residual between the fault planes. Thus it is expected that this process should be also emerged during the kHz EM activity that refers to the last stage of the EQ generation process. Should this case exist, the two-stage model needs to be extended with supplementary evidence that verify the existence of more than one fracture mechanisms that govern the last stage of EQ generation process. On these grounds, the present study deals with this suggestion focusing on the analysis of the preseismic kHz EM emissions that refer to last stage of the EQ generation process building on the two-stage model mentioned above.

2^{nd} argument: A critical-controversial issue facing the scientific community involved with materials science, is the interpretation of scaling laws, on material strength. Specifically, scientists concentrate on whether the spatial and temporal complexity of EQ and fault structures emerges from geometry or from the chaotic behaviour inherent to the nonlinear equations governing the dynamics of these phenomena. In effect this reflects on whether the variations in seismicity can be used to successfully forecast the occurrence of earthquakes. Rundle et al. (2003) [198] suggested that these events can be regarded as a type of generalized phase transition, similar to the nucleation and critical phenomena that are observed in thermal and magnetic systems. In contrast to this argument, Carpinteri and Pugno (2005) [30], purely based on geometry, stated that *"as happened for relativity, geometry could again hold an unexpected and fundamental role."*. Against these arguments the study of preseismic EM emissions seems to provide a relevant framework for examining the nature of the spatiotemporal complexity and fault structures emerged by such phenomena.

3^{rd} argument: It should be stressed that statistical analysis itself, cannot adequately provide sufficient criteria for the seismogenic origin of these kHz EM anomalies and even more their association with the fracture of asperities that are distributed along the fault sustaining the system [54]. In addition, there are very few studies that investigate whether the universal features of fractures and faulting are included in the recorded kHz EM precursors. Specifically, analysis in terms of the G-R formula and the nonextensive Tsallis framework, mentioned in previous sections, have been poorly applied to specific parts of recorded kHz EM emissions [172, and references therein]. Thus it would be challenging to extend this type of research in terms of these methods, in the prospect to identify features that link these EM precursors with EQ dynamics on one hand and to further provide evidence of repeatability of the other. Therefore, it would be challenging to apply a comparative spatiotemporal analysis with new

metrics and models for EQ dynamics that includes both the recorded kHz EM precursors and the regional seismicity around ensuing EQ epicenters. Such analysis could reveal the common existence of fracture regimes that govern these systems and provide further information of the spatial scale that these emissions refer to. In effect obtained information could provide the appropriate framework to investigate whether the statistics of regional seismicity could be merely a macroscopic reflection of the physical processes in the EQ source, as it has been suggested by Huang and Turcotte [108] and even more, whether the associated kHz EM precursors that refer to the activation of a single fault reflect to a reduced self-affine image of regional seismicity [172].

Motivated by this plurality of arguments, a critical concern of this study was to find the appropriate models and methods that include both complexity issues and earthquake dynamics, in the above mentioned context. In this direction, the nonextensive model for EQ dynamics was considered to be the most appropriate approach. Specifically it includes both the entropic content and complexity issues that derive from the nonextensive Tsallis theoretical framework [245], and further involves a profile of EQ dynamics that includes the interference between fragments that comprise the residual between two fault planes. Such an approach could possibly answer on the first question which states on *whether the generation process of an extreme event has more than one facet prior to its final appearance*. Characteristically, Eftaxias (2012) [54], has mentioned that *"seismicity and the precursory MHz EM activity are two faces of the same coin"*. Should this case exists, a combined spatiotemporal analysis on both the seismicity and the preseismic kHz EM emissions by means of the underlying models and methods, could possibly penetrate and elucidate several viewpoints in the field of seismology and geodynamics.

1.3.2 Is there a unified approach for the study of catastrophic events?

The identification of universal principles that may be used to describe the dynamics of complex systems has attracted evolving interest [20, 220, 221, 214, 265, 266]. Several studies, in disciplines such as physics, biology and economics, have applied nuanced analyses indicating that certain similar quantitative features underlie the study of complex systems [180, 45, 131, 214, 2, 76, 176]. In particular, strong analogies between earthquake dynamics and neurodynamics have been reported in the last two decades, suggesting that epileptic and seismic crises can be analyzed within similar mathematical frameworks [107, 105, 197, 122, 169]. On these grounds, the present study extends the focus of inquiry to the study of both scalp-recorded and intracranial electroencephalogram (EEG) recordings related to epileptic seizures.

From the perspective of complexity theory, it has been stated that the laws that describe the behaviour of a complex system are qualitatively different from those that govern its individual units [266]. This implies to the fact that it is almost impossible to understand and interpret the behaviour of a brain focusing on the behaviour of one single neuron. On the other hand it is expected that the simultaneous alteration of a population of neurons, should manifest a new peculiar behaviour-structure with universal characteristics. A challenging issue would be to examine whether the nonextensive formula for EQ dynamics which is routed in a nonextensive Tsallis framework [245, 208], can adequately describe the electric events during the epileptic seizure activity. In addition, a comparative study between the preseismic kHz EM emissions and epileptic seizure recordings, could provide important information that cross-fertilize the knowledge of both biological and geophysical shocks. Even more, from the perspective of self-affinity, it would be very interesting to examine the fractal nature of such phenomena using common methods and metrics.

1.4 Collection of EM data and development of software interface

Since 1994, 11 prototype field stations have been installed in the grater region of Greece under the supervision of Prof. Nomikos, from the *Department of Electronic Engineering of TEI of Athens*, and Prof. K. Eftaxias from the *Physics Department of the National and Kapodistrian University of Athens*. Note that all the stations have the same installed equipment. The installation includes six loop antennas that detect the electromagnetic variations at three different directions (EW, NS, and vertical) and two different frequencies: 3 kHz and 10 kHz respectively. Additionally two vertical $\lambda/2$ electric dipole antennas have been installed, detecting the electric field variations at 41 and 46MHz respectively.

A data acquisition system especially designed for a variety of environmental field measurements has been used for the underlying network, which is based on two parametric custom designed receivers: one for the kHz frequencies and one for the MHz frequencies. Each receiver is working at one of the two, kHz or MHz, desired frequencies using the appropriate antennas. The main core of the data acquisition system, consists of a programmable microcontroller interconnected with five peripheral sub-units [132, 133]. The use of $\lambda/2$ dipole antennas for the reception of the variations of the geo-electromagnetic field at the kHz band is prohibitive due to the excessive dipole lengths required (50 km and 15 km for 3 kHz and 10 kHz, respectively). Therefore, for the sensing of the electromagnetic variations at the kHz band, two standard small loop antennas tuned at 3 kHz and 10 kHz, respectively, were designed. These low frequency small loop antennas are usually referred to as "magnetic loops" to denote that

they are sensitive to the magnetic field variations. For further detail about the electronic part of the devises used for this network please refer to a previously PhD work of Koulouras [133].

For the data collection and preliminary analysis of the detected available signals, a set of software applications have been developed in C++ language, using features and tools of the Integrated Development Environment (IDE) of Borland C++ Builder 6. This was an initial phase which aimed to observe and understand the overall network response (station gaps, battery failures, noise, etc) and to create an earthquake database with the basic tools for combining the EM activity with seismicity. Fig. 1.2 depicts a screen shot of the implemented software used for the data collection. The observed EM recordings refer to those obtained from Zante (ZAKYNTHOS) station prior to the major EQ occurred in L'Aquila (Italy) on 06-Apr-2009.

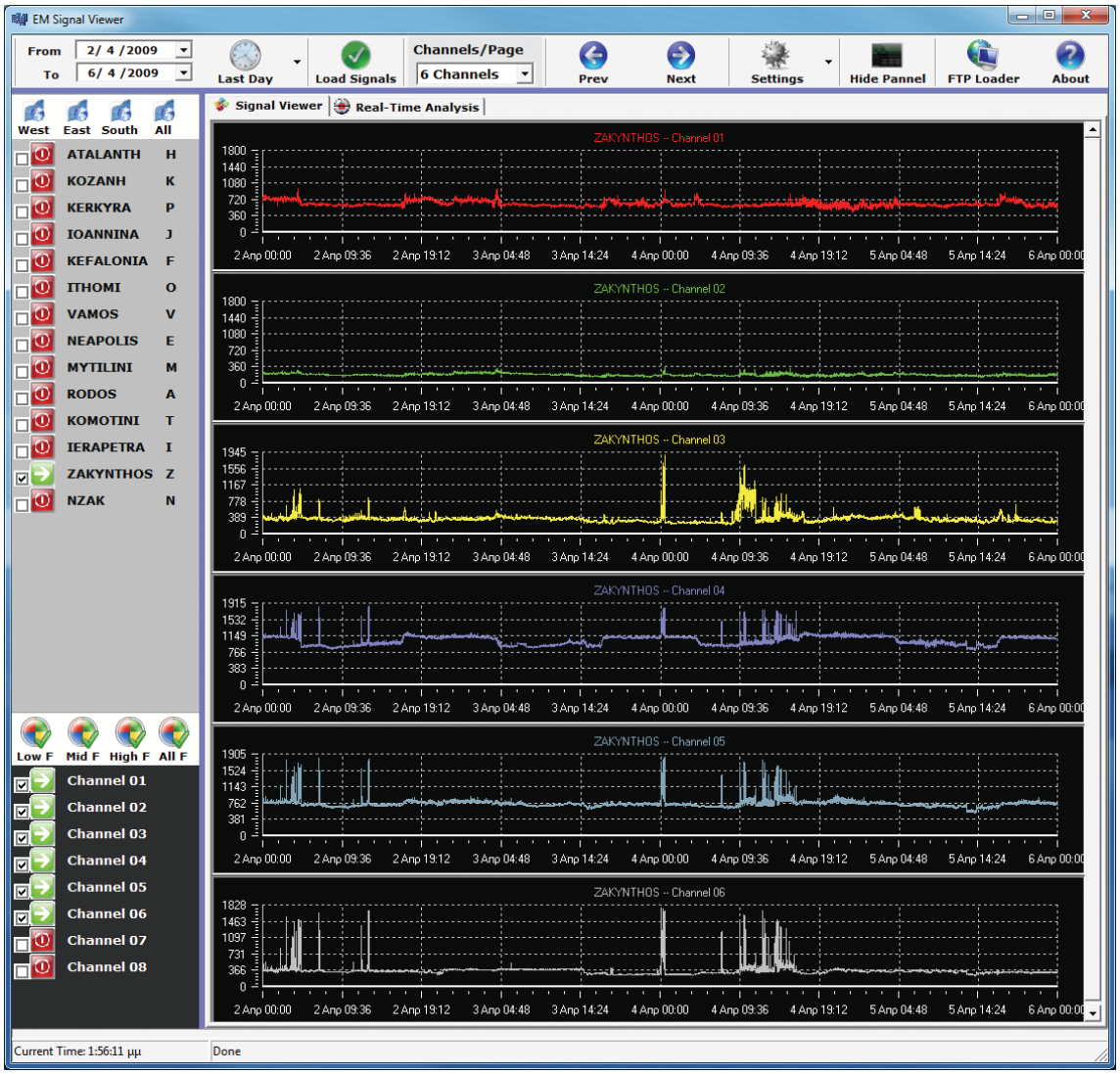

Figure 1.2: A screen shot of the implemented software used for the data collection

Fig. 1.3 depicts the software application for the comparison of EM signals with seismicity at specific regions of interest. The observed EM recordings refer to those obtained from Zante station prior to the major EQ occurred in Athens (Greece) on 7-Sep-1999 (see yellow mark).

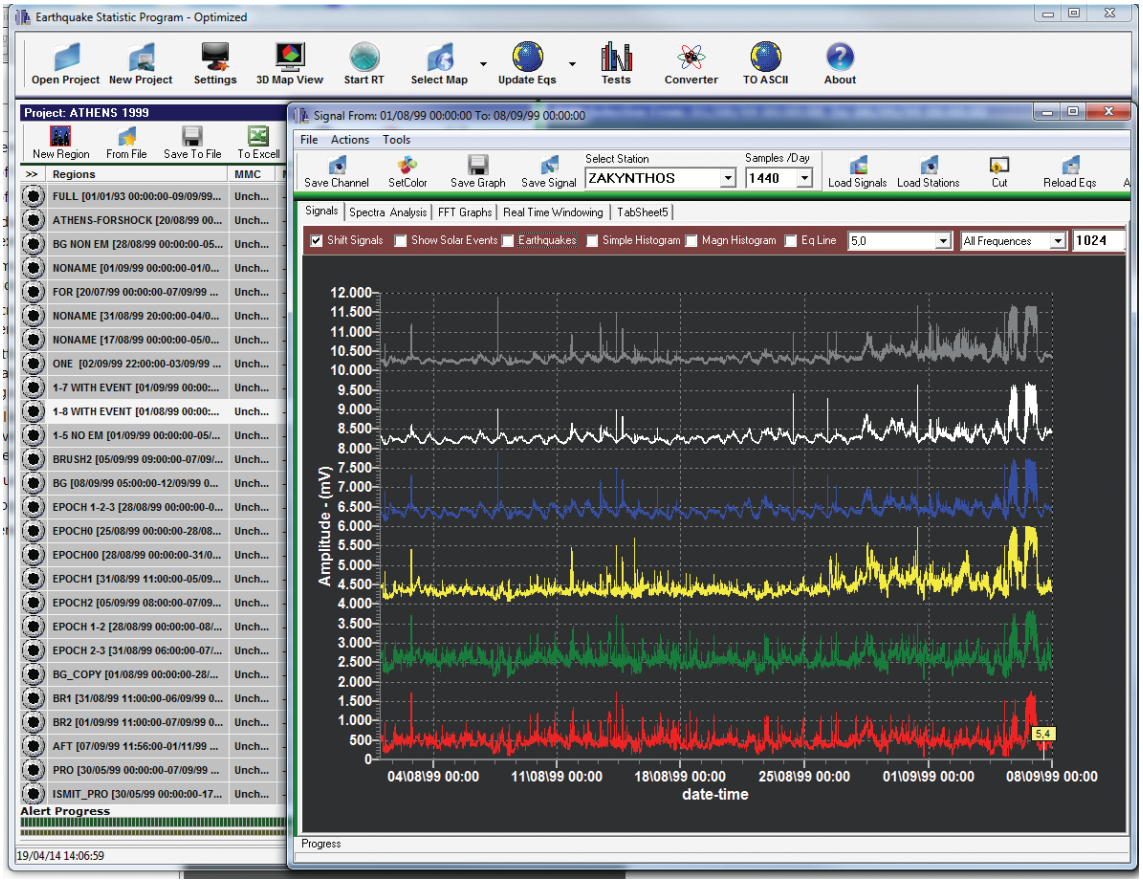

Figure 1.3: Screen shot of the software application for the comparison of EM signals with seismicity at specific regions of interest. The yellow mark at the bottom indicated the time of earthquake occurrence.

Analysis concerning the seismicity, includes EQ catalogs from different geographical regions, namely, Greece, Italy and Southern California. The Greek catalog used has been provided from the website of the *Institute of Geodynamics of the National Observatory of Athens*, (http://www.gein.noa.gr). The Italian catalog used, has been provided by the website of *Istituto Nazionale di Geofisica e Vulcanologia (INGV), Italy*, (http://www.ingv.it) and the Southern California Catalog form the *Southern California Earthquake Data Center (SCEDC)*, (http://www.ingv.it). Fig. 1.4 gives an example 2D and 3D representation of Greek seismicity related to major EQ occurred in Methoni on 14-Feb-2008 10:09:23 with magnitude $M = 6.2$.

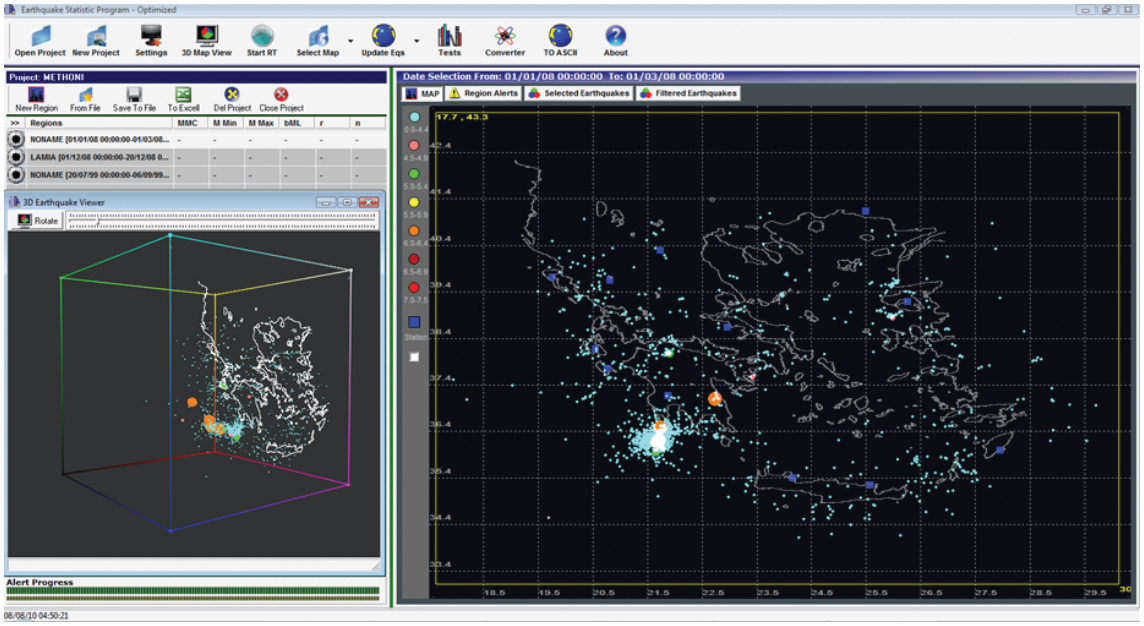

(a)

Figure 1.4: A screen-shot of the software interface implemented for seismicity observations

Herein, it should be noted that the selection of the location where an EM station should be installed is of crucial importance, since the right geoelectrical environment is one of the main considerations for such an installment. Firstly, the station should be away from any man-made radiation and any parasitic signals which may affect the emerged fracture-induced EM emissions. Secondly, according to the literature it has been stated that the MHz EM emissions are more efficiently captured when the Earth's conductivity is relatively low, while for the kHz EM emissions the Earth's should be relative high [61, 15]. For the case of Zante station, its location was selected after a detailed magnetotelluric and magnetic prospection measures that revealed the most appropriate place for its installation. Specifically, the geo-electrical structure beneath the station has been found to be with $1D$ symmetry and very high conductivity with $\rho \approx 100\Omega m$, compared to the typical value of $1000\Omega m$, while the upper is of $2D$ symmetry with characteristic principal axis strike direction $N35^{\circ} \pm 5^{\circ}W$ [63, 61, 9, 148]. Unfortunately, for the rest of the prototype field stations, the corresponding measurements were not performed since their locations were provided (freely) by the Greek Institude of Geodynamics. It should also be noted that the most part of the theoretical background as given by the literature derives from the available preseismic EM emissions recorded from Zante station.

On these grounds, since one the main perspective of this study is to further penetrate on the seismogenic origin of kHz EM precursors, analysis was focused on well documented signals that derive from Zante station. Algorithms and methods implemented and rooted in the above mentioned software interface, have been mainly used for: (i) preliminary observation,

(ii) selection and extraction of the eligible epochs under study and (iii) evaluation of results. Those methods were also implemented using the Matlab software application in order cross-check the validity of the experimental findings presented in this thesis.

In the following section the structure of this work is presented, followed by further arguments that support the context of the proposed analysis.

1.5 Structure of the thesis

Analysis contained in Chapters 2-3 and 4 has been mainly focused on the seismogenic origin of the candidate kHz EM emissions while in Chapter 5, a detailed comparative analysis between epileptic seizures, earthquakes and preseismic kHz EM emissions is performed. Chapter 6 contains a set of proposed formulas in a common framework that manifests the generation process of such phenomena. Chapter 7, summarizes the key findings of this work, in view of future research considerations. During the course of this research report, issues that interest the scientific community such as: universal features of fracture and faulting, the behaviour of propagating stress waves, the self-affinity and complexity, are further discussed and analysed in the context of the analysis performed. A brief description of these chapters follows along with the prospective results:

Chapter 2 - Linking electromagnetic precursors with earthquake dynamics: Analysis in this chapter, attempts to further penetrate and elucidate the link of the precursory kHz EM activity with the last stage of EQ generation building on two theoretical models for EQ dynamics. The first one concerns a self-affine model according to which an EQ is due to the slipping of two rough and rigid fractional Brownian profiles, one over the other, when there is an intersection between them. The second one is the fragment-asperity model mentioned in previous section which is rooted in a nonextensive Tsallis framework starting from first principles [245] and concerns two rough profiles interacting via the fragments filling their gap-residual. This study examines whether these models of EQ dynamics can be linked with the detected kHz EM emission: the possibility to discriminate whether a seismic shock is sourced in the fracture of fragments filling the gap between the rough profiles or in the fracture of "teeth" distributed across the fractional Brownian profiles that sustain the system.

Chapter 3 - Linking preseismic kHz EM emissions with seismicity: This chapter examines whether the transient stresses of seismic waves from a major earthquake (EQ) can trigger a considerably distant significant EQ using three different analytical approaches: (i) a recently introduced fragment-asperity interaction model for EQ dynamics based on nonextensive Tsallis

statistics; (ii) the Hurst exponent; (iii) organization in terms of Fisher information. Using the same approaches, the link beteewn associated precursory kHz EM activity and the last stage of the impending EQ generation is also examined in the prospect to identify whether the statistics of regional seismicity could be a macroscopic reflection of physical processes in the EQ source, as would be expected by the fractal nature of fracture and faulting.

Chapter 4 - Identifying the self-affine nature of fracture and faulting: The aspect of self-affine nature of faulting and fracture is widely documented from the data analysis of both field observations and laboratory experiments. Analysis in this chapter focuses on whether the activation of a single fault is a reduced self-affine image of regional seismicity. Building on a recently introduced model for earthquake dynamics which leads to a Gutenberg-Richter type law, a comparative spatiotemporal analysis is mainly performed that involves seismicity and preseismic kHz EM emission. More precisely, it is examined whether the population of: (i) the earthquakes that precede of a significant event and occur around its the epicentre, and (ii) the "fracto-electromagnetic earthquakes" that emerge during the fracture of strong entities distributed along the activated single fault sustaining the system follow the same statistics, namely, the relative cumulative number of earthquakes against magnitude. Such analysis enhances the physical background of the underlying self-affinity.

Chapter 5 - From earthquakes to the dynamics of regional brain activity in epileptic seizures: The purpose of this chapter is to further examine whether dynamical analogy between ESs and EQs and at the level of a single fault / seizure activation. Such analysis will further support the aforementioned suggestion at lower scale, elucidating the ways in which opening cracks and firing neurons organize themselves to produce *a single* EQ or ES respectively. The results are further verified using the traditional Gutenberg & Richter law and an alternative method for the magnitude-frequency relation for earthquakes. From the perspective of self-affinity, the different placement/locality of the electrodes used for the scalp-recorded and intracranial EEG recordings, provides a relevant framework to examine the fractal nature of such phenomena at two different scales of the regional ES activity in the brain. In this direction, applying different thresholds of EEG-EQ magnitudes contained in both types of EEG recordings under study, the behavior of the parameters included in the nonextensive formula is examined. It is expected that such analysis will verify the common scale-free nature of such phenomena and provide a preliminary indication of the self-affine nature of the regional ES activity in the brain, in terms of nonextensivity.

It should be noted that the initial impetus for the comparative study of earthquake dynamics and regional brain activity was given from previous collaborative work published in Eftaxias

et al [63]. However, the analysis presented in this chapter has been extended to the study of different kinds of data (i.e. including intracranial EEG recordings of epileptic seizures) and undertaking of different approaches in analyzing and interpreting issues pertinent to the main questions and directions of the overall thesis.

Chapter 6 - Spatiotemporal analysis of catastrophic phenomena: a set of proposed formulas: This chapter addresses a number of concerns raised during the course of this research. With a view to consider a different approach on key theoretical principles associated with the generation process of catastrophic phenomena, analysis here is focused on parameters such as: the energy of earthquakes, the mean and maximum magnitude of the sample, the probability that two samples may come from the same population, and the long-range correlations in terms of a nonextensive model for earthquake dynamics. The present study endeavors to provide a relevant framework which is based on new proposed algorithms for the study of catastrophic events. Such an attempt aims to contribute to the knowledge of natural phenomena, providing a few more ways for their interpretation.

Chapter 7: Discussion and conclusions: This chapter summarizes the key findings of this work, in view of future research considerations.

Chapter 2

Linking electromagnetic precursors with earthquake dynamics

The study of precursory phenomena in terms of preseismic electromagnetic (EM) precursors is still questionable, from the most part of the scientific community, since they have not been adequately accepted as real physical quantities [179, 259, 54]. Characteristically, Pham et al. [179], commented that the analysis of these signals *"did not present a quantitative and objectively testable model of the relation between the observed signals and the earthquake source parameters"*. In this direction, the need of using the basic principles of fracture mechanics in the prospect to link these precursors with a distinctive stage of EQ preparation comprises is a crucial open issue under study implying to a better understanding on whether an EM precursor is related to the physical process of the earthquake (EQ) generation. Motivated by such comments and criticisms related to the preseismic nature of these EM emissions, the analysis in this chapter is mainly focused on two key fundamental questions in strength considerations of materials:

(i) When does it fail?

(ii) Are there signals that can warn of imminent failure?

Several studies have shown that fracture induced electromagnetic (EM) physical fields allow real-time monitoring of damage evolution in materials during mechanical loading. EM emissions in a wide frequency spectrum ranging from kHz to MHz are produced by opening cracks, which can be considered as precursors of general fracture [11, 74, 77, 166, 136, 144, 156, 165, 171]. These precursors have been detected at both laboratory [11] and geophysical scale [192, 82]. According to the two-stage model described in Sec. 1.2.1, an important feature that has been observed on both scales, is that the MHz radiation systematically precedes the kHz one

[60, 58, 123, 36]. More precisely, the MHz EM activity can be attributed to phase transition of second order [36], while a Levy walk type mechanism can explain the observed critical state [40]. The finally emerged kHz EM emission, from approximately one week up to a few hours before the main shock occurrence, is rooted in the final stage of EQ generation, namely, the fracture of entities sustaining the system [123, 36, 117, 172, 55].

Drawing from the aforementioned two-stage model, the present work in this chapter endeavors to further penetrate and elucidate the link of the precursory kHz EM activity with the last stage of EQ generation building on two models for EQ dynamics. The first one concerns the work of De Rubeis et al., (1996) [47] and Hallgass et al., (1997) [93] who introduced a self-affine model related to fault dynamics by means of the slipping of two rough and rigid Brownian profiles one over the other. According to this self-affine asperity scheme, an individual EQ occurs when there is intersection between these two profiles. The second model concerns a recently introduced fragment-asperity model for EQ dynamics, by Solotongo-Costa and Posadas (SCP) [218], which is rooted in a nonextensive Tsallis framework [245, 246, 247], starting from first principles. This model is related with a scheme of two rough profiles interacting via fragments filling the gap. These fragments are mainly coming from the residues of the breakage of the tectonic plates, from where the faults have originated. The motion of the fault planes can be hindered not only by the overlapping of two irregularities of the profiles, but also by the eventual relative position of several fragments. The mechanism of triggering EQs is established through the combination of the irregularities of the fault planes on one hand and the fragments between them on the other hand.

Focusing on the kHz EM emissions (that refer to the last stage of EQ generation process), analysis in this chapter argues that the aforementioned two models for EQ dynamics are identified in two qualitatively different epochs of kHz EM precursory activity:

(i) the first epoch of the kHz EM precursor reflects the breakage of the fragments filling the gap between the two profiles.

(ii) the second epoch is emitted during the fracture of large and strong entities ("teeth") which are distributed along these two rough profiles of the fault.

The structure of this chapter is mainly organized as follows: In section 2.1, the aforementioned self-affine and fragment-asperity models for EQ dynamics are described in details. Sec. 2.2 sets the context for the proposed approach drawing on recent studies of kHz EM precursory activity in terms of complexity-organization. In Sec. 2.3 the kHz EM recordings by means of the Hurst's rescaled range analysis are analyzed, distinguishing two emitted epochs that

reflect on two different fracture regimes. In Sec. 2.4 the definition of the "electromagnetic earthquake" (EM-EQ) is firstly given, and secondly the nonextensive behaviour of the kHz EM activity is examined focusing on the link between the two identified epochs associated with the last stage of EQ preparation process. In Sec. 2.5, spectra-wavelet analysis is applied providing footprints of fractal Brownian motion (fbm) profile and roughness of surface fracture related with the two epochs of kHz EM activity. Finally, in the remaining sections, arguments for the association of the second epoch with the self-affine model are provided summarizing the key findings that support the proposed approach.

2.1 Overview of models for earthquake dynamics and metrics used for the analysis

2.1.1 Fundamentals of symbolic dynamics

Symbolic time series analysis is one of the most common methods used by the literature for modelling and characterization of nonlinear dynamical systems [268]: a way of simplifying or even coarse-graining the description of a system under study [95]. According to this method, the time series are transformed into a series of symbols by applying an appropriate partition-threshold which results to a new symbolic time series array with significantly fewer variety of symbols. A construction of a new array is then developed, that contains sequences of symbols ("words") in temporal order. To be more precise, a threshold C is usually applied on the available raw data, which in most cases is the mean value of the sample under study. The simplest possible coarse-graining of a time series is achieved by assigning the symbols "1" and "0" to the signal, depending on whether it is above or below the threshold C. This process generates a symbolic time series that contain a two-letter alphabet $[(0,1), \lambda = 2]$ which is then interpreted in terms of sequential blocks (words) of length $n = 2$. For example, a symbolic sequence of 16 words $(0110100110010110\ldots)$ becomes $01/10/10/01/10/01/01/10/\ldots$ where the number of all possible kinds of words is $\lambda^n = 2^2 = 4$, namely $00, 01, 10, 11$. The probabilities p_{00}, p_{01}, p_{10}, p_{11} are calculated using the fractions of the number of repeated blocks of $00, 01, 10, 11$ included in the symbolic time series divided by the total length of the symbolic data: $0/16$, $4/16$, $4/16$, and $0/16$, where 16 is the total length. In a symbolic time series of W symbols, $\{A_i\}, i = 1, 2, ..., W$, one can read it by words of length $L = n,\ (n < W)$. For each word length, there are λ^n possible combinations of the symbols that may be found in a word, here $\lambda^n = 2^n$, since $\lambda = 2$. The probability of occurrence $p_j^{(n)}$ of the $j-$th combination of symbols $(j = 1, 2, ..., 2^n)$ in a word of length n, can be denoted as:

$$\frac{\#\text{of the } j-th \text{ combination found in words of length } n}{\text{total}\#\text{of words of length } n \text{ (by lumping)}} \tag{2.1}$$

Based on these probabilities we can estimate, the probabilistic entropy or information measures. For example, the probabilistic entropy measure H_S introduced by Shannon (1948) [205], reads as follows:

$$H_S = -\sum p_i \ln p_i \tag{2.2}$$

where p_i are the probabilities associated with the microscopic configurations, calculated according to the above described process.

2.1.2 Principles of Tsallis entropy: definition of the term "nonextensivity"

It is generally accepted that the science of statistical mechanics aims to establish a direct link between the mechanical laws and classical thermodynamics. Within this framework of analysis, the term "extensivity" has been defined as one of the crucial properties of the Boltzmann-Gibbs entropy (S_{B-G}), that expresses the proportionality with the number of elements of the system under study. It has been shown that S_{B-G} satisfies this rule for the case where the subsystems are statistically (quasi-) independent, or typically if the correlations developed between the entities and within the system under study, are essentially local. In such cases the system is called "extensive". As opposed to extensive systems, when the correlations within a system may be far from negligible at all scales, the S_{B-G} is called "nonextensive". Inspired by multi-fractal concepts, Tsallis [245] proposed a generalization of the B-G statistical mechanics, by introducing an entropic expression characterized by an index q which leads to the nonextensive statistics. The formula reads as follows:

$$S_q = k\frac{1}{q-1}\left(1-\sum_{i=1}^{W} p_i^q\right), \tag{2.3}$$

where p_i are the probabilities associated with the microscopic configurations, W is their total number, q is a real number, and k is Boltzmann's constant. $q \to 1$ corresponds to the standard extensive B-G statistics. Indeed, using $p_i^{(q-1)} = e^{(q-1)\ln(p_i)} \sim 1 + (q-1)\ln(p_i)$ in the limit $q \to 1$, we obtain the standard B-G entropy:

$$S_1 = -k\sum_{i=1}^{W} p_i \ln(p_i)$$

The entropic index q characterizes the degree of non-additivity. Given two independent sub-systems A and B with probabilities p^A and p^B, the entropy of a composed system (A+B)

is reflected in the following pseudo-additivity rule, where additivity exists only for $q = 1$:

$$S_q(A + B) = S_q(A) + S_q(B) + (1 - q)S_q(A)S_q(B)$$

The cases $q > 1$ and $q < 1$, correspond to sub-additivity, or super-additivity, respectively. Note that the parameter q itself is not a measure of the complexity of a time series but measures the degree of nonextensivity of the corresponding system. A metric of the dynamic changes of the complexity of a system is the time variations of the Tsallis entropy for a given q (S_q). In the following subsection, a recently introduced fragment-asperity model for earthquake dynamics coming from nonextensive Tsallis statistical mechanics is presented.

2.1.3 A fragment-asperity model for earthquake dynamics coming from nonextensive statistical mechanics

In seismology, the scaling relation between magnitude and the number of EQs is given by the Gutenberg-Richter (G-R) relationship (described analytically in Sec. 1.2.2.1 [89]):

$$\log N(> M) = c - bm, \tag{2.4}$$

where, $N(> M)$ is the cumulative number of EQs with a magnitude greater than M occurring in a specified area and time and b and c are constants. The b-value, which is determined by the least squares method, is regarded as one of the important parameters representing the nature of the occurrence of EQs. However, it should be noted that the G-R empirical relation is not related with general physical principles.

Herrmann and Roux (1990) [104] who studied the phenomenon of fault slipping from a geometric viewpoint, offered an idealized representation of the fragmented core of a fault (gouge), focusing on the material filling the gap between the fault planes. The authors presented the gouge as a self-medium formed by circular disk-shaped pieces which act like bearings filling the space between two planes [103]. In that direction, Sotolongo-Costa and Posadas (SCP) [218] have developed a model for EQ dynamics coming from a nonextensive Tsallis formalism, starting from fundamental principles. In particular, the geometric form of this model refers to the fragments that fill the gap between two fault planes according to the following rules:

(i) *The mechanism of relative displacement of fault plates is the main cause of EQs.*

(ii) *The surfaces of the tectonic plates are irregular. The space between fault planes is filled with the residue of the breakage of the tectonic plates, from where the faults have originated.*

(iii) *The fragments are very diverse and have irregular shapes. The motion of the fault planes can be hindered not only by the overlapping of two irregularities/asperities (teeth) of the profiles, but also by the eventual relative position of several fragments. Thus, the mechanism of triggering EQs is established through the combination of the irregularities of the fault planes on one hand and the fragments between them on the other hand.*

(iv) *In this regard, the authors studied the influence of the size distribution of fragments on the energy distribution of EQs.*

Applying the maximum entropy principle [68] with the Tsallis entropy [245] and comparing the results with those obtained using the Boltzmann entropy, the latter nonextensive approach leads to a G-R type law for the magnitude distribution of EQs:

$$\log(N(M>)) = \log N + \left(\frac{2-q}{1-q}\right) \times \log\left[1+\alpha(q-1)\times(2-q)^{(1-q)/(q-2)} \times 10^{2M}\right] \quad (2.5)$$

where, N is the total number of EQs, $N(M>)$ the number of EQs with magnitude larger than M, and $M \approx \log(\varepsilon)$. The parameter α is the constant of proportionality between the EQ energy, and the size of fragment, r. More precisely, SCP assumed that $\varepsilon \propto r$ and so the energy distribution of the EQs generated by this mechanism can reflect the size distribution of the fragments in the gouge.

The latter fragment-asperity (SCP) model has been recently revised by Silva et al. [208] by applying two crucial updates. Their revision was based on a different definition of the mean values in the context of Tsallis nonextensive statistics as proposed by Abe and Bagci [1], by introducing a new scale law between the released energy ε and the size r of fragments, namely, $\varepsilon \propto r^3$. The new scale proposed by Silva et al. [208] is in full agreement with the standard theory of rupture, namely, the well-known seismic moment scaling with rupture length (see Ref. [267] for details). Finally, their approach leads to the following G-R type law for the magnitude distribution of EQs:

$$G(>M) = \frac{N(>M)}{N} = \left(\frac{2-q}{1-q}\right) \times \log\left[1-\left(\frac{1-q}{2-q}\right)\left(\frac{10^{2M}}{a^{2/3}}\right)\right] \quad (2.6)$$

where,

$$G(>M) = \frac{N(>M)}{N} \quad (2.7)$$

where, N is the total number of EQs, $N(>M)$ the number of EQs with magnitude larger than M, and $M \approx \log(\varepsilon)$. The parameter α is the constant of proportionality between the EQ energy, ε, and the size of fragment r.

Importantly, from most geological analysis performed so far, values of $q \sim 1.6 - 1.8$ seem to be universal, in the sense that different data sets from different regions of the globe indicate a value for the nonextensive parameter lying in this interval [218, 208, 267, 229, 230]. Note that the q-parameter included in the non-extensive formula (Eq. (2.6)) is associated with the b parameter of Gutenberg & Richter formula (Eq. (2.4)), by the relation [202]:

$$b = 2 \times \frac{2-q}{q-1} \tag{2.8}$$

At this point, it should be noted that the theoretical framework of Boltzmann-Gibbs statistical mechanics described in previous subsection, seems to fit properly when dealing with systems composed of either independent subsystems or interacting via short-range forces, and whose subsystems can access all the available phase space. On the contrary, for systems exhibiting long-range correlations, memory, or fractal properties, nonextensive statistical mechanics becomes the most appropriate mathematical framework [245, 247] for analyzing such systems. The aforementioned Eq. (2.6), is not a trivial result, and incorporates the characteristics of nonextensivity into the distribution of EQs by magnitude. This fragments size distribution function comes from a nonextensive Tsallis formulation, starting from first principles: a nonextensive formulation of the maximum entropy principle [218]. Englaman et al. [68] showed that the standard Boltzmann-Gibbs formalism, although useful, cannot account for an important feature of the fragmentation process, i.e., the presence of scaling in the size distribution of fragments, which is one of the main ingredients of the SCP approach.

Focusing on the EQ preparation process a central property of such systems is the occurrence of coherent large-scale collective with a very rich structure, resulting from the repeated nonlinear interactions among its constituents [212]. On these grounds, the nonextensive statistical mechanics seems to be an appropriate framework for investigating the last stage of EQ preparation process in terms of the preseismic kHz EM time series.

2.1.4 A self-affine asperity model for earthquake dynamics: experimental and theoretical evidence

In a pioneer work of De Rubeis et al., (1996) [47] and Hallgass et al., (1997) [93], the authors proposed a model for regional fault dynamics by means of the slipping of two rough and rigid Brownian profiles, $h1(x)$ and $h2(x)$, of length L, one over the other. According to this scheme, an individual EQ occurs when there is intersection between the two profiles. The rules of this scenario read as follows [47]:

(i) *The initial condition is obtained by putting two rigid profiles in contact in the point where the height difference is minimal, so that* $h1 \leq h2, \forall x \in [0, L]$.

(ii) *The successive evolution is obtained by drifting a profile in a parallel way with respect to another, at a constant speed* v*, so that* $h1(x;t) = h1(x - vt)$;

(iii) *At each time step* t*, one controls whether there are new contact points between the profiles, i.e. whether* $h1(x;t) - h2(x) < 0$ *for some* x *value. An intersection represents a single seismic event and starts with the collision of two asperities of the profile*

(iv) *The authors excluded the case of the developing of new earthquakes in a region where a seismic event is already taking place*

The authors assumed that the energy released is proportional to the extension of the overlap between the two asperities in contact. More precisely, it has been stated that the probability $P(E)dE$ that an earthquake releases an energy in the interval $[E, E+dE]$ follows a power law $P(E) \sim E^{-\beta-1}$ with an exponent β of order of the unity[167]. In the framework of this model the authors showed that it is possible to relate the value of the exponent β to the geometrical properties of the faults according to the following equation:

$$\beta = 1 - \frac{H}{(d-1)} = \frac{D_F - 1}{(d-1)} \tag{2.9}$$

where, this relation accounts for the direct dependence of the β-exponent on the roughness of the faults H related to the fractal dimension $D_F = d - H$.

In summary, the authors proposed a model of earthquakes where the critical behavior is generated by a pre-existent fractal geometry of the fault, showing that a specific fault can be regarded as a statistically self-affine profile. It has been shown that this model has exhibited a good interpretation of the seismicities generated in a large geographic areas around the world usually identified as "seismic regions". Ample experimental and theoretical evidence have been provided supporting the aforementioned scheme. Indicatively, some of these studies will be mentioned in the next paragraph in prospect to provide evidence for the validity of this model.

Several studies related to the kinematic or dynamic source of EQs have suggested that the final slip (or the stress drop) has a heterogeneous spatial distribution over the fault [87, 24, 178]. In addition, Power et al. (1987), who applied power-spectrum analysis of the fault surface suggested that heterogeneities are observed over a large range of scale lengths [189, see in particular Fig. 4]. Further investigations in the field of EQ dynamics have already pointed out that the fracture mechanics of the stressed crust of the earth forms self-similar fault patterns,

with well-defined fractal dimensionalities [116, 199, 21]. Chakrabarti et al. (1999) [32], based on observations of the self-similarity in various length scales in the roughness of the fractured solid surfaces, proposed that the contact area distribution between two fractal surfaces follows a unique power law. Huang and Turcotte [108] who studied the fractal distributions of stress in terms of the b-value of Gutenberg & Richter formula (see Eq. 2.4), pointed out that natural rock surfaces can be represented by fractional Brownian surfaces over a wide range. Interestingly, Hallgass et al. (1997) [93] have emphasized that *"what is lacking is the description of what happened locally, i.e., as a consequence of a single event"*.

Motivated by the suggestion of Huang and Turcotte [108], the theoretical approach of the nonextesive model for EQ dynamics, seems to provide the appropriate framework to show that the statistics of regional seismicity could be merely a macroscopic reflection of the preparation process of a single EQ. Thus the analysis that follows builds on this theoretical framework.

2.2 Setting the context for the proposed approach

This chapter focuses in its most part on a well documented [123, 36, 40, 172] kHz EM precursor associated with the Athens EQ that occurred on September 7, 1999 at 11:56 (GMT) with magnitude $M_W = 5.9$. The associated precursor is depicted in Fig. 2.1 recorded from the 10 kHz East-West (EW) sensor.

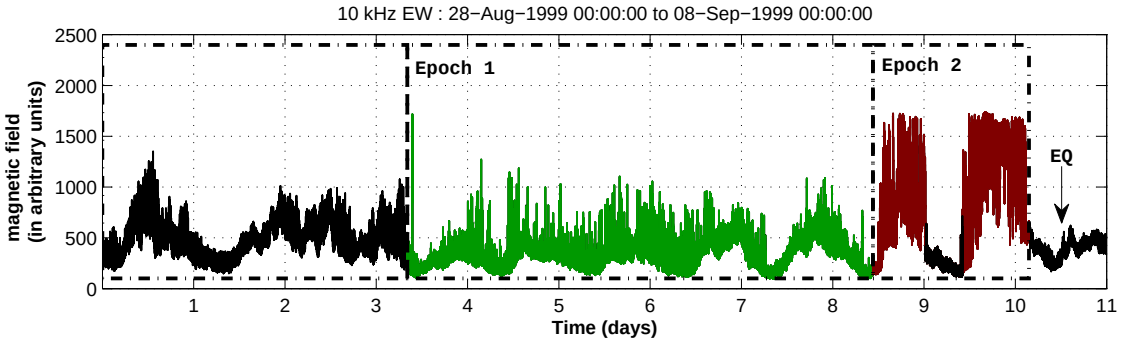

Figure 2.1: View of the preseismic EM emission (green and red) recorded by the 10 kHz EW magnetic field sensor. The vertical arrow indicates the time of the Athens EQ occurrence.

Drawing from recent studies, analysis applied so far on the raw-data from 10 kHz EW sensor, in terms of entropy concepts and information theory, has shown that the black part in Fig. 2.1 refers to the EM background activity (noise) which has been characterized by a low organization (or high complexity) [124, 125, 117]. The first part of the precursor (see epoch 1, depicted with green color) has been characterized by the appearance of a population of EM events sparsely distributed in time with noteworthy higher order of organization in comparison

to that of the noise. The strong bursts A and B included in epoch 2 (depicted with red color) have been characterized by a population of EM events of significantly higher organization in comparison to that of epoch 1 which are densely distributed in time.

Herein, since one of the prospects of this work is to penetrate on the seismogenic origin of preseismic kHz EM anomalies, it would be reasonable to focus the analysis on well documented cases of preseismic EM observations prior to large EQs. The case of Athens EQ is a characteristic well documented case [63, 61, 123, 36, 40, 172, 117]. Thus analysis that follows is based on the preseismic magnetic field recorded by the 10 kHz North-South (NS) sensor depicted in Fig. 2.2. This signal refers to a well documented case on one hand, and here is studied for the first time on the other. It is expected that such an attempt should provide further evidence that verify the repeatability of the literature results, with new findings that may contribute to the knowledge of the generation process of such phenomena.

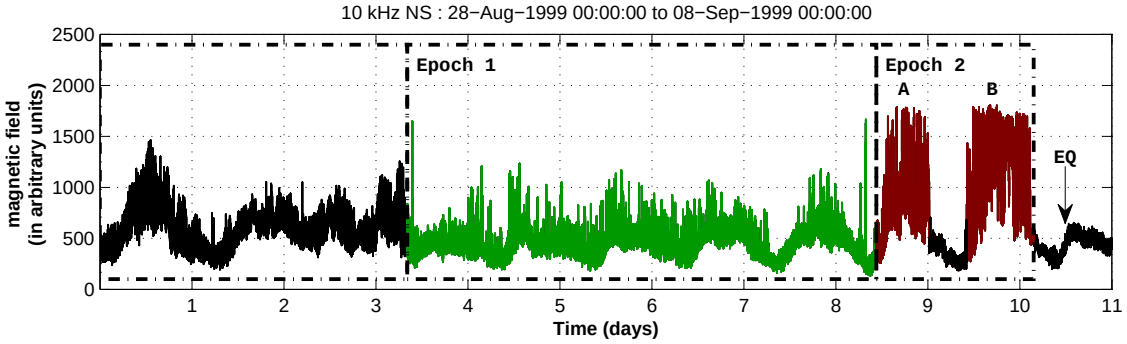

Figure 2.2: View of the preseismic EM emission (green and red) recorded by the 10 kHz NS magnetic field sensor. The vertical arrow indicates the time of the Athens EQ occurrence.

Analysis here is first focused on the degree of organization between the two distinctive underlying epochs included in the 10 kHz NS time series, namely Epoch 1 and Epoch 2, respectively. This process is mainly applied in order to verify that these epochs found in the EW component are also identified in the NS component in terms of complexity-organization measures. A robust grammar-based complexity/information technique was used, namely the T-Entropy introduced by Titchener [244]. T-entropy is based on the intellectual economy one makes when rewriting a string according to some rule. The estimation method and the theoretical background of T-Entropy has been presented in [244, 124, 55]. The analysis has been applied in terms of symbolic dynamics by using sequential successive windows of 1024 samples each. From Fig. 2.3, it is observed that the same results obtained from the 10 kHz EW sensor, are also obtained by the analysis of the 10 kHz NS sensor. More precisely, the second epoch (red bullets) is characterized by higher organization (lower complexity) in contrast to epoch 1 (green bullets). In addition, epoch 1 is characterized by higher levels of organization

in contrast to the black part of the signal which refers to the background noise and lower organization that epoch 3. These results provide a first indication, in terms of complexity, which intuitively leads to the suspicion that epochs 1 and 2, possibly refer to different fracture mechanisms with negative-feedback and positive-feedback, correspondingly.

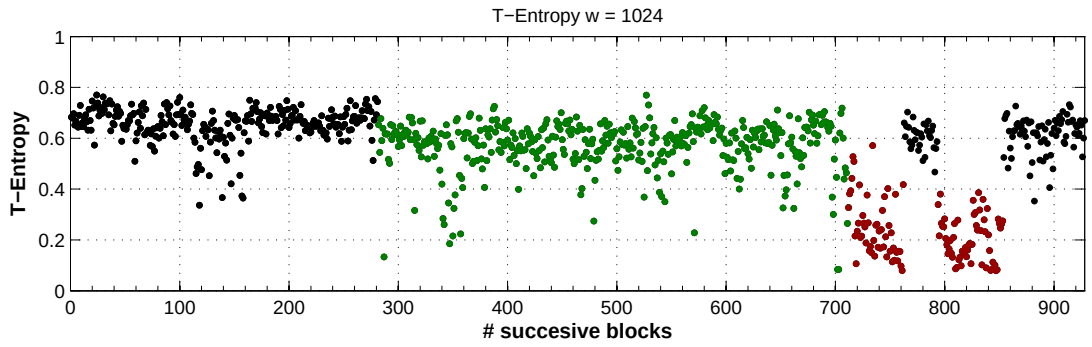

Figure 2.3: Temporal evolution of T-Entropy using sequential blocks of 1024 samples each

Against the theoretical background set in the previous section, herein the proposed approach aims to prove that the two models for EQ dynamics, described in Sec. 2.1, are identified in two qualitatively different epochs of the kHz EM precursory activity as follows:

(i) The first epoch (Fig. 2.2, green color) of the kHz EM precursor may reflect the breakage of the fragments filling the gap between the two profiles that sustain the fault (Fig. 2.4a). In this scheme, EM fluctuations are emitted during the fracture of fragments.

(ii) The second epoch (Fig. 2.2, red color) is possibly emitted during the fracture of large and strong entities ("teeth") which are distributed along two rough and rigid fractal Brownian profiles one over the other (Fig. 2.4b). In this scheme, EM fluctuations are emitted during the fracture of strong and large "teeth".

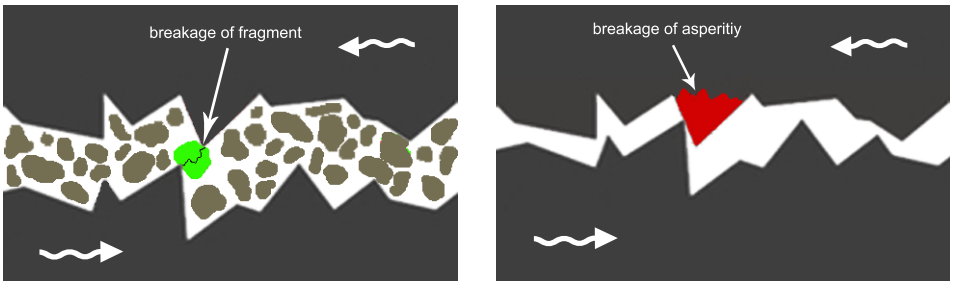

(a) (b)

Figure 2.4: (a) An illustration of the fragment-asperity model. EM fluctuations are emitted during the fracture of fragments. (b) An illustration of the self-affine model. EM fluctuations are emitted during the fracture of strong and large "teeth".

According to this scheme, along with the prospect to verify whether the two precursory epochs are rooted in different fracture regimes, the "Rescaled Range Analysis (R/S)" introduced by Hurst [110], seems to provide an appropriate mathematical and theoretical framework for such an approach. Thus in the following section the analysis of the of the 10 kHz NS sensor in terms of the Hurst exponent is provided.

2.3 The Rescaled Range analysis as a method for distinguishing different fracture regimes

After the works of Hurst et al. [109, 110], Mandelbrot and Wallis [151] and Feder [70], Hurst's rescaled analysis has been used as a method to detect correlations in time series. This method attempts to find patterns that might repeat in the future by using two main variables: the range of the data, R, as it is measured by the highest and lowest values in the time period, and the standard deviation of the data S. The so-called rescaled range is exactly the ratio of R and S. Hurst, in his analysis, first transformed the natural records in time $X(N) = x(1), x(2), ..., x(N)$, into a new variable $y(n, N)$, the so-called accumulated departure of the natural record in time in a given year $n(n = 1, 2, ...N)$, from the average, $< x > (n)$, over a period of N years. The transformation formula reads as follows:

$$y(n, N) = \sum_{i=1}^{n} (x(i) - \langle x \rangle) \tag{2.10}$$

Then, he introduced the rescaled range

$$R/S = \frac{R(N)}{S(N)}, \tag{2.11}$$

in which the range $R(N)$ is defined as a distance between the minimum and maximum value of y by

$$R(N) = y_{max} - y_{min}, \tag{2.12}$$

and the standard deviation $S(N)$ by

$$S(N) = \sqrt{\frac{1}{N} \sum_{i=1}^{N} [y(i) - \langle x \rangle]^2} \tag{2.13}$$

R/S is expected to show a power-law dependence on the box size n:

$$R(n)/S(n) \sim nH, \tag{2.14}$$

where H is the Hurst exponent. R is the difference between the maximum and minimum amounts of accumulated departure of the time series from the mean over a time span τ and S is the standard deviation calculated over the time span τ. The correlation of the past and the future in the observational time series can be described by the Hurst exponent H. For $H = 0.5$, there is an independent random process, with no correlations among samples. For $H > 0.5$, the sequence is characterized by a persistent behaviour, which means that the increasing or decreasing trend is more likely to be conserved, implying a positive feedback mechanism. For $H < 0.5$, the sequence is characterized by the anti-persistent behaviour, which means that an increasing or decreasing trend is more likely to be reversed, implying a negative feedback mechanism.

Focusing on the first epoch, the temporal evolution of the H exponent is studied by applying a sequence of successive fixed time windows of 1024 samples each. Fig. 2.5 shows this temporal evolution of the calculated Hurst exponents obtained by the linear fitting process of the $(log_2(R/SAve)$ vs $log_2(\tau))$ representation of the experimental data. As it is observed from the left part of Fig. Fig. 2.5, the first epoch is really characterized by anti-persistent behaviour $(0 < H < 0.5)$ in its most part with a mean $\bar{H} = 0.38$ and with only 3% of the experimental windows with persistent behaviour. This evidence is consistent with the hypothesis that the first epoch is characterized by a negative feedback.

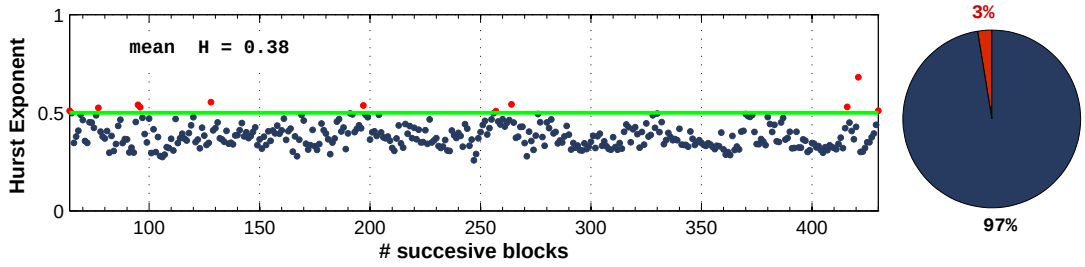

Figure 2.5: Temporal evolution of Hurst exponent (H) for epoch 1, deriving from fixed sequential windows of 1024 samples each. The green line is the threshold of the transition from antipersistent to persistent behavior. The pie shows that 97% of the blocks calculated, are antipersistent.

Focusing on the second epoch, the same windowing method is used as that applied for epoch 1. Figs 2.6a and 2.6b depict the temporal evolution of H exponent for the two strong EM bursts contained in epoch 2. Results obtained from these figures reveal that both the two EM bursts contained in epoch 2, are characterized by a 100% persistent behaviour $(0.5 < H < 1)$, with a mean $\bar{H} = 0.69$ and $\bar{H} = 0.71$ respectively. This evidence is consistent with the hypothesis that the second epoch is characterized by a positive feedback. However, in order to further support the persistency of the two strong EM bursts the R/S method was applied to the

whole part of each one of them. More precisely, Figs 2.6c and 2.6d depict the slopes deriving from the linear regression fitting of R/S method with $H = 0.69 \pm 0.05$ and $H = 0.71 \pm 0.05$ for the first and second EM bursts, respectively. The derived H exponents along with those of the windowing method strongly reveal that both EM bursts are characterized by an onset of persistency indicating the aforementioned positive feedback.

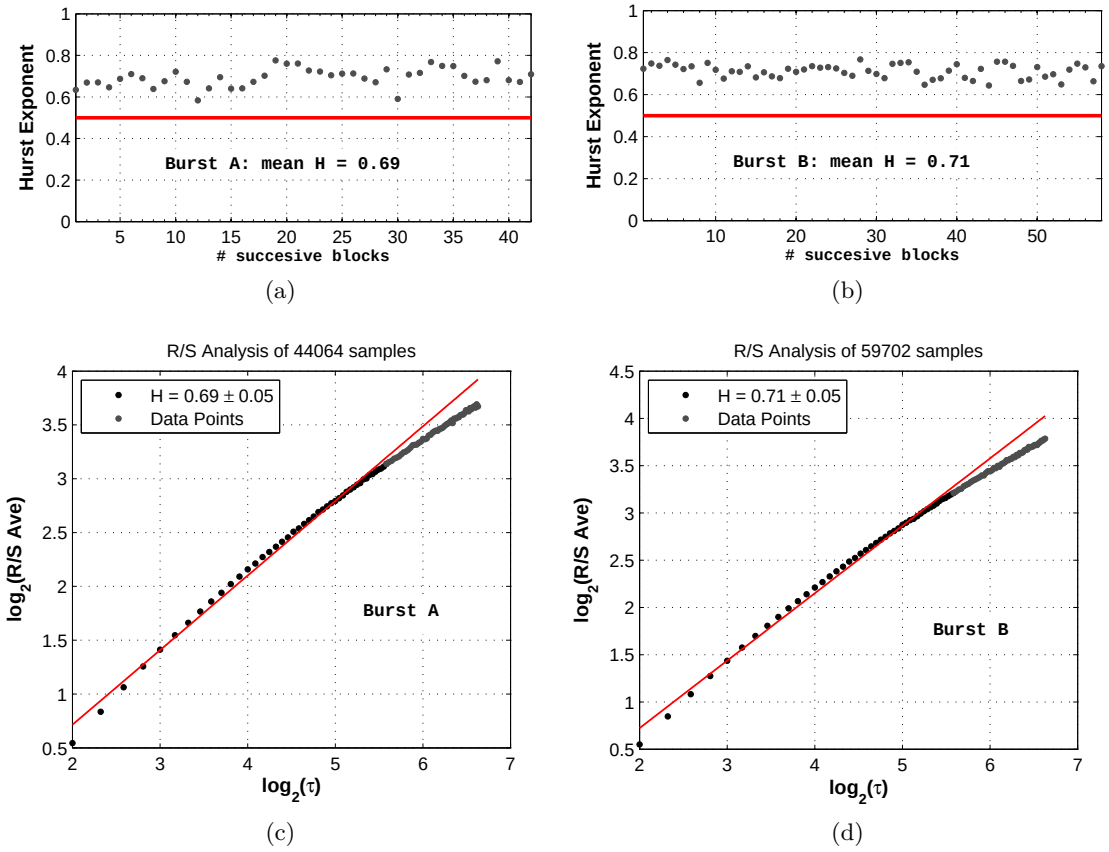

Figure 2.6: (a,b) Temporal evolution of Hurst exponent (H) for the two strong EM bursts contained in epoch 2. (c,d) Hurst exponent estimated in terms of R/S analysis for the whole part of each one of the two strong EM bursts contained in epoch 2.

Summarizing at this point of analysis, the results obtained from R/S analysis strongly support the hypothesis that the two preseismic epochs are rooted in different regimes characterized by negative and positive feedback correspondingly. However, the question whether these epochs are related with different fracture mechanisms is still open. Thus, in the following section the analysis turns to the nonextensive model as described in section 2.1.3 in the prospect to investigate this link.

2.4 Nonextensive approach of the two distinct epochs of kHz EM activity

The first question that this section deals with is whether the nonextensive formula 2.6 can adequately describe the sequence of "electromagnetic earthquakes" (EM-EQs) included in the recorded EM precursor. Should this case exist, analysis go on to further examine the variations/behaviour of the non-extensive parameter q and energy density α for different thresholds of magnitudes of the detected sequence of the EM-EQs. Note that the notion of "Electromagnetic earthquake" for the preseiemic kHz EM time-series has been described in details in Sec. 1.2.2.1, however for the purposes of analysis is also presented here.

The definition of electromagnetic earthquake: As amplitude A of a candidate "fracto-electromagnetic fluctuation" is regarded the difference $A_{f_{EM}}(t_i) = A(t_i) - A_{noise}$, where A_{noise} is the background (noise) level of the kHz EM time series. The "EM-EQ" is refereed as the sequence of k successively emerged "fracto-electromagnetic fluctuations" $A_{f_{EM}}(t_i)$, $i = 1, \ldots, k$ that represent the damage of a fragment or a "tooth" contained in the irregular surfaces of the fault planes. Since the squared amplitude of the fracto-EM emissions is proportional to their power ε_{EM}, the magnitude M of the candidate EM-EQ is given by the relation:

$$M = \log \varepsilon_{EM} \sim \log \left(\sum \left[A_{f_{EM}}(t_i) \right]^2 \right) \tag{2.15}$$

One of the conditions that have to be satisfied in order to be possible to extract the eligible information of these signals concerning the preparation of the last stages of the EQ process, is that the recorded radiation must be emerging clearly from the EM background. This means that the detected kHz EM radiation has not been significantly absorbed by conducting layers of the crust or the even more conductive sea. This implies to the fact that the useful EM precursor must be associated with an on-land seismic event which is both strong, i.e., with magnitude 6 or greater, and shallow. In this case, the fracture process is extended up to the surface layer of the earth's crust. During the evolution of fracture the precursory kHz, MHz EM emissions are mainly produced by a population of EM emitters that sufficiently represent the overall behaviour of their total number of the opening-activated cracks [30].

In order to achieve an efficient and accurate fit for the estimation of the nonextensive parameters q and α, the Levenberg-Marquardt (LM) method [142, 152, 78, 22, 190] was applied. The LM method has been used in several studies in order to solve nonlinear least squares problems when fitting a parameterized function to a set of given data points [155]. Fitting is basically achieved by minimizing the sum of the squares of the errors between the data points and the given function. Figs. 2.7a and 2.7b show that Eq. (2.6) along with the

use of LM method provides an excellent fit to the kHz EM-EQs included in epochs 1 and 2, respectively, incorporating the characteristics of nonextensivity statistics into the detected kHz EM precursor. The green and red lines depicted in the bottom charts of Fig. 2.7, represent the fitting of Eq. (2.6) respectively for epochs 1 and 2. Herein, N is the total number of the detected EM-EQs, $G(>M) = N(M >)/N$ the normalized cumulative number of EM-EQs with magnitude larger than M, and α the constant of proportionality between the EM energy released and the size of fragment [218, 208]. The best-fit parameters for this analysis are given by $q = 1.739 \pm 0.001$ for epoch 1 and $q = 1.834 \pm 0.001$ for epoch 2 respectively. As it was expected, these values evidently reveal that both epochs are characterized by high nonextensivity.

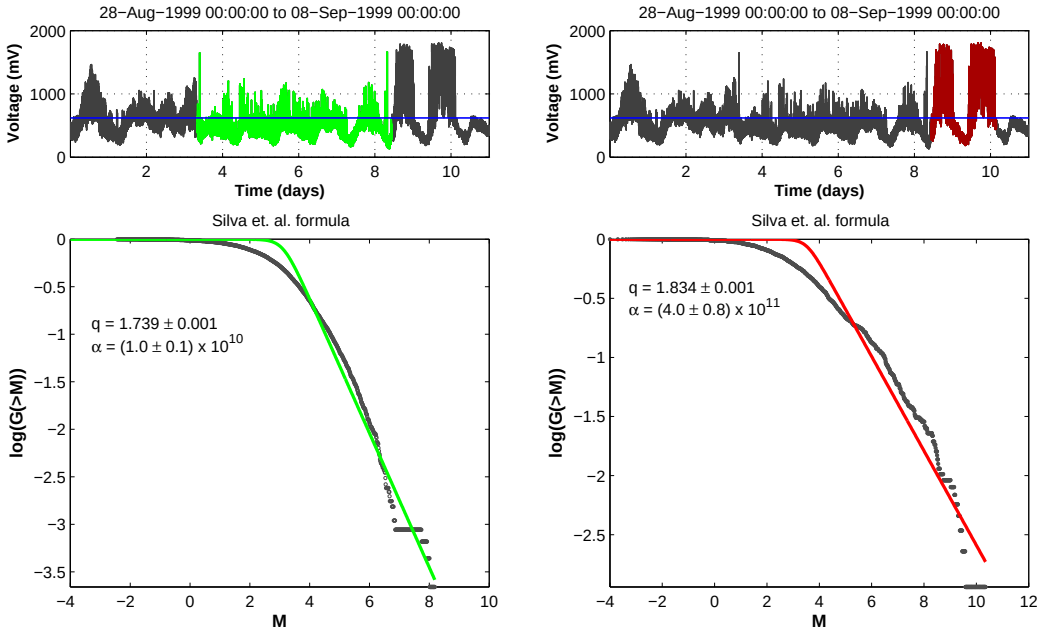

(a) (b)

Figure 2.7: Eq. 2.6 was used to calculate the relative cumulative number of EM-EQs, $G(>M)$, for epochs 1 and 2 respectively. As A_{noise} the threshold of $620mV$ was used for the calculation of EM-EQs.

Note that for the most of geological analysis applied so far in terms of Eq. (2.6), the q parameter lies between the interval $q \sim 1.6 - 1.8$ [218, 208, 155, 267, 229, 230], as well as for all the precursory sequences of EM-EQs under study. According to the two-stage model the preseismic kHz EM time series refer to the last stage of the generation of a single EQ. This observed similarity in the q values indicates that the activation of a single EQ (fault) could be considered as a reduced self-affine image of the whole regional seismicity. These results are consistent with the self-affine nature of fracture and faulting processes [150], issues that will be examined in the next chapters of this study.

As A_{noise} for the calculation of EM-EQs the threshold of $620mV$ was empirically estimated by analysing the mean daily variation of 18 days of quiet signal [121, 55, 56]. From Fig. 2.7, a relative deviation from the experimental data at the intermediate region of the analytical expression of Eq. (2.6), is observed. This is an expected result since it is reasonable to accept that due to the previously discussed absorption of the EM emissions, most of the lower magnitudes "EM-EQs" are placed near the level of the background EM activity at the station area (EM noise). It is obvious that the lower the magnitude of "EM-EQs" the higher the population of "EM-EQs" which are lost. However, the reported data and curves depicted in Fig. 2.7, are considered to be representative of the nature of the studied precursor signal, in the context explained above. The argument that the finally acquired EM emissions are representative of the underlying fracture phenomenon has already been documented based on the fact that there is a remarkable quantitative resemblance between the acquired EM emissions and the seismicity either at laboratory or geophysical scale [123, 36, 172].

Taking into account the recently proposed relation between the b-exponent of G-R Law and the nonextensive q-parameter (see Eq. (2.8)), the estimated b-values were found $b_{est} = 0.71$ and $b_{est} = 0.40$, for the calculated q values of the Figs. 2.7a and 2.7b respectively. These results are consistent with the corresponding results of Scholz (1968) [204] for the last stages of fracture in laboratory experiments. Similar values have already been published in Papadimitriou et al. (2008) [172]. Thus, if the background noise threshold is decreased from $620mV$, which has been considered in the analysis as the absolute maximum value of the background noise, to $480mV$, a better fitting to the analytical expression could be achieved as shown in Fig. 2.8. Nevertheless, this means that a population of "EM-EQs" of lower magnitudes that are of questionable validity (probably correspond to noise) have been encountered in the study although the q-parameter and the b_{est} provide consistent results.

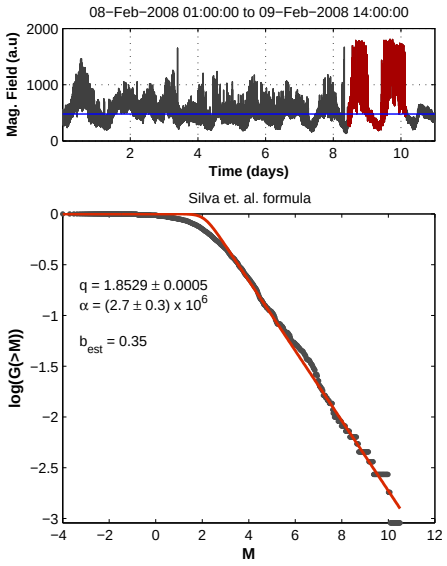

Figure 2.8: Eq. 2.6 was used to calculate the relative cumulative number of EM-EQs, $G(>M)$, for epoch 2. As A_{noise} the threshold of $480mV$ was used for the calculation of EM-EQs.

It should be clarified that the q-parameter itself is not a measure of the complexity-

organization of the system but only a measure for the degree of nonextensivity as derives from revised nonextensive model for EQ dynamics. On the contrary, the dynamic changes of the complexity of the system can be quantified by applying the given Tsallis entropy equation (S_q, see Eq. 2.3) to the time variation of the signal with a given nonextensive parameter q [117]. Against this framework of analysis the lower S_q values characterize the sequential portions of the signal with higher organization, namely lower complexity. Note that analysis applied so far from recent studies in terms of Tsallis entropy the optimal q-parameter is obtained by using different values of q. Such analysis has been already performed for the 10 kHz sensor by [117]. Herein, in order to test this theoretical ingredient the q-parameter included in the formula of Tsallis entropy (see Eq. 2.3), was replaced by the estimated parameters q as derived from Eq. (2.6): $q = 1.739$ for epoch 1 and $q = 1.834$ for epoch 2, respectively. More precisely, Figs. 2.9a and 2.9b depict the temporal variation of the Tsalis entropy for the epochs 1 and 2 respectively. The analysis has been applied in terms of symbolic dynamics by using sequential successive windows of 1024 samples each. It is observed that the results of this statistical analysis are consistent with those obtained from the T-Entropy in section 2.2. As shown, epoch 2 is characterized by a high organized population of EM events which are densely distributed in time in contrast to epoch 1, which is characterized by a population of lower organization sparsely distributed in time. Note that both epochs present higher organization in respect to that of the background noise. The blue line depicts the of entropy level between the background EM activity and the eligible signal.

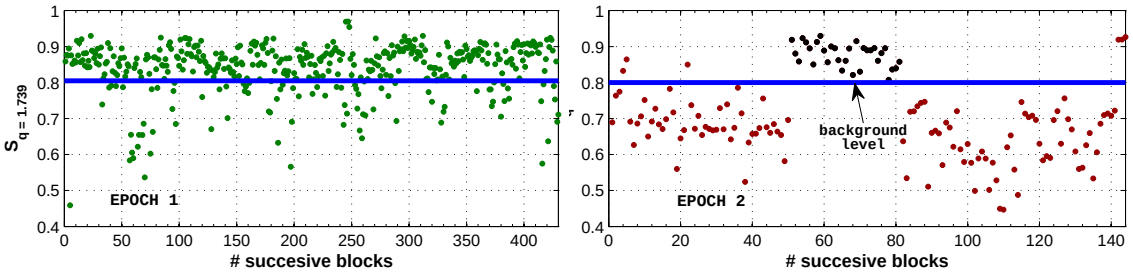

(a) epoch 1 (b) epoch 2

Figure 2.9: Temporal evolution of Tsallis entropy for epochs 1 and 2 respectively. The blue line depicts the entropy level that refers to the background EM activity.

The latter results support the hypothesis that the two epochs of the precursory kHz EM activity are really rooted in different regimes. Thus, since this the nonextensive formula can adequately describe the sequence of "electromagnetic earthquakes" (EM-EQs) included in the two epochs of the recorded EM precursor the analysis is focused on the variation of the nonextensive parameter q and the volumetric energy density α in the prospect to identify possible

differences that may distinguish the seismogenic origin of these epochs. In this direction, different cutoffs of magnitudes M_c were used, of the detected EM-EQs, included in the two epochs of the emerged EM precursor using a serial step of $M_c = 0.1$. For each step, Eq. (2.6) was used to fit the experimental data using a minimum event number of 50 events as a criterion for statistical completeness. The LM method was also used for optimizing the fitting process and ensure the efficiency and accuracy of the algorithm.

In Figs. 2.10a and 2.10b the black curves depict the variation of the q-parameter for different M_c. The observed high q-values for different threshold magnitudes reveal that the nonextensivity in the underlying fracture mechanism remains high in both epochs. This evidence is consistent with the hypothesis that the recorded EM precursor is associated with the final stage of EQ generation. Additionally, the prospective decrement of the nonextensive parameter q as the magnitude threshold increases is explained by the fact that the larger the magnitude threshold the larger the number of EM-EQs/fractures is omitted. Indeed, it has been stated that the large number of the small fractures along with the corresponding redistribution of stresses significantly contributes to the increment of the correlation length during the fracture process [214, and references therein]. The characteristic value that governs the overall system is the one that corresponds to the smaller magnitude threshold for each period. It should also be noted that although the nonextensive parameter q decreases at higher magnitude thresholds it still remains high. This evidence further verifies that strong correlations have developed within the system. Note that the standard error of these serial calculations of the q-parameter was not exceeded the value of ± 0.001, indicating the accuracy of the process.

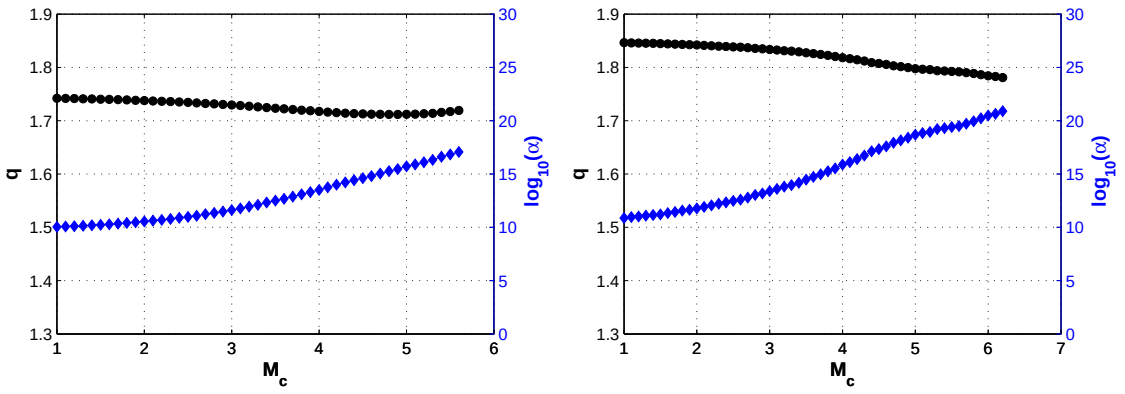

Figure 2.10: Variation of nonextensive parameter q and the volumetric energy density α, for different thresholds of magnitudes of the detected EM-EQs for epoch 1 and epoch 2 respectively.

As opposed to the behaviour of q-parameter, the blue curves in figs. 2.10a and 2.10b show

that the characteristic value of the volumetric energy density α, increases at higher threshold values. This is not an unexpected result since α is the coefficient of proportionality between fragment size and released energy as defined from the fragment-asperity model [208]. More precisely, this observation is consistent with the hypothesis that larger EM-EQs are rooted in larger and stronger entities. Special attention should be given to the following points of differentiation between the two highly nonnonextensive epochs 1 and 2: (i) The maximum magnitude of EM-EQs included in epoch 1 has been found to be $M_{max} = 8.19$, while in epoch 2 it is $M_{max} = 10.36$. (ii) The EM-EQs contained in the abruptly emerged epoch 2 reach significantly higher values of energy density α in the order of 10^{21} while in epoch 1 reach values in the order of 10^{17}.

Herein it should be noted that the method applied here is an interactive method employed to study only the behavior of these parameters and not the natural meaning of the high energies observed by this method for larger magnitude threshold. Besides, the characteristic value that governs the overall system is the one that corresponds to the smaller magnitude threshold which in turn characterizes the original nature of the population under study [172, 214]. The values that correspond to this minimum threshold are also consistent with recent studies [208, 172, 19]. Moreover, Chester et al. (2005) [35] have stated that the energy required to create the fracture surface area in the fault is about 300 times greater than the energy where seismological estimates would predict for a single large EQ.

Summarizing, up to this stage of the analysis, the following findings have been obtained:

- *Analysis in terms of T-Entropy and Tsallis Entropy showed that the degree of the organization of the two strong EM bursts included in epoch 2 is significantly higher than in epoch 1.*
- *R/S analysis has shown that the abrupt emerged two kHz EM bursts contained in epoch 2 are characterized by persistency in contrast to epoch 1 which is characterized by antipersistency.*
- *Nonextensive analysis in terms of the fragment-asperity model for EQ dynamics has shown that both two epochs are characterized by strong nonextensivity*.
- *The behaviour of the volumetric energy density α has revealed that the second epoch is rooted in the fracture of larger and stronger entities in comparison to the first epoch*.

The above mentioned characteristics provide strong evidence supporting the hypothesis that the two epochs of preseismic kHz EM activity under study refer to different models of EQ dynamics. Thus in the following section this hypothesis will be established showing that the

first and second epochs are consistent with the nonextensive fragment and self-affine model, correspondingly.

2.5 The persistent-fBm profile of fracture surfaces in the second epoch of kHz EM activity

The complex nature of the Earth's crust has been globally accepted from the scientific community. However despite its complexity there are several universally holding scaling relations [55, and references therein] that may explain individual processes such as EQs [55, and references therein]. The present section examines whether such universal structural patterns of fracture and faulting process should be included into an associated kHz EM precursor observed prior to Athens EQ. Additionally, further arguments will be provided along with the appropriate analysis, in the prospect to link the two models for EQ dynamics (see Sec. 2.1), with the two distinctive epochs of preseismic kHz EM activity.

Beginning with the pioneer work of Maslov et al. (1994) [154], the authors have formally established the relationship between spatial fractal behavior and long-range temporal correlations for a broad range of critical phenomena. They showed that both the temporal and spatial activity can be described as different cuts in the same underlying fractal. In addition, from the early work of Mandelbrot (1982) [149], much effort has been put to statistically characterise the resulting fractal surfaces in fracture processes focusing on two crucial theoretical ingredients:

- *Fracture surfaces have been found to be self-affine following the fractional Brownian motion (fBm) model over a wide range of length scales [47, 93].*

- *The spatial roughness of fracture surfaces has been interpreted as a universal indicator of surface fracture, weakly dependent on the nature of the material and on the failure mode [146, 94, 186, 162, 272].*

Therefore, focusing on the first ingredient, a fracture surface follows the persistent fBm-model, and consequently, an associated EM precursor should behave as a persistent fBm temporal fractal [57]. Special attention should be given to the following point: *the characteristic of the persistent fBm model does not refer to a population of residual-fragments coming from previous fractures. Consequently, if this hypothesis is true, this characteristic should be contained only in epoch 2 due to the interference of the large and strong teeth.*

Focusing on the second ingredient, it has been stated that the Hurst Exponent H specifies the strength of the irregularity ("roughness") of the surface topography [248]. In addition several studies have shown that the Hurst exponent has been interpreted as a universal indicator

of fracture surfaces [146, 94, 272, 162]. The height-height correlation function of a surface $\Delta h(r) =< [h(r+\Delta r) - h(r)]_r^{1/2} >$ computed along a given direction has been found to scale as $\Delta h \sim (\Delta r)^H$, where H refers to the Hurst exponent. The characteristic value of the Hurst exponent $H \sim 0.7$ has been interpreted as a universal indicator of surface fracture, weakly dependent on the nature of the material and the failure mode [146, 94, 186, 162, 272]. Importantly, Renard et al., (2006) [193] measured the surface roughness of a recently exhumed strike-slip fault plane by three independent 3D portable laser scanners. Their statistical scaling analyses revealed that the striated fault surface exhibits self-affine scaling invariance that can be described by a scaling roughness exponent, $H_l = 0.7$ in the direction of slip.

Concerning the analysis in this chapter by means of Hurst exponent (see Sec. 2.3) it has been shown that the "roughness" of the profile of the two strong kHz EM bursts, is distributed around the value of 0.7. Thus, the universal spatial roughness of fracture surfaces nicely coincides with the roughness of the temporal profile of the recorded two strong preseismic kHz EM bursts included in the second epoch. As opposed to the first epoch, this feature does not coincide with the temporal profile of the preseismic time series of the first epoch in which the mean Hurst exponent was found $\bar{H} = 0.38$.

2.5.1 Footprints of fractional-Brownian-motion model of fracture surfaces

In this section the hypothesis whether the kHz EM precursor behaves as a temporal fractal following the fractional Brownian motion model [47], is examined. According to the literature, if a pre-seismic EM time series behaves as a persistent temporal fractal, then, a power-law of the form $S(f) \propto f^{-\beta}$ is obeyed, with $S(f)$ the power spectral density (PSD) and f the frequency. In a $\log S(f) - \log f$ representation the power spectrum is a line with slope β. The spectral scaling exponent β is a measure of the strength of time correlations, while the quality of the fit of a time series to the power-law is represented by the linear correlation coefficient r [57]. In this direction, the wavelet transform along with the "morlet" wavelet as a mother function was applied, in order to provide an unbiased and consistent estimation of the true power wavelet-spectrum of the given kHz EM time-series. A fixed moving window of 1024 samples was used with no overlapping sequence for the bursts, 2(A) and 2(B), depicted in Fig. 2.11 respectively. For each window the local parameters β and r were derived. Figs. 2.11a and 2.11b shows the calculated wavelet-spectrograms of epochs 2(A) and 2(B) while Figs. 2.12a and 2.12b, the distribution of the β- exponents with $r \geq 0.95$. Two classes of signal have been widely used to model stochastic fractal time series: fractional Gaussian noise (fGn) and fractional Brownian motion (fBm) [102]. For the case of the fGn model the scaling

exponent β lies between $-1 < \beta < 1$, while the regime of fBm is indicated by β values from 1 to 3. As it is observed from Figs. 2.12a and 2.12b, the mean β- exponents of $< \beta >= 2.28$ and $< \beta >= 2.43$, indicate that the profile of the two strong EM bursts indeed follows the fBm-model ($1 \leq \beta \leq 3$).

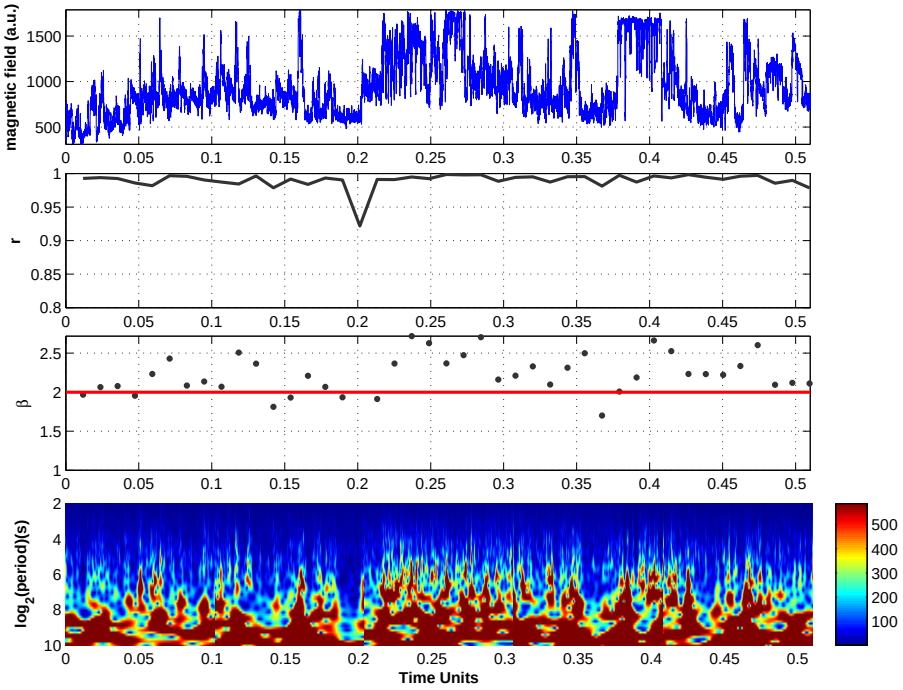

(a) Epoch 2(A)

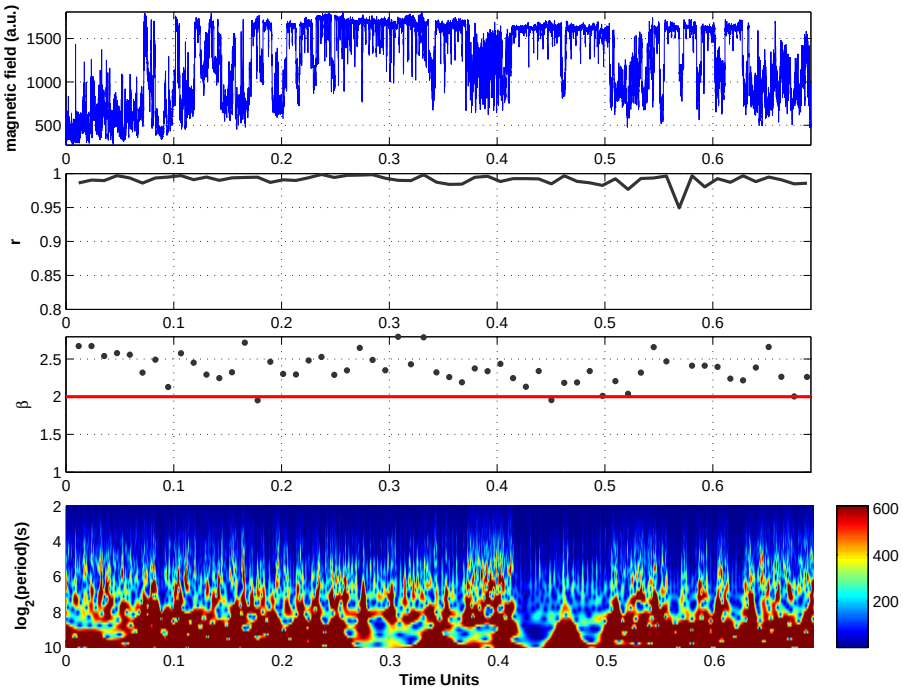

(b) Epoch 2(B)

Figure 2.11: (a,b) depict the wavelet spectrogram of epochs 2(A) and 2(B), respectively along with the local parameters β and r.

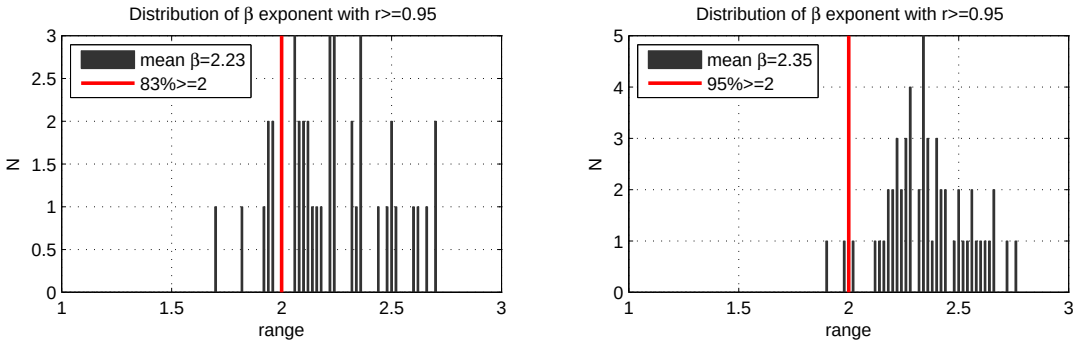

(a) Epoch 2(A) (b) Epoch 2(B)

Figure 2.12: (a,b) depict the distribution of the β - exponents with $r \geq 0.95$ as applied to epoch 2(A) and 2(B) respectively.

However, in order to further verify this finding, in Figs. 2.13a and 2.13b the linear regression fitting derived from the overall estimation of the $\log S(f) - \log f$ representation of the experimental data. It is observed that the estimated β-exponents of two strong EM bursts are $\beta = 2.28 \pm 0.06$ and $\beta = 2.43 \pm 0.09$ for the epochs 2(A) and 2(B), respectively. This finding verifies that the profile of the second epoch of the candidate kHz EM precursor is qualitatively analogous to the fBm-model ($1 < \beta < 3$), indicating that those bursts could be originated during the slipping of two rough and rigid Brownian profiles [47] that follow the fBm-model. The β exponent is related to the Hurst exponent, H, by the formula $\beta = 2H + 1$ with $0 < H < 1$ ($1 < \beta < 3$) for the fBm model [102]. Figs. 2.13a and 2.13b show the estimated values of Hurst exponent, $H = 0.64$ and $H = 0.72$, calculated by applying the β - exponent to the formula: $\beta = 2H + 1$.

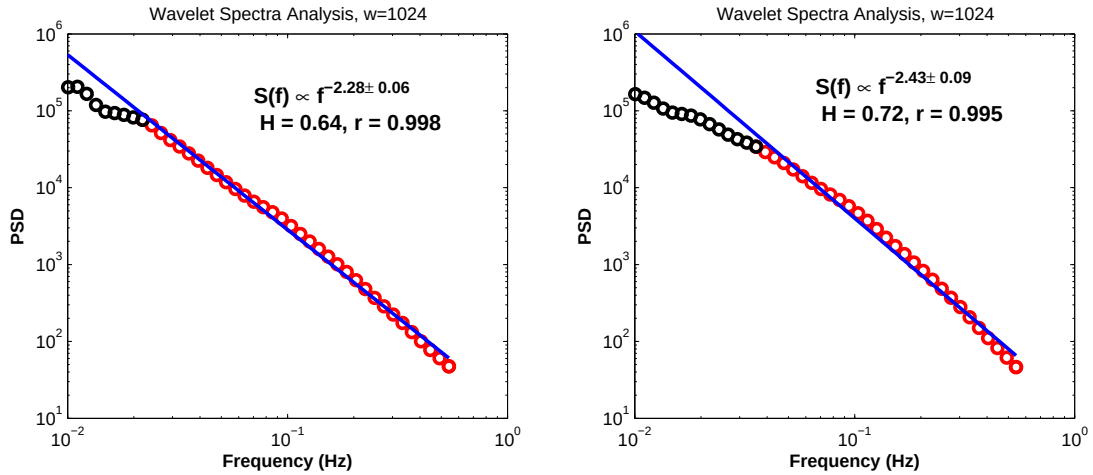

(a) Epoch 2(A) (b) Epoch 2(B)

Figure 2.13: Overall linear regression fitting for the estimation of the β exponent of the power spectra density function: $S(f) \propto f^{-\beta}$

The latter finding further verifies that two strong EM bursts follow the persistent fBm-model, a result that links these precursors with the universal indicator of fracture according to the aforementioned arguments provided in the beginning of this section. In addition, Fig. 2.14 depicts the distribution of H-exponents deriving from the formula $\beta = 2H + 1$ in relation to the distribution of H-exponents as they have been estimated in terms of R/S analysis in Sec. 2.3. We observe that the distributions depicted in Figs. 2.14a and 2.14b that refer to the epochs 2(A) and 2(B), namely the two strong EM bursts contained in epoch 2, are almost concurrent, supporting the persistent-fBm temporal profile of the second epoch. On the contrary the H-exponent distributions of epoch 1 as provided in Fig. 2.14c, verify the antipersistent profile which is not consistent with the universal indicator of fracture surfaces ($H \sim 0.7$).

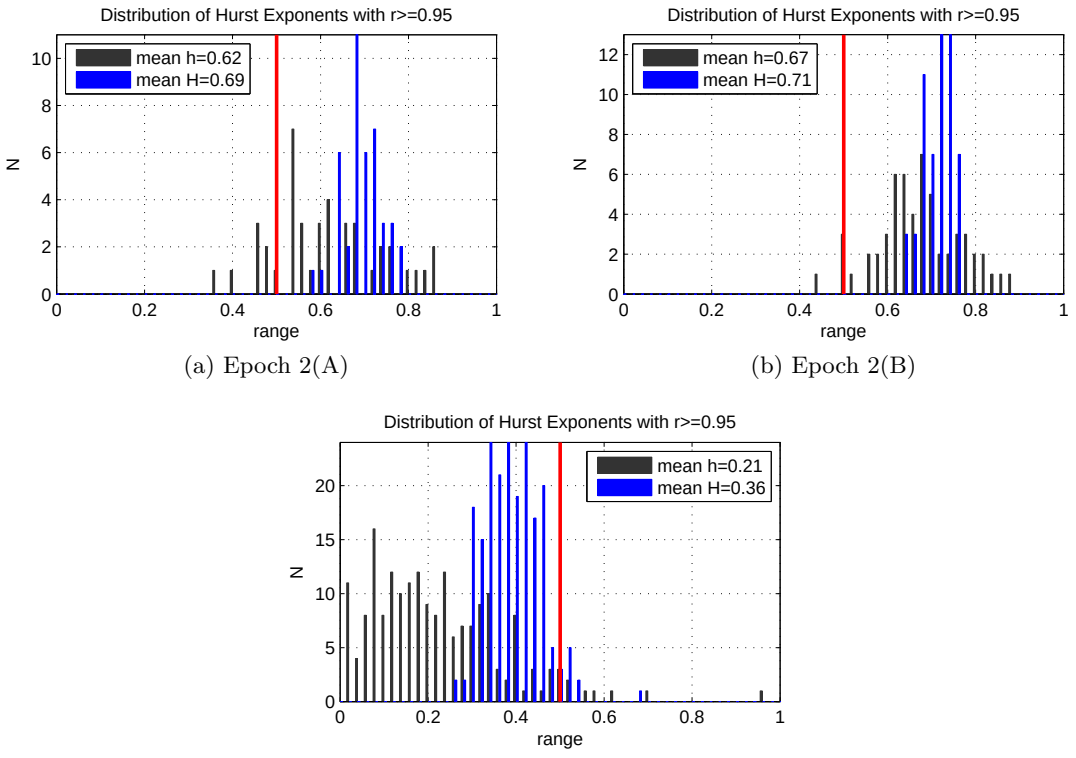

(a) Epoch 2(A)

(b) Epoch 2(B)

(c) Epoch 1

Figure 2.14: The distribution of H-exponents deriving from the formula $\beta = 2H + 1$ in relation to the distribution of Hurst h-exponents as they have been estimated in terms of R/S analysis, respectively from epoch 2(A), 2(B) and epoch 1.

The above mentioned profile of epoch 1 can also be shown in the detailed spectra analysis depicted in Fig. 2.15, where all the β-exponents are distributed below the red line which indicates the transition from antipersistent to persistent behaviour.

According to the self-affine asperity model, the distribution of areas of the asperities broken A, follows a power law $P(A) \sim A^{-\delta}$, with an exponent δ, which could be related to the Hurst

exponent $(0 < H < 1)$ that controls the roughness of the fault. The former relation is obtained by supposing that the area of the broken asperities scales with its linear extension l as $A_{asp} \sim l^{1+H}$. The H-exponent associated with the second epoch of the kHz EM activity is distributed around the value 0.7. It is reasonable to assume that the broken teeth scaled with its linear dimension l as $A_{asp} \sim l^{1.75}$. Importantly, numeric analysis performed by de Arcangelis et al. (1989) [46] has shown that the number of bonds that break, scale during the whole process of fracture as 1.7. This consistency further supports the association of the second epoch with the self-affine asperity model. Moreover, the self-affine model also reproduces the Gutenberg-Richter law suggesting that a seismic event releases energy in the interval $[E, E + dE]$ with a probability $P(E)dE$, $P(E) \sim E^{-B}$, where $B = \alpha + 1$ and $\alpha = 1 - H/2$ with $\alpha \in [1/2, 1]$. In the present case, the Hurst-exponent $H \sim 0.7$ leads to $\alpha \sim 0.65$. Thus, the fracture of asperities released EM energies follow the distribution $P(E) \sim E^{-B}$, where $B \sim 1.65$. This value is in harmony with geophysical data. Indeed, the distribution of energies released at any EQ is described by the power-law, $P(E) \sim E^{-B}$, where $B \sim 1.4 - 1.6$ [89]. The latter results and arguments strongly verify that the aforementioned two models for EQ dynamics are identified in two qualitatively different epochs of kHz EM precursory activity.

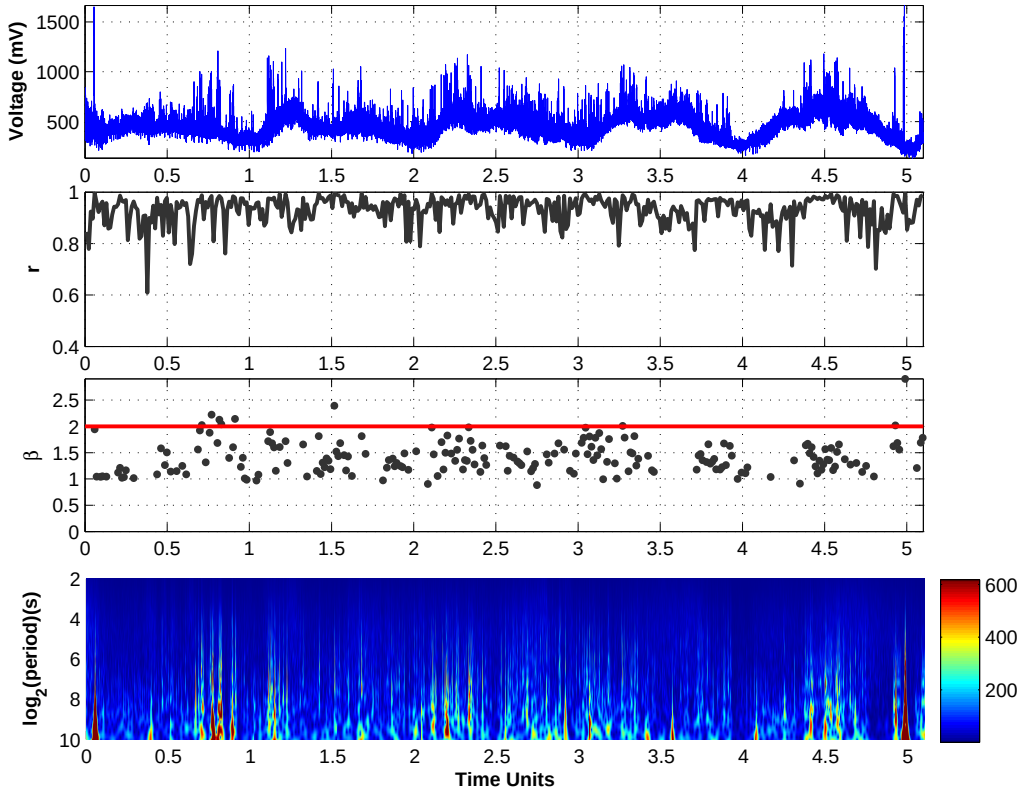

Figure 2.15: Spectra analysis of epoch 1 along with the local parameters β and r.

2.6 The case of Methoni 2008 earthquake: evidence of fbm-model

This section focuses on the case of Methoni (Greece) EQ occurred on 14-Feb-2008 10:09:23 with magnitude $M = 6.2$ at 41km depth, very near to the coastline. Although the earthquake was not very shallow, a strong kHz EM burst was recorded by the 10 kHz EW component of Zante station, approximately six days before the main event, as shown by the red part depicted in Fig. 2.16. Note that the first (black) part contained right before the strong EM burst under study, has been violated by artificial shifts in its intermediate temporal region, and for this reason will not be examined in the present study in order to avoid inconsistencies.

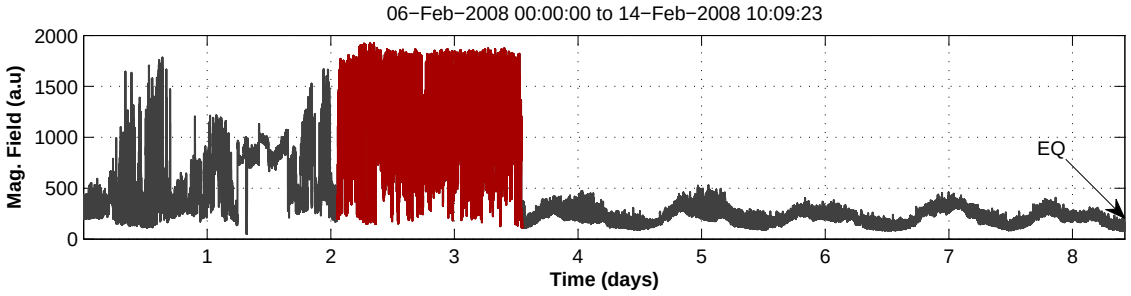

Figure 2.16: A strong kHz EM burst (with red color) recorded approximately six days before the occurrence of Methoni EQ by the 10 kHz EW component. The black arrow indicates the time where the main EQ occurred.

Drawing from the findings in this chapter, it is expected that these strong avalanches are possibly refer to the last stage of the EQ generation process, namely the 2nd epoch as described in previous sections for the case of Athens EQ. In this direction it is expected that the specific red part of these recordings should present both higher organization and high persistent behaviour. Moreover it is also expected that the profile of this burst should be qualitatively analogous to the fBm-model as provided by De Rubeis te al. [47]. A preliminary analysis in terms of T-Entropy, using sequential blocks of 1024 samples each, has revealed that this burst is characterized by high organization levels in contrast to the background activity as shown in Fig. 2.17. The estimation method and the theoretical background of T-Entropy has been analytically described in Sec. A.3. As observed from Fig. 2.17, the part included between the two red lines is characterized by low complexity (high degree of organization). On the contrary the background activity, right after the strong EM burst, is characterized by low organization (or high complexity).

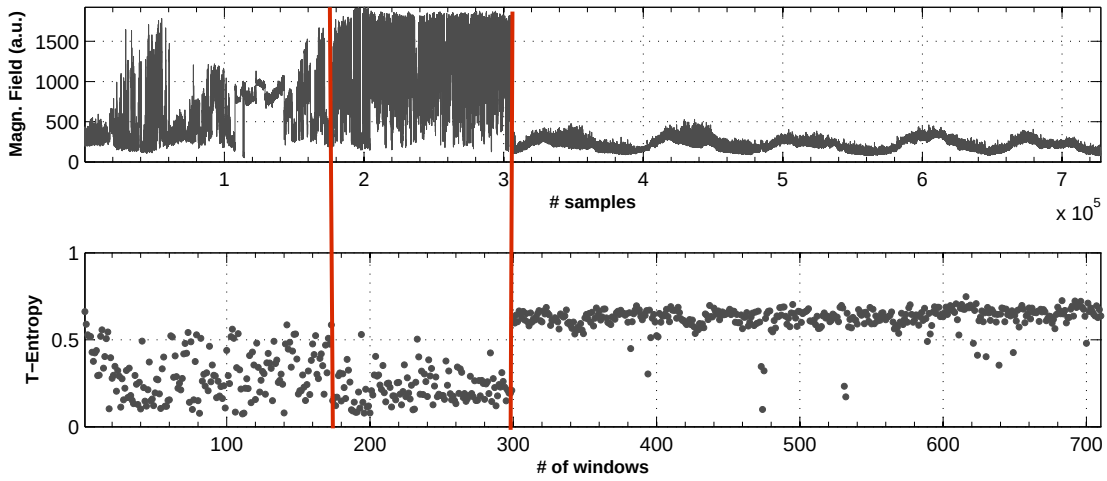

Figure 2.17: Temporal evolution of T-Entropy using sequential blocks of 1024 samples each.

From the perspective of nonextensivity, it is expected that the underlying strong EM burst should present high values of q-parameter that indicate the long-range correlations developed in the system. Thus, Eq. (2.6) was applied to the cumulative number of EM-EQs contained in the signal under study as shown in Fig. 2.18b.

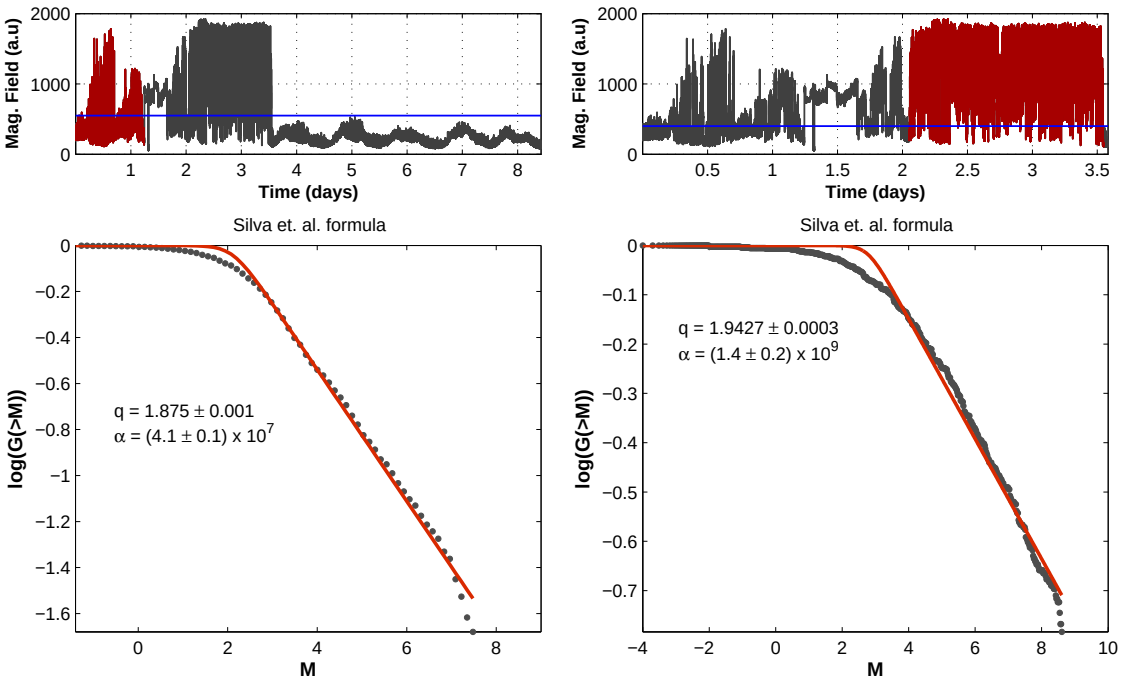

(a) (b)

Figure 2.18: Eq. 2.6 was used to calculate the relative cumulative number of EM-EQs, $G(> M)$, contained in the two epochs depicted in red, related to Methoni EQ. The blue line refers to the threshold of $550mV$ and $400mV$ correspondingly, that used for the calculation of EM-EQs.

Herein, for reasons of completeness, the first part of the signal was also examined by excluding the part of the signal that has been violated by artificial shifts. However the seismogenic origin of this part is still questionable. Therefore, the suggestions in present study will be based only from the results obtained from the second epoch. Specifically, Fig. 2.18a depicts the fitting of the experimental data that refer to the red part of the signal that contained the first epoch of the corresponding EM activity, yielding $q = 1.875 \pm 0.001$. Fig. 2.18b depicts the fitting of the experimental data that refer to the red part of the signal that contained the second epoch, namely the strong EM burst, of the corresponding EM activity, yielding $q = 1.9427 \pm 0.0003$. It is observed that both epochs reveal higher nonextensivity with even higher values observed in the case of the second strong EM burst. It is also observed that the second burst presents higher values of energy α in contrast to the first epoch. Additionally, Fig. 2.19 depicts the Tsallis entropy using a fixed/non-overlapping moving window of 1024 samples. The q-parameter used for the calculation of Tsallis entropy is that derived from the nonextensive analysis in Fig. 2.18b. As it is observed from Fig. 2.19, the part between the two red lines which refer to the strong EM burst is characterized by higher degree of organization in contrast to the preceding epoch 1 where the data are spread in more spatial way reaching the levels of the silent part that follows.

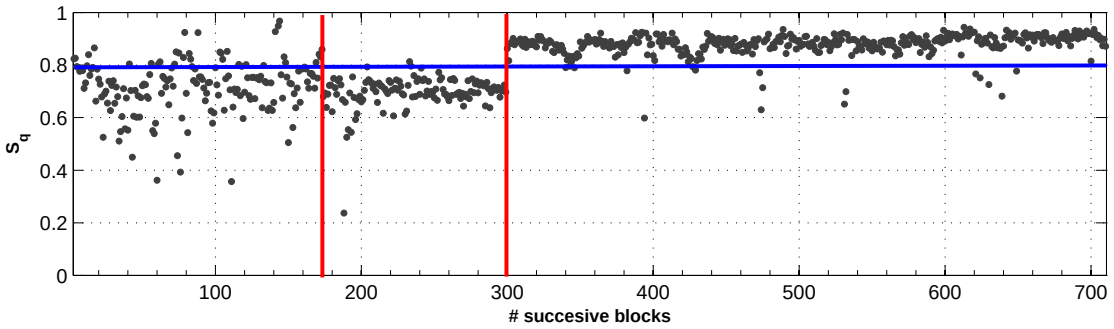

Figure 2.19: Tsallis entropy of the strong EM burst related to Methoni EQ, using a fixed/non-overlapping moving window of 1024 samples.

The wavelet transform along with the "morlet" wavelet as a mother function, was also applied here in order to provide an unbiased and consistent estimation of the true power wavelet-spectrum of the given kHz EM time-series. A fixed moving window of 1024 samples was used with no overlapping sequence for the strong EM burst depicted with red in Fig. 2.16. Fig. 2.20a shows the distribution of the β- exponents with $r \geq 0.95$, while Fig. 2.20b depicts the distribution of H-exponents deriving from the formula $\beta = 2H + 1$ in relation to the distribution of H-exponents as they have been estimated in terms of R/S analysis.

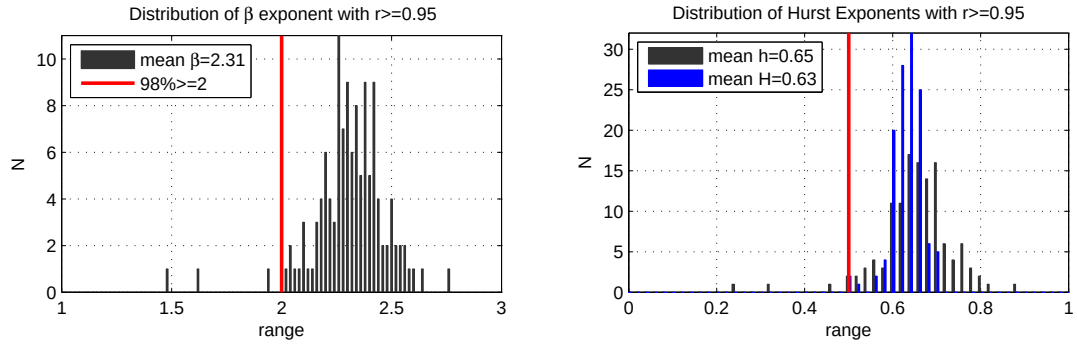

(a) (b)

Figure 2.20: (a,b) depict the distribution of the β exponents with $r \geq 0.95$ and Hurst exponents, respectively.

Fig. 2.21 shows the detailed calculated wavelet-spectrogram along with the calculated local parameters β and r. Note that the blue dots refer to the Hurst exponents as they have been estimated in terms of R/S analysis.

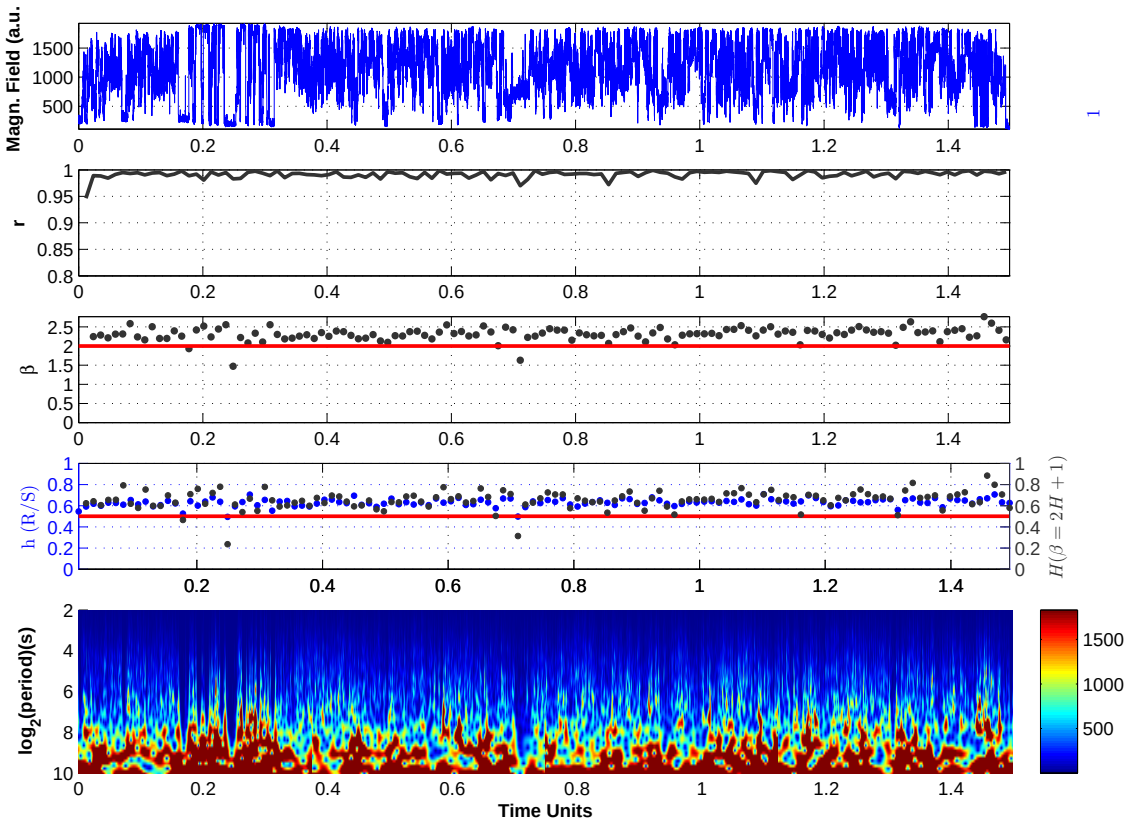

Figure 2.21: (a) depicts the wavelet spectrogram of the strong EM burst observed from the vertical kHz EM sensor prior to Methoni EQ, along with the local parameters β and r.

As it is observed, from both the analysis by means of wavelet-spectra and R/S method, the distributions of H exponents obtained by the two different methods are almost concurrent.

This consistency supports the suggestion that the persistent-fBm temporal profile of the strong EM burst observed prior to Methoni EQ, is analogous to the fBm-model as provided by De Rubeis te al. [47]. However, in order to further support the persistent fbm profile of the aforementioned strong EM burst, in Fig. 2.22a, the linear regression fitting derived from the overall estimation of the $\log S(f) - \log f$ representation of the experimental data, has been estimated. The estimated β-exponent $\beta = 2.50 \pm 0.07$, verifies that the profile of the second epoch of the candidate kHz EM precursor is qualitatively analogous to the fBm-model $(1 < \beta < 3)$, indicating that this burst could be originated during the slipping of two rough and rigid Brownian profiles [47] that follow the fBm-model. In addition, Fig. 2.22b depicts the overall linear regression fitting for the estimation of the Hurst exponent in terms of R/S analysis. The value of $H = 0.67$ is consistent with the universal indicator of fracture surfaces $(H \sim 0.7)$.

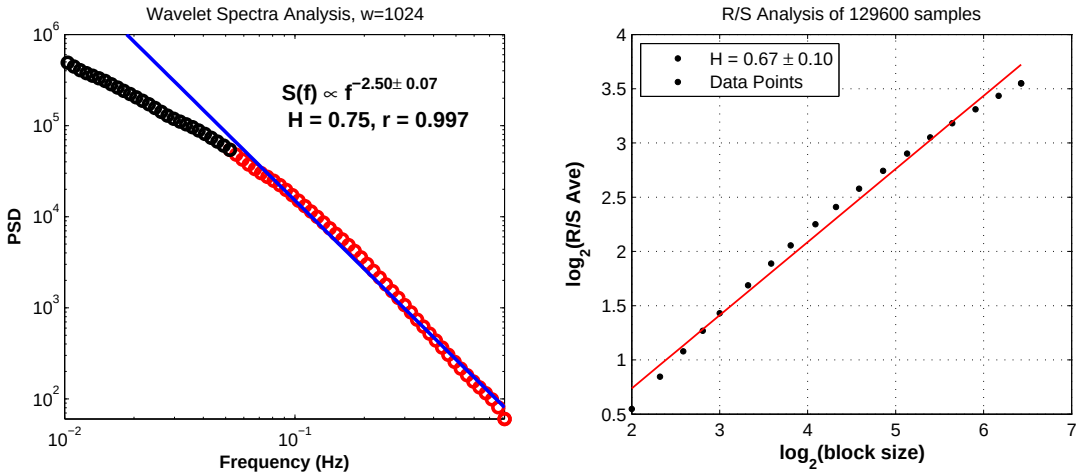

(a) (b)

Figure 2.22: (a)Overall linear regression fitting for the estimation of the β exponent of the power spectra density function: $S(f) \propto f^{-\beta}$. (b) Overall linear regression fitting for the estimation of the Hurst exponent in terms of R/S analysis.

The link between EM precursors and EQ dynamics was supported in this work using two cases of large EQs occurred in the area of Greece. A short discussion follows with arguments in this direction.

2.7 Discussion & Conclusions

It has been stated that preseismic EM emissions in a wide frequency spectrum ranging from kHz to MHz are produced by opening cracks, which can be considered as precursors of general fracture. A recently proposed two-stage model that refers to preseismic EM activity observed prior to large EQs has provided an initial framework for the analysis and classification of these

kHz-MHz EM anomalies. More precisely, the MHz EM emission refers to the fracture of the highly heterogeneous system that surrounds the fault while the kHz EM emission is rooted in the final stage of EQ generation, reflected to the fracture of entities sustaining the system. Drawing from this framework of analysis, the present chapter has been mainly based on two kHz EM precursors recorded from the Zante station, prior to large catastrophic EQs occurred in Greece: the case of Athens (Central Greece) EQ and the case of Methoni (South-West Greece) EQ. Building on two theoretical models for EQ dynamics, the link of the precursory kHz EM activity with the last stage of EQ generation has been further examined, in the prospect to elucidate and penetrate the seismogenic origin of these precursors. The first self-affine asperity model states that the EQ is due to the slipping of two rough and rigid Brownian profiles one over the other in which an individual EQ occurs when there is an intersection between them. The second model which is routed in a nonextensive Tsallis framework starting from first principles, concerns two rough profiles interacting via fragments filling the gap, in which the mechanism of triggering EQ is established through the interaction of their irregularities and the fragments included between them.

The present study attempts to show that the aforementioned two models for EQ dynamics supplement each other, in a sense that both are mirrored in two qualitative different epochs of the preseismic kHz EM emission observed prior to large EQs. It is argued that the profile of first epoch of the emerged precursory activity follows the nonextensive model for EQ dynamics, reflected to the fracture of fragments filling the gap between the two rough planes of the activated fault. The second epoch refers to the emerged precursory activity that contains the abruptly emerged strong impulsive EM bursts which in turn follow the self-affine asperity model. Focusing on the case of Athens EQ, the analysis results illustrate that both the detected epochs are characterized by strong nonextensivity supporting their association with the final stage of EQ generation. Analysis in terms of Hurst Exponent (R/S analysis), wavelet-spectra analysis, complexity theory (T-Entropy, Tsalis Entropy) and nonextensive dynamics, has revealed significant differentiations between the two distinct epochs of the recorded kHz EM activity which in turn verify the aforementioned link with the two models of EQ dynamics. The findings of this analysis read as follows:

(i) The degree of the organization of the two strong EM bursts included in the second epoch, is significantly higher than in the first one.

(ii) The abrupt emerged two kHz EM bursts observed in the tail of the preseismic EM activity of the second epoch, are characterized by persistency in contrast to epoch 1 which is characterized by antipersistency.

Characteristically, Sammis and Sornette (2002) [201] who reviewed the "critical point" concept for large earthquakes and they enlarged it in the framework of so-called *finite-time singularities* presented the most important mechanisms for such positive feedback. In addition, Laboratory experiments based on the study of acoustic and EM emissions have shown that the main rupture occurs after the appearance of persistent behaviour ([185, 4, 5]. Lei et al. (2000, 2004) [140, 139] who studied the individual and coupled asperities fracture as well as the role of asperities in fault nucleation, as potential precursors prior to dynamic rupture, have stated that the self-excitation strength, which expresses the strength of the effect of excitation associated with the preceding event on succeeding events, or equivalently, the degree of positive feedback in the dynamics, reaches the maximum value of ~ 1 during the nucleation.

(iii) The second epoch is rooted in the fracture of larger and stronger entities in comparison to the first epoch. This is verified by the maximum magnitude of EM-EQs where in the first epoch is founded $M_{max} = 8.19$ while in the second epoch it is $M_{max} = 10.36$.

(iv) The EM-EQs contained in the abruptly emerged second epoch reach significantly higher values of energy density a of the order of 10^2. On the contrary in epoch 1 the energy reaches values up to 10^{17}. Herein, it should be emphasized that the breakage of fragments filling the gap between two rough fault planes, is easier than the breakage of teeth distributed along them [218].

(v) The kHz EM precursor of the second epoch includes crucial universal feature of fracture of surfaces: it follows the persistent fBm-model with a roughness consistent with the universal roughness of fracture surfaces ($H \sim 0.7$). Importantly this universal footprint is not mirrored in the first epoch.

Focusing on the case of Methoni EQ, analysis in terms of the Hurst exponent and wavelet-spectra analysis has also revealed that the strong abrupt emerged kHz EM burst observed approximately six days before the main event also follows the persistent fBm-model profile with a roughness consistent with the universal roughness indicator of fracture surfaces ($H \sim 0.7$).

Drawing from the above mentioned findings, the following scenario is supported: the first epoch refers to the fracture of fragments intervening between the two anomalous surfaces of the fault that contributes to the hindering of their relative motion. Once the fracture of one fragment has occurred, there is a reformation of fragments followed by a redistribution of stresses. This process practically results to a relative displacement of the fault planes (fault slip). The next EM-EQ will emerge when a new fragment breaks under the impact of the

increased tensions. This process is consistent with the antipersistent character of the first epoch. As the fragments are broken, the two rough planes of the fault approaches each other. The abruptly emerged second epoch of large EM-EQs is the reflection of collision and breakup of large and strong teeth of the irregular surfaces. The persistent behaviour, the increased degree of organization, the corresponding higher magnitudes M and energy density α provide evidence that support this scenario.

An important question in the present analysis is whether the generation of an EQ can be adequately explained by the both aforementioned models for EQ dynamics, namely the self-affine model (see Sec. 2.1.4 and the nonextensive fragment-asperity model (see Sec. 2.1.3). Confronted with such a question, we may not seek answers merely in the statistics of EQs since both two models of EQ dynamics lead to a power-law distribution of magnitudes. The self-asperity model leads to the traditional power-law distribution of magnitudes, known as Gutenberg-Richter law. The fragment-asperity model as described by Eq. 2.6 also leads to a Gutenberg-Richter-type - law above some magnitude threshold, though Sarlis equation (2.8) [202].

The fact that both models find quantitative expression through the latter equation is not an unexpected result from the viewpoint that some generic behaviour seems to be shared by fragmenting systems whatever their size, material, or typical interaction energy. For instance, as observed in a large variety of experiments [203, 249] and natural phenomena [249, 200, 118, 30], the fragment size distribution frequently exhibits a power law behavior, the origin of which is still unknown. In this direction, it should be mentioned that Scholz (1989) [204] has provided several examples of power-law fragmentation. Moreover, as stated by Silva et al. [208], the released energy ε is proportional to fragment size ($\varepsilon \propto r^3$). Thus it is reasonable to assume that the magnitudes of EQs which are rooted in the fracture of the population of fragments filling the space between fault planes also follow a power-law distribution.

In the research prospect of discriminating whether a seismic shock is sourced in the fracture of fragments filling the gap between the rough profiles or in the fracture of teeth distributed across the fractional Brownian profiles, it would be more appropriate to focus on the generation of a single EQ and not on the statistics of a population of different EQs. On these grounds, the reported significant differentiations of the two epochs imply that the fracture induced kHz pre-seismic EM emissions seem to offer such a possibility. However the proposed approach cannot claim any universal applicability or objective truth. The results presented in this work simply justify the link between nonextensive fragment-asperity and self-affine asperity models for EQ dynamics with preseismic kHz EM activity.

Chapter 3

Linking preseismic kHz EM emissions with seismicity: the role of propagating stress waves in geophysical scale

3.1 Overview

This chapter examines whether the transient stresses of seismic waves from a major earthquake (EQ) can trigger a considerably distant significant EQ, using three different analytical approaches: (i) a recently introduced fragment-asperity interaction model for EQ dynamics based on nonextensive Tsallis statistics (described in Sec. 2.4) [218] (ii) the Hurst exponent [110], and (iii) organization in terms of Fisher information [14, 239]. The analysis has been focused on the major catastrophic earthquake (EQ) occurred in the metropolitan region of Athens (Greece) on 7-Sep-1999 (11:56:50.5 GMT) with magnitude $M = 5.4ML$. The selection of Athens EQ was mainly based due to the fact that a few weeks prior the mainshock, on 17-Aug-1999, another major catastrophic EQ took place on Izmit (Turkey), which is located approximately 650km North-East of Athens EQ. This coincidence, along with the available preseismic kHz EM emissions observed prior to Athens EQ, provides an appropriate framework for such an analysis.

In a recent study, Brodsky et al. [28] reported that the Turkish event was followed immediately by small earthquakes occurring throughout much of continental Greece. Characteristically, the authors mentioned that the Turkish EQ triggered widespread regional seismicity in Greece over a study region extending from 400 km to nearly 1000 km away from the epicenter.

Drawing from the analysis of EQ catalogues, the authors found that small events began immediately after the occurrence of the mainshock suggesting that the transient stresses of the seismic waves were the trigger. An increase in cataloged earthquakes was observed in ordinary continental crust of Greece and the activated seismicity occurred entirely in non-volcanic areas, with statistical significance of 95%. It should be noted that the aforementioned suggestion is in agreement with evidence deriving from laboratory experiments: Krysac and Maynard [134] have shown that, during the fracture of a brittle material, the breaking of a bond launches a propagating stress wave which may trigger the breaking of other bonds. The time interval between the Turkish EQ and Greek EQ, along with the distance between them ($\approx 650km$), strongly supports the hypothesis that the large amplitude dynamic strain of the surface waves was responsible for triggering the regional seismicity.

Against this evidence, the present study examines whether the transient stresses from the Turkish event were responsible for the triggering of the Athens EQ. Drawing from a recently introduced model for EQ dynamics [218, 208], which is routed in a nonextensive Tsallis statistics framework [245, 247], the Greek seismicity is examined in terms of the nonextensive q-parameter, which characterizes the intensity of long-range interactions between fracture events. Note that the model has been described analytically in Sec. 2.1.3, according to which, two rough profiles interact via fragments that fill the gap between them [218, 208].

Focusing on seismicity, analysis in this direction has shown that before the Izmit EQ, the seismicity in Greece presents increased nonextensivity centered on central and western Greece. On the contrary, after the Izmit EQ, the higher nonextensivity is shifted towards the central Greece around the metropolitan area of Athens. In addition, analysis applied on inter-event times in terms of Fisher information and Rescaled Range Analysis, has revealed that higher organization and higher persistent behaviour were mainly developed around the Athens EQ epicenter, for the period after the occurrence of the Izmit EQ.

Focusing the well documented preseismic kHz electromagnetic (EM) activity observed a few tens of hours before the Athens EQ [123, 36, 40, 172], it was found that the preseismic kHz EM emissions share similar nonextensive features with those obtained from seismicity. In addition, the analysis in Chapter 2, along with the analysis form recent studies [123, 117], has verified the high persistent behaviour and high organization levels of these signals. This correlation with the corresponding seismicity further verifies the seismogenic origin of these signals on one hand and further supports the suggestion that the activation of a single fault in terms of preseismic kHz EM emissions behaves as a reduced self-affine image of regional seismicity [108].

This chapter is organized as follows. In Sec. 3.2, the basic principles of Tsallis nonextensive statistical mechanics and a fragment-asperity model for EQ dynamics are described. In Sec. 3.3, a spatial-nonextensive analysis of Greek seismicity focusing on the periods before and after the occurrence of the Turkish event, is applied. The results of this analysis are further investigated in terms of complexity/organization. In Sec. 3.4, analysis is focus on the regional seismicity around the Athens EQ epicenter using the Rescaled Range Analysis as a method to show the persistence of the system under study. In Sec. 3.5, the nonextensive model for EQ dynamics is used in order to examine the relation between the kHz EM emissions and the foreshock activity of the Athens EQ. Sec. 3.7 summarizes the key findings.

3.2 Theoretical background

A nonextensive model for EQ dynamics consisting of two rough profiles interacting via fragments filling the gap has been recently introduced by Sotolongo-Costa and Posadas (SCP) [218]. The model has been analytically described in Sec. 2.1.3, while the related equations used in this Chapter can also be found in Sec 0.6.

3.2.1 Introduction to Fisher Information

Fisher information has been used as a metric of the level of disorder of a system or phenomenon, providing a powerful tool for the investigation of complex and non-stationary signals [153, 187, 238, 236, 147, 240]. The results deriving from Fisher information behave inversely to the corresponding entropic measures, For example, the increased order of the deriving values is characterized by decreased entropy correspondingly, and so called as increased Fisher information. Note that Fisher information, has been applied in several studies related to geophysical and environmental phenomena, divulging its ability to describe the complexity of a system [14, 239, and references therein].

$$I_x = \sum_{n=1}^{N-1} \frac{\left[p\left(x_{n+1}\right) - p\left(x_n\right)\right]^2}{p\left(x_n\right)} \tag{3.1}$$

The discrete probability distribution $p\left(x_n\right)$ corresponds to the specific values of the unknown underlying probability density function at the centre values of the intervals $\{x_n\}$, which are not necessarily of equal length. The probability density function is usually approximated by the histogram, or by the kernel density estimator technique, employing different kernel functions like Gaussian kernel, or Epanechnikov kernel [187, and references therein].

3.3 Investigation of Greek seismicity in terms of nonextensive statistical mechanics

In order to clarify whether the Turkish EQ was possibly triggered the Athens EQ, in this section the seismicity of Greece is first examined for the periods before and after the time of the Izmit EQ occurrence up to the time of the Athens EQ occurrence. Figs. 3.1a and 3.1b depict the overall Greek seismicity of both periods under study.

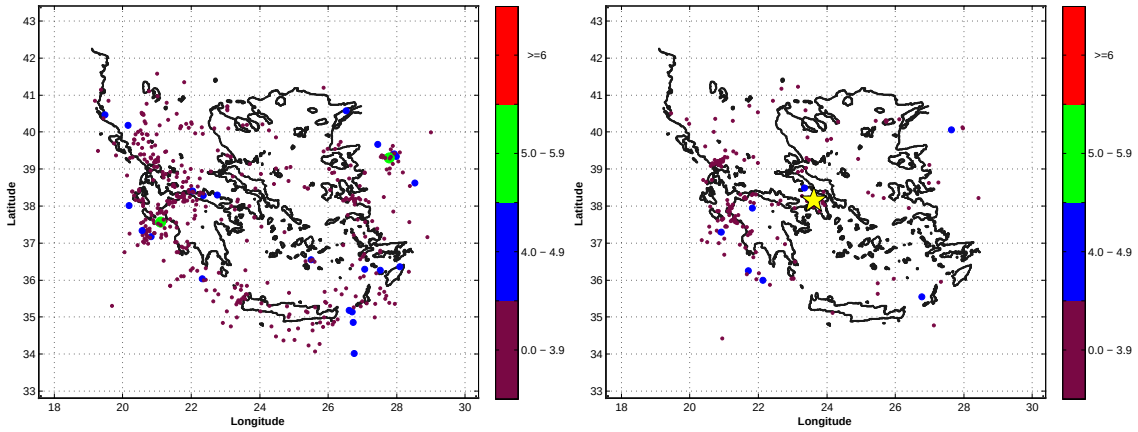

(a) Before Izmit EQ (b) After Izmit EQ

Figure 3.1: Spatial distribution of EQs for the periods before and after the occurrence of Izmit EQ. (a) refers to a time window from 1-Jun-2009 00:00:00 up to 17-Aug-1999 00:01:39.80 and (b) to a time window from 17-Aug-1999 00:01:39.80 up to 7-Sep-1999 01:56:50. The star indicates the Athens EQ epicenter. The data derive from the EQ catalogue provided by the website of the Institute of Geodynamics of the National Observatory of Athens (www.gein.noa.gr).

Herein, the period before the Izmit EQ refers to a time window from 1-Jun-1999 00:00:00 up to 17-Aug-1999 00:01:39.80, whereas the period after the Izmit EQ refers to a time window from 17-Aug-1999 00:01:39.80 up to 07-Sep-1999 01:56:50. In order to examine the spatial variation of the nonextensive q-parameter between the two periods under study, the Greek territory was scanned using a shift of 0.2° in longitude and latitude directions. Using Eq. (2), along with the use of the Levenberg-Marquardt (LM) fitting method [142, 152], a spatial area of 160 km around each relative point was examined. For each calculation, the obtained parameters (q and α) were graphically placed at the center of each scanned area with different colors. A minimum number of 20 events was used as a criterion for the statistical completeness of each calculation. Figs. 3.2a and 3.2b show a contour plot of the spatial distribution of the q-parameter depicted with different colors, for both periods under study. Focusing on the period before the Izmit EQ (Fig. 3.2a), it is observed that higher nonextensivity was mainly

developed at the central and western Greece, as shown by the dark-red areas in Fig 3.2a. On the contrary, for the period after the occurrence of Izmit EQ, the higher nonextensivity is observed around the Athens EQ epicenter within a range of approximately 160km, as shown by the dark-red areas Fig. 3.2b).

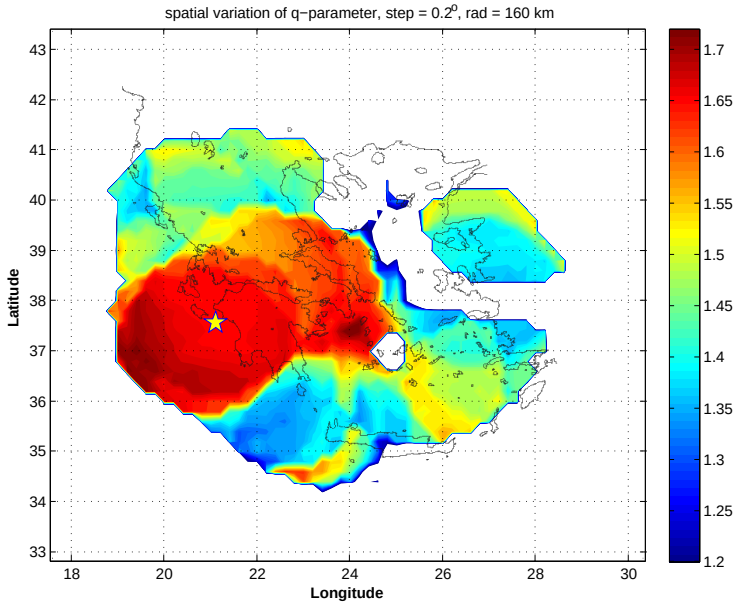

(a) Before Izmit EQ

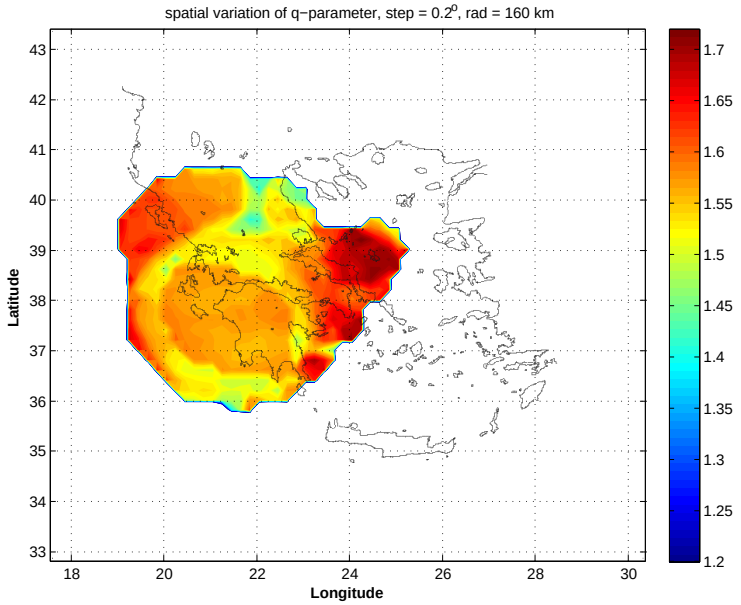

(b) After Izmit EQ

Figure 3.2: Spatial distribution of q-parameter for the periods (a) before and (b) after the occurrence of Izmit EQ. The star-marks indicate the EQs with magnitude larger than or equal to $5.0M_L$. The colored bar indicates the range of variation of the q-parameter.

In the prospect to further support the latter results for their consistency and to show the accuracy of the fitting process, in Figs. 3.3a, 3.3b, 3.3c and 3.3d, the fitting of Eq. (2), with

the lowest and largest number of events included in the grids of 3.2a and 3.2b respectively. It is observed that the relative standard error for the estimation of q-parameter varies between $0.002 - 0.008$, indicating the good approximation of the fitting.

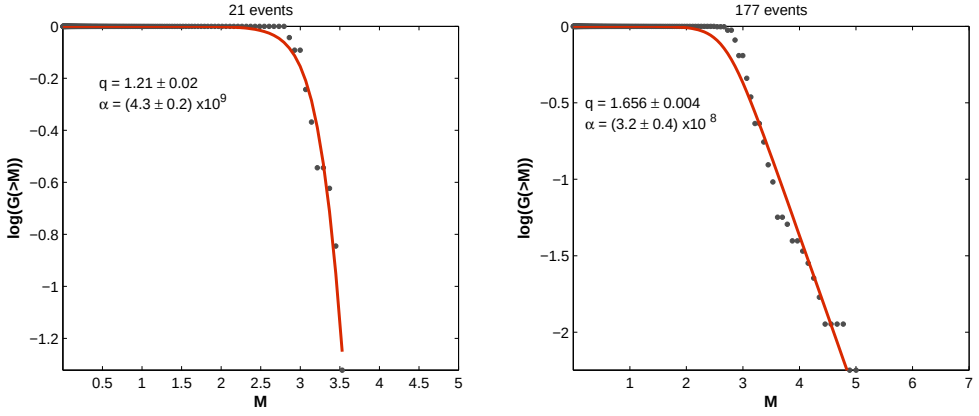

(a) Before (smallest sample) (b) Before (largest sample)

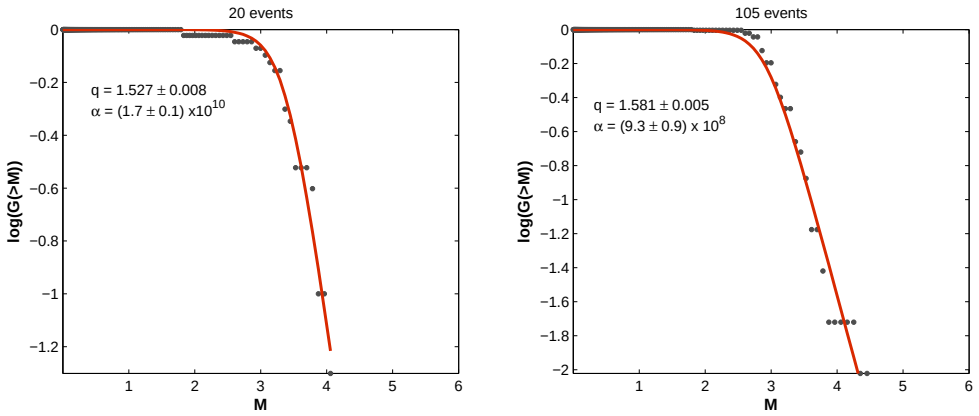

(c) After (smallest sample) (d) After (largest sample)

Figure 3.3: (a,b,c,d), depict the fitting of Eq. (2), with the lowest (a,c) and largest (b,d) number of events included in the two grids of figure 3.2, correspondingly.

Herein it should be noted that the period before the Izmit EQ that refers to a time-frame from 1-Jun-1999 00:00:00 to 17-Aug-1999 00:01:39, was mainly selected in order to achieve sufficient number of EQ events mainly for the range of 0-160km around the Athens EQ epicentre. If the analysis in this chapter was only focused on the behaviour of the nonextensive q parameter (Eq. (2)), then a shorter time window closer to the Izmit EQ could be used which in turn might give even better results, further enhancing the suggestion. Indeed, in the following figure 3.4a, the same spatial nonextensive analysis for a shorter time-frame, namely from 1-Jul-1999 00:00:00 to 17-Aug-1999 00:01:39 has been applied. The white areas in the grid (in central Greece) indicate a q parameter lower than 1.2. This result is consistent with the hypothesis that before the Izmit EQ the nonextensivity was relative low. In addition, Fig.

3.4b shows the same analysis as that in Fig. 3.2b, but includes the Athens EQ event.

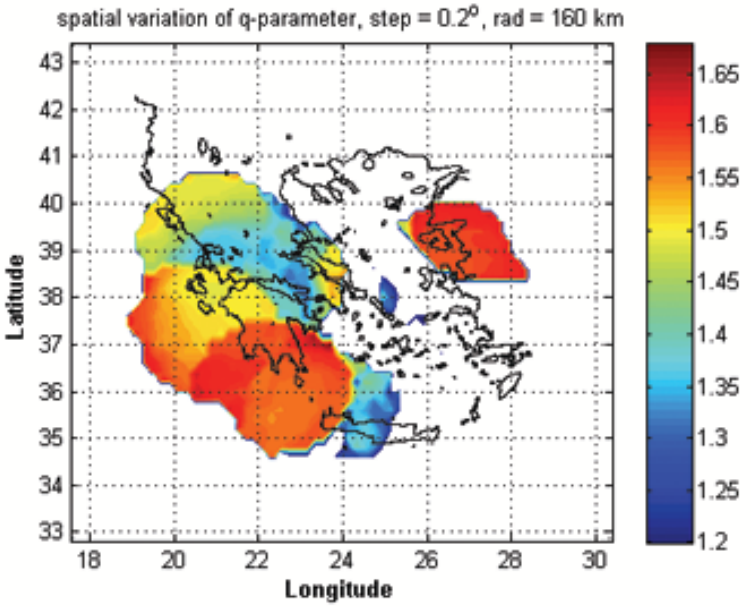

(a) Before Izmit EQ

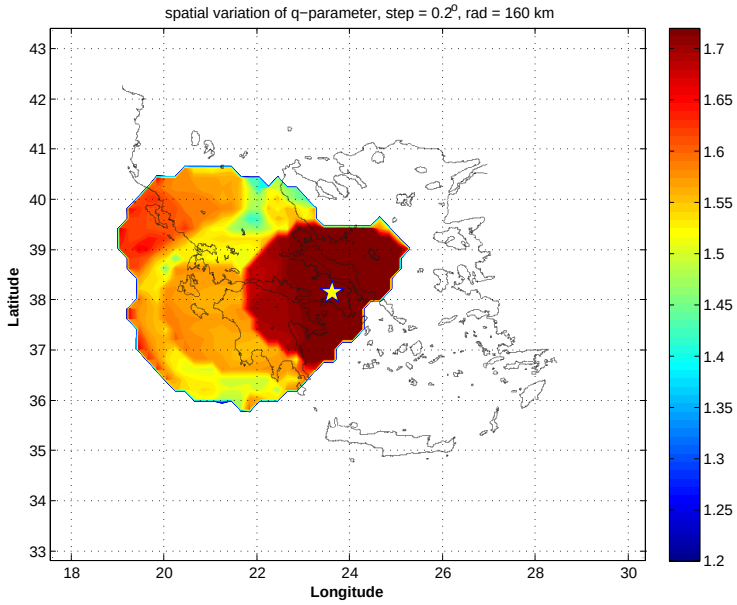

(b) After Izmit EQ with Ath. EQ

Figure 3.4: Spatial distribution of q-parameter for the periods (a) before and (b) after the occurrence of Izmit EQ but with Athens EQ included. The star-marks indicate the EQs with magnitude larger than or equal to $5.0M_L$. The colored bar indicates the range of variation of the q-parameter.

The aforementioned results provide a first indication that increased correlations were mainly developed around the Athens EQ, namely, after the occurrence of Izmit EQ. Thus in the following section analysis is focused on the regional seismicity around the Athens EQ epicenter in the prospect to further ensure this suggestion.

3.3.1 Focusing on the regional seismicity around the Athens EQ epicenter

In the prospect to further test the validity of the results obtained in previous section, analysis here is focused on the regional seismicity around the Athens EQ epicenter. Two different geographic areas were mainly selected for the analysis: (i) *within a circular area of 0-160 km around the Athens EQ epicenter*, and (ii) *within a circular ring from 160-400 km away from the Athens EQ epicenter*. Eq. (2) was used to fit the seismic data on the relative cumulative number of EQ magnitudes $G(> M)$, for the periods before and after the Izmit EQ. Fig. 3.5 shows that Eq. (2), along with use of the LM method, provides an excellent fit to the relative cumulative number of EQs contained in both geographic areas, with a standard error ranging between the interval $[0.003 - 0.006]$.

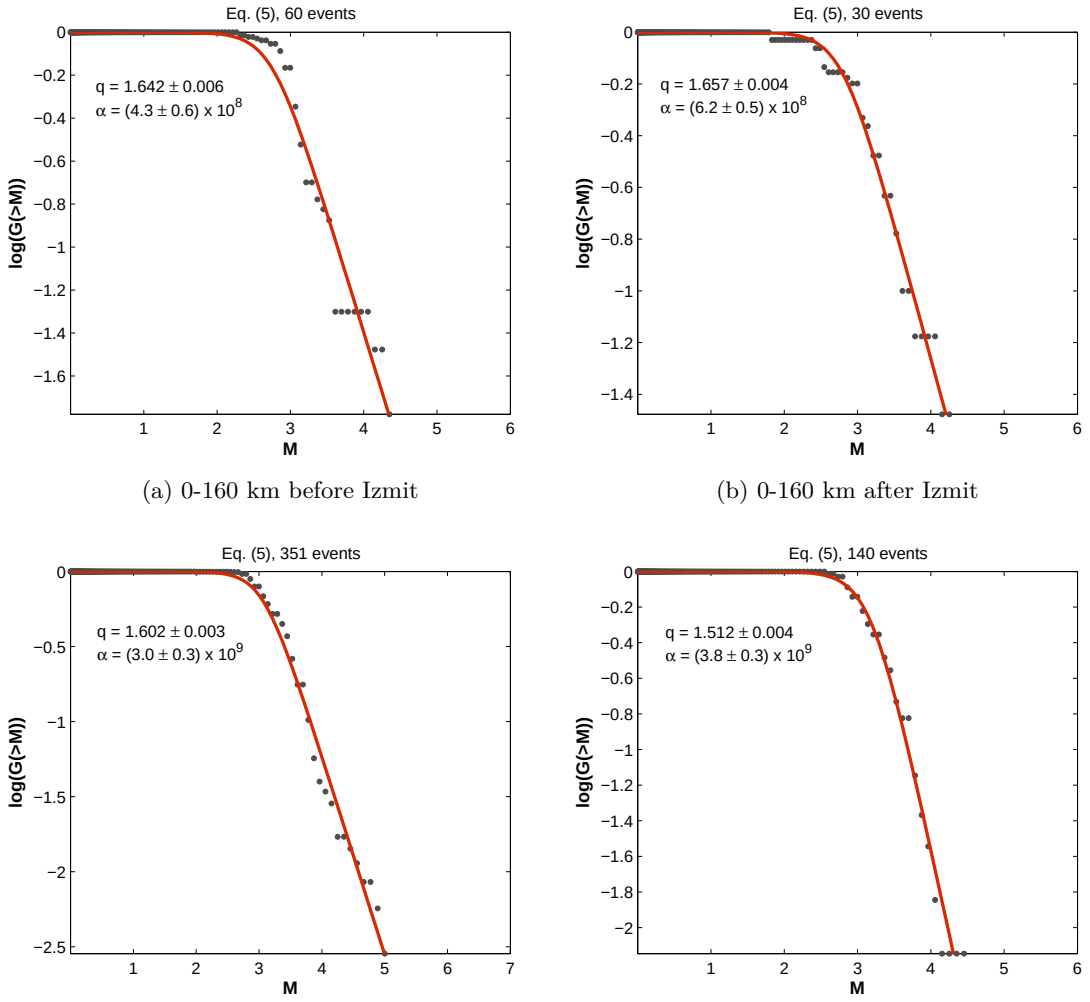

(a) 0-160 km before Izmit

(b) 0-160 km after Izmit

(c) $160 - 400$ km before Izmit

(d) $160 - 400$ km After Izmit

Figure 3.5: Eq. (2) was used to fit the seismic data in terms of the relative cumulative number of EQs included in the area, (0-160) km around Athens EQ epicenter and (160-400) km away from Athens EQ epicenter: (a,c) for the period before Izmit EQ and (b,d) for the period after Izmit EQ.

It is observed that both periods under study which refer to the range of 0-160km (see Figs. 3.5a and 3.5b, respectively), present higher q-parameters in contrast to the period before the Izmit EQ. However, the highest q-parameter is observed in Fig. 3.5b, with $q = 1.657 \pm 0.004$, which refers to the period after the occurrence of the Izmit EQ. On the contrary, focusing on the area between 160-400 km, a reduction in the nonextensive q-parameter, for the period after the Izmit EQ is observed (see Figs. 3.5c and 3.5d, respectively). The latter observations are consistent with those obtained in previous section, supporting the statement that, after the occurrence of the Izmit EQ, markedly higher nonextensivity was sustained around the near-Athens EQ epicenter. Herein, it should be noted that the analysis in this work mainly compares the seismicity for the periods before and after the Izmit EQ, focusing on the seismicity associated with the behaviour of a single fault (mainly 160km around the Athens EQ location). The range of 160-400km is mainly used for comparison reasons. There is a significant difference on the event-populations between these two geographic areas mainly for the period before the Izmit EQ, that someone could consider that should have any effect on the results. It should be stated that this difference of the number of EQs between the two geographic areas under study, is an evidence that characterizes the phenomenon itself. Thus, if the number of EQ was different then the results would come up with different values of q parameter indicating a different phenomenon.

The relation between the nonextensive q-parameter and the b-value associated with the G-R formula (Eq. 1) has been given by Sarlis et al. [202] (see Eq. 3). In Fig. 3.6 the blue line, depicts this theoretical relationship, indicating that the higher the nonextensivity, the lower the associated b-value. Note that the lower b-values express the increase of accumulated stresses in the region under study. Thus, the analysis that follows, examines whether the increased accumulated stresses and the shift to higher nonextensivity around the Athens EQ epicenter are combined with a higher degree of organization of the corresponding regional seismicity.

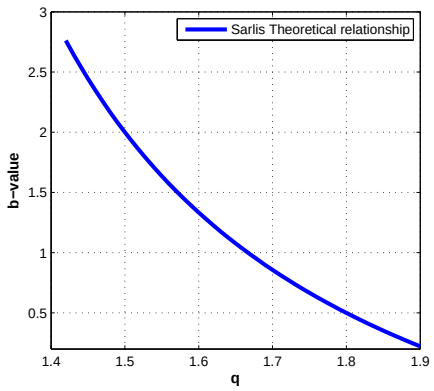

Figure 3.6: Scatter plot of the theoretical relationship between the b-value and q-parameter as derives from Sarlis Eq. (3)

At this point of analysis, it should be noticed that the parameter q itself is not a measure of the complexity-organization of the system but only a measure of the degree of nonextensivity

[117]. The dynamic changes of the complexity of the system can be quantified by applying the Tsallis entropy equation (S_q) to the time variation of a given signal having a given nonextensive parameter q [117]. However, Tsallis entropy requires a sufficient number of samples and stationarity of the data in the sample, conditions that are not fulfilled in the case of seismicity. On the contrary, Fisher information [72, 14, 237], does not have such requirements, since it has been accepted as a powerful tool for the investigation of complex and non-stationary signals. The theoretical content of Fisher Information is that where the entropy decreases, the Fisher information increases. Moreover, unlike entropy, Fisher Information is sensitive to changes in the shape of the probability distribution corresponding to the measured variable [188, and references therein]. Fig. 3.7, depicts the calculated Fisher information applied to the time intervals between EQs, for the two aforementioned periods under study. The results indicate a significant increment of organization in the range 0-160km after the occurrence of the Izmit EQ.

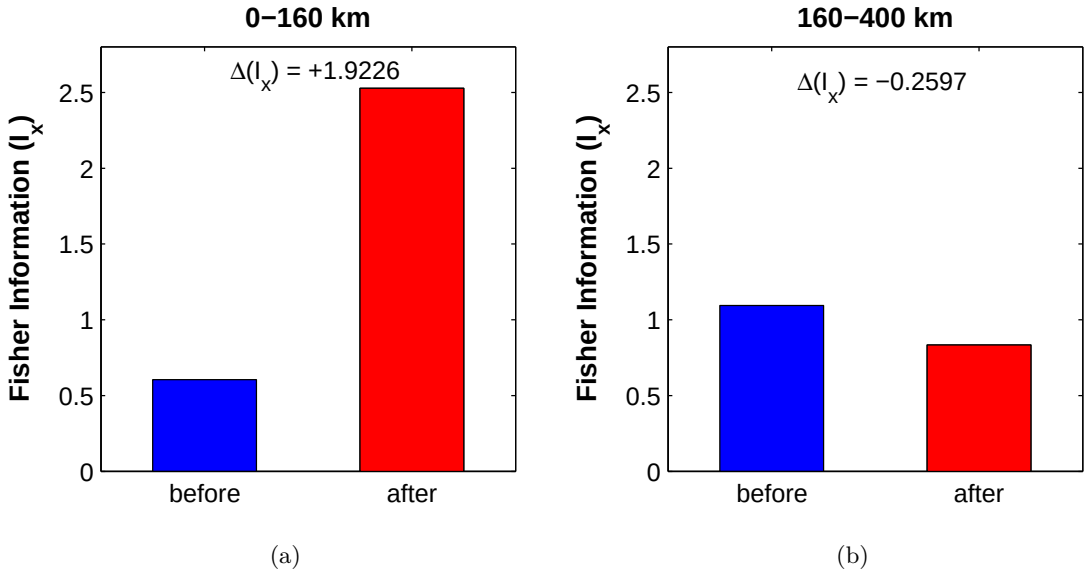

(a) (b)

Figure 3.7: Fisher information applied to the time intervals between EQs: (a) within the range 0-160 km around the Athens EQ epicenter; (b) within the range 160-400 km away from the Athens EQ epicenter. The parameter $\Delta(I_x)$ indicates the differences in the calculated Fisher information between the periods under study, for (a) and (b) respectively.

Against this evidence, it is argued that this higher organization, along with the increased nonextensivity, may indicate the appearance of higher persistent behaviour of the overall area around the Athens epicenter EQ. In this direction, the following section is focused on the Rescaled Range Analysis (R/S), which seems to be a particular method for investigating this argument.

3.4 Evidence of persistent behaviour of the regional seismicity related to Athens EQ

The method for estimating the Hurst exponent H has been analytically described in Sec. 2.3. Thus briefly speaking, Hurst's [109] rescaled analysis has been used as a method to detect correlations and memory effects in a time series according to the following relation:

$$R/S = (\tau/2)^H, \tag{3.2}$$

where R is the difference between the maximum and minimum amounts of accumulated departure of the time series from the mean over a time span τ and S is the standard deviation calculated over the time span τ. The correlation of the past and the future in the observational time series can be described by the Hurst exponent H. For $H = 0.5$, there is an independent random process, with no correlations among samples. For $H > 0.5$, the sequence is characterized by a persistent behaviour, which means that the increasing or decreasing trend is more likely to be conserved, implying a positive feedback mechanism. For $H < 0.5$, the sequence is characterized by the anti-persistent behaviour, which means that an increasing or decreasing trend is more likely to be reversed, implying a negative feedback mechanism.

The calculation of the H-exponent has been proved very important issue for the understanding the EQ preparation process and the behaviour of seismic series [34, 271]. Studies on R/S analysis applied to earthquake series both in time and space evolution, suggest that this particular temporal occurrence of seismicity is a persistent process [145, 42, 271, 115]. Specifically, Xu et al. [271], who examined the earthquake occurrence density in time, found that the seismic frequency textures in all cases have Hurst index exceeding 0.70 suggesting long memory interactions. Moreover, it has been stated that the spatial roughness of fracture surfaces $H \simeq 0.7$ has been interpreted as a universal indicator of surface fracture, weakly dependent on the nature of the material and on the failure mode [146, 94, 186, 162, 272, and references therein].

Motivated by the theoretical framework of previous section, it is believed that R/S analysis is a particular case to enhance the suspicion that higher organization and nonextensivity are combined by the appearance of increased persistent behaviour. Using the same geographic areas and periods as those used in Sec. 3.3.1, the seismicity around the Athens EQ epicenter is examined here, by means of R/S analysis applied on the time intervals between time-neighbouring events as shown in Fig. 3.8. Specifically, Figs. 3.8a and 3.8b depict the Hurst exponents (H) for the two epochs under study for the range 0-160km around the Athens EQ epicenter. Figs. 3.8c and 3.8d, depict the same analysis for the range 160-400km away

from the Athens EQ epicenter. It is observed that both geographic areas are characterised by persistent behaviour ($H > 0.5$) for both periods under study, with an H index varying between $H \in [0.61, 0.77]$. However, the period after the Izmit EQ is characterized by significantly higher persistent behaviour, with H-values of 0.77 ± 0.11 for the area 0-160km compared to 0.73 ± 0.14 for the area 160-400km. The highest H-exponent is observed in the area of 160km around the Athens EQ epicenter (Fig. 3.8b).

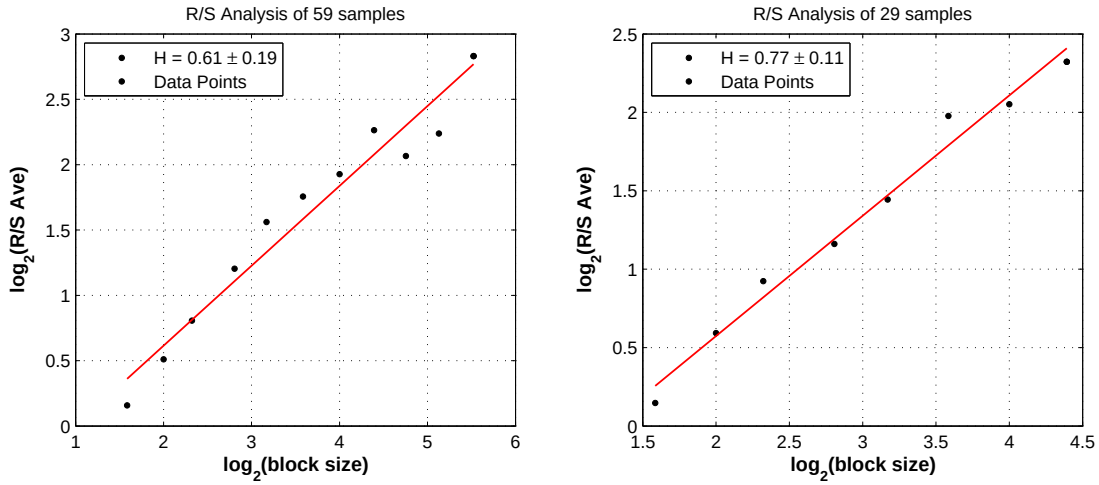

(a) 0-160 km before Izmit

(b) 0-160 km after Izmit

(c) 160-400 km before Izmit

(d) 160-400 km after Izmit

Figure 3.8: R/S analysis of time intervals (0-160) km around Athens EQ epicenter and (160-400) km away from Athens EQ epicenter; (a,c) for the period before Izmit EQ and (b,d) for the period after Izmit EQ.

Summarising at this point analysis, after the occurrence of the Izmit EQ, higher nonextensivity, higher organization and higher persistent behaviour were developed mainly within the area $\approx 160km$ around the Athens EQ epicenter. The latter footprint has been further justified in Chapter 2, for the second epoch that includes the two strong EM bursts of preseismic kHz

EM activity related to Athens EQ. Thus, an interesting issue here would be to examine whether the whole sequence of preseismic kHz EM emissions that have been characterized as a fracture process (fragment-asperity interaction) observed prior to Athens EQ, can also be described by the nonextensive Eq. (2). Expecting to find similar q-parameters with those obtained from seismicity the following section focuses on this suggestion.

3.5 Linking the kHz electromagnetic activity with seismicity

In chapter 2, by giving the definition of the "fracto-electromagnetic earthquake" (EM-EQ) (see Sec. 2.4, Eq. 2.15), it was shown that the nonextensive Eq. (2), can adequately describe the EM-EQs included in the two distinctive identified epochs of kHz EM activity observed prior to Athens EQ. In this section, for the first time, all the six observed magnetic fields recorded by the 3 kHz (NS, EW and V) and 10 kHz (NS, EW and V) sensors, are analysed in the framework of nonextensivity, and the seismicity occurred within the same time period. More precisely, analysis is focused on whether the whole sequence of EM-EQs included in the two identified epochs of preseismic kHz EM time-series can also be described by Eq. (2). Should this case exists, it is expected that similar q-values should characterize the seismicity occurred within that period on one hand and such analysis will further verify the results obtained in chapter 2. These signals can be observed in Fig. 3.9, where the top charts in each one of the depicted subfigures, show the six observed magnetic fields recorded on the period from 28-Aug-1999 00:00:00 to 08-Sep-1999 00:00:00. The red parts refer to the period where the kHz EM anomalies observed and have been well justified for their seismogenic origin [123, 36, 40, 172].

Against the latter arguments, Eq. (2) was used to fit the EM data in terms of the relative cumulative number of electromagnetic earthquakes $G(> M)$, included in the period that refers to the red part of these signals. The results are depicted in the bottom charts, included in Fig. 3.9. It is observed that Eq. (2) provides an excellent fit to the preseismic kHz EM experimental data associated with the Athens EQ for all six recorded components, revealing the characteristics of nonextensivity statistics of the distribution of the detected precursory EM-EQs. Here, N is the total number of the detected EM-EQs, $N(M >)$ the number of EM-EQs, with magnitude larger than M, $G(> M) = N(M >)/N$ the relative cumulative number of EM-EQs with magnitude larger than M, and α the constant of proportionality between the EM energy released and the size of the fragment r [208]. It is observed that the resulting q-values lie within the interval $q \in [1.78 - 1.82]$ for all the recorded channels. It should be noted that these calculated nonextensive q-parameters are in general agreement with those obtained from several independent studies, related to seismicities generated in various large geographic areas, in the

context of Tsallis nonextensive framework [208, 267, 229, 228, 230, 155]. Characteristically, Telesca [228], found a value of ($q = 1.74$) for the preseismic activity of the L'Aquila EQ. These findings reveal that the higher levels of the nonextensive q-parameter could be considered as a universal footprint of fracture and faulting. On these grounds, analysis further focuses on seismicity included in the period where the kHz EM emissions observed, in the prospect to make a concurrent-comparative analysis between the two different data sets.

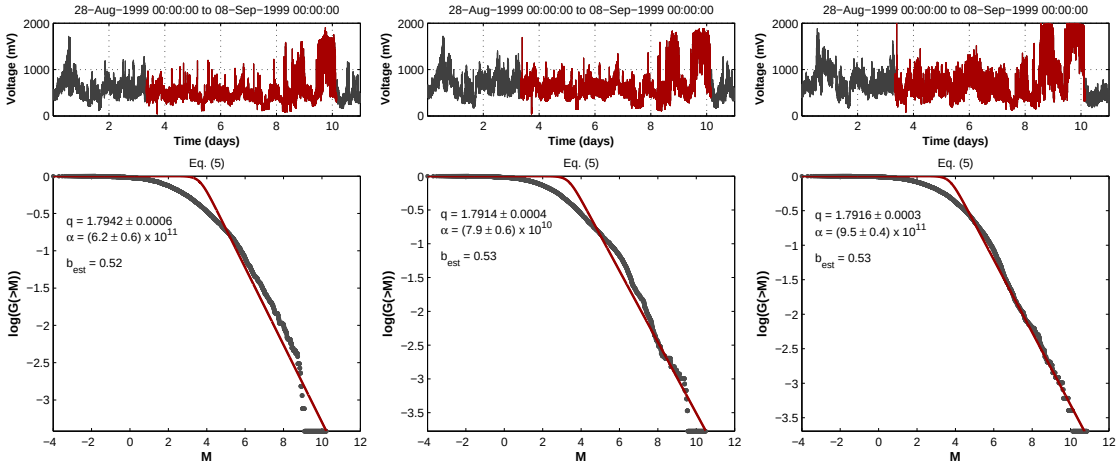

(a) 3 kHz NS (b) 3 kHZ EW (c) 3 kHz V

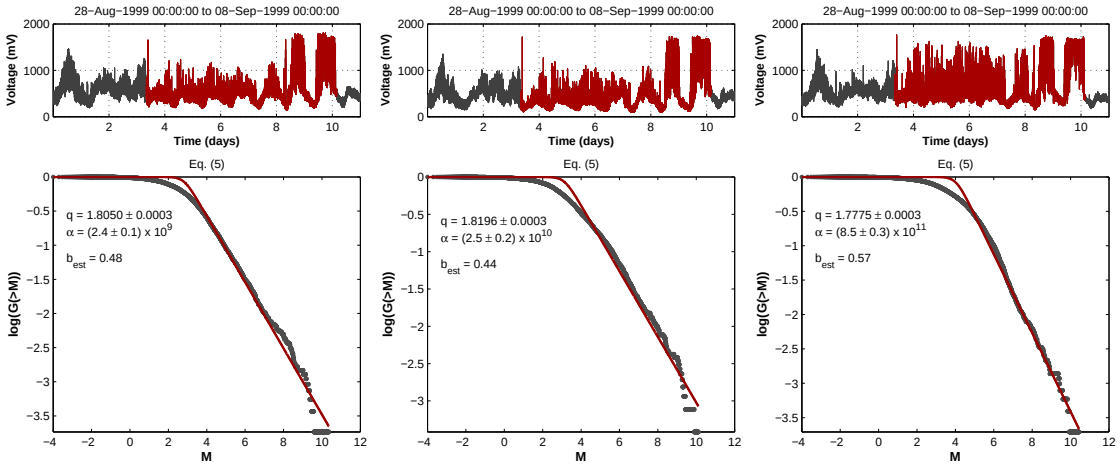

(d) 10 kHz NS (e) 10 kHz EW (f) 10 kHz V

Figure 3.9: Six observed magnetic fields recorded on the period from 28-Aug-1999 00:00:00 to 08-Sep-1999 00:00:00. The selected red parts of each recorded signal refer to the period where the kHz EM anomalies observed and have been well justified for their seismogenic origin [123, 36, 40, 172]. The bottom charts of each subfigure, refer to the fitting of the EM data in terms of the relative cumulative number of electromagnetic earthquakes $G(> M)$ (see Eq. (2)), included in the observed period (red-part) prior to Athens EQ.

Focusing on the seismicity, Eq. (2) was used to fit the relative cumulative number of EQ magnitudes $G(> M)$, occurred in the period from when the kHz EM emission started, up to the occurrence of the Athens EQ. However, due to the fact that the time-frame was very short

with limited number of EQs, analysis was focused on two different regions around the Athens EQ epicenter in the prospect to avoid possible inconsistencies. Thus the selected regions refer to 160km and 200km around the Athens EQ epicenter. The fittings are depicted in Fig. 3.10.

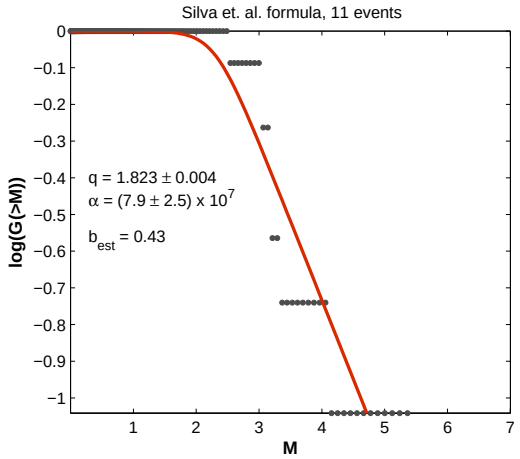

(a) 0-160 with EQ

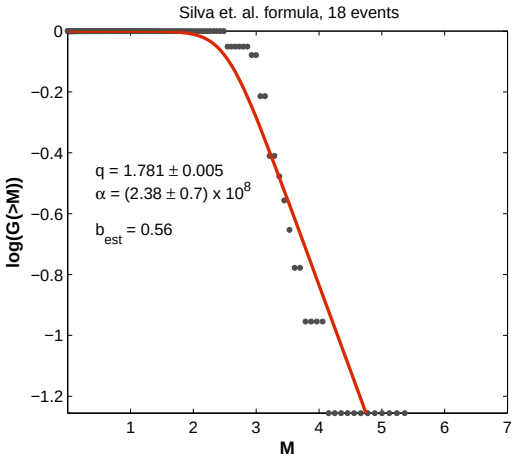

(b) 0-200 with EQ

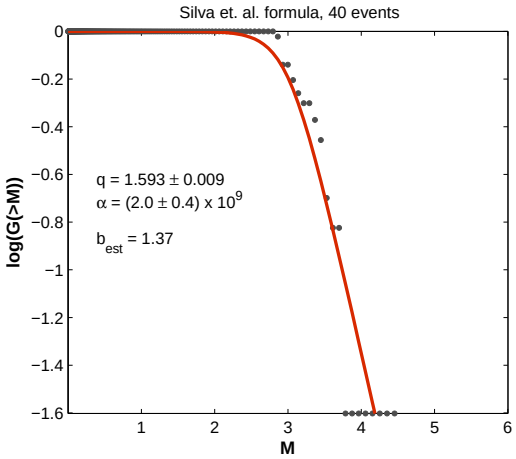

(c) 160-400

Figure 3.10: Eq. (2) was used to fit the seismic data in terms of the relative cumulative number of EQ magnitudes $G(> M)$, included in the period where the kHz EM emission started, up to the occurrence of the Athens EQ.

Specifically, from Figs. 3.10a and 3.10b, it is observed that the highest q-parameter is that of the region 0-160 km around the Athens EQ epicenter, but also the area of 0-200km presents high q-value. Note that similar results have been obtained in Fig. 3.5b that refers to the period after the Izmit EQ. In addition, the calculated values of $q = 1.823 \pm 0.004$ (Fig. 3.10a) and $q = 1.781 \pm 0.005$ (Fig. 3.10b) are consistent with the q-parameters derived from the analysis of the preseismic kHz EM emissions (see Fig. 3.9), which vary between $1.78 \sim 1.82$. On the contrary, the seismicity within the geographic area of 160-400 km (Fig. 3.10c), is characterized

by a relatively lower q-parameter (1.593 ± 0.009), similar to Fig. 3.5d which refers to the area of (> 160)km away from Athens EQ.

Finally, focusing on the b-values related to the theoretical background of the Gutenberg & Richter formula, the estimated b-values as derived from Sarlis Eq. (3), depicted in Figs. 3.10a and 3.10b from seismicity, are consistent with those obtained from the analysis of kHz EM activity depicted in Fig. 3.9, with $b_{est} \in [0.44 - 0.57]$. In addition, the b-values obtained from the analysis in terms of traditional empirical G-R law (Eq. (1)), were found to be $b = 0.43 \pm 0.15$ for the seismicity contained 0-160 km around the Athens EQ epicenter and $b = 0.56 \pm 0.17$ for the range 0-200 km, respectively. A graphical representation of this consistency is depicted in Fig. 3.11. The different red marks indicate the b-values calculated directly from G-R Eq. (1), corresponding to the q-values calculated in Fig. 3.5. It is observed that both of the b-values calculated in this way are consistent with Eq. (3).

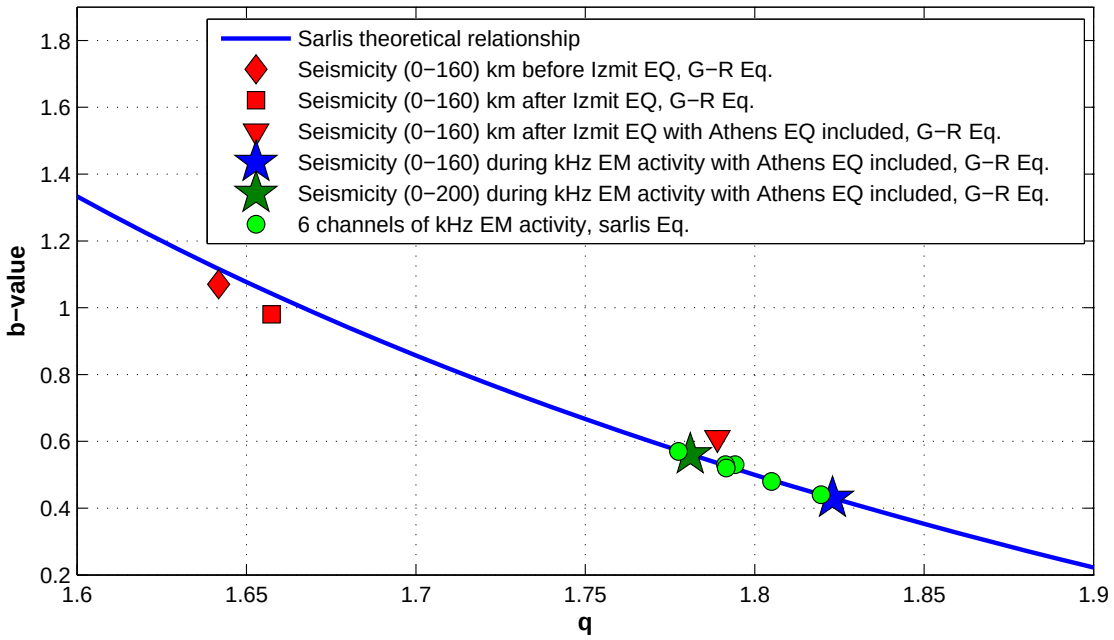

Figure 3.11: Scatter plot of the calculated relationship between the b-value and q-parameter. The blue line indicates the theoretical relationship between the b-value and q-parameter, Eq. (3). The red marks depict the b-values calculated by Eq. (1) (G-R formula) for the already calculated q-values through fitting of Eq. (2), for the periods before and after the occurrence Izmit EQ. The green circles refer to the nonextensive analysis of preseismic kHz EM emissions in Sec. 3.5, while the green and blue stars refers to the seismicity of that period.

The latter results evidently reveal the way in which the preseismic kHz EM activity is mirrored in the seismicity of that period with similar nonextensive q-values. Drawing from the fractal nature of fracture and faulting, Huang and Turcotte [108] suggested that the statistics

of regional seismicity could be merely a macroscopic reflection of the physical processes in the EQ source. The analysis presented here strongly supports this suggestion. In addition, previous studies along with the analysis in Chapter 2, have also verified the high persistent behaviour and high organization levels of these signals [123, 117].

3.6 Precursory evidence from different disciplines: the case of Athens EQ

It is recalled that Athens EQ arrived very shortly after the major 17/8/1999, $Mw = 7.4$, EQ of Izmit, Turkey, which occurred approximately 650 km North-East of Athens. According to the literature, several precursory symptoms from different disciplines have been provided all related to the specific EQ. This section mainly summarizes these precursory symptoms, in view of the sequence that have been reported, as follows:

(i) Focusing on seismicity, Tzanis et al. (2002) [251], reported precursory power-law-type acceleration of the seismic energy release, in which the apparent onset of power-law behaviour began approximately 20 days before the Athens EQ. The authors suggested that the Athens EQ may have been hastened by long range interaction with the Izmit event. Additionally, Papadopoulos (2002) [173], provided historical, stochastic and geophysical evidence, suggesting that the Athens EQ was likely advanced in time: the possible acceleration of the failure process of Athens EQ, caused by remote stress changes associated with the Izmit large EQ.

(ii) Varotsos et al. [261] have reported a series of Ultra-Low-Frequency(ULF) seismic electric signals (SES - VAN signals) on September 1-2, 1999 recorded from Lamia (Central Greece) station with duration ~ 9 hours, with the following peculiarity: this lasts several hours, but its last portion has a larger amplitude and also changes polarity. However, there still remains a problem of explaining a VLF wave propagation from ~ 10 km depth to the surface. One of the possible mechanisms is the effective radiation in the inhomogeneous crust using fractal geoantenna [58].

(iii) A sequence of MHz EM anomalies were simultaneously recorded at 41, 54, and 135 MHz on August 29, 1999 [62, 36]. According to the two-stage model described in Sec. 1.2.1.1, these anomalies can be attributed to a phase transition of second order.

(iv) Filizzola et al. [71] reported that clear TIR * signals over the area around the Athens EQ epicentre have been detected from satellites during the last days prior to the Athens

*Earth's thermally emitted radiation measured from satellite in the Thermal Infrared (8Ű14 lm) spectral range is usually referred to as TIR signal and given in units of brightness temperature (BT).

EQ. More specifically they mentioned that after the 28-Aug-1999, a progressive increase (in extension and intensity) of the area affected by over-threshold pixels started, reaching its maximum on 05-Sep-1999 (i.e. two days before the earthquake) and progressively dissipated after the event. As it has been stated by the literature related to the specific EQ, the appearance of TIR emissions indicates the possibility that the fracture process has been extended up to the surface layers of the crust [54].

(v) The sequence of two strong kHz EM anomalies (bursts) analysed in chapter 2, were simultaneously recorded from both 3 and 10 kHz components (antennas) before the occurrence of the main EQ [63, 61, 58, 123, 122, 172]. More precisely, the first one had 12 hours duration followed by a cease of 9 hours and the second one had 17 hours duration which ceased about 9 hours before the main EQ. According to the two-stage model described in Sec. 1.2.1.2, these anomalies can be attributed to the last stage of the EQ generation process, namely the breakage of the asperities between the two profiles (fault planes).

(vi) In a pioneer study based on information obtained by radar interferometry (ERS-2 satellite) [129] for the case of Athens EQ, the authors suggest the following modeling scheme that predicts two faults: the main fault segment is responsible for 80% of the total energy released, with the secondary fault segment for the remaining 20%. In addition, Kikuchi [127] who studied the seismic data of that period using standard methodology, mentioned that a two-event solution for the Athens EQ is more likely than a single event solution since there was a subsequent ($M = 5.5$) EQ after about $3.5s$ of the main EQ ($M = 5.8$). Moreover, concerning the two strong impulsive kHz EM bursts emerged in the tail of the preseismic kHz EM emission, it has been found that the first one contains approximately 20% of the total EM energy received while the second one the remaining of 80% [61].

The latter evidence along with the results of this study strongly verify that the underlying kHz EM emissions analysed in this chapter, are related to Athens EQ. Even more, the time interval between the Turkish EQ and Greek EQ, the common persistent and nonextensive behaviour, the higher organisation and the increased accumulated stresses developed around the Athens EQ epicenter indirectly support the hypothesis of this study: that the large amplitude dynamic strain of the surface waves was responsible for triggering the regional seismicity.

3.7 Discussion & Conclusions

Laboratory studies have shown that during a fracture, the breaking of a bond launches a propagating stress wave which may trigger the breaking of other bonds [134]. Analysis in this chapter examined whether this suggestion holds on a geophysical scale as well. The possibility that the transient stresses of the seismic waves of a major EQ can trigger a considerably distant significant EQ at a later time was examined, in terms of a nonextensive model for EQ dynamics. The analysis was mainly focused on a major catastrophic EQ (M=5.4ML) occurred in the metropolitan area of Athens (Greece) on 7-Sep-1999. The EQ arrived very shortly after the major 17-Aug-1999, $Mw = 7.4$, EQ of Izmit, Turkey, which occurred approximately 650 km North-East of Athens.

Focusing on seismicity of that period, it was found that before the major Turkish event, the seismicity in the wider Greek area presented increased nonextensivity centered on central and western Greece. On the contrary, after the Turkish event, the higher nonextensivity was shifted towards the central Greece around the metropolitan area of Athens, with even higher values of the nonextensive q-parameter. Moreover, analysis in terms of Fisher information on the one hand and the Hurst exponent, applied to inter-event times, on the other, revealed that higher levels of organization and higher persistent behaviour were developed mainly around the ensuing EQ epicenter. Against this evidence the present work provided a first indication in terms of nonextensive statistics that the transient stresses of the seismic waves of a major EQ can trigger a considerably distant significant EQ.

In the prospect to link the associated precursory kHz EM activity observed at that period with the last stage of the ensuing EQ generation, analysis examined whether the statistics of regional seismicity could be merely a macroscopic reflection of the physical processes in the EQ source as has been suggested by Huang and Turcote [108]. Indeed, the analysis revealed that the sequence of electromagnetic EQs (EM-EQs) contained in the preseismic kHz EM signal emitted before the impending EQ, also follow the theoretical approach of the nonextensive model for EQ dynamics, providing similar q-parameters with those derived from seismicity. On these grounds, the present work suggests that such similarity indicates that these preseismic kHz EM signals originate from the EQ preparation process. Thus the activation of a fault could be considered as a reduced self-affine image of the regional seismicity. This suggestion is further examined in Chapter 4 from the perspective of self-affinity.

Chapter 4

Identifying the self-affine nature of fracture and faulting

The aspect of self-affine nature of faulting and fracture has been widely documented from the data analysis of both field observations and laboratory experiments [149, 108, 248, 213, 163]. Characteristically, Huang and Turcotte (1998) [108], have stated that *"the statistics of regional seismicity could be merely a macroscopic reflection of the physical processes in earthquake source"*. This suggestion, from the perspective of self-affinity, implies that the activation of a single fault is a reduced self-affine image of regional seismicity. In this direction, the present chapter deals with this suggestion focusing on both the regional seismicity around the epicenter of a significant event and the preseismic kHz EM emissions which have been well justified for their seismogenic origin. In the prospect to enhance the physical background of the underlying self-affinity, analysis is mainly performed by means of a recently introduced nonextensive model for earthquake dynamics [218, 208], which leads to a Gutenberg-Richter (G-R) type law and is routed on the nonextensive Tsallis statistical approach [245, 246, 247]. Since the latter model has been analytically described in Sec. 2.1.3, shortly speaking, its theoretical ingredient concerns two rough profiles interacting via the fragments filling the gap between them. The model leads to a nonextensive G-R type formula that describes the frequency distribution of earthquakes (EQs) against magnitude including two parameters: (i) the entropic index q, which describes the deviation of Tsallis entropy from the standard Boltzmann-Gibbs entropy, and (ii) the physical quantity α, which is a constant of proportionality between the energy released during the fracture of a fragment and its size r.

In the prospect to capture the underlying self-affinity in terms of nonextensive dynamics, a suggested framework would be to focus on two different scales of populations of fracture events, as follows:

(i) *The fractures-EQs that precede a significant seismic event occurring in the region which surrounds its epicenter (foreshock activity).*

(ii) *The fractures of strong entities which are distributed along the single activated significant fault sustaining the system.*

In the following section arguments that support this framework of analysis are analytically presented.

4.1 Overview: setting the context for the analysis

A crucial question that is aptly emerged according to the latter proposed framework, is: *"How can we know the sequence of magnitudes of fractures of strong entities which are evolved during the activation of a significant fault?"*.

Confronted with such a question, it has been stated that crack propagation is the basic mechanism of material failure [59]. Additionally, it has been shown that during the mechanical loading, fracture induced acoustic and electromagnetic (EM) fields have been observed, mainly produced by opening cracks, in a wide frequency spectrum ranging from kHz to MHz. These precursors, have been detected at both laboratory [11, 165, 166, 144, 171, 74, 156, 77, 135, 10] and geophysical scale [269, 81, 99, 98, 63, 61, 100, 164, 60, 62, 58, 123, 36, 124, 66, 172, 117, 40, 55, 53, 191, 73, 82, 161], including those under study, which in turn have been considered as the so-called precursors of general fracture.

An important feature that has already mentioned in literature and has been observed at both scales, is that the MHz radiation precedes the kHz one [60, 58, 123, 36, 55, 56]. Drawing from the two-stage model described analytically in Sec. 1.2.1, the MHz EM emission is due to the fracture of the highly heterogeneous system that surrounds the fault, attributed to a phase transition of second order [36], while a Levy walk type mechanism can explain the observed critical state [40]. It should be noticed that the heterogeneity and long-range correlations are two of the key features of material failure, providing an appropriate framework for their study in terms of statistical mechanics. In addition, several authors have suggested that ruptures of heterogeneous systems is a critical phenomenon (indicatively see [6, 33, 104, 217, 137, 7, 210, 7, 213, 80]). Continuing with the two stage model, the kHz EM phenomenon/emission, refers to the final stage of EQ generation, that reflects the fracture of backbone of entities that prohibit the relative slipping of the two profiles of the fault [123, 36, 117, 172, 55]. Moreover, analysis in chapter 2, has shown that the aforementioned nonextensive G-R type formula can adequately describe the "fracto-electromagnetic earthquakes" (EM-EQs) included in the

preseismic kHz electromagnetic (EM) emissions observed prior to large EQs. More precisely, using two models for earthquake dynamics it has been shown that the kHz EM emissions refer to the last stage of a single EQ generation and not on the statistics of a population of different EQs, representing the population of fractures that occur during the relative displacement of fault plates. Characteristically, studies on the small (laboratory) scale have shown that the kHz EM emission is launched in the tail of pre-fracture EM emission from 97% up to 100% of the corresponding failure strength [60, and references therein]. At the geophysical scale the kHz EM precursors are also emerged in the tail of preseismic EM emission, namely, from a few days up to a few hours before the EQ occurrence [123]. Thus, the association of MHz, kHz EM precursors with the last stages of EQ generation seems to be justified on one hand, with the kHz EM emissions representing the population of fractures that occur during the relative displacement of fault plates on the other hand.

It should be noted that the aforementioned proposal has been partly supported by a multi-disciplinary analysis, e.g., in terms of extensive and non extensive statistical physics [125, 172, 117, 40], information theory, complexity [124, 187], laboratory experiments [60, 66, 65], fault modeling [61], fractal electrodynamics [58], self-affinity in fracture and faulting [53], nonextensive model for earthquake dynamics [172], and mesomechanics [65]. More precisely, it has been shown that the strong impulsive kHz EM time series show strong persistent behaviour mirroring a non-equilibrium process without any footprint of an equilibrium thermal phase transition. Additionally, the fracture surfaces have been found to be self-affine following the persistent fractional Brownian motion (fBm) model over a wide range of length scales, while, the spatial roughness of fracture surfaces $H \simeq 0.7$ has been interpreted as a universal indicator of surface fracture, weakly dependent on the nature of the material and on the failure mode [146, 94, 186, 162, 272, and references therein]. Note that the latter footprint has been further justified in Chapter 2, for the second epoch of preseismic kHz EM activity.

Summarizing at this point, the present study attempts to provide evidence that the activation of a significant single fault (routed in the preseismic kHz EM emissions as argued above) is a reduced self-affine image of the regional seismicity, namely, the foreshock neighboring activity associated with the activation of the main fault. In this direction, analysis will be first focused on whether the aforementioned nonextensive G-R type formula can adequately describe both:

(i) the populations of EQs included in different radius around the epicenter of a significant seismic event (namely the foreshock activity).

(ii) the populations EM-EQs reflecting the fracture of strong entities distributed along the

main fault that sustain the system.

Secondly, the variation of parameters q and α included in the nonextensive formula for both populations using different thresholds of magnitudes will be examined in the prospect to find similar behaviour at all the aforementioned scales of fracturing. In this direction, two well documented cases that fulfil the needs of such analysis, with available data for both the seismicity and preseismic kHz EM emissions observed prior to large EQs, are: (i) the case of Athens EQ ($M = 5.9$) occurred on 07-Sep-1999, in Greece and (ii) the case of L'Aquila EQ ($M = 6.3$) occurred on 06-Apr-2009 in Italy.

Such analysis enhances the underlying self-affinity, suggesting that the activation of a single fault is a reduced self-affine image of regional seismicity. It also supports the hypothesis that the statistics of regional seismicity is a macroscopic reflection of the physical processes in the earthquake source as has been suggested by Hung and Turcotte [108].

4.2 A fragment-asperity model for earthquakes coming from a nonextensive Tsallis formulation

A nonextensive model for EQ dynamics consisting of two rough profiles interacting via fragments filling the gap has been recently introduced by Sotolongo-Costa and Posadas (SCP) [218]. The model has been analytically described in Sec. 2.1.3, while the related equations used in this Chapter can also be found in Sec 0.6.

Herein, the main target of this work is to verify the self-affine nature of fracture and faulting in the framework of nonextensive Tsallis statistics. However a still open question is whether the underlying self-affinity can be adequately explained by the nonextensive G-R type formula (Eq. (2)). Conformed with such question, it has been stated that the traditional G-R formula leads to the power-low distribution of magnitudes which in turn expresses the fractal nature of the system under study [203, 249, 200, 118, 30]. Several studies in a large variety of experiments [203, 249] and natural phenomena [249, 200, 118, 30], have reported that the fragment size distribution frequently exhibits a power law behavior, the origin of which is still unknown. Characteristically, Scholz [204] have reported several examples of power-law fragmentation indicating the fractal nature of such systems. On the other hand, Eq. (2) is directly connected to the traditional G-R law (Eq. 1), above some magnitude threshold through Eq. (3) [202, 227, 231]. Moreover, since the released energy ε is proportional to fragment size ($\varepsilon \propto r^3$) [208], it is reasonable to assume that the magnitudes of EQs which are rooted in the fracture of the population of fragments-asperities filling the space between fault planes, also follow a power-law distribution.

In the following sections the two aforementioned cases of strong EQs are examined, for both the seismicity and the observed preseismic kHz EM emissions.

4.3 The case of L'Aquila 2009 earthquake

The analysis here is focused on a recent catastrophic EQ occurred on 6 April 2009 in L'Aquila, Central Italy, at 01:32:39 UTC. The EQ was very shallow ($\approx 8km$) with magnitude Mw $= 6.3$. Focusing on studies related to seismicity of that period, Papadopoulos et al. [174], reported that from the beginning of 2006 up to the end of October 2008 no particular earthquake activation was noted in that seismogenic area. On the contrary, from 28-October-2008 up to 27-March-2009 the seismicity was in the state of weak foreshock activity, and dramatically increased 10 days prior the main event (from $\approx$ 26-Mar-2009) [174]. Drawing from this evidence, the period from 28-Oct-2008 00:00:00 up to 6-April-2009 01:32:00 (a few seconds before the mainshock) was selected as the most appropriate time-frame in order to examine the underlying self-affinity. The seismicity of that period is depicted in Fig. 4.1, 400 km around the epicenter of the L'Aquila EQ. The yellow star indicates the location of the mainshock. For the analysis, the Italian EQ catalogue which is available on the website of the *Istituto Nazionale di Geofisica e Vulcanologia* (INGV: `http://bollettinosismico.rm.ingv.it`), was used.

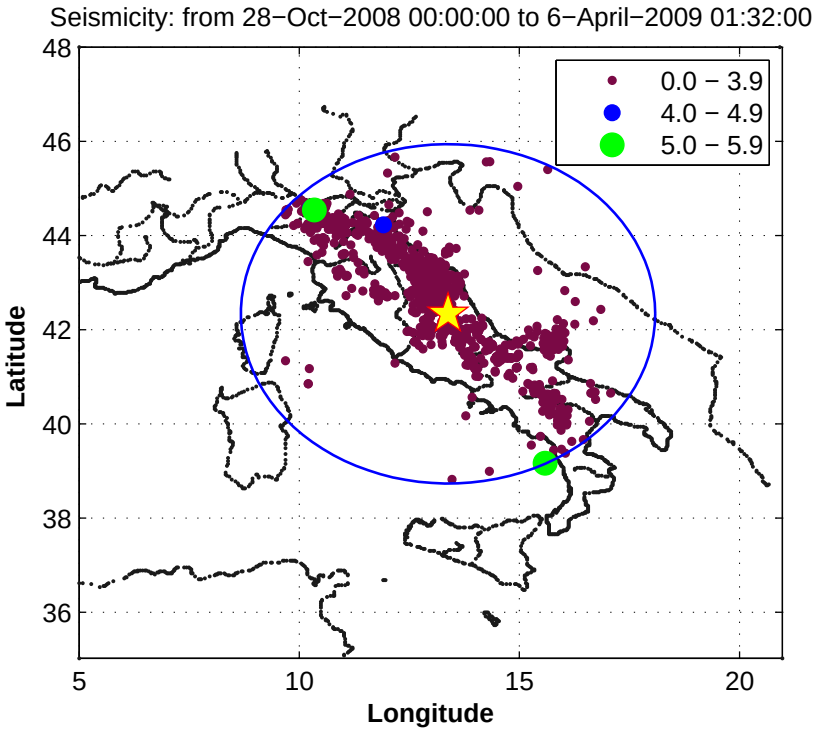

Figure 4.1: (a) Seismicity 400km around the L'Aquila EQ epicenter included in period from 28-Oct-2008 00:00:00 up to 6-April-2009 01:32:00. The colored bullets represent the magnitude ranges of the EQs occurred within the selected period under study.

Herein, analysis is first focused on seismicity in order to examine whether the nonextensive G-R type formula (Eq. (2)) can adequately describe the populations of EQs included within different radii around the epicenter of L'Aquila EQ. Should this case exist, the variation of the parameters included in Eq. (2) will be further examined. Thus firstly, Eq. (2) was used to fit the seismic data of six different selected geographic areas around the EQ epicenter, for the period under study: 0-400km, 0-300km, 0-200km, 0-100, 0-50km and 0-30km respectively. Fig. 4.2 shows the results of this process. Note that in order to achieve the optimal fitting, the Levenberg-Marquardt (LM) fitting method [142, 152] was used. From Fig. 4.2, we observe that Eq. (2) provides an excellent fit on the relative cumulative number of magnitudes ($G(>M)$) related to the populations of EQs included in each one of the six selected geographic areas. The nonextensive q-parameter varies between $[1.644 \sim 1.694]$ with a relative small standard error ranging between $[0.002 \sim 0.003]$.

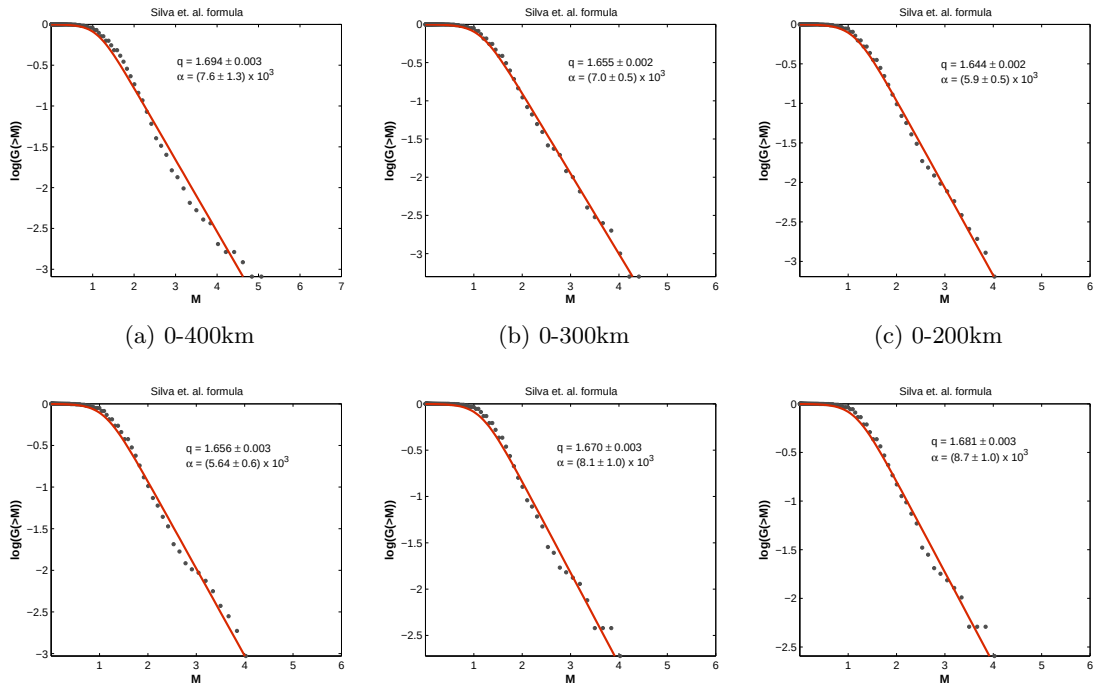

(a) 0-400km (b) 0-300km (c) 0-200km

(d) 0-100km (e) 0-50km (f) 0-30km

Figure 4.2: Eq. (2) was used to fit the foreshock seismic data in terms of the relative cumulative number of EQs included in six different geographic areas around the L'Aquila EQ epicenter. The yellow star indicates the location of the mainshock.

Secondly, in the prospect to examine the behaviour of parameters q and α included in the nonextensive formula, different thresholds of magnitudes cut-offs (M_c) were applied using an increasing step of 0.1. For each step, formula (2) along with the use of Levenberg-Marquardt (LM) fitting method, were used to fit the seismic data in terms of the relative cumulative number of EQs. A minimum number of 20 events was considered as a criterion for the

statistical completeness of each calculation. The derived parameters q and α, were graphically placed on to a common x-axis chart as shown in Fig. 4.3. It is observed that both the nonextensive q-parameter and the energy α, present similar behaviour, for all the selected geographic areas around the EQ epicenter. More specifically, the nonextensive parameter q (depicted with black bullets) remains relative stable with minor increment at intermediate thresholds of magnitudes ($M_c \approx 1.5 - 2.5$). On the contrary, the characteristic value of the volumetric energy density α (depicted with blue-rhombuses), increases at higher magnitude thresholds (M_c), reaching values in the order of $\approx 10^{10}$.

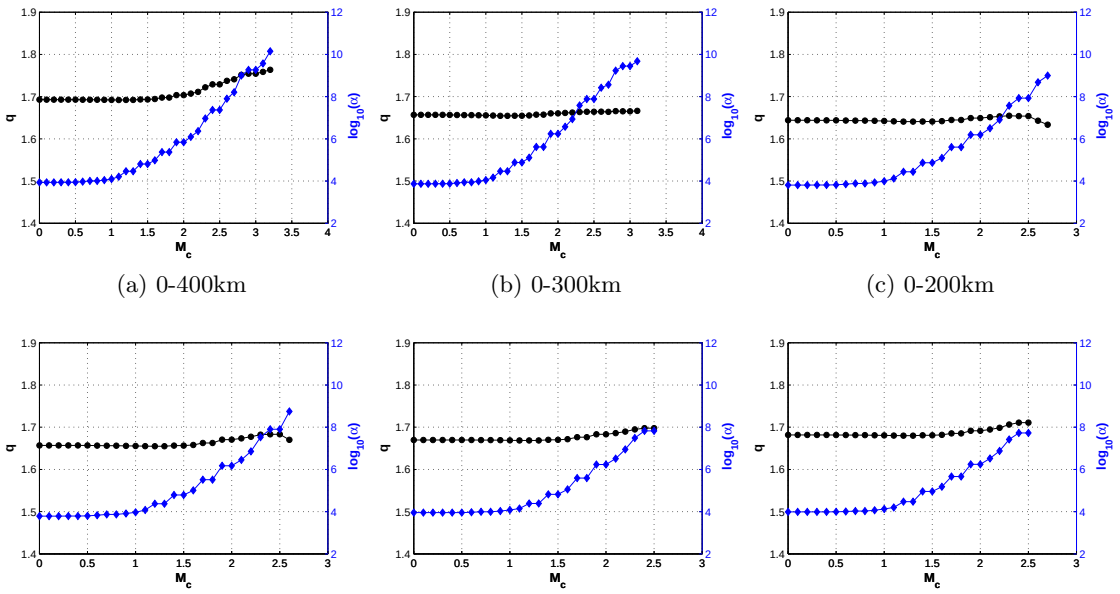

(a) 0-400km (b) 0-300km (c) 0-200km

(d) 0-100km (e) 0-50km (f) 0-30km

Figure 4.3: (a) Variation of nonextensive parameter q (see black-bullets) and the volumetric energy density α (see blue-rhombuses), for different thresholds of magnitudes of the detected EQs included in the period from 28-Oct-2008 00:00:00 up to 6-April-2009 01:32:00, for different geographic areas around the EQ epicenter: (a) 0-400km (b) 300km, (c) 0-200km (d) 0-100km (e) 0-50 and (f) 0-30km around the epicenter of L'Aquila EQ.

Since the analysis of seismicity at different geographic scales revealed similar footprints for both the parameters included in the nonextensive formula it is expected that similar behaviour should be observed at even lower scales of fracture, namely, the preseismic kHz EM anomalies observed prior to L'Aquila EQ. Thus, the analysis further focuses on the kHz EM emissions detected by the 10kHz (NS-EW-V) component, located at a mountainous site of Zante Island in the Ionian Sea (Western Greece). During the aforementioned 10-day foreshock activity, well documented [55, 56], preseismic kHz EM anomalies were observed on 4-Apr-2009, two days after the MHz EM anomalies of 2^{th} Apr, verifying the two-stage model described in the beginning of this chapter (see Sec. 4.1). The detected anomalies followed the temporal scheme

listed below:

(i) The MHz EM anomalies were detected on 26 March 2009 and 2 April 2009.

(ii) The kHz EM anomalies emerged on 4 April 2009.

(iii) The ULF EM anomaly was continuously recorded from 29 March 2009 up to 2 April 2009.

In Fig. 4.4, the three observed magnetic field strengths are depicted, recorded from the 10 kHz (NS,EW,V) sensors, on 4-Apr-2009. Note that the NS and EW components are analyzed here for the first time.

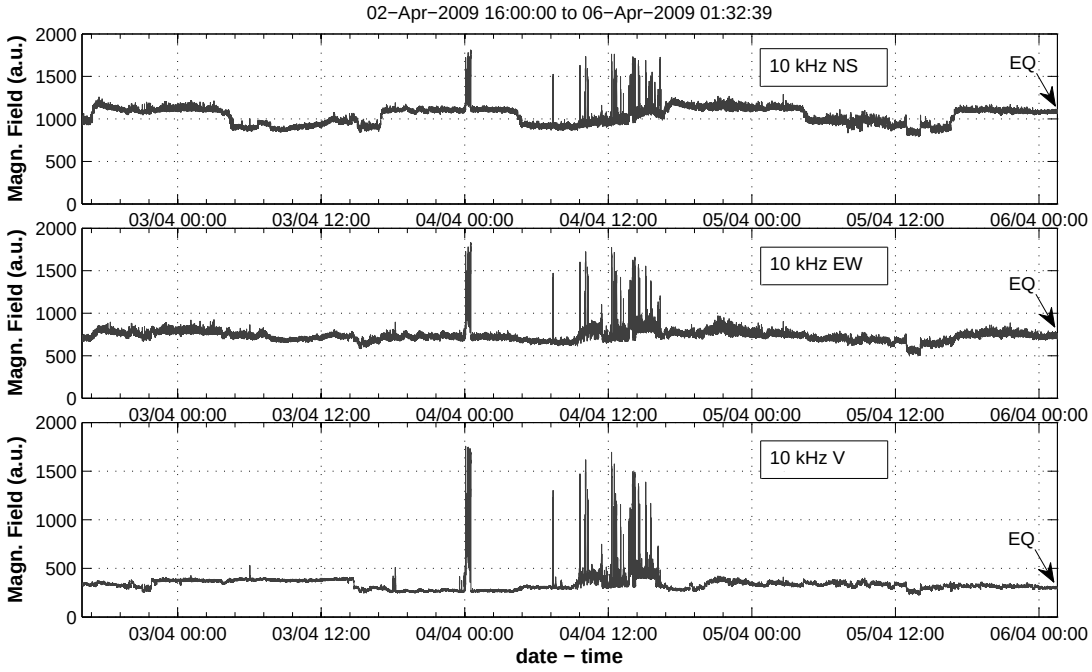

Figure 4.4: Three magnetic fields recorded on 02-Apr-2009 16:00:00 to 06-Apr-2009 01:32:39 from the 10 kHz NS,EW and V sensors respectively.

As in the case of seismicity, herein it is first examined whether the aforementioned nonextensive G-R type formula (Eq. (2)) can adequately describe the populations of EM-EQs included in the preseismic kHz EM time series. Thus Eq. (2) was used to fit the EM data in terms of the relative cumulative number of electromagnetic earthquakes $G(> M)$, included in the period that refers to the red part of the signals depicted in Fig. 4.5. Focusing on the intermediate subfigures ,it is observed that Eq. (2) provides a satisfactory fit to the preseismic kHz EM experimental data associated with the L'Aquila EQ for all the three recorded components correspondingly. Characteristically, the nonextensive q-parameter varies between $[1.818 \sim 1.838]$ with a relative small standard error ranging between $[0.001 \sim 0.002]$. Secondly, since Eq. 2, can adequately describe the populations of EM-EQs included in the preseismic kHz EM time

series, analysis is focused on the variation of nonextensive q-parameter the volumetric density α. Different thresholds of magnitude cut-offs (M_c) were applied on the EM-EQs contained in each one of the aforementioned channels using an increasing step of 0.1. For each step, Eq. (2) along with the use of LM method, was used to fit the EM data in terms of the relative cumulative number of EM-EQs contained in each channel. In Fig. 4.5, the bottom charts of each sub-figure, depict the variation of the nonextensive q-parameter (black bullets) and the volumetric energy density α (blue rhombuses), for different thresholds of magnitudes (M_c). As it is observed from the bottom charts of Fig. 4.5, the variation of the nonextensive q-parameter remains relative constant with minor decrement at higher thresholds of magnitudes. On the contrary, the energy density α mirrors the behaviour of q-parameter, presenting a relative increment at higher thresholds.

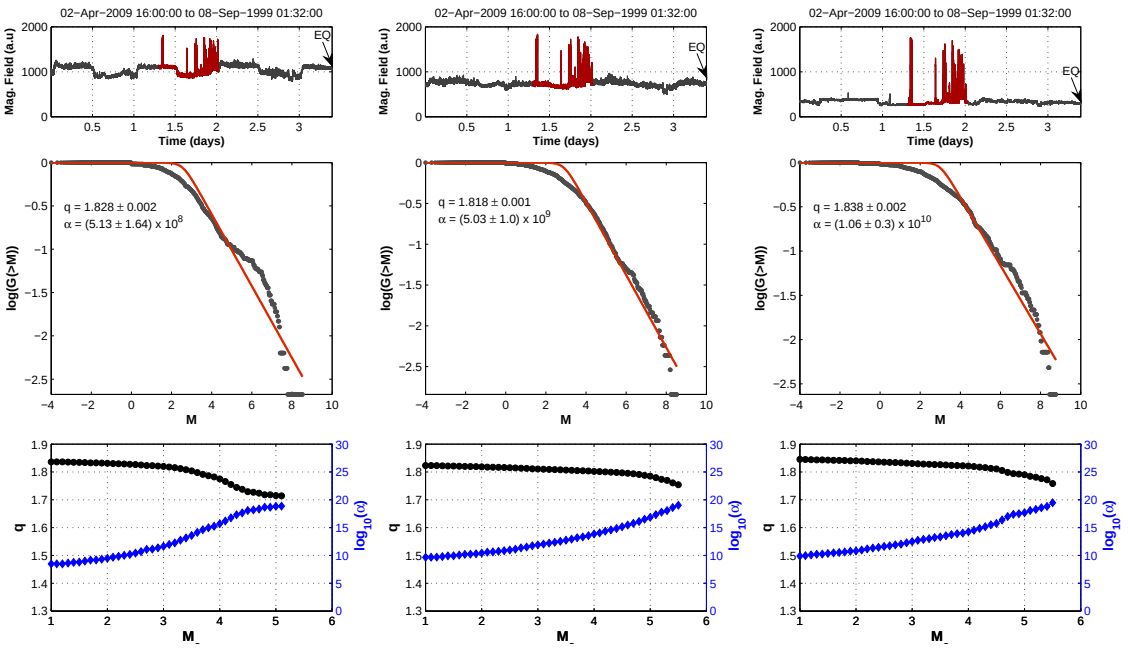

(a) 10 kHz NS (b) 10 kHZ EW (c) 10 kHz V

Figure 4.5: Three observed magnetic fields recorded on 02-Apr-2009 16:00:00 to 06-Apr-2009 01:32:39. The selected red parts of each recorded signal refer to the period where the kHz EM anomalies observed and have been well justified for their seismogenic origin ([55, 56]). The middle charts of each subfigure, refer to the fitting of the EM data in terms of the relative cumulative number of EM-EQs $G(> M)$ (see Eq. (2)), included in the period under study (red-part). The bottom charts of each subfigure, refer to the corresponding variation of the nonextensive q-parameter (black-bullets) and the volumetric energy density α (blue-rohmbs), for different thresholds of magnitude cut-off (M_c).

These latter results evidently show the similarity with the results obtained from the analysis of regional seismicity (see Fig. 4.3) at different radii around the EQ epicenter. Such evidence indicate the self-affine nature of fracture and faulting, from the large scale of foreshock seismic-

ity, to the fault-generation of a single EQ in terms of preseismic kHz EM emissions. However, in order to further verify this suggestion in the following section, the case of Athens 1999 EQ is examined in terms of the nonextensive model for EQs.

4.4 The case of Athens 1999 earthquake

This section focuses on the case of the catastrophic EQ ($Mw = 5.9$) occurred in the metropolitan region of Athens (Greece) on 07-Sep-1999 11:56:50 UTC. It should be noted that Athens EQ occurred very shortly after the major 17/8/1999, $Mw = 7.4$, catastrophic EQ which took place on Izmit, Turkey, approximately 650 km North-East of Athens. Characteristically, Brodsky et al. (2000) [28] showed that the Izmit EQ, was followed immediately by small earthquakes occurred throughout much of continental Greece, which in turn, followed by the Athens EQ in less than a month period. Against this evidence, the period from 17-Aug-1999 00:01:39.80 up to 07-Sep-1999 01:56:49 (right before the EQ occurrence), was selected as the most appropriate period that can be considered as the regional seismicity prior to Athens EQ. Fig. 4.6 depicts the seismicity contained within the period under study, for 400km arround the Athens EQ epicenter (see yellow star). The EQ catalog used, has been provided by the website of the Institute of Geodynamics of the National Observatory of Athens (www.gein.noa.gr).

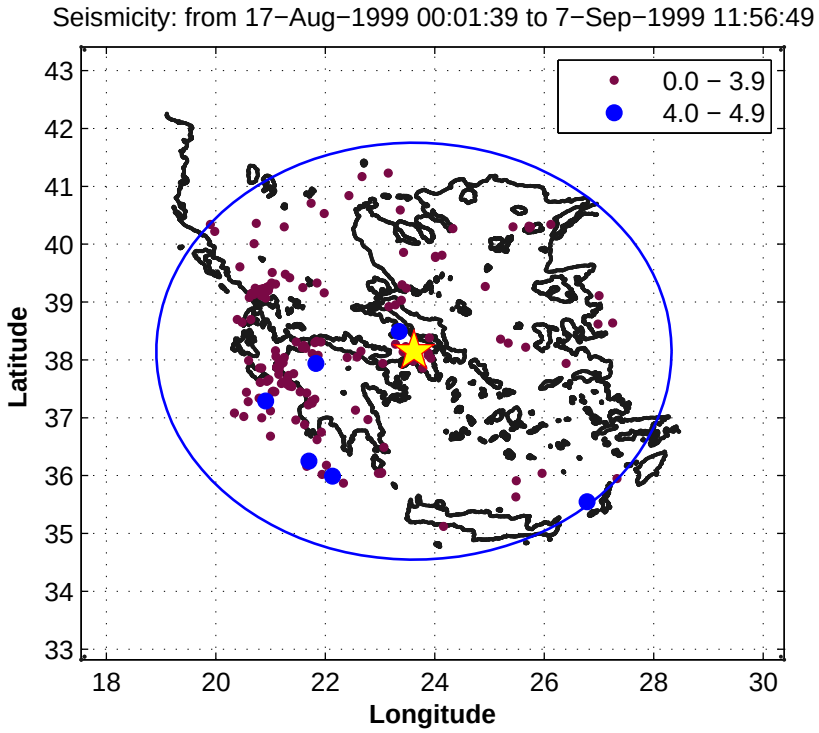

Figure 4.6: (a) Seismicity 400km around the Athens EQ epicenter included in period from 17-Aug-1999 00:01:39.80 up to 07-Sep-1999 01:56:49. The colored bullets represent the magnitude ranges of the EQs occurred within the selected period under study.

Focusing on the analysis of seismicity, four different geographic areas were selected around the Athens EQ epicenter for the period under study: $0-400km$, $0-300km$, $0-200km$ and $0-160km$ respectively. Fig. 4.7, depicts the fitting of Eq. (2) applied on the relative cumulative number of magnitudes ($G(>M)$) for the populations of EQs included in each one of the four geographic areas under study. As it is observed, the nonextensive q-parameter varies between $[1.532 \sim 1.664]$ with a relative small standard error ranging between $[0.003 \sim 0.004]$.

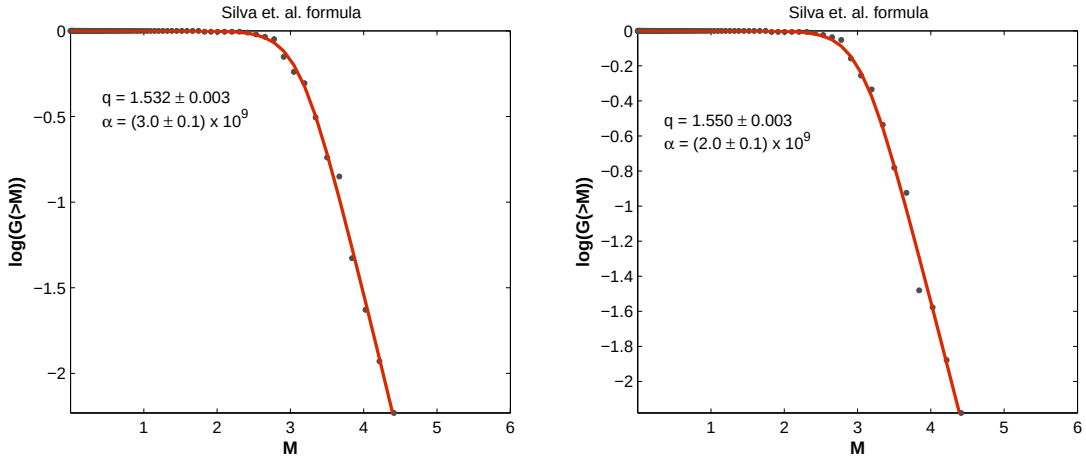

(a) 0-400km

(b) 0-300km

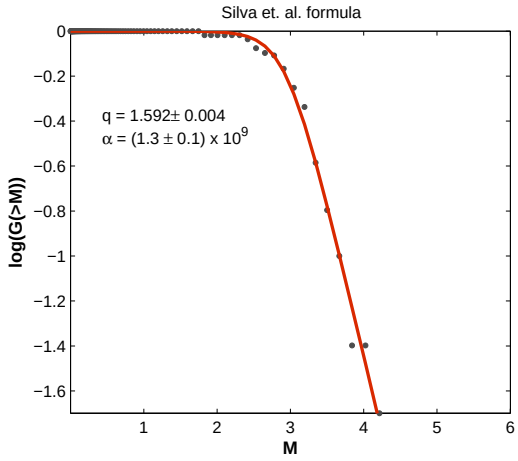

(c) 0-200km

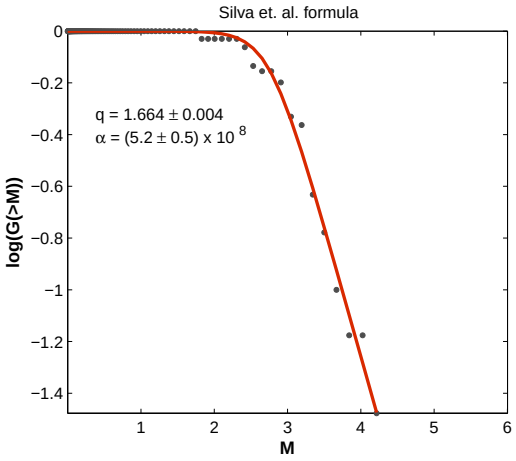

(d) 0-160km

Figure 4.7: Eq. (2) was used to fit the seismic data in terms of the relative cumulative number of EQs included in four different geographic areas around the Athens EQ epicenter.

Focusing on the behaviour of parameters included in the nonextensive Eq. (2), the same method has been used as that described in Sec. 4.3. Fig. 4.8, depicts the variation of nonextensive parameter q (see black-bullets) and the volumetric energy density α (see blue rhombuses), at different thresholds of magnitudes (M_c). It is observed that both the nonextensive q-parameter and the energy α, present similar behaviour, for all the selected geographic areas around the EQ epicenter. More specifically, the nonextensive parameter q (depicted with

black bullets) remains relative stable with minor decrement at higher thresholds of magnitudes, while the characteristic value of the volumetric energy density α (depicted with blue rhombuses), increases at higher magnitude thresholds (M_c).

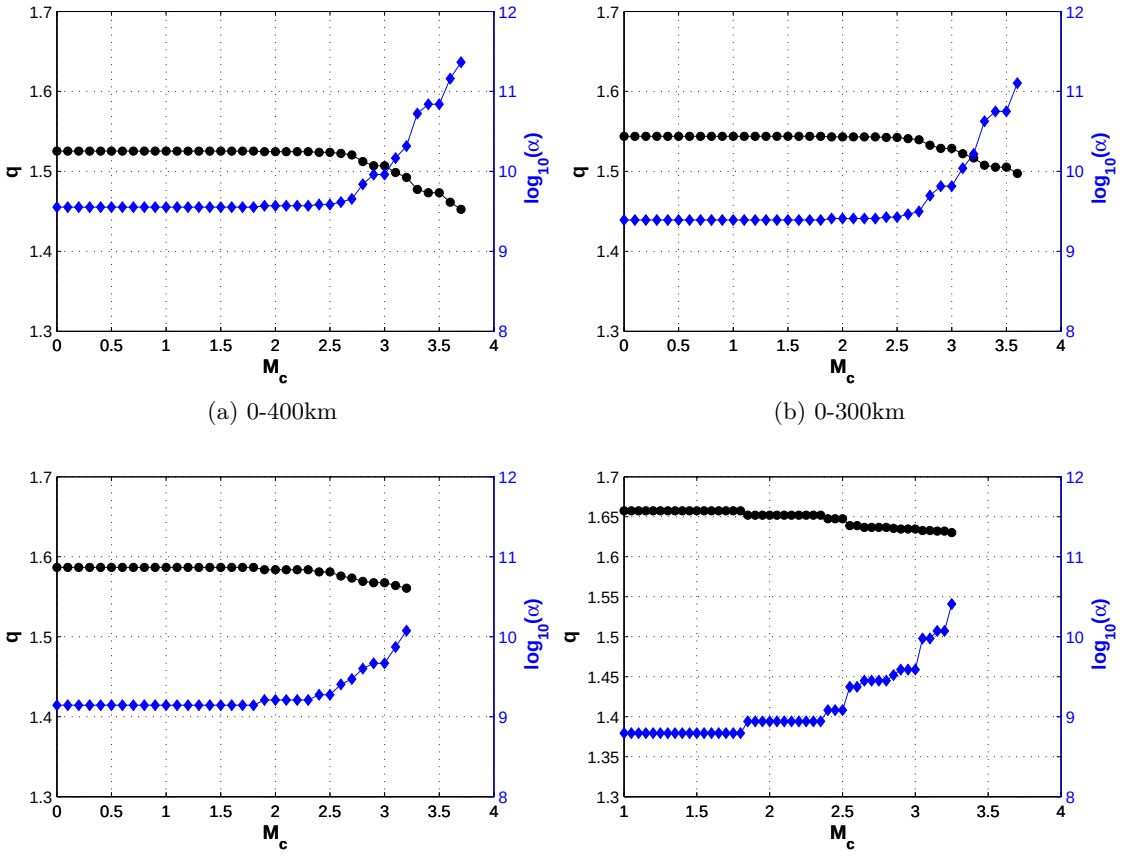

(a) 0-400km (b) 0-300km

(c) 0-200km (d) 0-160km

Figure 4.8: Variation of nonextensive parameter q (see black-bullets) and the volumetric energy density α (see blue-rhombuses), for different thresholds of magnitudes of the detected EQs included in the period from 17-Aug-1999 00:01:39.80 up to 07-Sep-1999 01:56:49, for the range (a) 0-400km (b) 0-300km, (c) 0-200km and (d) 0-160km around the Athens EQ epicenter.

A characteristic differentiation that should be discussed here in order to avoid possible inconsistencies, is that the q-parameter presents relative different behaviour with that of the case of L'Aquila EQ (see Fig. 4.3). More precisely, for the case of L'Aquila EQ, a relative increment of the q parameter is observed at higher magnitude thresholds as opposed to the case of Athens EQ, where a relative decrement is observed (see Fig. 4.8) correspondingly. This observation is not a trivial result, because if we get a closer look to Athens case in Fig. 4.8, this variation is mainly observed for larger thresholds of magnitude in contrast to the case of L'Aquila EQ where the increment is observed at intermediate thresholds of magnitude. This evidence enhances the suggestion that the small fractures along with the corresponding

redistribution of stresses, contributes to the increment of the correlation length during the fracture process [214]. Indeed, focusing on the EQ catalogs that refer to the periods under study, the mean magnitude of the EQs included in the area of 0-400km around the epicenter, for both the examined periods and has been found to be: $\bar{M} = 1.60$ for the case of Italy EQ and $\bar{M} = 3.00$ for the case of Greece, respectively. Fig 4.9 shows the distribution of EQ magnitudes that correspond to the areas under study for the specific periods. It is clearly observed that in the case of the Italian territory, EQs with lower magnitudes are more frequent in contrast to the Greek territory which is characterized by relative higher events. This evidence explains this inconsistency in the sense that the absence of small EQs results to a decrement of the nonextensive parameter q, as shown in the case of Athens EQ. On the contrary, for the case of Italian catalog, the abundance of small events keeps the correlations at higher levels even for intermediate magnitude thresholds. Thus the increment of q-parameter mentioned above is probably a finding that further supports the theoretical background of the nonextensive model.

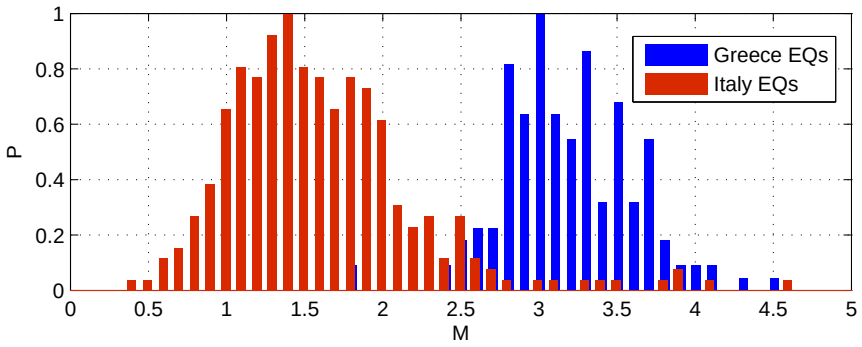

Figure 4.9: Distribution of EQ magnitudes included in the area of 0-400km around the Italian EQ (red bars) and Greek EQ (blue bars), correspondingly.

Along with these results, another feature that is also observed as approaching to the EQ epicenter, is that the smaller the area under study around the epicenter, the higher the nonextensive q-parameter, namely for the cases of: 300km, 200km and 160km around the Athens EQ epicenter. This evidence further verifies the increased correlations developed as approaching to the EQ epicenter. On the contrary the energy α, presents a relative decrement that mirrors the behaviour of q-parameter. This mirroring behavior has also been observed in a recent study of Matcharashvili et al. [155], who studied the area of Javakheti, Georgia in terms of a nonextensive statistical analysis. However, this behaviour is still an open issue for the scientific community and will be further analysed in the present thesis.

Since the analysis of seismicity at different geographic scales revealed similar footprints for both the parameters included in the nonextensive formula, it is expected that similar behaviour

should be observed at even lower scales of fracture, namely, the preseismic kHz EM anomalies observed prior to Athens EQ. Thus in the following section the analysis of the kHz EM emissions detected by the 3 kHz and 10kHz (NS-EW-V) components, prior to Athens EQ is presented.

4.4.1 Analysis of preseismic kHz EM emissions related to Athens EQ

Herein analysis is further focuses on the kHz EM emissions detected by the 3 kHz and 10kHz (NS-EW-V) components, located at a mountainous site of Zante Island in the Ionian Sea (Western Greece). These precursors can be seen in the top charts of each sub-figure depicted in Fig. 4.10, recorded on the period from 28-Aug-1999 00:00:00 to 08-Sep-1999 00:00:00. Athens EQ occurred on 07-Sep-1999 07-Sep-1999 01:56:50 UTC as shown by the black-arrow. The selected red parts refer to the period where the kHz EM anomalies observed. Note that although the seismogenic origin of the kHz EW component has been well justified by the literature [123, 36, 40, 172], herein for the first time all the six detected components are further analysed from the perspective of self-affinity.

It should also be noted that in Sec. 3.5, the six observed magnetic fields have been analyzed in the context of nonextensive Tsallis statistics showing that the q-parameter lies within the interval $q \in [1.78 - 1.82]$ with a relative small standard error ranging between $[0.0003 \sim 0.0006]$, for all the recorded channels. Thus, since the nonextensive Eq. 2 can adequately describe the "fracto-electromagnetic earthquakes" (EM-EQs) included in the preseismic kHz electromagnetic (EM) emissions, the analysis further focuses on the behaviour of parameters included in the nonextensive formula from the perspective of self-affinity. In this direction, the bottom charts of each sub-figure contained in Fig. 4.10, depict the variation of the nonextensive q-parameter (black bullets) and the volumetric energy density α (blue rhombuses), for different thresholds of magnitudes (M_c). As in the case of L'Aquila recordings, It is also observed that the variation of the nonextensive q-parameter remains relative constant with minor decrement at higher thresholds of magnitudes. On the contrary, the energy density α mirrors the behaviour of q-parameter, presenting a relative increment at higher thresholds.

The latter results evidently reveal the similarity with the results obtained from the analysis of L'Aquila EQ. This consistency indicates the self-affine nature of fracture and faulting, from large-scale seismicity, to the fault-generation of a single EQ in terms of preseismic kHz EM emissions.

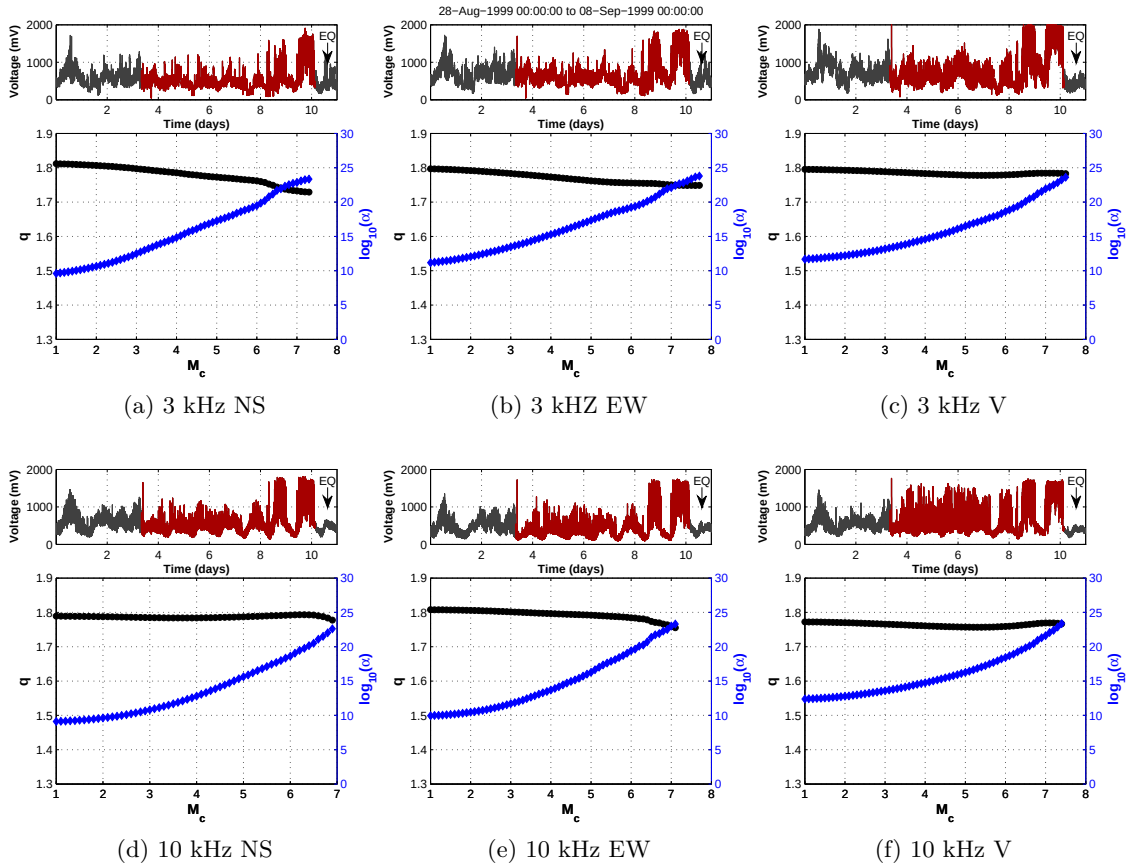

(a) 3 kHz NS (b) 3 kHZ EW (c) 3 kHz V

(d) 10 kHz NS (e) 10 kHz EW (f) 10 kHz V

Figure 4.10: Six observed magnetic fields recorded on the period from 28-Aug-1999 00:00:00 to 08-Sep-1999 00:00:00. The selected red parts of each recorded signal refer to the period where the well justified for their seismogenic origin kHz EM anomalies have been observed ([123, 36, 40, 172]). The bottom charts of each sub-figure, refer to the corresponding variation of the nonextensive q-parameter (black-bullets) and the volumetric energy density α (blue-rhombuses), for different thresholds of magnitude cut-off (M_c).

4.5 Further Discussion

Analysis applied so far in this chapter, on both the populations of EQs included in foreshock activity and the populations of EM-EQs included in preseismic kHz EM emissions (see Figs. 4.2,4.5 and 4.7), has shown that similar footprints of nonextensivity have been observed in both populations, verifying the seismogenic origin of these precursors. Characteristically, for the case of L'Aquila EQ, analysis has shown that the nonextensive q-parameter varies between $q \in [1.644 \sim 1.694]$ for the seismicity and between $q \in [1.818 \sim 1.838]$ for the preseismic kHz EM emissions, correspondingly. In addition, for the case of Athens EQ, the q-parameter has been found between $q \in [1.532 \sim 1.664]$ for the seismicity and between $q \in [1.78 \sim 1.82]$ for the preseismic kHz EM emissions. It should be noted that these results are in general agreement with those obtained from several independent studies, related to seismicities generated in

various large geographic areas, involving the Tsallis nonextensive framework [208, 229, 228, 230, 155]. Indicatively in a recent study, Telesca [228], who examined the preseismic activity of L'Aquila EQ included in the foreshock period from 30-Mar-2009 to 06-Apr-2009, found a value of ($q = 1.742$).

As concerns the method applied for the estimation of the behaviour of parameters q and α, by using different magnitude thresholds (M_c), similar behaviour has also been found for both the populations of EQs included in foreshock activity and the populations of EM-EQs included in preseismic kHz EM emissions. More precisely, for the case of seismicity related to Athens EQ (Fig. 4.8), it is observed that the nonextensive parameter q and energy α, present similar behaviour, for all the selected areas around the Athens EQ epicenter. Characteristically, the nonextensive parameter q (depicted with black bullets) remains relative stable for different magnitude thresholds while the situation changes for even larger thresholds, where a relative decrement is observed. Such behaviour is also observed from the analysis of preseismic kHz EM emissions as shown in Figs 4.5 and 4.10. This prospective decrement can be explained by the fact that the larger the magnitude threshold the larger the number of the omitted EQs. The absence of the small fractures along with the corresponding redistribution of stresses, contributes to the decrement of the correlation length during the fracture process [214]. The smaller magnitude threshold is the one that governs the overall system (e.q for $M_c = 0$). It should also be noted that although the nonextensive parameter q decreases at higher magnitude thresholds it still remains high verifying the strong correlations that have been developed. Concerning the volumetric energy density α (depicted with blue-rhombuses), its characteristic value, increases at higher thresholds of magnitude (M_c). Note that according to the fragment-asperity model (SCP), α is the coefficient of proportionality between fragment size and released energy [218, 208]. This evidence is consistent with the hypothesis that larger EQs are rooted in larger and stronger entities [158, 172] that sustain the system.

4.6 Conclusions

Building on the self-affine nature of fracture and faulting theory, this work supports the hypothesis that the statistics of regional seismicity is a macroscopic reflection of the physical processes in the earthquake source, as has been initially suggested by Huang and Turcotte [108]. This suggestion implies that the activation of a single fault is a reduced self-affine image of regional seismicity. Focusing on two well documented cases of large earthquakes, similar behaviour has been found of the corresponding variation of the parameters q and α, which are included in the nonextensive law for different thresholds of magnitudes. More precisely, this similar behaviour

has been founded on: (i) the population of EQs contained in different radii around the epicentre of a preceding large earthquake and (ii) the population of "fracto-electromagnetic earthquakes" that emerge during the fracture of strong entities distributed along the activated single fault sustaining the system. Analysis revealed that these two populations follow the same statistics, namely, the relative cumulative number of earthquakes against magnitude. The results have been further supported from recent studies in terms of the traditional Gutenberg-Richter law, enhancing the physical background of the underlying self-affinity.

Chapter 5

From earthquakes to the dynamics of regional brain activity in epileptic seizures

5.1 Overview

Complexity nowadays is a frequently used - yet quantitatively poorly defined - concept that embraces a great variety of scientific and technological approaches of all types of natural, artificial and social systems [247]. As noted in the relevant literature, complex systems are those which consist of a large number of units which strongly interact together in a nonlinear basis. A common basis of the various catastrophic phenomena is that their generation is the result of a collective process: the repeated interactions in many spatial scales progressively lead to the development of large-scale correlations between the entities and finally to the crisis. Several examples have been given in this direction providing evidence that support such definition [20, 180, 45, 131, 214, 2, 76, 176].

Recently, the unified study of complex systems which lead to catastrophic events, has been recognized by the scientific community as a new field of research [220, 221, 222, 265, 266]. An apparent paradox on this suggestion is how such a multifaceted concept as complexity, can adequately serve such a unified approach of catastrophic complex phenomena. Conformed with such a question, it should be noted that the laws governing the behavior of complex systems are completely different from the laws governing their respective units. Characteristically, Vicsek (2002) [266] mentioned that: *"a phenomenon that is "complex" refers to a system whose phenomenological laws, which describe the global behaviour of the system, are not necessarily directly related to the "microscopic" laws that regulate the evolution of its elementary parts"*. For example, it is not possible to understand the generation of a single epileptic seizure by

studying the behavior of a single neuron. When the units begin to interact each other, the behavior of each one of these is determined by the interactions with their neighbors. This results to a simultaneous alteration of their behaviour where the system displays a new peculiar common structure. This process involves interactions hierarchy governed by mechanisms of negative and positive feedback, self-organization and eventually develops fractal structures in space and in time (memory effects). The science of complexity is about revealing the principles that govern the ways in which new properties appear as these interactions move from one scale to another [266].

Towards the generation of a catastrophic event, it has been established that the corresponding time series are governed by: memory effects, gradually increment of the correlation length between the nonlinear domination of the neighbor units, transition from a negative to a positive feedback mechanism, development of fractal structures, gradual improvement of quality of the fractal structure and its transition at larger spatial scales with maintaining self-similarity. These dynamics of complex systems are founded on universal principles that may be used to describe disparate problems [20]. On these grounds, the present study explores physical and mathematical principles with universal character (universality) that govern the way to the generation of a catastrophic event in complex systems, as a result of the interaction of its ordinary members [20, 214, 196].

Theoretical studies have been made by eminent scientists from the fields of Medicine and Geophysics expressing the view that the same laws govern the preparation-emergence of a seizure or an earthquake [107, 196, 105, 184]. In this direction, emphasis will be placed on analyzing of electroencephalograph (EEG) recordings containing seizures and on well documented electromagnetic (EM) kHz time-series that contain seismic disturbances related to the activation of seismic faults. The purpose of this study will be to further verify the suggestion that the same laws govern the preparation-emergence of a seizure or an earthquake. The results will be extended-compared with already published studies [59, 124, 17, 18], related to catastrophic events such as magnetic storms and solar flares, in order to verify the universality of the symptoms that lead to the crisis.

It should be noted that the initial impetus for the comparative study of earthquake dynamics and regional brain activity was given from previous collaborative work published in Eftaxias et al [53], in the context of this thesis. The analysis presented in this chapter has been extended to the study of different kinds of data (i.e. including intracranial EEG recordings of epileptic seizures) and undertaking of different approaches in analyzing and interpreting issues pertinent to the main questions and directions of the overall thesis.

5.2 Setting the context of the analysis

Several complexity measures have been performed in order to monitor possible structures, patterns and correlations that sustain systems and generation processes. However the definition of the term "complexity" is still not unique since its quantification has received considerable attention due to the different contexts and different fields of application [147, and references therein]. Quantities such as: randomness or uncertainty, the degree of order or organization and disequilibrium, have played significant role on defining the term [147, and references therein]. Some of the common features that have been seen in many complex systems is the self-affinity and the fractional power law relationship which is a classic expression of a self-affine structure, namely the fractal [203, 249, 200, 118, 30]. Tsallis (1988) [245], proposed a generalization of the B-G statistical mechanics, by introducing an entropic expression characterized by an index q leading to nonextensive statistics. He mentioned that complex systems seem to occur close, in some sense, to the frontier between order and disorder where most of their basic quantities exhibit nonexponential behaviours, very frequently power laws [247]. It happens that the distributions and other relevant quantities that emerge naturally within the frame of nonextensive statistical mechanics are precisely of this type [247].

Epileptic seizures (ESs) and earthquakes (EQs) seem to be complex phenomena since they have highly intricate cluster and hierarchical structures, they are governed by feedback mechanisms with spatial and temporal correlation, they provide footprints of self-organization and connection diversity [169]. Against these features, several authors have suggested that dynamics of EQs and neurodynamics can be analyzed within similar mathematical frameworks [105, 197]. Driven systems of interconnected blocks with stick-slip friction have been found to capture these main features of EQs [107, 105]. Herz (1995) [105] suggested that such models may also represent the dynamics of neurological networks. Characteristically, Hopfield (1994) [107], proposed a model for a network of N integrate-and-fire neurons in which the dynamical equation of k^{th} neuron is based on the Hodgekin-Huxley model for neurodynamics and represents the same kind of mean field limit that has been examined in connection with earthquakes (EQs) [197]. Beggs and Plenz [23], who used neuronal cultures and cortical rat slices found that the size of local field potentials generated by these preparations have, as earthquakes and avalanches, no characteristic scale, and their probability density function (pdf) is described by a power law with an exponent of -1.5.

From the perspective of universality, it has been stated that the dynamics of complex systems, are founded on universal principles that may be used to describe disparate problems ranging from particle physics to economies of societies [20, 220, 221, 214, 265, 266]. Sufficient

studies have reported evidence for universality supporting the hypothesis that a number of systems under study in disciplines as diverse as physics, biology, engineering, and economics may have certain quantitative features that are intriguingly similar [180, 45, 131, 214, 2, 76, 176]. The latter arguments support this suggestion.

Recently, Osorio et al. [169] in a pioneering work have shown in terms of "scale-free statistics" that a dynamical analogy exists between ESs and EQs. More precisely, the authors performed a two directional analysis as follows: (i) they used a population of different EQs in the Southern California between 1984-2000, and (ii) they used a population of different ESs, collected between 1996 and 2000, from 60 human subjects with epilepsy undergoing surgical evaluation at the University of Kansas Medical Center. Their suggestion was supported using five scale-free statistics: the Gutenberg-Richter distribution of event sizes, the distribution of intervals, the Omori laws, and the conditional waiting time until the next event [169].

Analysis in this chapter is mainly focused on a recently introduced nonextensive model for EQ dynamics [218] (analytically described in Sec. 2.1.3), which is routed in the nonextensive Tsallis statistical framework [245]. In addition entropic measures including the Tsallis entropy have been also considered. A challenging issue would be to examine whether this dynamical analogy between ESs and EQs, also exists at the level of a single fault / seizure activation. Such analysis will further support the aforementioned suggestion at lower scale, elucidating the ways in which opening cracks and firing neurons organize themselves to produce *a single* EQ or ES respectively. Thus an appropriate framework would be to examine whether the above mentioned nonextensive statistical law can adequately describe the following populations:

(i) electric pulses included in a single ES, referring to the EEG time-series

(ii) fracto-electromagnetic pulses rooted in the activation of a single fault, referring to the preseismic kHz electromagnetic (EM) time series

(iii) different ESs occurred in different human's brains

(iv) different EQs occurred in different faults in various seismic regions

Building on that framework of analysis, a question that naturally arises is *"how the fluctuations included in a single EQ / ES precursory signal correlate in time"*. Conformed with such question, natural phenomena as well as human activities have been found to share common time-clustering behaviour [241, 235, 226, 234, 233, 232, 225]. In addition, in order to verify the aforementioned dynamical analogy the results should at least provide power-law correlations in both space and time. Thus, the analysis in this chapter also investigates the existence of a

common potential power-law distribution of burst lifetime (duration) [169], in the populations of: (i) electric pulses included in a single ES, (ii) fracto-electromagnetic pulses rooted in the activation of a single fault, and (iii) acoustic pulses in laboratory.

Summarizing at this point, the results in this study were positive since the performed analysis revealed common principal laws behind the exciting variety of complex phenomena under study. Moreover since the nonextensive model also leads to a fractional power-law relationship [202, 231], the results of this study were further verified using an alternative method, proposed by Utsu (1964) [252], which is based on the maximum likelihood estimation of the b-value included in the Gutenberg & Richter (G-R) formula. Finally the present study was further extended on the behaviour of the parameters included in the nonextensive formula at different threshold of magnitudes, enhancing the physical background of the underlying dynamical analogy and providing evidence of the scale-free and self-affine nature of the regional ES brain activity.

5.3 Analysis in terms of Hurst exponent, organization and information content

As already mentioned in the literature, a promising and globally accepted way to investigate such transient phenomena is to analyze the experimental time-series as a sequence of distinct time windows of short duration or even in some cases as a sequence of separate epochs. Such an approach along with the appropriate methods of analysis, could clearly differentiate the possible dynamical characteristics, as the catastrophic event is approaching, and furthermore to reveal-discover the basic mechanism that characterize such phenomena. Analysis here is first focused on the nonextensive statistical mechanics framework [245], namely the Tsallis entropy (see Sec. 2.1.2 for details). Herein, for reasons of clarity, the Tsallis entropy for the word length n, $S_q(n)$, is recalled and given by:

$$S_q = k\frac{1}{q-1}\left(1-\sum_{i=1}^{W} p_i^q\right), \tag{5.1}$$

where p_i are the probabilities associated with the microscopic configurations, W is their total number, q is a real number, and k is Boltzmann's constant. $q \to 1$ corresponds to the standard extensive B-G statistics.

An EEG recording from an adult Sprague-Dawley rat was firstly used in which a bicuculline injection was applied in order to induce the rat epileptic seizures [143, 122]. This selection was mainly made because it refers to a a controlled epilepsy where the temporal stages (injection, pre-ictal, ictal and post-ictal), have been well determined and justified for their origin. Fig. 5.1

shows the analysis of the aforementioned EEG signal in terms of Tsallis entropy in its symbolic form for word length 5 and $q = 1.7$ [117]. As it is observed from Fig. 5.1, the black part refers to the healthy state right before the injection, followed by the pre-ictal (green) state which has higher organization in comparison to the healthy state. On the contrary the initial stage of the red part that includes the ictal state, presents much higher degree of organization in contrast to the previous two phases, which is gradually increasing up to the healthy state as the rat is recovered from the effect of the drug.

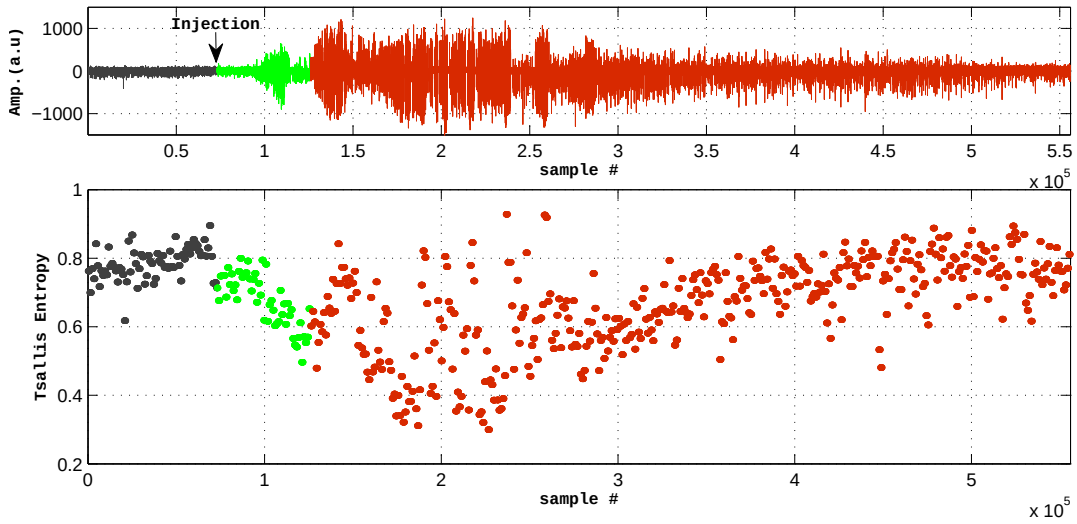

Figure 5.1: The top graph depicts an evoked seizure of a rat EEG. The arrow shows the time of injection while the black, green and red parts refer to the normal, pre-ictal and seizure epochs, correspondingly. The bottom graph shows the temporal evolution of Tsallis entropy, at non-overlapping windows of 1024 samples each.

Parallelizing the aforementioned results with the preseismic kHz EM emission associated with the Athens EQ, the analysis in chapter 2, in terms of T-Entropy and Tsalis entropy has revealed the higher degree of organization in contrast to the background EM activity, for the two epochs of EQ dynamics that have been justified for their seismogenic origin. Herein, the same results are also depicted in Fig. 5.2, where the three distinct phases of time series are also identified in the symbolic form of Tsallis entropy for a word length 5 and $q = 1.7$. More precisely, recalled that the first (black) part corresponds to the normal state, namely the EM background, followed by an epoch that includes a population of EM events sparsely distributed in time, with higher organization in comparison to the EM background. The third epoch that refers to the red part, is characterized by an ensemble of intense EM events, that present much higher degree of organization even in respect to those contained in the second epoch. Note that it has been shown that the two EM bursts refer to the fracture of the family of large high-strength entities distributed along the fault sustaining the system

[61, 123, 36, 124, 66, 172, 117].

The latter similarity obtained from Figs 5.1 and 5.2, provides a first indication that the Tsallis entropy clearly discriminate the emergence of shocks in EEGs and kHz EM-seismograms by means of order of organization. Note that Kapiris et al. (2005) [122] in a recent study in terms of wavelet-spectra and rescaled range analysis, applied on the same data, the authors have shown that the two examined events have also been characterized by persistency, while the normal states that refer to the black epochs, have been characterized by antipersistency (see Sec. 2.3 for definition).

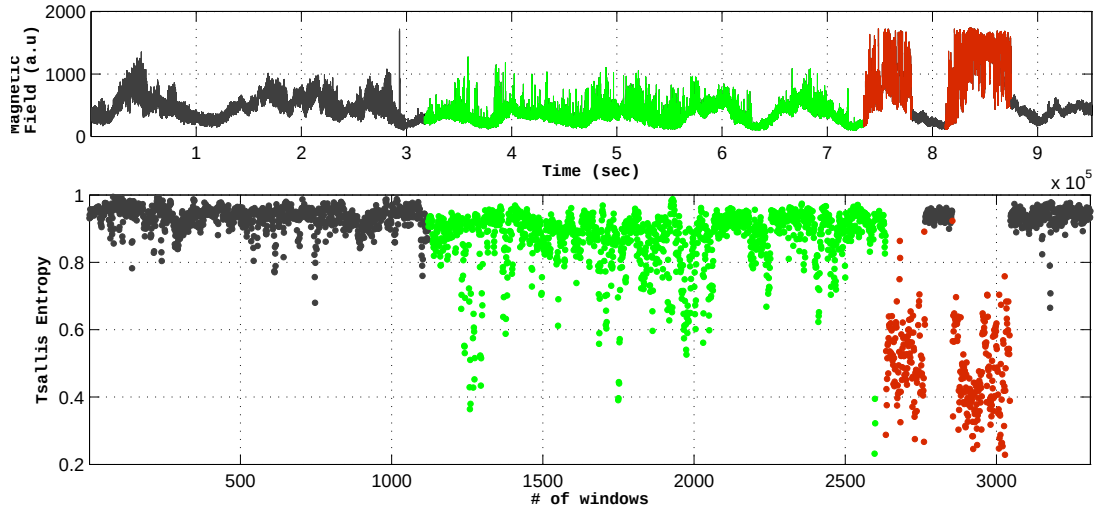

Figure 5.2: The EM time series associated with the Athens EQ recorded by the 10 kHz magnetic sensor. The black part refers to the background noise, while the green and red parts refer to the two distinct epochs of the emerged seismic EM activity (see text). The bottom graph shows the temporal evolution of Tsallis entropy, using non-overlapping windows of 1024 samples.

In order to further test the above mentioned suggestion, a humman EEG seizure available from the on-line PhysioNET database (http://physionet.org/pn6/chbmit/), collected at the Children's Hospital Boston, has also been analyzed in this study. It should be stated that PhysioNet is an open access web portal that provides a large collections of recorded EEG signals. Verbatim copying and redistribution of any material available from PhysioNet is permitted. The recorded EEG is depicted in the top part of Fig. 5.3. The red part corresponds to the ictal phase as has been annotated in the PhysioNET database [83]. The intermediate graph depicted in Fig. 5.3 shows the analysis of a human EEG in terms of Tsallis entropy in the framework of symbolic dynamics, using a word length 2. The bottom graph depicts the Rescaled Range analysis (R/S) [109, 110], described in Sec. 2.3, using successive non-overlapping windows of 1024 samples each. As it is observed, the red part which corresponds

to the ictal phase, is characterized by higher degree of organization and persistent behaviour ($H > 0.5$) in contrast to the previous part of the signal under study. The appearance of a high organization dynamics, which is simultaneously characterised by a positive feedback mechanism is consistent with the emergence of a catastrophic phenomenon and seems to clearly discriminate the pathological from the healthy state.

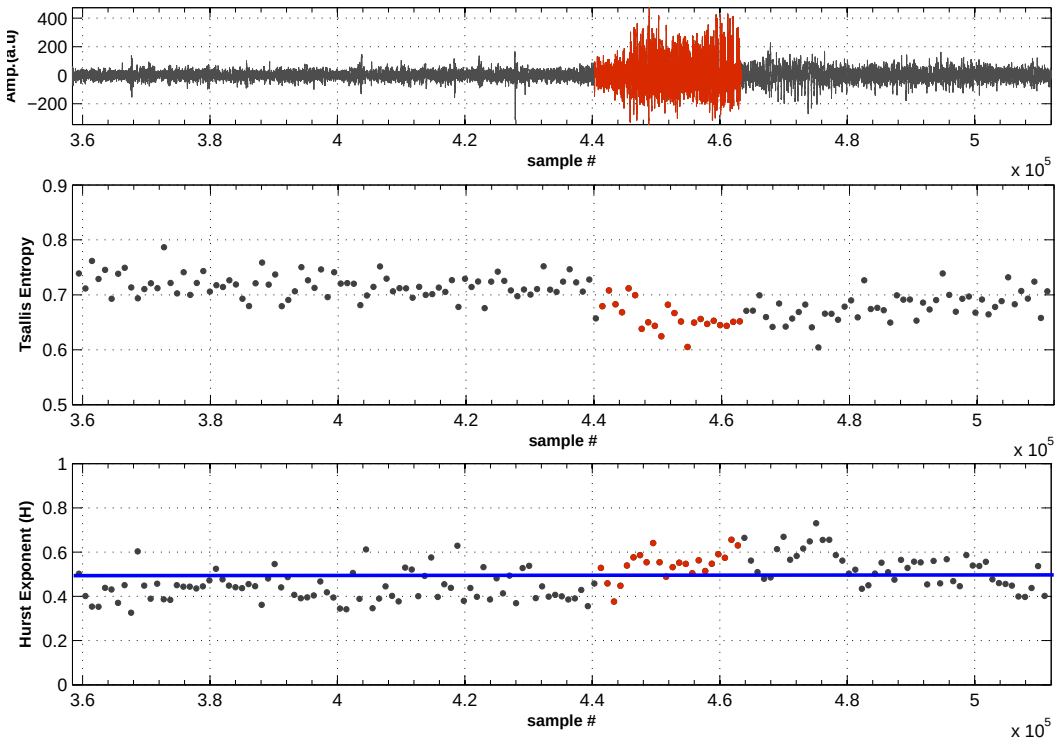

Figure 5.3: The top graph depicts a human EEG that contains a seizure (red color), as given from the PhysioNET database [83]. The bottom graph, shows the temporal evolution of Tsallis entropy using successive non-overlapping windows of 1024 samples each.

In the prospect to further verify the aforementioned suggestion and to show the repeatability of the results, the analysis further focuses on 100 healthy and 100 patient human EEG recordings offered by Andrzejak et al. [8]. In this direction, two more entropic methods have been employed in order to cross-fertilize the results: The T-Entropy [244] which is analytically described in Sec. A.3 and the Approximate Entropy [117, and references therein], which is analytically described in Sec. A.2 using the symbolic form for a word length 2 (see Sec. 2.1.1 for details). Note that both methods have been successfully applied to biological systems [182, 183, 243]. Focusing on the Tsallis entropy estimation depicted in Fig. 5.4, it is observed that the temporal evolution of the complexity in the EEGs time-series, is in full agreement with the upper limit $q < 2$ obtained from several studies involving the Tsallis non-extensive framework [267, and references therein]. However, it is expected that, for every specific system,

better discrimination will be achieved with appropriates ranges of q values [245]. Moreover, the results are in consistent with an underlying sub-extensive system, $q > 1$, verifying the emergence of strong interactions in the brain, especially during the occurrence of an ES. As concerns the rest of the estimated entropies, it is observed that both reveal the increased levels of organization of the patient EEGs in contrast to the healthy ones. Note that the most part of this work has been published in [64] where further analysis in terms of Shanon entropy has revealed similar results, while the estimation the appropriate value of q-parameter which is associated with the generation of ESs, was found to be $q = 1.55$.

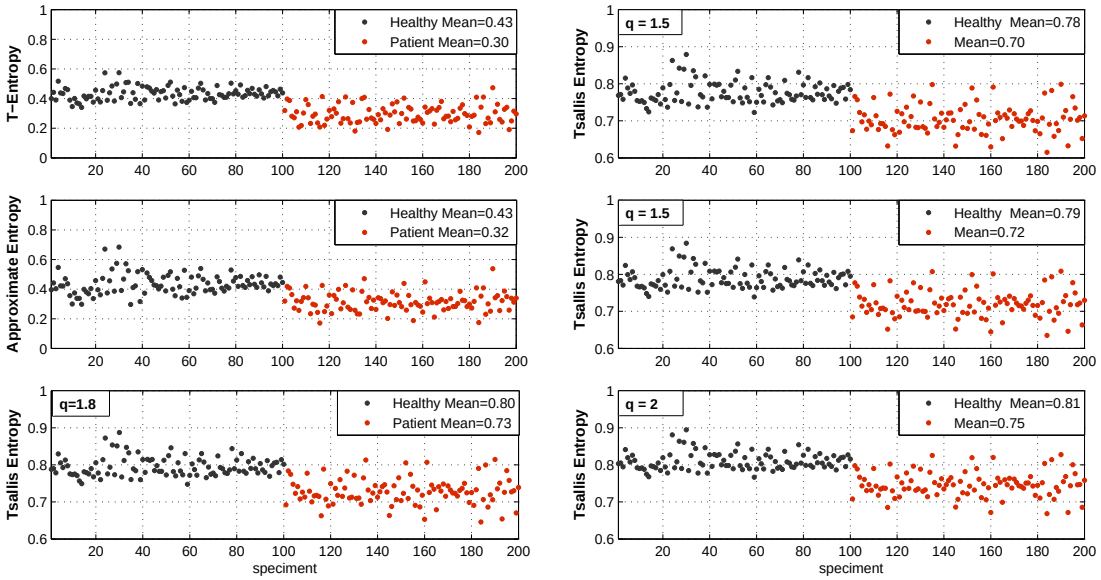

Figure 5.4: T-Entropy, Approximate Entropy and Tsallis entropy for different values of q, applied on 100 healthy and 100 patient human EEGs [8]. The healthy EEGs are black colored while the patient EEGs are red coloured.

5.4 Dynamical analogy in terms of energy: the Gutenberg-Richter scaling law

In order to meet the analysis performed by Osorio et al. [169], this section focuses on the traditional Gutenberg-Richter law (G-R) which states that the number of EQs with magnitude greater than M follows the relation (1) described in Sec. 0.6. Note that in terms of energy the G-R law states that, the probability density function of having an EQ energy E is denoted by the power-law $P(E) \sim E^{-B}$ where $B \sim 1.4 - 1.6$ [89]. According to Osorio et al. [169], the authors found that the probability of an ES in a population of different events having energy E is proportional to E^{-B}, where $B \sim 1.5 - 1.7$. In this direction analysis here is focused on the sequences of electrical pulses included in a single ES and on the sequence of

EM pulses included in preseismic kHz EM emissions that refer to a single fault. More precisely, it is examined whether both sequences follow a power-law $P(E) \sim E^{-B}$, with a compatible exponent B.

Focusing on the electrical pulses included in a single ES, Fig. 5.5a shows that the energies, E, of the electrical pulses included in the single rat seizure follow the power-law $N(>E) \sim E^{-0.62}$, or equivalently, the power-law $N(E) \sim E^{-1.62}$. In addition, Fig. 5.5b, shows that the energies, E, of the electrical pulses included in a human ESs follows the power-law $N(>E) \sim E^{-0.72}$, or equivalently, the power-law $N(E) \sim E^{-1.72}$. As regards the case of the kHz EM precursor associated with the Athens EQ (Fig. 5.2, upper panel), it has been shown that the cumulative number $N(>A)$ of pre-seismic EM pulses having amplitudes larger than A follows the power-law $N(>A) \sim A^{-0.62}$ [121]. Thus, the probability of an EM-pulse having energy E is proportional to $E^{-1.31}$ [58].

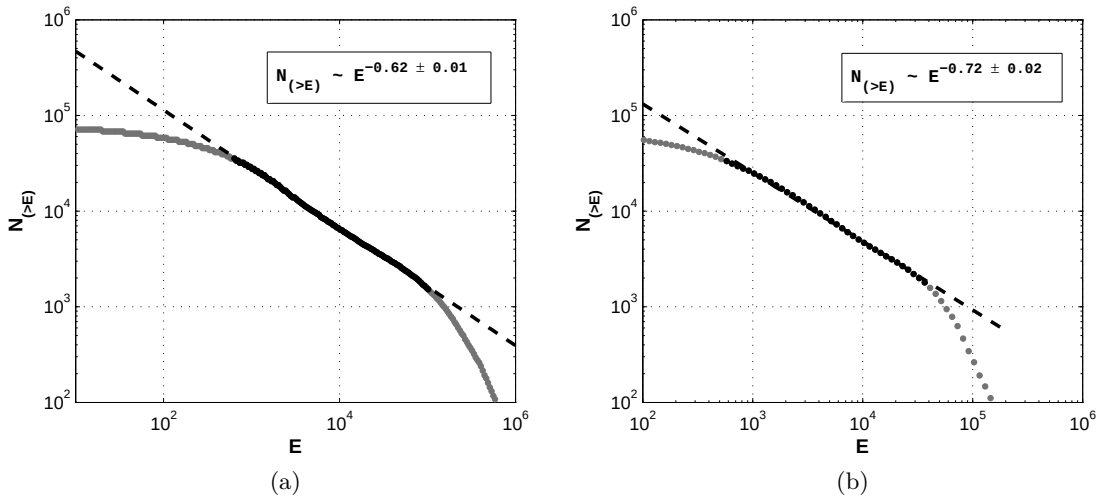

(a) (b)

Figure 5.5: (a) The distribution of energies, E, of the electrical pulses included in the rat seizure depicted in Fig. 5.1 follows the power-law $N(>E) \sim E^{-0.62}$. (b) The distribution of energies, E, of the electrical pulses included in a human ES, depicted in Fig. 5.3, follows the power-law $N(>E) \sim E^{-0.72}$.

The latter results along with the results of the analysis obtained by Osorio et al. [169], strongly indicate that sequences of: (i) fracto-EM-pulses included in a single EM-precursor associated with the activation of a single fault, (ii) electric pulses included in a single ES, (ii) different EQs occurred in various areas included many faults, and (iv) different ESs, follow the power-law $P(E) \sim E^{-B}$ with rather compatible B-exponents. It should be noted that Osorio et al. were mentioned that in general, differences in constituting elements (organic vs inorganic), in scale, and in other properties between the earth and brain may account for dissimilarities in the values of exponents. This suggestion implies that further consideration

should be taken in this direction. Moreover the dynamical analogy that the authors suggested, is further extended to lower scale in terms of energy, namely to the activation of a single ES / EQ.

By extending this suggestion to laboratory seismicity, in terms of acoustic / EM emissions detected in rocks, Rabinovitch et al. [192] who studied the fractal nature of EM radiation induced by rock fracture have found similar results. More precisely, the authors found that the pre-fracture EM time series reveals that the cumulative distribution function of the amplitudes contained in the pre-fracture EM time series, follows the exponent $N(>A) \sim A^{-0.62}$, and, consequently, the distribution function of the energies follows the power-law $P(E) \sim E^{-1.31}$. In addition, Petri et al. [177] who studied the acoustic emission in terms of energy, found a power-law scaling behaviour in the acoustic emission energy distribution with $B = 1.3 \pm 0.1$. On the other hand, Cowie et al. (1993) [44], Sornette et al. (1994) [215] and Cowie et al. (1995) [43], who worked on a model of self-organized EQs occurring on self-organized fault, suggested that the theoretical value of the B exponent should be $B = 1.3$. These arguments verify the above mentioned dynamical analogy also for the experiments employed at laboratory scale.

As already mentioned in introduction in order to have an overall view of the underlying dynamical analogy between different catastrophic events, these power-law correlations should be at least observed in both space and time scales. Thus in the following section analysis is focused on the dynamical analogy in terms of waiting times.

5.5 Dynamical analogy in terms of waiting times

Motivated by the analysis employed by Osorio et al. [169], herein, the temporal clustering in terms of burst lifetime (duration) is investigated from the perspective of potential power-law distribution. More precisely, the authors showed that the probability-density-function (pdf) for intervened intervals τ as calculated for a population of different ESs, follows a power-law distribution $\sim 1/(\tau^{1+\beta})$, with $\beta \sim 0.5$ for interseizure intervals. In this direction, Figs. 5.6a and 5.6b, depict the distributions of the lifetimes of the electric pulses included in the rat seizure depicted in Fig. 5.1 and the human ES depicted in Fig. 5.3. It is observed that both distributions follow a power-law of $\sim 1/{\tau_w}^{1.7}$ and $\sim 1/{\tau_w}^{1.8}$, correspondingly. As concerns the preseismic EM activity dipicted in Fig. 5.2 which is associated with the Athens EQ, from Fig. 5.6c it is observed that the distribution of durations (lifetimes) displays a power-law in the order of $\sim 1/{\tau_w}^{1.6}$. Extending these results to laboratory scale, Vespignani et al. (1995) [264] measured an exponent $= 1.6$ via acoustic signals recorded from laboratory samples subjected

to an external stress. These arguments along with the analysis applied in this chapter up to this point, further enhance the view that a dynamical analogy exists between the two catastrophic events (EQs and ESs).

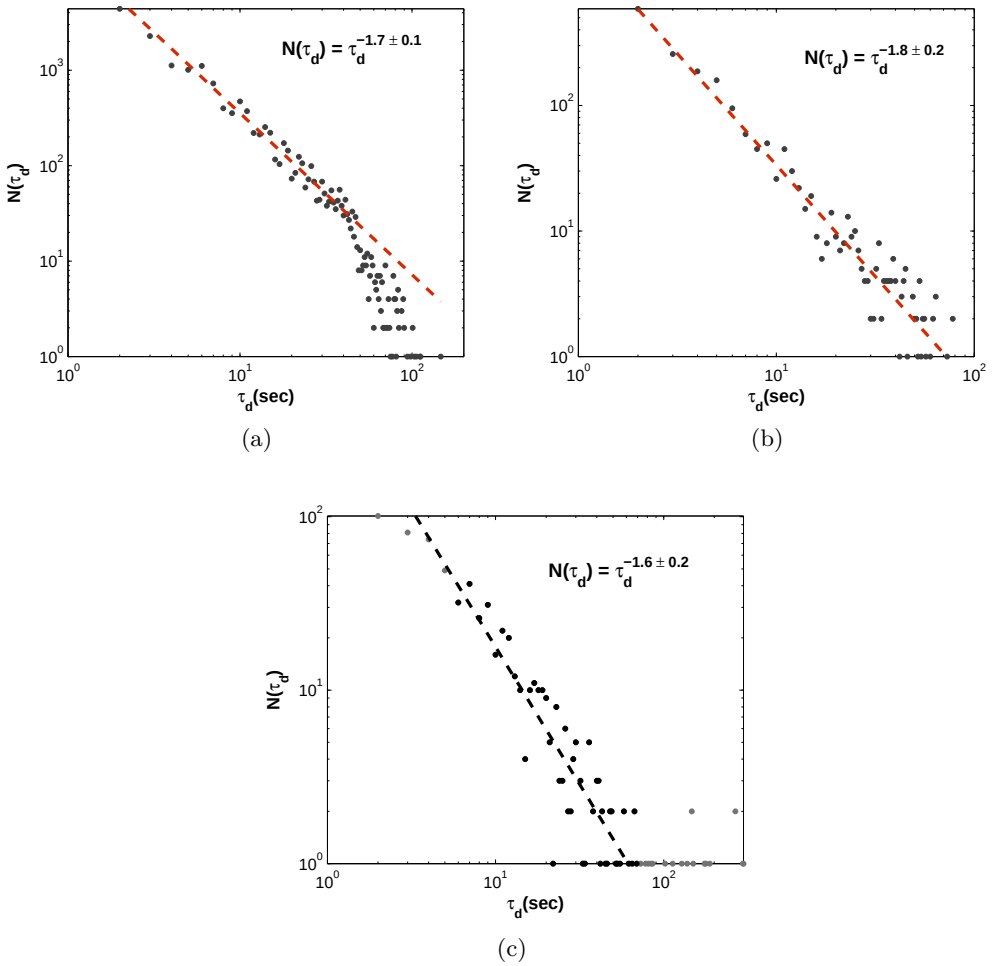

Figure 5.6: (a and b) Distributions of the lifetimes of the electric pulses included in a rat and a human ESs, correspondingly. (c) Distributions of the lifetimes of the EM pulses included in the precursory kHz EM activity associated to Athens EQ, following a power-law distribution $\sim 1/\tau^{1.6}$.

5.6 Dynamical analogy in terms of nonextensive model for earthquake dynamics

This section refers to a nonextensive model for EQ dynamics [218], in which the mechanism of triggering EQs is established through the combination of the irregularities of the fault planes, on one hand, and the fragments between them, on the other hand. The model has been analytically described in Chapter 2, thus for clarity reasons the nonextensive formula is only

presented, as given by Silva et al. [208]:

$$G(>M)=\frac{N\left(>M\right)}{N}=\left(\frac{2-q}{1-q}\right)\times\log\left[1-\left(\frac{1-q}{2-q}\right)\left(\frac{10^{2M}}{a^{2/3}}\right)\right], \tag{5.2}$$

where N is the total number of EQs, $N(>M)$ the number of EQs with magnitude larger than M, and $M\approx\log\varepsilon$. α is the constant of proportionality between the EQ energy, ε, and the size of fragment.

Sarlis et al. [202] have shown that the nonextensive Eq. (5.2) is related to the G-R law, above some magnitude threshold, as follows:

$$b=2\times\left(\frac{2-q}{q-1}\right) \tag{5.3}$$

Note that in previous chapters analysis has further verified that the nonextensive formula (5.2) can adequately describe the sequences of fracto-EM events, namely the EM-EQs, associated with the activation of a single fault [172, 117, 55, 56], as well as the populations of EQs included in the regional seismicities of various seismic regions [218, 208, 155, 229]. Characteristically, for the cases of Athens EQ and L'Aquila EQ, analyzed in this study, the best-fit parameter for these two precursors has been given by $q\sim1.80$, which is clearly in harmony with the exponents obtained in studies of regional seismicities, at the interval $q\in[1.6,1.8]$ [218, 208, 172, 229, 228, 227], suggesting that the activation of a single fault behaves as a "reduced image" of the regional seismicity as it was expected. Even more, analysis up to now has provided evidence of the self-affine nature of regional seismicity in the context of nonextensive Tsallis framework (see Chapter 4), identifying the self-affine nature of fracture and faulting. Herein, a challenging issue would be first to examine whether the same formula can adequately describe the sequences of electric events included in a single ES as well as in the case of EM-EQs included in preseismic kHz EM time series and the regional seismicity. The notion of "electric earthquake" (EL-EQ) is given here in the same way that has been calculated from the time-series of preseismic kHz EM emissions, by the relation:

$$M=\log\varepsilon\sim\log\left(\sum\left[A_{fem}(t_i)\right]^2\right), \tag{5.4}$$

where A_{fem} , $i=1,\ldots,k$ represents the EM energy released, ε, during the damage of a fragment calculated by the difference between the time series $A(t_i)$, from its background (noise) level A_{noise}: $A_{fem}(t_i)=A(t_i)-A_{noise}$.

In this direction, analysis here is first focused on in three single ESs available on the Internet from PhysioNET database * [83]. From Fig. 5.7, it is observed that the distribution

* http://physionet.org/pn6/chbmit/chb01/chb01_04.edf, Channel 14: F8-T8 /

of magnitudes of electric pulses included in two of the aforementioned single ESs, follow the nonextensive Eq. (5.2) with $q = 1.70 \pm 0.03$ and $q = 1.76 \pm 0.01$, respectively. Herein, $G(>M)$ vs M, is the fitting of the distribution of the relative normalized cumulative number of EL-EQs against magnitude, where $G(>M) = N(>M)/N_{tot.}$, with $N_{tot.}$ the total number of events.

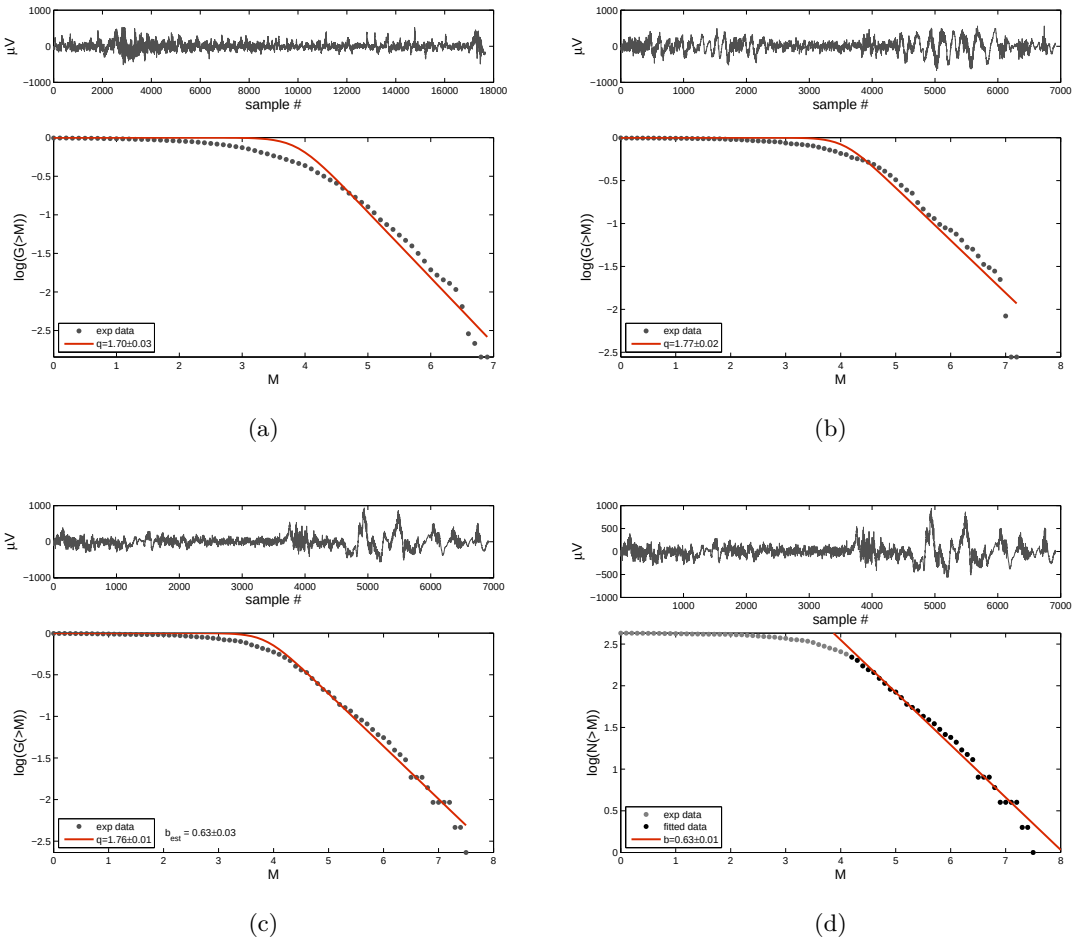

Figure 5.7: (a,b,c) Eq. (5.2) was used to fit the distribution of the magnitudes of electric events included in three single human epileptic seizures available from PhysioNET database [83]. (d) depicts the fitting of the same experimental data of (c) analyzed by means of the G-R law.

Herein, for reasons of completeness and in the prospect to meet the analysis performed by Osorio et al. [169], analysis here further refers to the comparison between the traditional Gutenberg-Richter law (G-R) that represents the frequency magnitude distribution of EQs (see Eq. 1), and the nonextensive Eq. (5.2). Fig. 5.7c shows that the distribution of magnitudes of electric pulses included in the third of the aforementioned single ESs, follow the nonextensive

http://physionet.org/pn6/chbmit/chb01/chb01_04.edf, Channel 22: FT10-T8 /
http://physionet.org/pn6/chbmit/chb03/chb03_03.edf, Channel 14: F8-T8.

Eq. (5.2) with $q = 1.76 \pm 0.01$. Additionally, Fig. 5.7d shows the fitting of the experimental included in Fig. 5.7c, directly fitted to G-R law for events with magnitude larger than $M = 4.2$, yielding a $b = 0.63 \pm 0.01$. Moreover, by replacing the q-parameter obtained by the fitting shown in Fig.5.7c, the estimated b-value through equation 5.3 has been found to be $b_{est} = 0.63$. This similarity in the b-values indicates the consistency with the G-R law.

The above presented results provide a first indication that the nonextensive formula which is routed in the Tsallis statistical mechanics framework, can adequately describe the sequences of electric events included in a single ES. However, analysis up to now has been mainly focused on "scalp-recorded" EEG recordings obtained from patients which suffer from ESs. Thus in order to further support the existing dynamical analogy between ESs and EQs, in the following sections an alternative approach is examined with new data deriving from intracranial EEG recordings. A redefined version of the notion of the electric event is presented which is mainly based on specific characteristics of ES EEG recordings.

5.7 Evidence of nonextensivity on both scalp-recorded and intracranial epileptic EEG recordings

Analysis in this section is focused on EEG recordings provided due to the collaboration with the Department of Neurosurgery, University of Athens, Evangelismos Hospital, Greece. The study was undertaken with the understanding and written consent of each subject, and the study conforms with "The Code of Ethics" of the World Medical Association (Declaration of Helsinki), printed in the British Medical Journal (18 July 1964). The study was also approved from the Evangelismos Hospital committee. After several meetings arranged with doctors involved in this collaboration, in the prospect to empirically find artificially clear EEG recordings for the specific analysis, the final data collection took place in the Epilepsy Telemetry Unit during longterm video/EEG for pre-surgical evaluation, using a sampling rate of $400Hz$, with 12 bits A/D resolution. Eight EEG recordings were collected (2 intracranial and 6 scalp-recorded), from patients which suffer from epileptic seizures and were for pre-surgical evaluation. A Beehive Millennium Digital Recording System was used with Grass Telefactor Twin Recording unit and the available software interface was used to mark the beginning of the seizure parts of each epilepsy recorded. The results in this section are also compared with the available 100 seizure parts analysed in Sec. 5.3.

It should be noted that the notion of "fracto electromagnetic earthquake" (EM-EQ), that has been validated in previous studies [124, 63, 172, 158], states that the recorded radiation must be emerging clearly from the EM background. This means that the detected EM radiation

has not been significantly absorbed by conducting layers of the crust or the even more conductive sea, implying that useful EM precursor must be associated with an on-land seismic event which is both strong, i.e., with magnitude 6 or greater, and shallow. In a manner analogous to the notion of EM-EQ, the present study seeks to identify specific "electric events" in the EEG recordings, corresponding to specific electric "pulses". According to this line of thought, the term "electric earthquake" (EEG-EQ) and the corresponding "fracto-electric emission", referring to the electric potential pulses that can be characterized as "events" of interest, is used. The theoretical background of this assumption reads as follows.

A characteristic feature that can be observed in EEG recordings is that the electric field balances around a specific (inactive) reference point (Pt_r) [219], which in most cases is observed around the zero value and usually forms a Gaussian (normal) like distribution in it's most part [67]. This feature can be verified by Elul (1969) [67], who investigated the probability distribution of the amplitude of a scalp EEG recording. He found that the idle state of the EEG of the sample under study follows a Gaussian (normal) probability function 66 percent of the time. On the contrary, during performance of mental task (arithmetic), the portion of Gaussian electroencephalogram decreases to 32 percent. This evidence implies to the fact that the cooperative activity of cortical neuronal elements increase during the performance of mental task [67]. The degree of mutual interaction of individual cellular generators of wave activity in the tissue located underneath the recording electrode is mainly the reason that forms the probability function which in turn characterizes the gross electroencephalographic activity. A challenging issue would be to examine whether this increased cooperative activity can be adequately explained through the notion of the "electroencephalograph earthquake" (EEG-EQ) for the case of EEG recordings related to ESs.

Indeed, Figs 5.8a, 5.8b and 5.8c depict the histograms of the fluctuations of the electric potential, recorded during the idle time behavior of three different patients. On the contrary, Figs 5.8d, 5.8e and 5.8f depict the histograms of the fluctuations of the electric potential recorded during the time of epileptic seizure. The samples S1 and S2 refer to intracranial EEG recordings while the S3 sample refers to scalp-recorded one. As it is observed from all the signals depicted in Fig. 5.8, the aforementioned Gaussian distribution is obvious, where the most frequent occurrence of the electric potentials concentrates within a zone around zero. It should be pointed out that although the distribution of the electric potentials included in the seizure EEG recordings, differs from that of the idle ones, the most frequent occurrence still remains within a zone around the zero point. In the present analysis this zone is defined as "balance zone". Two criteria have been considered in order to establish the start and the

end of each candidate electric EEG emission: (i) the electric emission starts when the pulse leaves the balance zone and ends the time where the pulse enters the zone, and (ii) the time duration where the pulse stays in the balance zone is considered as a criterion of state-changing (start-end). Note that for an ideal case (without noise), this balance zone could be limited very close to the "inactive" reference point (Pt_r).

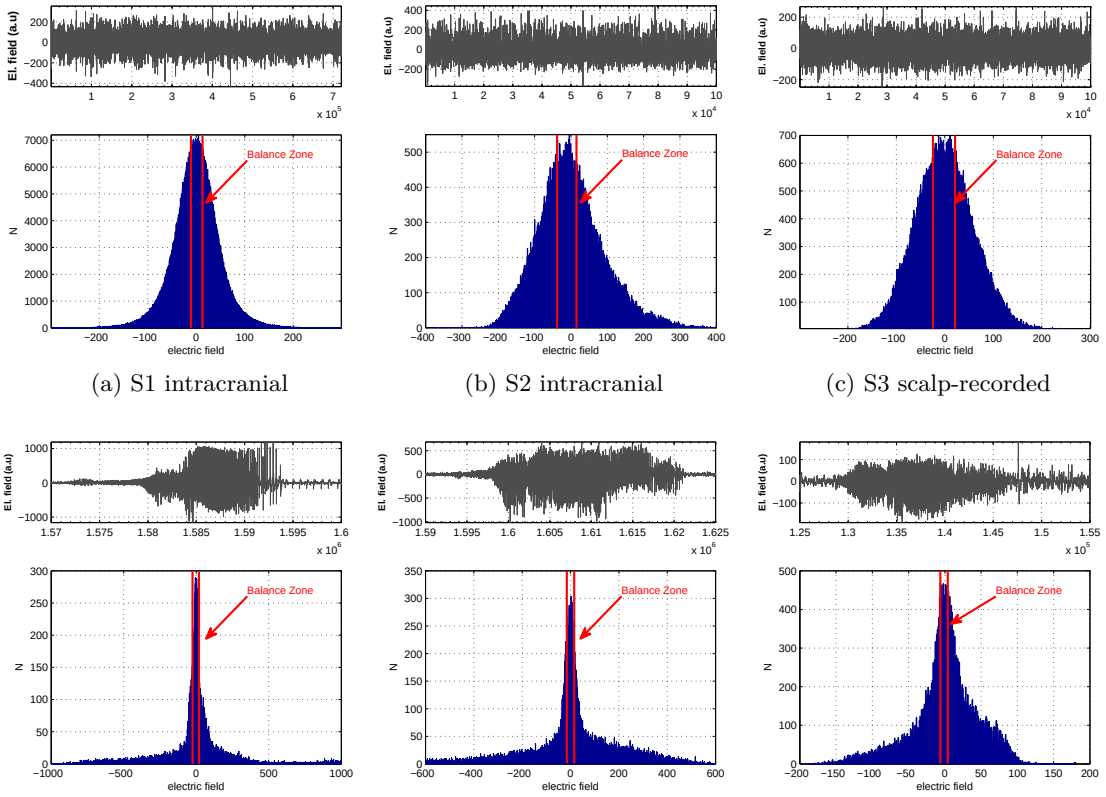

(a) S1 intracranial (b) S2 intracranial (c) S3 scalp-recorded

(d) S1 intracranial seizure (e) S2 intracranial seizure (f) S3 scalp-recorded seizure

Figure 5.8: Histogram distribution of the electric potentials recorded during the idle (a,b,c) and seizure (d,e,f) time behavior of three different patients. The range between the red lines indicates the "balance zone" around the "inactive" reference point (Pt_r)

Building from this feature, as eligible amplitude A of a candidate electric EEG time-series is considered the sequence of k successive units that exceed a threshold ($\pm Pt_{BG}$) around the balance point (Pt_r): $A_{eeg>|\pm Pt_{BG}|}(t_i)$, $i = 1, \ldots, k$. Since the squared amplitude of the "electric emission" is proportional to its power, the magnitude M of the candidate EEG-EQ is given by the relation:

$$M = \log \varepsilon \sim \log \left(\sum \left[A_{eeg}(t_i) \right]^2 \right), \tag{5.5}$$

In this direction, Figs 5.9a and 5.9b suggestively show that the distribution of magnitudes of electric pulses included in the ictal part of two intracranial EEG recordings, is also de-

scribed by the formula (5.2), yielding $q = 1.8838 \pm 0.0004$ and 1.8281 ± 0.0009, respectively. The Levenberg-Marquardt (LM) fitting method [142, 152] was used for optimizing the fitting process. Herein, N is the total number of the detected EEG-EQs, $N(M >)$ the number of EEG-EQs with magnitude larger than M, $G(> M) = N(M >)/N$ the relative cumulative number of EEG-EQs with magnitude larger than M, and α the constant of proportionality between the energy released and the size of fragment [208]. It should be noted that higher observed values of the nonextensive entropic index q characterize the strong correlations developed within the system under study [214].

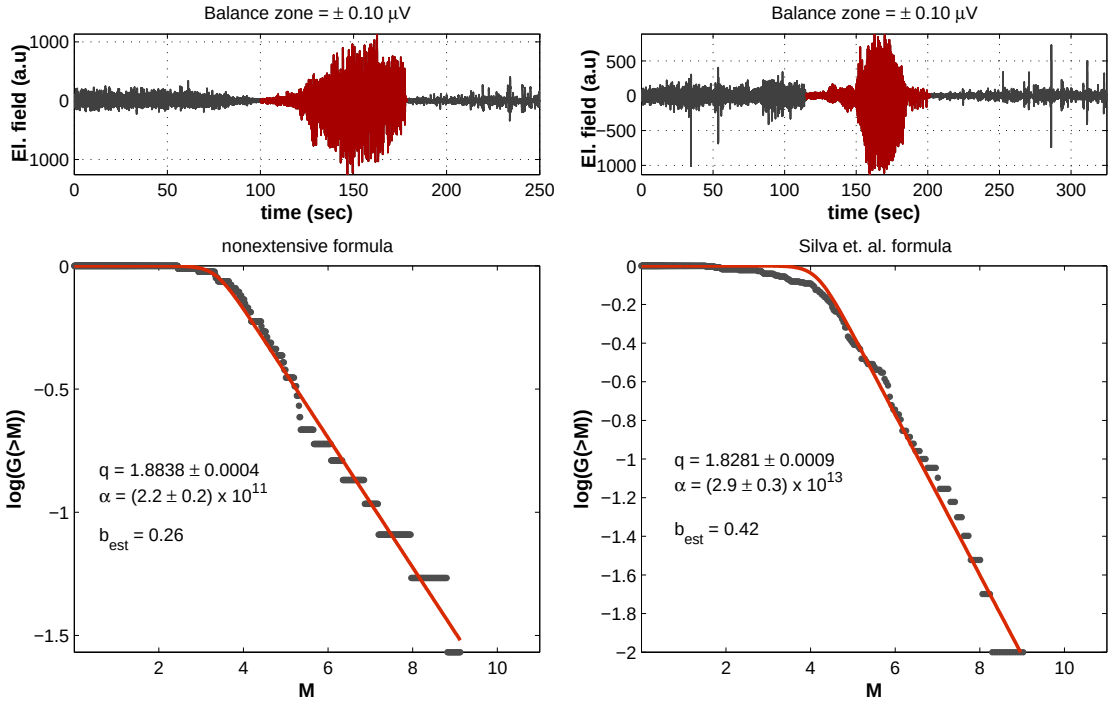

(a) Patient 1 (b) Patient 2

Figure 5.9: (a,b) Eq. 5.2 was used to fit the distribution electric events included in two intracranial EEG recordings. The red part refers the selected-calculated seizure part.

Figs 5.10a and 5.10b show the calculated nonextensive parameter q for all the electrodes used in the aforementioned EEG recordings. It is observed that the nonextensive parameter q varies between $1.41 \sim 1.9$ for all eight patients. The observed differentiation of q-parameter in the intermediate electrodes is not unexpected since the great variability in the morphology and mode occurrence of seizures, and the great variability of non-ictal EEG patterns, has already been emphasized [126]. On the other hand since there is not an optimal estimation of the levels of experimental noise within those signals, it is not clear whether the magnitudes lower than a specific threshold refer to the noise levels or to the eligible signal. However, the variation range of q-parameter with a mean $< q >= 1.768$ and $< q >= 1.722$ respectively, indicates

the nonextensive character of such phenomena.

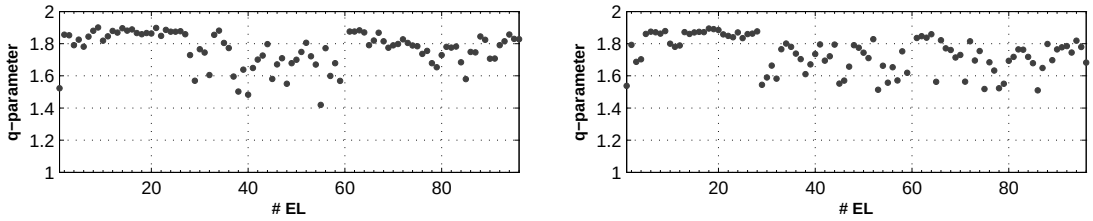

(a) intracranial 1 (b) intracranial 2

Figure 5.10: (a,b) depict the calculated q-parameter included in Eq. 5.2, for all the electrodes used in EEG recordings of Figs 5.9a and 5.9b, correspondingly.

In order to further test the results, the same analysis was applied to the set of 100 human ictal parts described in Sec. 5.3. Figs. 5.11a and 5.11b depict the analysis in terms of the nonextensive Eq. (5.2), using a balance zone of $Pt_{BG} = \pm 1\mu V$ and $Pt_{BG} = \pm 10\mu V$ respectively. It is observed that the obtained q-parameters vary between the intervals $q \in [1.257, 1.953]$ and $q \in [1.253, 1.817]$, with a standard error varying between $s_{err} \in [0.0024, 0.0254]$ and $s_{err} \in [0.0024, 0.0167]$, respectively.

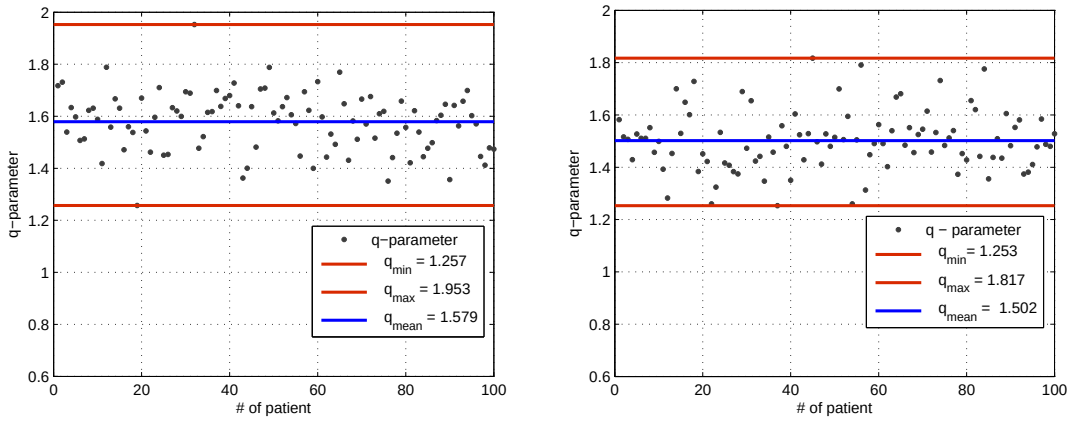

(a) (b)

Figure 5.11: Eq. 5.2 was used to fit the distribution of electric events included in 100 human ictal parts [8].

In Fig. 5.12, for repeatability reasons further evidence are provided, showing that the distribution of magnitudes of electric pulses included in the ictal part of all the rest six scalp-recorded EEGs, is also described by the formula (5.2). It is observed that the nonextensive q-parameter varies between $1.693 \sim 1.842$ for all the six recordings depicted in Fig. (5.12), with a standard error varying between $0.001 \sim 0.005$ indicating the excellent approximation of the fitting process. It should be noted that the fitting of some of the analyzed electrodes

of both the intracranial and scalp-recorded EEG recordings depicted in Figs 5.9 and 5.12, was relative poor. In addition relative poor fittings where also observed in the case of 100 human ESs. An empirical look of these fittings one by one, showed that approximately 80% of the analyzed ESs can be fitted by Eq. (5.2), while the rest of the EEGs ($\approx 20\%$) seemed to follow quite different statistics, than the one described by either Eq. (5.2) or the traditional G-R law.

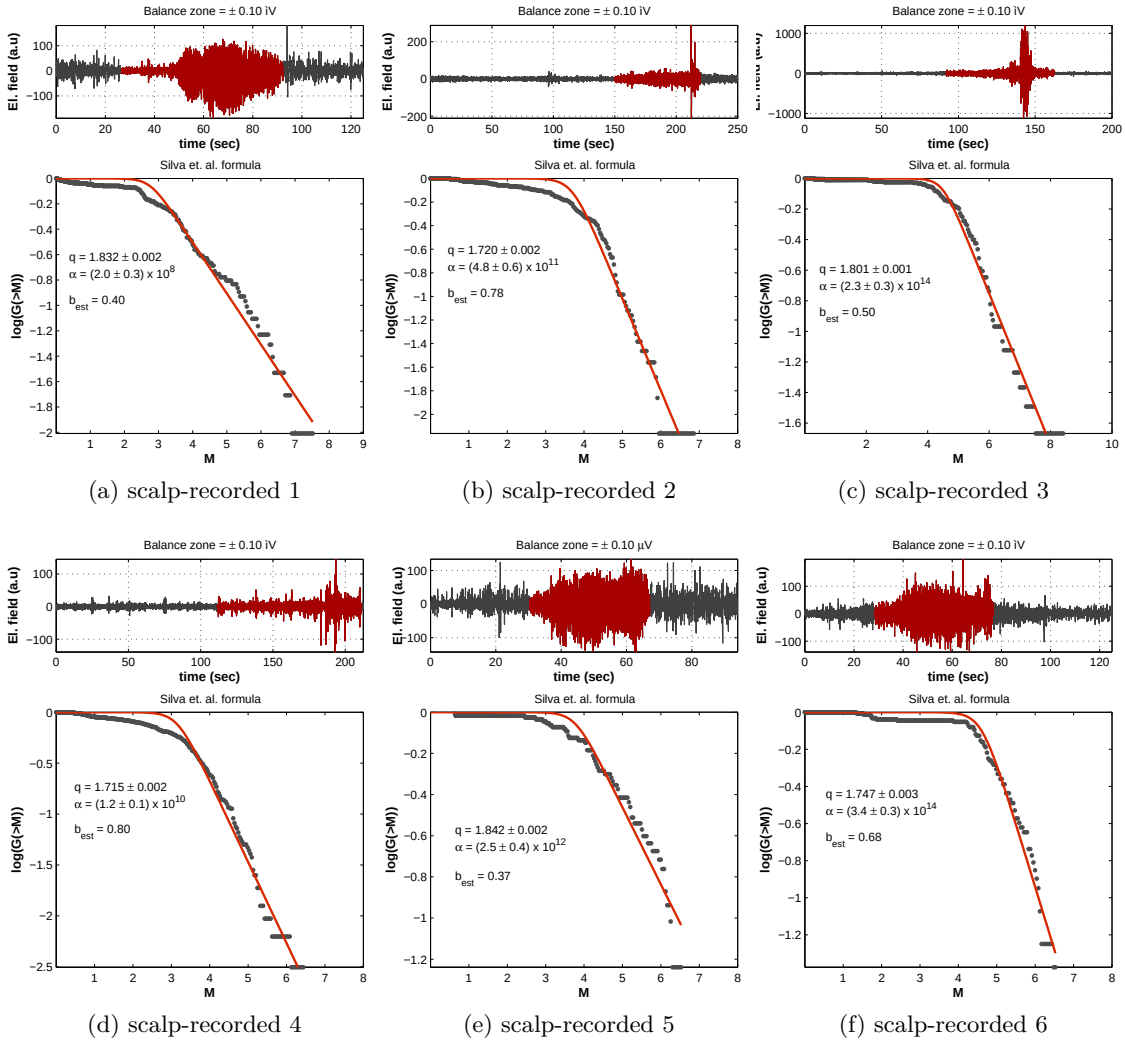

(a) scalp-recorded 1 (b) scalp-recorded 2 (c) scalp-recorded 3

(d) scalp-recorded 4 (e) scalp-recorded 5 (f) scalp-recorded 6

Figure 5.12: Eq. 5.2 was used to fit the distribution electric events included in six scalp-recorded EEGs. The red part indicates the seizure part of each EEG recording.

Indeed, following the latter argument, Osorio et al. [169] mentioned that "*increases in interneuronal excitatory coupling generate characteristic scale seizures regimes that coexist in space-time with scale-free ones, revealing the richness and complexity of pathological dynamics*". Characteristically, the authors provided a generic phase diagram which leads to the prediction that, if the degree of the coupling strength (or of the heterogeneity) between threshold oscillators is manipulated, transitions between the criticality and synchronized regimes will

not only occur but will be coextensive. They also mentioned a "shoulder" in the distribution of the Probability Density Function (PDF) estimation of seizure energies, which characterizes this transition. Analogous "shoulder" can also be observed in Fig. 5.12a which violates the linearity of the $\log G(> M) = N(M >)/N$ vs M representation of the cumulative number of magnitudes larger than M, indicating the existence of a 'characteristic" size (magnitude) in the distribution of M. Such evidence indicate that a study on the quantitative levels of such coexistence should be further explored in details.

As it is observed from Figs 5.10 and 5.11 respectively, there is a significant difference between the mean q-parameter obtained from the intracranial electrodes ($q_{mean} = 1.768$ and $q_{mean} = 1.722$) in contrast to the q-parameter obtained from the 100 cases of ESs ($q_{mean} = 1.579$ and $q_{mean} = 1.502$). This differentiation is mainly observed due to the fact that the data deriving data from the 100 patients, contain only a small part of 4096 samples included in the ictal part of the ES. However within the ictal part of an ES, the absence of the small events is a characteristic feature that governs the underlying interval. On the contrary the examined parts of the intracranial EEG recordings refer to the whole phenomenon that characterizes a single ES and includes a population of small events that contribute to increase correlations in the system under study [214]. This absence of small events possible leads to a decrement of correlation length which in turn leads to the decrement of the nonextensive q-parameter. On these grounds, a challenging issue would be to examine the behaviour of parameters q and α included in the nonextensive formula since such analysis has already been performed for both the EQs [228] and preseismic kHz EM emissions (See Chapter 2). Thus in the following section this issue is examined by applying different thresholds of magnitudes (cut-offs M_c) on the available EEG-EQs included in the EEG recordings depicted in Figs. 5.9 and 5.12.

5.8 Examining the behaviour of the parameters included in the nonextensive formula

Different thresholds of magnitudes cut-offs (M_c) were applied using an increasing step of 0.1. For each step, formula (5.2) along with the use of Levenberg-Marquardt (LM) fitting method, were used to fit the seizure data in terms of the relative cumulative number of EEG-EQs. A minimum number of 20 events was considered as a criterion for the statistical completeness. The derived parameters q and α, were graphically placed on to a common x-axis chart as shown in Fig. 5.13. Figs 5.13a and 5.13b, depict the analysis applied on the two intracranial EEG recordings S1 and S2, depicted in Fig. 5.9. The black-bullets refer to the variation of

nonextensive q-parameter at different thresholds, while the blue-rhombuses refer to the variation of the volumetric energy density α It is observed that the nonextensive parameter q (depicted with black bullets) remains relative stable for different magnitude thresholds. The situation changes for even larger thresholds of magnitude, where a relative decrement is observed. This prospective decrement of the q-parameter for larger thresholds of magnitude can be explained by the fact that the larger the magnitude threshold the larger the number of the omitted EEG-EQs. According to the fragment-asperity model (SCP), the absence of the small fractures along with the corresponding redistribution of stresses, contributes to the decrement of the correlation length during the fracture process [214]. The smaller magnitude threshold is the one that governs the overall system. It should also be noted that although the nonextensive parameter q decreases at higher magnitude thresholds it still remains high verifying the strong correlations that have been developed. As concerns the volumetric energy density α (depicted with blue-rhombuses), its characteristic value, increases at higher thresholds of magnitude (M_c). However, α is the coefficient of proportionality between fragment size and released energy [218, 208], as it has been stated by the SCP model. This evidence is consistent with the hypothesis that larger EQs are rooted in larger and stronger entities that sustain the system [172].

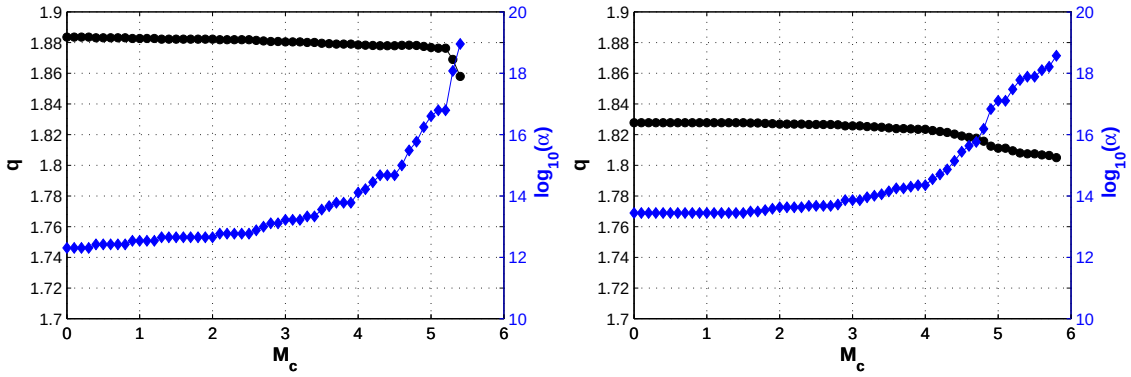

(a) S 1 (b) S 2

Figure 5.13: Variation of nonextensive parameter q (see black-bullets) and the volumetric energy density α (see blue-rhombuses), for different thresholds of magnitudes of the detected EEG-EQs included in the intracranial EEG recordings depicted in Fig. 5.9

The same analysis was applied on the scalp-recorded EEG recordings depicted in Fig. 5.12. More precisely, from Fig. 5.14, it is observed that the q-parameter derived from the analysis of patients 1,5 and 6 has the same behaviour with that of the analysis of intracranial ones, while for the rest the variation remains relative stable indicating the strong correlations in the sample. On the contrary the volumetric energy density α, has the same behaviour with that

depicted in Fig. 5.13. Note that although a minimum number of 20 events was selected for statistical completeness, inconsistencies may occur due to the reduce of the number of events at larger magnitude thresholds. However these inconsistencies do not seem to profoundly affect the results in this study.

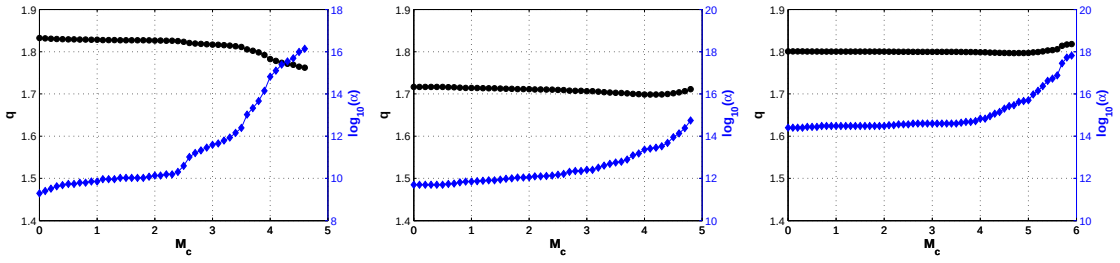

(a) scalp-recorded 1 (b) scalp-recorded 2 (c) scalp-recorded 3

(d) scalp-recorded 4 (e) scalp-recorded 5 (f) scalp-recorded 6

Figure 5.14: Variation of nonextensive parameter q (see black-bullets) and the volumetric energy density α (see blue-rhombuses), for different thresholds of magnitudes of the detected EEG-EQs included in the six scalp-recorded EEG recordings depicted in Fig. 5.12

At this point of analysis, it should be noted that the same method was applied in previous chapters namely for the seismicity and the preseismic kHz EM emissions that refer to the last stage of the EQ generation process. Such analysis further verifies the aforementioned dynamical analogy between the three different kinds of data sources suggesting that similar behaviour has been observed, namely for:

(i) both the intracranial and scalp-recorded EEG recordings, analysed in this chapter

(ii) the regional seismicity observed prior to Athens (Greece) EQ and the L'Aquila (central Italy) EQ, analysed in chapters 3 and 4.

(iii) the observed preseismic kHz EM emissions observed prior to Athens and Italy EQs, analysed in chapters 2 3 and 4.

Reminded that Sarlis et al. [202] have shown that above some magnitude threshold Eq. (5.2) leads to the traditional G-R law through Eq. (5.3). It has been shown that the latter

equation leads to the power-low distribution of magnitudes, expressing the fractal nature of the system under study [203, 249, 200, 118, 30]. Thus in the following section the consistency of results is further examined using the traditional G-R formula, and an alternative method which is based on the mean magnitude of the sample. Such analysis will further verify the validity of the estimations obtained up to now.

5.9 The consistency of results by means of Gutenberg & Richter law

Fig. 5.15, depicts the analysis of the intracranial EEG recordings by means of traditional G-R law (Eq. (1)) above some magnitude threshold (M_c). The experimental data shown in Fig. 5.15 were directly fitted to G-R law for events with magnitude larger than $M_c = 3.69$ and $M_c = 4.17$, yielding $b_{GR} = 0.26 \pm 0.06$ and $b_{GR} = 0.41 \pm 0.08$, respectively.

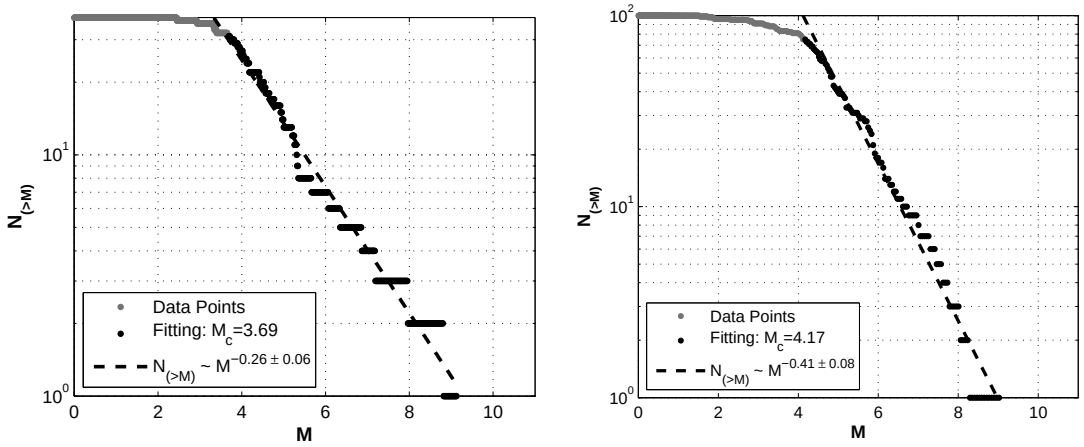

(a) intracranial 1 (b) intracranial 2

Figure 5.15: (a,b) Eq. 1 was used to fit the distribution electric events included in two intracranial EEG recordings depicted in Fig. 5.9. The straight line represents the fitting to the plotted points on a $log(N_{>M})$ vs M diagram by the method of least squares.

As shown by the nonextensive analysis depicted in Fig. 5.9 of Sec. 5.7, the q-parameters that derive from the fitting of Eq. (5.2) to the experimental data of intracranial EEG recordings, leads to an estimated, by Eq. (5.3), $b_{est} = 0.26$ (see Fig. 5.9a) and $b_{est} = 0.42$ (see Fig. 5.9b), respectively. Even more, the estimated b-values that derive from the scalp-recorded EEG recorgings depicted in Fig. 5.12, vary within the range of $b_{est} \in [0.4, 0.68]$. This observation is consistent with recent studies on premonitory behaviour of b-value before EQs which have shown that foreshock temporal EQ series and main shocks are characterized by a much smaller b-exponent ($b < 1.0$) compared to aftershock sequences [92, 128, 172]. In addition, Eq. 1 was also applied on the experimental data of the scalp-recorded EEG recordings shown in Fig.

5.12, yielding: $b_{GR} = 0.43 \pm 0.11$, $b_{GR} = 0.82 \pm 0.14$, $b_{GR} = 0.46 \pm 0.07$, $b_{GR} = 0.85 \pm 0.09$, $b_{GR} = 0.4 \pm 0.1$, $b_{GR} = 0.59 \pm 0.09$, respectively. The latter b-values are consistent with the estimated ones deriving from Eq. (5.3).

Paradimitriou et al. [172] who studied the EM-EQs included the preseismic kHz EM time series observed prior to Athens (Greece) EQ (see Sec. 5.8), found that they follow the G-R law with a b-value of 0.51. As regards the energy, Rabinovitch et al. [192] who studied the fractal nature of EM radiation induced by uni-axial and tri-axial rock fracture, have found that the amplitudes of the pre-fracture EM timeseries, follows a "Gutenberg-Richter type" law with a b-value of 0.62. Additionally, in the present study the energies, E, of the electrical pulses included in the single rat ES and in a human ES were found to follow the power-law $N(>E) \sim E^{-0.62}$ and $N(>E) \sim E^{-0.72}$, respectively, or equivalently, the power-law $N(E) \sim E^{-1.62}$ and $N(E) \sim E^{-1.72}$ (analysis was published in [64]).

Herein it should be noted that the value of b included in the traditional G-R Eq. (1) for a given group of EQs, is determined usually from the slope of a straight line fitted to the plotted points on a $log(N_{>M})$ vs M diagram by the method of least squares. However, such determination of $b-value$ may give inaccurate results that are subjected to the following criticisms [252, 258]: (i) the ordinary least squares method gives too heavy weight to the points for large magnitude. (ii) different b-values are obtained according to the choice of the length of interval ΔM of magnitude in classifying EQs. Further criticisms can be raised concerning the need for the determination of the magnitude cut-off completeness threshold, which is also a crucial choice for estimating the slope that refers to the linear part of the $log(N_{>M})$ vs M distribution of the experimental data. On the other hand the nonextensive Eq. (5.2) seems to be superior to the traditional G-R one since the characteristic value that governs the overall system is the one that corresponds to the smaller magnitude threshold.

On these grounds, along with the prospect to ensure the validity of the above mentioned results, in the following section, an alternative method for the estimation of the value of b in Eq. (1) is examined for the first time. This formula has been widely used in statistical seismology and has proved its superiority in contrast to the traditional G-R law for a large number of regions under study [252, 253, 255, 256, 258].

5.10 Dynamical analogy between ESs and EQs: an alternative approach which derives from statistical seismology

Utsu on 1965 [253], proposed an alternative method for determining the b-value of the Gutenberg & Richter formula, showing that it is inversely proportional to the mean magnitude $\overline{M}$,

given the minimum magnitude, M_{min}, of the EQ magnitudes. More precisely, if the magnitude frequency distribution of EQs obey the Gutenberg-Richter law, we get the following approximate relation for the moment of order n:

$$\sum_{i=1}^{N} (M_i - M_c)^n \approx \frac{N\Gamma(n+1)}{(b\ln 10)^n} \tag{5.6}$$

where, N is the total number of EQs and M_c is the smallest magnitude in the sample. For the case of $n = 1$, Eq. (5.6), is given by:

$$b = \frac{N\log_{10} e}{\sum_{i=1}^{N} M_i - NM_c} = \frac{\log_{10} e}{\overline{M} - M_c} \tag{5.7}$$

where $\overline{M}$ is the average magnitude and M_c is the minimum magnitude in a sample. At the same year, Aki [3] showed that Eq. (5.7), is equivalent to the maximum likelihood estimation, and provided the confidence limits for this estimation from a given sample. For the case where there is no uncertainty in magnitude, the approximate 95% confidence limit of b is $\pm 1.96(b/\sqrt{N})$. Later on, Utsu (1966) [254] suggested slight modification of Eq. (5.7) addressing the use of the binned magnitudes. The final equation reads as follows:

$$b_{utsu} = \frac{\log_{10} e}{\overline{M} - (M_c - \frac{\Delta M}{2})} \tag{5.8}$$

where, ΔM, is the lowest binned magnitude in the sample.

It has been shown that the latter equation gives unique, unbiased and accurate estimation of b-values [258]. Characteristically, Monte Carlo simulations applied on Eq. (5.8) have shown that this method is superior to the least squares estimation of the b-value in the case of $N = 50 \sim 100$ samples at least [252, 253, 255, 256]. Another strength is that it does not require any fitting process but only a good approximation of the cut-off completeness threshold which in turn can be found from the G-R distribution of the experimental data.

Herein, it is recalled that studies on premonitory behavior of b-value before EQs which have shown that foreshock temporal EQ series and main shocks are characterized by a much smaller b-exponent ($b < 1.0$) compared to aftershock sequences [92, 128], while several studies from different disciplines have shown this corresponding behavior of the b-value [64, 192, 123, 172]. Characteristically, [174] who studied the foreshock seismicity prior to L'Aquila EQ (see Sec. 4.3) in terms of Eq. (5.8), found that in the last 10 days before the mainshock, the b-value dropped significantly to $b = 0.68$.

On these grounds, the present study examines the applicability of Eq. (5.8) to the study of epileptic EEG recordings, in order to explore the consistency of results of this alternative

approach with those retrieved when using the traditional G-R law. In addition, since the nonextensive formula leads to the G-R law through the [202] equation (5.3), a comparative study of b-values is applied. Such analysis aims to subsequently enhance the validity of the nonextensive formula, on the one hand, and further elucidate the suggested dynamical analogy between the two phenomena (EQs and ESs), on the other. Table 5.1 shows a comparative list of the calculated b-values derived from equations (1), (5.3) and (5.8) applied on both the experimental data of the intracranial EEGs depicted in Fig. 5.9 and the scalp-recorded ones depicted in Fig. 5.12. It is observed that the later Eq. (5.8) provides similar b-values with those deriving from the rest two equations, ranging within the interval $b_{utsu} \in [0.27, 0.76]$. This similarity indicates the consistency with the theoretical background supported from equations (1) and (5.3).

Table 5.1: Comparative table between Equations (1),(5.3) and (5.8)

specimen	$b_{GR}, Eq.(1)$	$b_{est}, Eq.(5.3)$	b_{utsu}, Eq. (5.8)
intracranial 1	0.26 ± 0.06	0.26	0.27
intracranial 2	0.41 ± 0.08	0.42	0.33
scalp-recorded 1	0.43 ± 0.11	0.40	0.38
scalp-recorded 2	0.82 ± 0.14	0.78	0.76
scalp-recorded 3	0.46 ± 0.07	0.50	0.40
scalp-recorded 4	0.85 ± 0.09	0.80	0.64
scalp-recorded 5	0.40 ± 0.10	0.37	0.38
scalp-recorded 6	0.59 ± 0.09	0.68	0.47

Expanding on the relevance of Eq. (5.8) to the study of ESs, the analysis of table 5.1 is applied on all the electrodes used for each one of the two intracranial EEG recordings depicted in Fig. 5.9. Fig. 5.16 shows two scatter plots of the calculated relationship between the obtained b-values and q-parameters. More precisely, the relation between the nonextensive q-parameter and the b-value associated with the G-R formula (Eq. (1)) has been given by [202] (see Eq. (5.3)). In Fig. 5.16 the solid blue line, depicts this theoretical relationship, indicating that the higher the nonextensivity, the lower the associated b-value. Note that the lower b-values express the increase of accumulated stresses in the region under study. The black marks indicate the b-values calculated directly from Eq. (1) (G-R formula), corresponding to the q-values calculated respectively. The blue marks indicate the b-values calculated directly from Eq. (5.3) (Sarlis formula) while the square-marks refer to Eq. (5.8) (Utsu Formula). As observed in Fig. 5.16, most of the b-values that derive from Eq. (1) and (5.8) are very close to the theoretical ones (see solid line) indicating the consistency with Eq. (5.3). Note that for the estimation of b-values related to equations (1) and (5.8), the same cut-off completeness threshold M_c was applied, which is mainly determined by the experimental data that refer to

the linear part of the $log(N_{>M})$ vs M distribution of the G-R law representation.

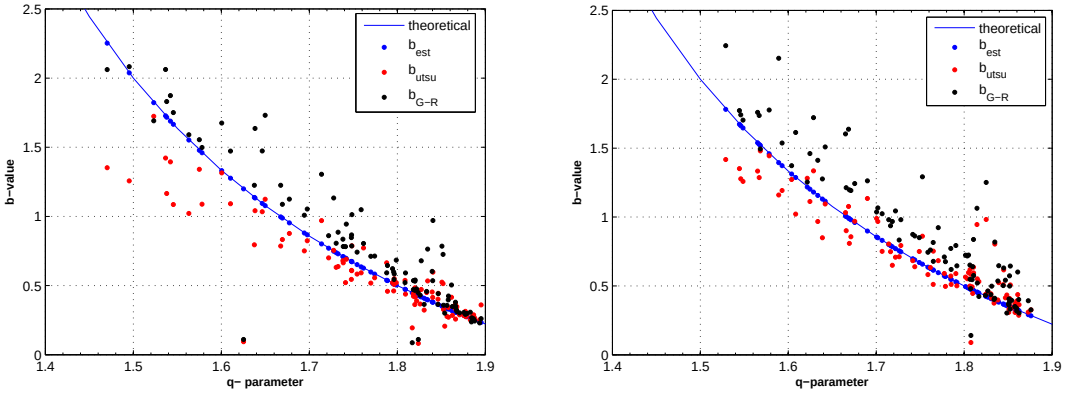

(a) intracranial 1 (b) intracranial 2

Figure 5.16: Scatter plot of the calculated relationship between the b-value and q-parameter. The blue line refers to the theoretical curve of Eq. (5.3). The blue, red and black bullets refer to the estimated b-values calculated from equations (5.3)(5.8) and (1) respectively.

Following on this line of analysis, Table 5.2 provides a quantitative expression of the close relevance of experimental results to the theoretical background this study deals with. Specifically, we present the percentage analysis of the calculated parameters that derive from the three aforementioned equations. As shown for the first intracranial EEG (Fig. 5.16a), 82% of the calculated electrodes gave a $b_{est} < 1$, 84% gave $b_{utsu} < 1$ and 74% gave $b_{G-R} < 1$, respectively. As concerns the q-parameter, 89% of the calculated electrodes were found with $q \geq 1.6$. For the second intracranial EEG recording (Fig. 5.16b), we get 66% of $b_{est} < 1$, 79% of $b_{utsu} < 1$, 80% of $b_{G-R} < 1$ and 89% of $q \geq 1.6$ respectively.

Table 5.2: Comparative table between Equations (1),(5.3) and (5.8), percentage results

specimen	$b_{GR} < 1$, Eq. (1)	$b_{est} < 1$, Eq. (5.3)	$b_{utsu} < 1$, Eq. (5.8)	$q \geq 1.6$,
intracranial 1	74%	82%	84%	89%
intracranial 2	66%	79%	80%	89%

The latter quantitative results reveal that more than $\approx 80\%$ of the electrodes are consistent with the "scale free" nature of the ES phenomenon under study. This suggestion is justified in the present analysis by nonextensive dynamics and the three formulas related with the b-value estimation. Moreover, the scalp-recorded EEG recordings have also revealed similar behaviour with the intracranial ones as shown in Sec. 5.8.

A crucial differentiation here is that the electrodes of an intracranial EEG recordings are mainly located very near to the brain area that is considered to be the possible source of the

ES problem. The selection of this area mainly results from examinations applied to the patient using scalp-recorded EEG recordings or even tomographic methods that may reveal a possible pathogenesis. On the contrary the electrodes that refer to scalp-recorded EEG recordings are mainly located over an area that covers the most part of the brain activity, according to the 10-20 electrode placement system [101]. A crucial importance in this differentiation is that the intracranial EEG recordings are actually refer to the "regional seismicity" of the brain activity, namely the EEG-EQs over the possible epicenter of the pathogenic region in contrast to the scalp-recorded which refer to a greater region of interest. Thus from the perspective of self-affinity, we have evidence of similar behaviour by two different scales of brain. It seems that the self-affine nature of "fracture and faulting in the brain" can be adequately explained by the nonextensive equation (Eq. 5.2), as well as from the traditional G-R law (Eq. 1) which leads to the power-low distribution of magnitudes [203, 249, 200, 118, 30]. Such analysis provides a preliminary indication that further verifies the self-affine nature of ESs, at two different scales of regional brain activity.

Summarizing at this point of analysis, the existence of dynamical analogy between earthquake dynamics and neurodynamics has been further supported in this work by means of the nonextensive Eq. (5.2) on one hand and an alternative formula (Eq. (5.8)) which is based on the mean magnitude of the sample. The applicability of such models for EQ dynamics in epileptic seizures indicates that such phenomena obey laws which have the property of "self-similarity" or "scale-invariance". This means that these laws are universal in the sense that the shape of the distribution of physical quantities such as magnitudes of EEG-EQs examined in this study are "scale-free" or insensitive to fluctuations in the scale at which they are observed [168]. This implies that they do not depend on details concerning the actual species [64].

5.11 Discussion & Conclusions

Numerous authors have reported strong analogies between earthquake dynamics and neurodynamics suggesting that epileptic and seismic crises can be analyzed within similar mathematical frameworks [107, 105, 197, 122, 169, 64]. Motivated by the universal principles rooted in disparate problems ranging from particle physics to economies of societies, the main interest in this study was the dynamics of complex systems [20, 220, 221, 214, 265, 266, 180, 45, 131, 214, 2, 76, 176]. In this direction, analysis in this chapter revealed both spatially and temporally, common "pathological symptoms" governing the generation of two seemingly different extreme events: epileptic seizures and earthquakes. More precisely, using entropic metrics such as T-Entropy [244] and nonextensive Tsallis entropy [245], it was found that the generation of

a single epileptic seizure/earthquake is accompanied by the appearance of higher organization. In addition using the Rescaled Range Analysis method [109], it was found that the underlying generation process is also characterized by persistent behaviour revealing a positive feedback mechanism that reflects the leading of complex systems out of equilibrium.

Drawing from a model for EQ dynamics which is routed on the concepts of nonextensive statistical mechanics, the present work reports further evidence that a dynamical analogy exists between the generation of a single epileptic seizure and an EQ. More precisely, it was shown that a recently introduced nonextensive formula for EQ dynamics which leads to a Gutenberg-Richter type law for the magnitude distribution of EQs (formula 5.2), can adequately describe (with 89%, $q \geq 1.6$) the electric events included in a single epileptic seizure not only for the EEG-EQs included in the scalp-recorded EEGs [64] but also for the intracranial ones.

The latter formula is directly connected to the traditional G-R law (Eq. 1), above some magnitude threshold through Eq. (5.3), which in turn leads to the power-low distribution of magnitudes, expressing the fractal nature of the system under study [203, 249, 200, 118, 30]. In this direction, the results of this study were further supported with an alternative formula which is based on the maximum likelihood estimation of the b-value included in the G-R law (see Eq. (5.8)), providing first indication of similar b-values (with approximately 80%, $b < 1$) with those deriving from Eq. (5.3) and the G-R formula.

Applying different thresholds of EEG-EQ magnitudes contained in both types of EEG recordings under study, it was found similar behaviour of the parameters included in the nonextensive formula with that founded on the analysis of the regional seismicity around the epicenter of large EQs [228, 159], and the EM-EQs contained on the preseismic kHz EM emissions which refer to the last stage of the generation process of EQs [158]. From the perspective of self-affinity, the different placement (spatially) of the electrodes of scalp-recorded and intracranial EEG recordings provides a relevant framework to examine the fractal nature of such phenomena at two different scales of the regional ES activity in the brain. This similarity further enhances the common scale-free nature of such phenomena and provides a preliminary indication of the self-affine nature of the regional (ES) activity in the brain, in terms of nonextensive dynamics.

Summarizing at this point, this work comes to further verify the suggestion that as long as similar properties and common distinctive features can be found in the two types of extreme events, it may be possible to draw on identified dynamic analogies in order to utilize transferable ideas and methods [168, 64]. Such analysis further enhances the aforementioned dynamical analogy suggesting that more exhaustive study of the aforementioned biological and geophysical shocks in terms of nonextensive Tsalis statistics is needed to give a deeper interpretation of

their generation. Results and insights from the study of epileptic seizures may provide useful approaches that can feed back into the analysis of EQs and vise versa.

Chapter 6

Spatiotemporal analysis of catastrophic phenomena: a set of proposed formulas

As we have seen so far form the analysis in previous chapters, a number of complex systems under study are governed by laws that have the property of "self-similarity" or "scale-invariance" [203, 249, 200, 118, 30, 168], such as: the Gutenberg & Richter Law and the fractional power law relationship. Earthquakes (EQs), preseismic kHz electromagnetic (EM) emissions and epileptic seizures (ESs) examined in this study, seem to follow these universal laws. The great variability of such systems is a crucial feature that complicates the study of such phenomena, especially when different regimes coexist during their generation process. For the most part of the literature review, the statistical tests and the energy calculations are of the most fundamental subjects, deriving through empirical Gutenberg-Richter energy-magnitude relationships. Although the precise physical significance of these relationships is somewhat uncertain, several attempts have been made from scientists to give a proper interpretation of the generation mechanism that exists behind a catastrophic phenomenon [88, 119, 29, 218]. This chapter addresses a number of concerns raised during the course of this research. With a view to consider a different approach on key theoretical principles associated with the generation process of catastrophic phenomena, analysis here is focused on parameters such as: the energy of EQs, the mean and maximum magnitude of the sample, the probability that two samples may come from the same population, and the long-range correlations in terms of a nonextensive model for EQ dynamics. Such an attempt aims to contribute to the knowledge of natural phenomena, providing a few more ways for their interpretation.

6.1 Relation between energy and mean magnitude of the sample

The present section deals with the analysis of seismicity catalogues within the framework of nonextensive Tsallis statistical mechanics, namely the revised version of a recently introduced model for EQ dynamics [218, 208], analytically described in Chapter 2. The non-extensive Gutenberg & Richter type formula which describes the earthquake (EQ) dynamics has been analytically described in Chapter 2. The entropic index q included in the non-extensive Gutenberg & Richter type formula (see Eq. (2), describes the deviation of Tsallis entropy from the standard Boltzmann-Gibbs entropy. The corresponding physical quantity α, is the constant of proportionality between the EQ energy, ε, and the size of fragment r.

As already mentioned in previous chapters, the relation between these two parameters is still an open issue since a relative mirroring behaviour was found due to the analysis in this study. This observation has also been justified from a previous study on regional seismicity in terms of the nonextensive model for EQ dynamics [155]. Specifically, Matcharashvili et. al [155], who studied the temporal evolution of both the q-parameter and the energy α mentioned that when a strong EQ occurs and much more correlated behavior of the system constituents is assumed to take place, the emergence of short and long range correlations is reflected in an increase of the nonextensive parameter q. On the contrary, lower nonextensive q-parameter indicates that the amount of accumulated stress is not yet enough to initiate a correlated behavior of the whole system under study. Concerning the energy, decreases of α are associated to activated movements of large size fragments, as opposed to quiet periods, when accumulated stress energy is mostly released through the relative movement of small fragments [155]. Additionally, Telesca (2010) [227] who studied the Italian territory by means of the nonextensive model, suggested that differences in q may characterise different EQ triggering mechanisms, namely, stick-slip-like for low q values and a fragment-asperity interaction-type for high values of q respectively.

Herein a challenging issue would be to examine the spatial variation of the nonextensive parameter q and the volumetric energy density α, in order to have an overall view that may elucidate the underlying relation. Two data sources were used in order to ensure that the results of this study are applicable in different regions of the globe: (i) the Greek seismicity catalog deriving from the website of the National Observatory of Athens (NOA) during the period from 01/01/1990 to 31/12/2009, and (ii) the Southern California catalogue of the *Southern California Earthquake Data Center (SCEDC)* (`http://www.data.scec.org/research-tools/alt-2011-dd-hauksson-yang-shearer.html`), from 1981 to 2011 [96].

6.1.1 Analysis of the Greek earthquake catalogue

Eq. (2) was used to examine the spatial variation of the nonextensive q-parameter and the volumetric energy density α, for the Greek seismicity included in the period from 01-Jan-1990 00:00:00 to 01-Jan-2011 00:00:00. The Greek territory was scanned using a shift of 0.2° in longitude and latitude, as shown in Fig. 6.1.

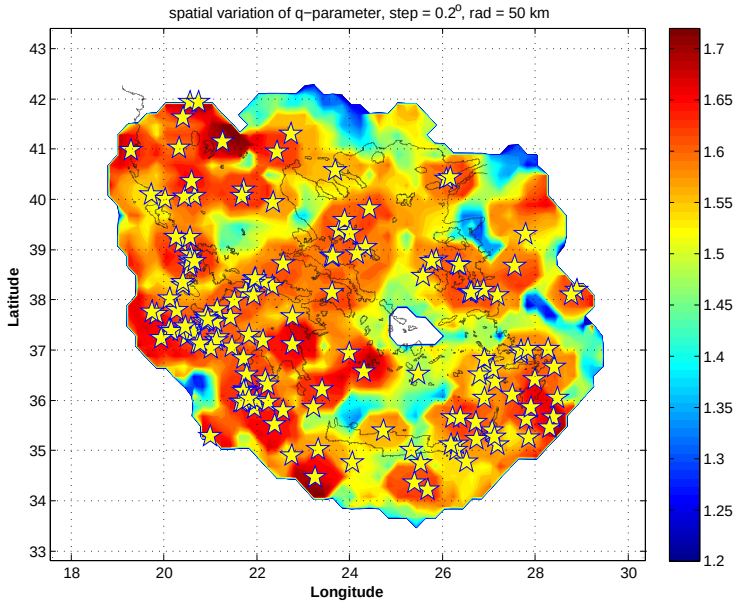

(a)

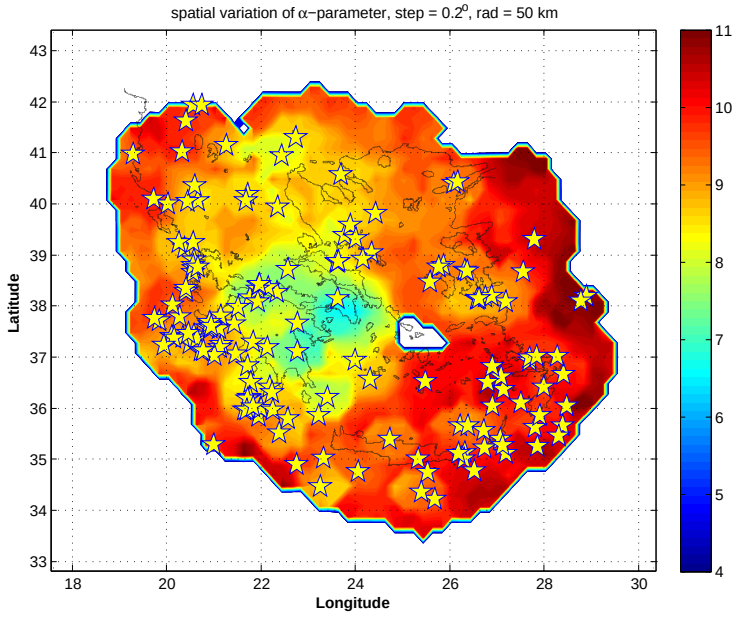

(b)

Figure 6.1: Spatial distribution of the nonextensive q-parameter and the volumetric energy density α, for the Greek seismicity included in the period from 01-Jan-1990 00:00:00 to 01-Jan-2011 00:00:00. The star-marks indicate the EQs with magnitude larger or equal than $5.0M_L$. The colored bars indicate the variation range of q and α respectively.

Herein, a spatial area of approximately 50 km around each relative point was examined. For each calculation, the obtained parameters were graphically placed at the center of each scanned area with different colors. A minimum number of 50 events was used as a criterion for the statistical completeness of each calculation. The Levenberg-Marquardt (LM) method [142, 152] was applied in order to achieve an efficient and accurate fit for the estimation of the nonextensive parameter q. Fig. 6.1 shows a contour plot of the spatial distribution of q-parameter and energy α. The star-marks indicate the EQs with magnitude larger or equal than $5.0M_L$. From Fig. 6.1a, it is observed that in geographic areas that have experienced with large EQs, the nonextensive parameter q presents higher values in contrast to the rest of the areas under study. On the contrary, the spatial distribution of the volumetric energy density α (see fig. 6.1b), presents both lower and higher values within the geographic areas where large EQs have occurred, resulting to a mirroring behaviour in contrast to the $q-parameter$. A characteristic example, is the cluster of large EQs ($> 5.0M_L$) contained in the south-east part of Greece which presents both high nonextensivity and high energy density α. On the other hand, the cluster of large EQs contained in the central-west part of Greece presents high nonextensivity and lower values of energy density α. Similar alternations can also be observed between other regions of Greece.

Drawing from these results, a challenging issue is to examine the way in which the occurrence of larger EQs reflects to an increase of nonextensivity on one hand and to further elucidate which regions reflect the above mentioned alternations of energy α, in relation to the nonextensive parameter q, on the other hand. Thus, an appropriate framework for such an analysis would be to examine the behaviour of these parameters in comparison to the maximum (M_{max}) and average magnitude (M_{av}) of the EQs contained in each one of the calculated areas derived from the spatial method, as applied in Fig. 6.1. Fig. 6.2, shows the scatter plots for each pair of the aforementioned parameters. Indeed, from Fig. 6.2a it is observed that the areas which contain large EQs ($M_{max} \geq 4.7$, see red-asterisks), present constantly higher values of nonextensivity ranging from $1.4-1.75$. On the contrary, the areas that contain lower values of the maximum magnitude ($M_{max} < 4.7$, see black-bullets), seem to be divided in two classes: those that develop relative higher nonextensivity and those which do not. However, the situation changes for the case of the comparison between the average magnitude (M_{av}) and the q-parameter, as shown in the scatter plot of Fig. 6.2b. It is observed that although both populations are characterized with different levels of nonextensivity, their average magnitude (M_{av}) does not seem to distinguish as well this feature, where similar values of M_{av} are observed in both populations. Furthermore, a crucial observation obtained from fig. 6.2b,

is that the population of the areas that contain smaller EQs ($M_{max} < 4.7$, see black-bullets), present higher nonextensivity at lower values of average magnitude, and lower nonextensivity at higher values of average magnitudes. On the contrary, this mirroring behavior is much less for the population of the areas that contain larger EQs ($M_{max} \geq 4.7$, see red-asterisks), which in turn present relative higher nonextensivity at all scales of average magnitude (M_{av}). In other words, this can be expressed as: *"the smaller the maximum magnitude of EQs within the area under study, the larger the mirroring alternations between the average magnitude and the nonextensivity."*

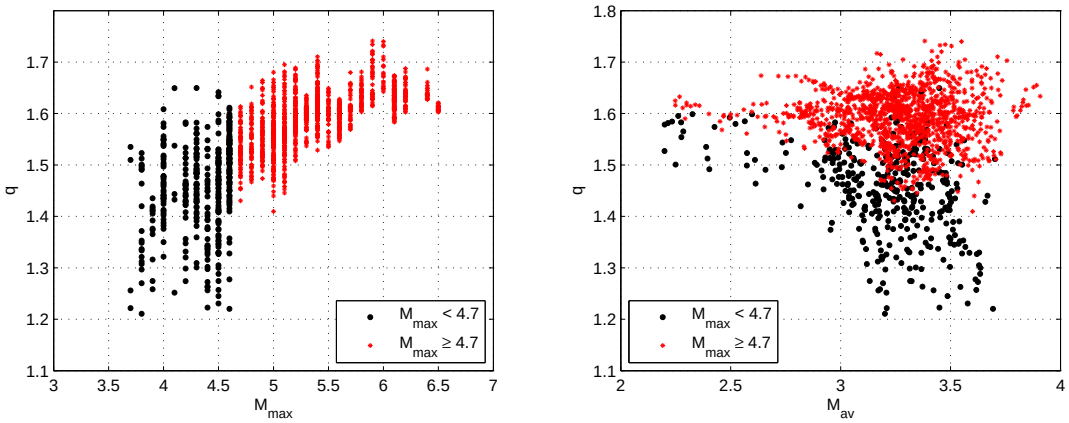

(a) (b)

Figure 6.2: (a) depicts the scatter plot between the nonextensive parameter q and the maximum magnitude of the EQs contained in each one of the calculated areas derived from the spatial method applied in fig. 6.1. (b) depicts the scatter plot between the q-parameter and the mean magnitude, respectively. The red-asterisks refer to the areas that contain EQs with $M_{max} \geq 4.7$, and the black-bullets refer to the areas that contain EQs with $M_{max} < 4.7$.

Since the seismic energy E released during an earthquake is related to the magnitude through $E \sim 10^{cM}$, where c is around 1.5 [120], the same comparison, between the spatial variation of the volumetric energy density α, and the parameters (M_{max}) and (M_{av}) was also applied, in the prospect to further examine the way in which the existence of larger EQs reflects to an increase (or to a decrease) of the levels of energy density, as revealed from Fig. 6.1. In Fig. 6.3, the scatter plots for each pair of the parameters: $log_{10}(\alpha) \sim M_{max}$ and $log_{10}(\alpha) \sim M_{av}$, are presented.

Focusing on Fig. 6.3a, it is observed that for higher maximum magnitude rates there is a relative decrease of the energy α. On the other hand, although the relation between $log_{10}(\alpha)$ and M_{max} is not depicted so clear for lower, intermediate and higher values of maximum magnitudes, it seems that for lower values of M_{max} there is a relative increase of the energy.

This evidence reveals that the value of maximum magnitude of EQs contained in the area under study seems to affect in a mirroring way the volumetric energy density of the system where this transition is observed at a specific magnitude threshold ($M = 4.7$). Moreover, it also seems to affect the levels of nonextensivity of a system, namely, the short-long range correlations developed between its entities, for higher values. On the other hand, from Fig. 6.3b, a linear relation between the average magnitude M_{av} and the logarithmic expression of the energy density α, is observed. More specifically, this can be expressed as: *"the larger the mean magnitude of the EQs within the area under study, the larger the volumetric energy density α"*. Furthermore, it is also observed that the regions that contain lower values of maximum magnitude cover the upper diagonal part of the linear distribution (see black-bullets in Fig. 6.3b), while larger values of M_{max} cover the lower diagonal part of this distribution (see the red-asterisks in Fig. 6.3b).

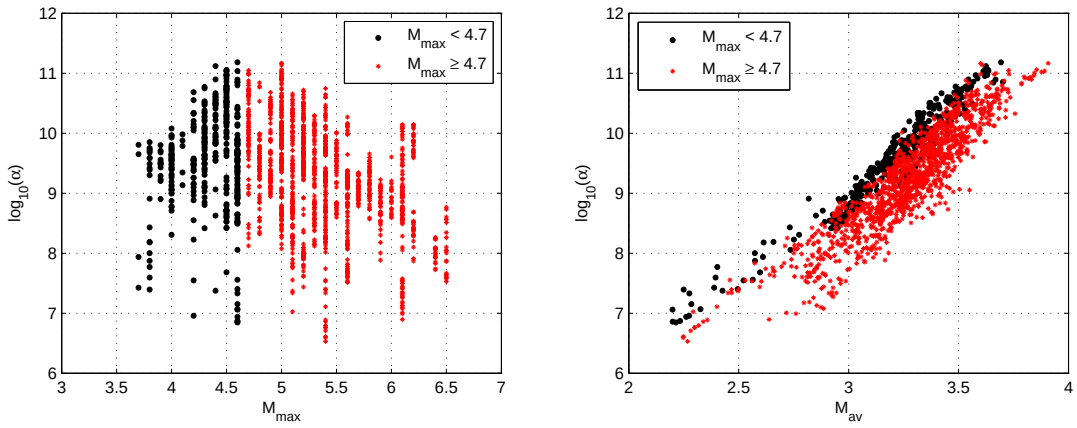

(a) (b)

Figure 6.3: (a) Scatter plot between the volumetric energy density α and the maximum magnitude M_{max} of the EQs contained in each one of the calculated areas derived from the spatial method applied in fig. 6.1. (b) Scatter plot between α and the average magnitude M_{av}. The red-asterisks refer to the areas with $M_{max} \geq 4.7$, and the black-bullets refer to those with $M_{max} < 4.7$.

Finally, since the main perspective in this work is to examine the relation between the nonextensive q-parameter and the volumetric energy density α, in order to explain the underlying mirroring behaviour, in Fig. 6.4 a scatter plot is presented depicting the corresponding values obtained from the spatial analysis of the Greek EQ catalog. As it is observed from Fig. 6.4, the higher alternations of energy are observed in regions that contain lower maximum magnitudes and in contrast to those that contain larger EQs. This insufficient behaviour is very similar with that described for Fig. 6.2b. However this was an expected result since there is linear relation between $log_{10}(\alpha)$ and the average magnitude M_{av} as shown in Fig. 6.3b.

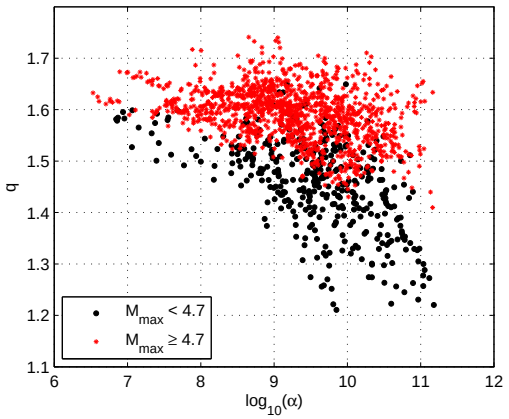

Figure 6.4: Scatter plot between the volumetric energy density α and the nonextensive q-parameter of the EQs contained in each one of the calculated areas derived from the spatial method applied in fig. 6.1. The red-asterisks refer to the areas that contain EQs with $M_{max} \geq 4.7$, and the black-bullets refer to the areas that contain EQs with $M_{max} < 4.7$.

At this point of analysis, the empirical findings of this work suggest that the logarithmic expression of the energy distribution of earthquakes is mostly dependent from the average magnitude (M_{av}) of the sample in a linear way, while the maximum magnitude seems to affect this expression in a mirroring way. Indeed, according to Utsu formula [252], the b-value obtained from the traditional Gutenberg & Richter equation ($\log N(> M) = \alpha - bm$) is inversely proportional to the mean magnitude M_{av}, given the minimum magnitude, M_{min}, of the EQ series under study [253, 3] as follows:

$$M_{av} \sim M_{min} + 1/2.3b \tag{6.1}$$

Thus, working the b-value is equivalent to working on the mean magnitude of the sample under study. Since the lower b-values express the increase of accumulated stresses in the region under study, the linear relation between M_{av} and $log_{10}(\alpha)$ obtained from fig. 6.3b, reveals that the lower the accumulated stresses that sustain the system the lower the energy density α. However in order to further verify this hypothesis, analysis in the following section focuses on the Southern California EQ catalogue.

6.1.2 Analysis of the Southern California EQ catalogue

Herein, the same spatial analysis with that on previous section was also performed for the case of Southern California EQ catalogue. It should be noted that this catalogue is a revised (relocated) version which is considered to be more accurate in contrast to the Greek EQ catalogue. The Southern California has experienced with large EQs coming from the well

known San Andreas Fault [242] which is a part of an active transform fault zone that connects the Pacific tectonic plate with the North American tectonic plate. The relative motions of these plates have been generated a series of EQs of significant size and interest [13] as shown in Fig. 6.5.

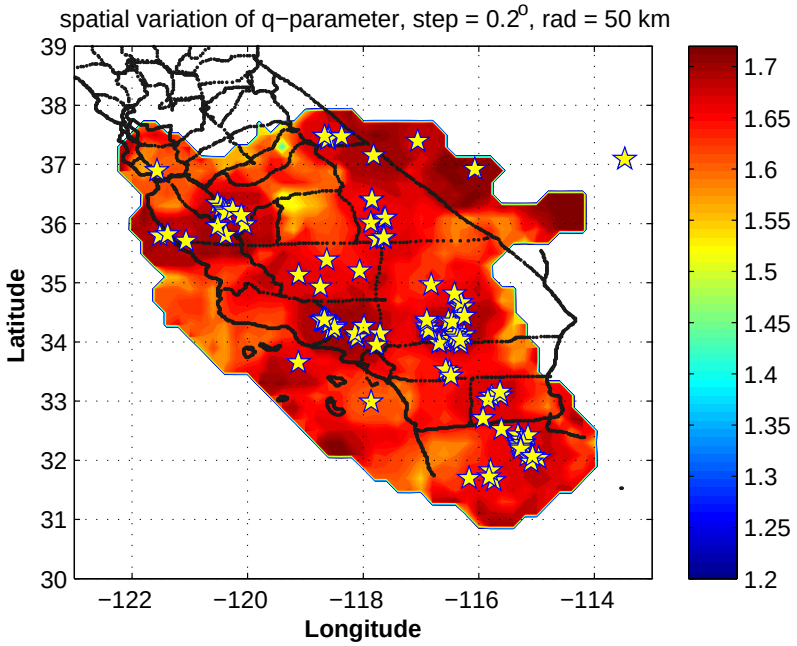

(a)

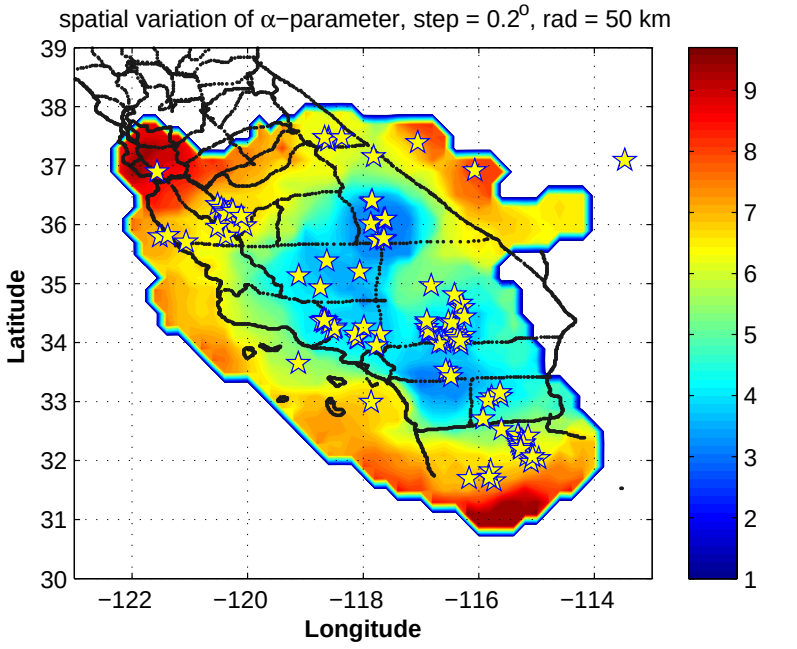

(b)

Figure 6.5: Spatial distribution of the nonextensive q-parameter and the volumetric energy density α, for the Southern California seismicity included in the period from 1981 to 2011. The star-marks indicate the EQs with magnitude larger or equal than $5.0M_L$. The colored bars indicate the variation range of q and α respectively.

The underlying mirroring behaviour between the two parameters, namely q and α, is also observed for the seismicity included across the central part of the map. On the contrary, although the data from the Northern California are missing, for the north-west part of the map this feature is not observed. Special attention should be given to the fact that the overall area of Southern California presents higher rates of nonextensivity in contrast to the Greek seismicity ($q \gtrsim 1.5$). In Fig. 6.6, the scatter plots between the maximum magnitude M_{max} and mean magnitude M_{av} versus the nonextensive parameter q are presented.

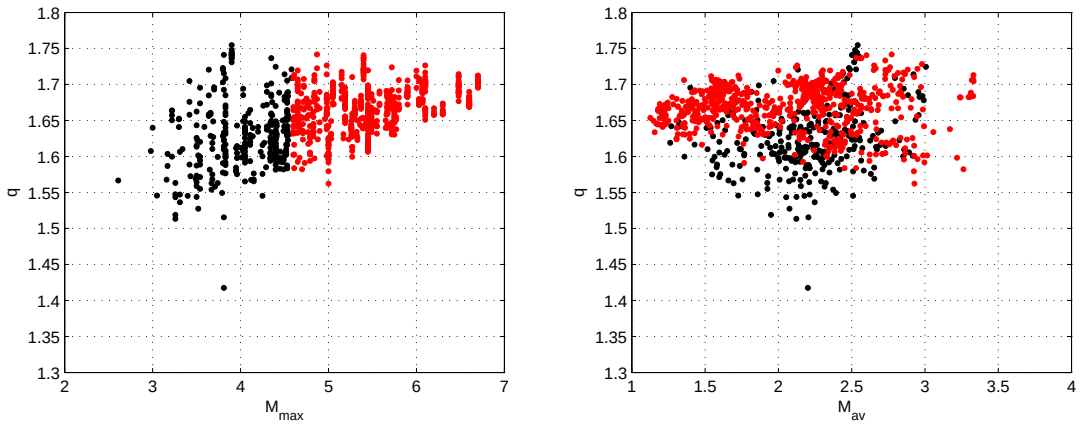

(a) (b)

Figure 6.6: (a) depicts the scatter plot between the nonextensive parameter q and the maximum magnitude of the EQs contained in each one of the calculated areas derived from the spatial method applied in fig. 6.1. (b) depicts the scatter plot between the q-parameter and the mean magnitude, respectively. The red-asterisks refer to the areas that contain EQs with $M_{max} \geq 4.7$, and the black-bullets refer to the areas that contain EQs with $M_{max} < 4.7$.

According to nonextensive model, the smaller fragments are those that increase the correlated behaviour of the system, thus it is expected that smaller earthquakes should be found in the seismicity under study. Indeed, it is observed that the mean magnitude varies within the interval $M_{av} \in [1.1, 3.4]$ while for the case of Greek Catalog varies within the interval $M_{av} \in [2.2, 3.8]$. This observation verifies the aforementioned suggestion. Moreover, comparing the results with those obtained fro the case of the Greek catalogue, it is observed all the parameters behave in the same way with a minor difference in Fig. 6.6b, at lower q-values where the mirroring range between q and m_{av} is less in contrast to the Greek catalog: $q_{greece} \in [1.2, 1.75]$ and $q_{clifornia} \in [1.5, 1, 75]$. This narrowness of the variation range of the distribution of the experimental data is also obvious in 6.6a. However the shape and the information that we get is the same with that of the Greek catalogue.

In Fig 6.7, the scatter plots between the maximum magnitude M_{max} and mean magnitude

M_{av} versus the energy density α are presented. It is observed that for lower maximum magnitudes ($M \leq 4.7$) there is a relative gradually increment as the as the maximum magnitude increases. This can be justified by the linear fitting of the experimental data depicted with black bullets. On the contrary for larger maximum magnitudes included in each sample under study, the energy is gradually decreases as shown for the linear fitting applied on the experimental data depicted with red bullets. It should be noticed that the threshold of $M = 4.7$ that characterizes the transition from one state to the other, was empirically estimated and was found to be the same as that for the case of the Greek catalogue. However, the relation between $log_{10}(\alpha)$ and M_{max} is not depicted so clear for lower, intermediate and higher values of maximum magnitudes as for the case of the Greek catalogue. There is a variety of energies observed fluctuating in the order of $\approx 10^4$, that characterizes the variety of the morphology of the occurring fractures. Focusing on Fig. 6.7b, a crucial characteristic that it is observed, is the linear relation between the logarithmic expression of the energy α and the mean magnitude M_{av}. This linearity has been also observed due to the analysis of the Greek catalogue. Moreover the observed thickness of the distribution of the experimental data strongly verifies the underlying relation.

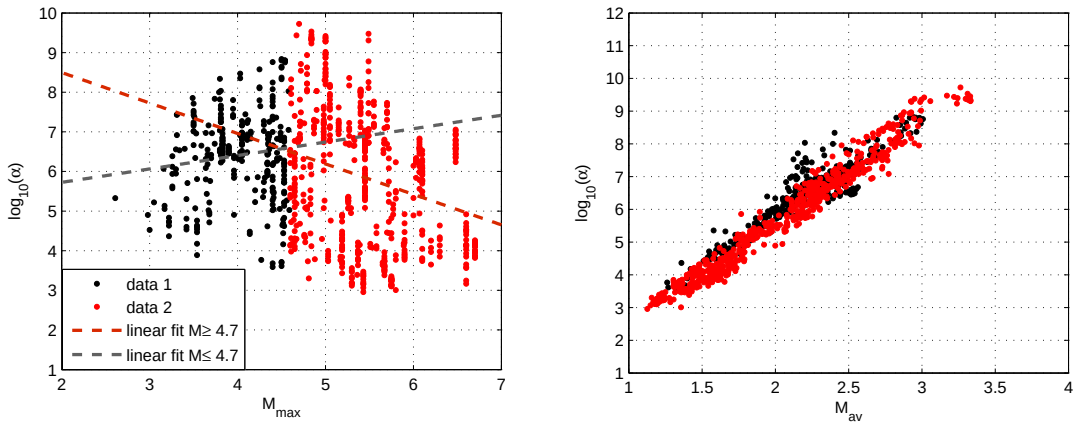

(a) (b)

Figure 6.7: (a) Scatter plot between the volumetric energy density α and the maximum magnitude M_{max} and the average magnitude M_{av}, for the case of Southern California catalogue. The red-asterisks refer to the areas with $M_{max} \geq 4.7$, and the black-bullets refer to those with $M_{max} < 4.7$.

Finally, in Fig. 6.8, the scatter plot between the volumetric energy density α and the nonextensive q-parameter is depicted, showing the aforementioned consistency with Fig. 6.6b, as described in previous section, for the case of Greek catalogue. Herein, it should be noted that the relative difference observed on the areas that contain EQs with $M_{max} < 4.7$ (black-bullets) is mainly due to the different way in which the EQ epicenters are produced. The accuracy of

California catalogue in contrast to the Greek catalogue has been repeatably mentioned by the literature [173, 174, 13, 242]. Thus the results obtained here are more consistent in contrast to those obtained from the case of Greek catalogue. Moreover, on 2001 the Geodynamic Institute of Greece has upgraded the technology related to the estimation of EQ magnitudes/epicenters providing more accurate estimations in contrast to previous years. Nevertheless, the overall observations are consistent with the theoretical framework this study deals with.

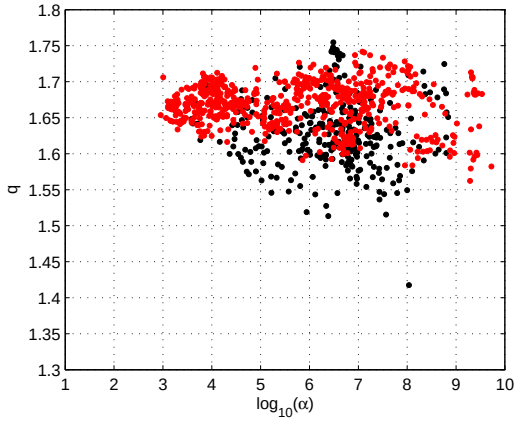

(a)

Figure 6.8: Scatter plot between the volumetric energy density α and the nonextensive q-parameter of the EQs contained in each one of the calculated areas derived from the spatial method applied in fig. 6.1. The red-asterisks refer to the areas that contain EQs with $M_{max} \geq 4.7$, and the black-bullets refer to the areas that contain EQs with $M_{max} < 4.7$.

Against these results, a possible empirical relation between the energy α and the mean magnitude M_{av} of the sample under study should read as follows:

$$log_{10}(\alpha) = b_x \; M_{av} + c, \tag{6.2}$$

where $log_{10}(\alpha)$ is the logarithmic expression of the volumetric energy density α, M_{av} the mean magnitude of the sample and b_x the slope of the linear regression fitting of the experimental data. Figs. 6.9a and 6.9b show the fitting of the experimental data by means of Eq. (6.2), for the Greek and Southern California catalogues, respectively. The slopes of the linear regression fitting process were found:$b_x = 3.0$ and $b_x = 3.1$, correspondingly. The similarity between the two aforementioned b_x values leads to the suspicion that there is a universal indicator that characterizes the underlying relation between the energy and the mean magnitude of the sample which is estimated $b_x \approx 3.0$. Thus in order to verify this suggestion, the Italian catalogue was further examined using the same spatial method applied to previous two catalogues, for the period between 01-Jan-2005 00:00:00 and 01-Jan-2009 00:00:00. Indeed, as shown in Fig. 6.9c, the estimated b_x-value was found $b_x \approx 2.8$.

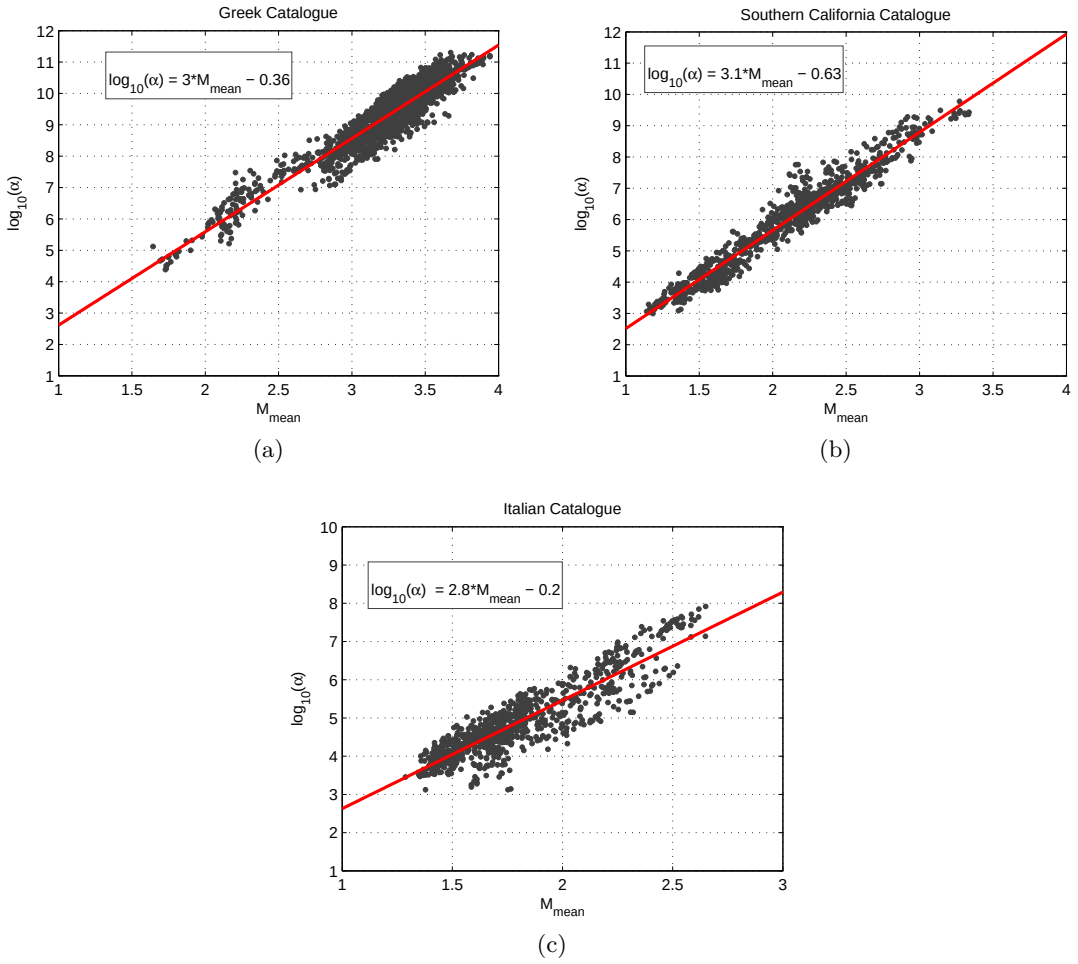

Figure 6.9: Scatter plot between the volumetric energy density α and the mean magnitude M_{av}, for the case of the Greek, Southern California and Italian catalogues respectively. The red line refers to the linear regression fitting of the experimental data.

The study of the energy release of earthquakes has been an challenging field of research since several ways have been proposed for its estimation [106, 119, 91, 88, 90, 114, 143]. In addition, a variety of physical parameters have been used such as: the fault-length, the fault-displacement, the fault-area, velocity-acceleration-complexity of the fault-motion, duration of faulting, in order to understand and quantify the process of the fracture, namely the earthquake. Among them the magnitude is one of the most fundamental physical parameters involved in the methods and formulas proposed by the literature. The energy-magnitude relation was first proposed by Gutenberg & Richter [88] after many revisions, given as follows:

$$logE = 1.5m_S + 11.8 \text{ or equivalently } logE = 2.4m_B + 5.8 \tag{6.3}$$

where E is the radiated energy (in ergs). m_S and m_B refer to the surface-wave magnitude and the body-wave magnitude scales proposed by G-R. Although this was an empirical relation it was considered as a good gross relation and it is sill widely used nowadays.

Later on, Kanamori (1977) [119] proposed an alternative formula between the radiation and the seismic moment M_0, that gave similar results compared to the previous formula, and reads as follows:

$$E = (\Delta\sigma/2\mu)M_0, \tag{6.4}$$

where $\Delta\sigma$ is the average stress drop in the earthquake, and μ is the rigidity of the medium near the fault.

The latter formula (6.2) does not claim any inconsistence of the previous two equations mentioned above, but just verifies a simple relation that has been empirically found in terms of a nonextensive model for EQ dynamics, which is also supported by the literature [119, 88]. A crucial characteristic that should be mentioned is the variety of the available magnitude scales used for the seismic catalogues, such as: M_L, M_S, M_B and M_W. These scales are mainly coming from the analysis of the seismic source spectrum of the wave data and they are very different concerning their saturation and accuracy. The magnitude scale used for the available data contained in the seismic catalogues under study, is the M_L local and regional scale, mainly used in the Western United States and also adopted by Italy and Greece. On these grounds, the fact that the latter formula is related to the mean magnitude of the sample (containing more that one single EQ), leads to a reasonable assumption that this parameter would be less affected from the saturation-accuracy of the magnitude scale that is described. On the other hand, the repeatability of the results at the seismic catalogues of three different countries, strongly supports the underlying relation.

To further test whether the results of this study are unified, in the following subsection focuses on the analysis of epileptic seizure recordings.

6.1.3 Spatial analysis of the brain

This section focuses on whether the linear relation between the volumetric energy density energy and the mean magnitude of the sample is also depicted in the case of the brain activity related to a single ES. Specifically, analysis builds on the two intracranial EEG recordings analysed in Chapter 5. Each one of these recordings contain 96 separate electrodes located near the brain area that is considered as the pathogenic region that triggers the epileptic seizure. Such topography provides a relevant framework for applying a spatial analysis similar to that of previous section, considering that each one of these electrodes refer to a regional brain activity beneath its location. Thus for each one of these electrodes, the electric events contained in the seizure part of these recordings were first calculated, using the method defined in Chapter

5. The nonextensive Eq. 2, was then applied on the distribution of events calculated, for each electrode. It should also be stressed that the selection of the seizure part was determined by the experienced surgeon who performed the operation.

Fig. 6.10, depicts the scatter plot between the volumetric energy density α and the mean magnitude of each sample under study. Herein, as opposed to the analysis of seismicity catalogues, the experimental data are more sparsely distributed along the two axes, while the b_x values obtained through Eq. (6.2) yield: $b_x = 4.1$ and $b_x = 3.9$ correspondingly. It is recalled that analysis in Chapter 5 showed that $\approx 80\%$ of the electrodes where found to follow the nonextensive formula while the rest of them seemed to follow quite different statistics. This observation was also justified by the study of Osorio et al. [169]. In addition the selected parts of these signal mainly refer to the seizure part which is expected to include in its most part large sizes of events. Indeed, the rates of the mean magnitude for both EEG recordings vary between the interval of $M_{av} \in [4.2, 6.2]$ for the first intracranial EEG and $M_{av} \in [3.9, 5.3]$ for the second one correspondingly. However, the underlying linear relation found due to the analysis of seismicity catalogues is also observed here.

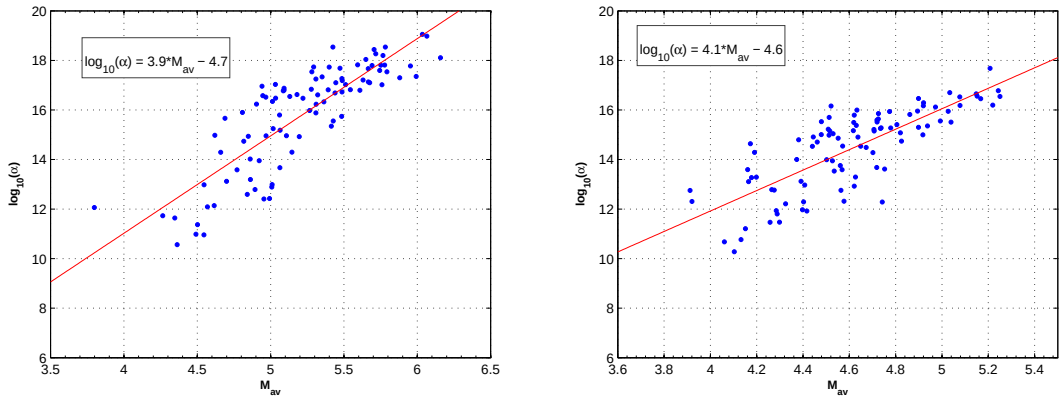

(a) intracranial 1 (b) intracranial 2

Figure 6.10: (a,b) Scatter plot between the volumetric energy density α and the average magnitude M_{av}, for the case of two intracranial EEG recordings.

The latter suggestion is further justified through the scatter plots between the q-parameter and the volumetric energy density α, as shown in Fig. 6.11. The underlying mirroring behaviour is also observed more clearly specially in higher rates of energy. In particular, it is observed that as the value of the volumetric energy density increases, the nonextensive parameter q constantly decreases without significant fluctuations. On the contrary, when the energy rate exceeds a certain threshold then the system seems to change its behavior, where high volatility of nonextensivity is observed.

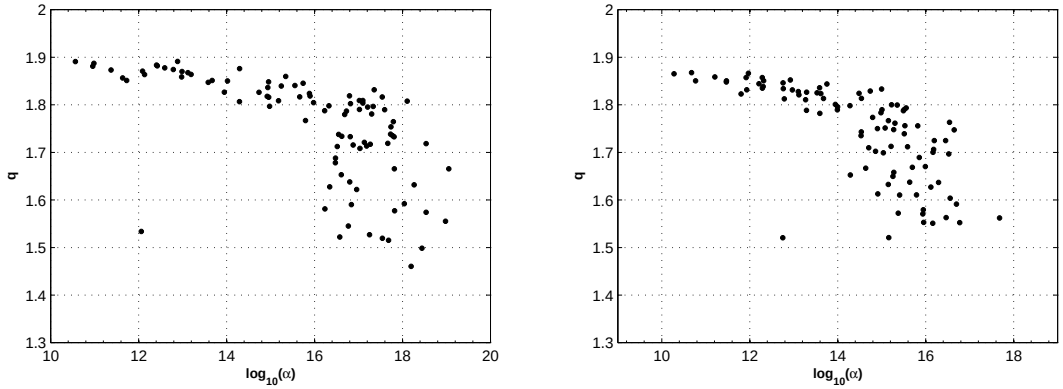

(a) intracranial 1 (b) intracranial 2

Figure 6.11: (a,b) Scatter plot between the q-parameter and the volumetric energy density α, for the case of two intracranial EEG recordings.

This behaviour leads to the suspicion that there are of two different "fracture regimes" on the same phenomenon. Specifically, drawing from the nonextensive model for earthquakes, when the system is governed by small events, this reflects to the fact that the developed stresses are not capable to exceed the breakage threshold of large fragments included in the system. The siege of fragments at lower energies leads to the increment of the correlation length keeping the system at higher nonextensive levels. As the developed stresses increase, the underlying threshold is gradually achieved by destroying most of the fragments involved in this process. This leads to the absence of small fragments where the interaction between larger and stronger entities takes place marking a new regime: the fragment-asperity interaction occurring at higher energies-stresses. On these grounds, the breakage of larger entities reproduces smaller fragments. These newly created fragments, along with the redistribution of stresses that follows, lead the system to the volatility of nonextensivity for larger energies. This scenario has been also verified through the temporal analysis of preseismic kHz EM emissions (see Chapter 2). Furthermore, for the case of the brain, the results reveal that these two regimes coexist under a single regional ES brain activity. Analogous coexistence has been also found from the study of Osorio et. al [169] who mentioned a synchronization shoulder that violates the linear part of the probability distribution of energies. The similarity of the behaviour with the seismicity, provides preliminary indication that verifies this coexistence of two different regimes, indicating that further consideration should be given on the common-universal character of such complex phenomena [54, 169] in terms of energy and nonextensivity.

6.2 A new approach for the estimation of nonextensivity

It is recalled that the frequency magnitude relationship for EQ dynamics is given by the Gutenberg & Richter formula [89], Eq. 1. Utsu on 1965 [253], proposed an alternative method for determining the b-value of the Gutenberg & Richter formula, showing that it is inversely proportional to the mean magnitude $\overline{M}$, given the minimum magnitude, M_{min}, of the EQ magnitudes (see Chapter 5, Eq. (6.5)). At the same year, Aki [3] showed that the latter equation, is equivalent to the maximum likelihood estimation, and provided the confidence limits for this estimation from a given sample. For the case where there is no uncertainty in magnitude, the approximate 95% confidence limit of b is $\pm 1.96(b/\sqrt{N})$. Later on, Utsu (1966) [254] suggested slight modification addressing the use of the binned magnitudes. The final equation reads as follows, for the case where the magnitude frequency distribution of EQs obey the Gutenberg-Richter law:

$$b_{utsu} = \frac{\log_{10} e}{\overline{M} - (M_c - \frac{\Delta M}{2})} \tag{6.5}$$

where, ΔM, is the lowest binned magnitude in the sample and M_c is the smallest magnitude in the sample. Moreover Sarlis et al. (2010) [202], mentioned that the q-parameter included in the nonextensive formula (2) is associated with the b parameter of Gutenberg & Richter formula (Eq. (1)), above some magnitude threshold, by the relation:

$$b = 2 \times \left(\frac{2-q}{q-1} \right) \tag{6.6}$$

Combining equations (6.5) and (6.6), along with some simple mathematics, we get a new estimation of q-parameter based on the mean magnitude of the sample:

$$q_{est} = \frac{\log_{10} e + 4(\overline{M} - M_k)}{\log_{10} e + 2(\overline{M} - M_k)} = \frac{\frac{4}{\log_{10} e}(\overline{M} - M_k) + 1}{\frac{2}{\log_{10} e}(\overline{M} - M_k) + 1} \simeq \frac{9.2103(\overline{M} - M_k) + 1}{4.6052(\overline{M} - M_k) + 1}, \tag{6.7}$$

where $M_k = M_c - \frac{\Delta M}{2}$, with M_c the smallest magnitude in the sample, and ΔM the lowest binned magnitude in the sample, respectively. The parameter $\overline{M}$ is the average magnitude of the sample. For further details about the solution please refer to Apendix Sec. A.1.

6.2.1 Applicability of the new formula to the regional seismicity of large earthquakes

In order to test the validity of the new derived formula, analysis is first focuses on the regional foreshock seismicity seismicity of two cases of large EQs: (i) the case of Athens EQ ($M = 5.9$)

occurred on 07-Sep-1999, in Greece and (ii) the case of L'Aquila EQ ($M = 6.3$) occurred on 06-Apr-2009 in Italy. Note that both cases have been described analytically in Chapter 4 along with the fittings in terms of Eq. (2). The q-parameter included in the nonextensive Eq. (2) was replaced by the estimated one (q_{est}). The experimental data were then fitted according to the given parameter q_{est} in terms of Eq. (2). The Levenberg-Marquardt (LM) method [142, 152] was also used in order to achieve an efficient and accurate fit.

Focusing on the Athens EQ, Fig. 6.12a depicts the fitting of Eq. (2) on the experimental data for a given q_{est} parameter as derives from Eq. (6.7). The data refer to the period from 17-Aug-1999 00:01:39.80 up to 07-Sep-1999 01:56:49, namely the period after the occurrence of the catastrophic EQ occurred in the Izmit region (North-West Turkey). The selected area is 160km around the Athens EQ epicenter. The green line refers to the cut-off completeness threshold used for achieving the optimal fitting-estimation of q_{est}. Fig. 6.12b, depict the fitting in terms of the original Eq. (2).

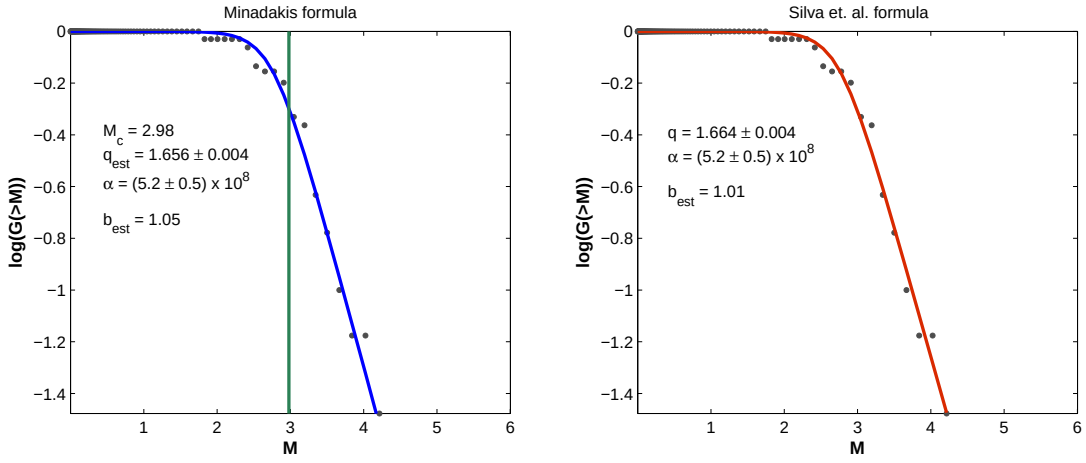

(a) Athens EQ, new formula

(b) Athens EQ, SCP formula

Figure 6.12: (a) depicts the fitting of Eq. (2) on the experimental data for a given q_{est} parameter as derives from Eq. (6.7). The data concern the foreshock activity related to the case of Athens EQ ($M = 5.9$) occurred on 07-Sep-1999, in Greece. (b) depicts the original fitting in terms of Eq. (2)

Additionally, for the case of L'Aquila EQ, Fig. 6.13 depicts the fitting of Eq. (2) on the experimental data for a given q_{est} parameter as derives from Eq. (6.7). The data refer to the period from 28-Oct-2008 00:00:00 up to 6-April-2009 01:32:00. As it is observed from both cases of EQs analysed above, the estimated (q_{est}) parameters are very close to those deriving from Eq. (2). More precisely, for the case of Athens EQ, the q-parameters were found to be: $q_{est} = 1.656 \pm 0.004$ and $q = 1.664 \pm 0.004$. For the case of L'Aquila EQ the parameters yield: $q_{est} = 1.680 \pm 0.003$ and $q = 1.681 \pm 0.003$, respectively. In addition, similar values

have been observed between the volumetric energy density α. Even more, similar values can also be observed between the estimated b-values obtained from Sarlis et. al [202] equation. This similarity indicates the validity of the suggested formula.

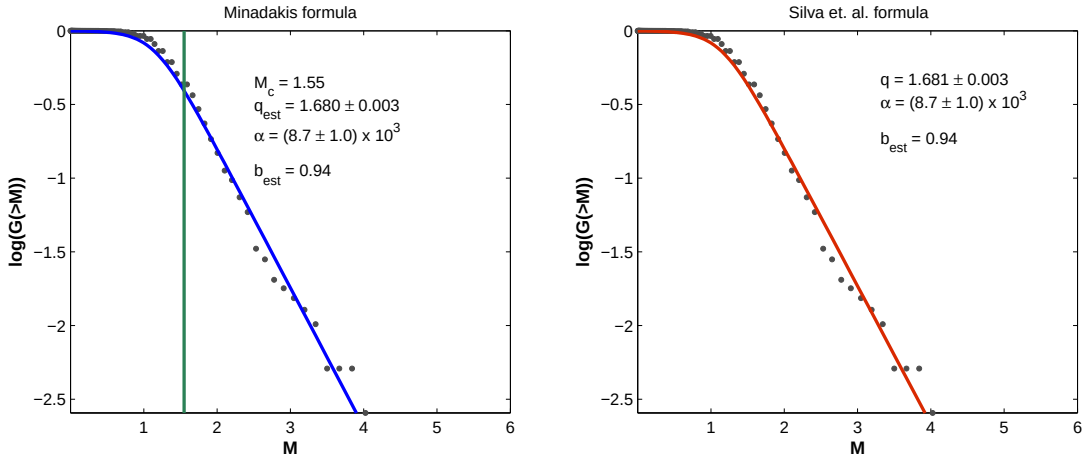

(a) L'Aquila EQ, new formula (b) L'Aquila EQ, SCP formula

Figure 6.13: (a) depicts the fitting of Eq. (2) on the experimental data for a given q_{est} parameter as derives from Eq. (6.7). The data concern the foreshock activities related to the case of L'Aquila EQ ($M = 6.3$) occurred on 06-Apr-2009 in Italy. (b) depicts the original fitting in terms of Eq. (2)

Table 6.1 shows a more detailed analysis of the experimental data that refer to the above mentioned EQs. Specifically, a comparison between the q and q_{est} is presented for different radii around the epicenter of the two aforementioned EQs.

Table 6.1: Comparison between q and q_{est} parameters for the different regions under study

Period	M_c	$Eq.(2)$	$Eq.(6.7)$
Athens EQ (0-160)	2.9	$q = 1.664 \pm 0.004$	$q_{est} = 1.656 \pm 0.004$
Athens EQ (0-200)	2.9	$q = 1.606 \pm 0.006$	$q_{est} = 1.585 \pm 0.007$
Athens EQ (0-300)	3.31	$q = 1.615 \pm 0.003$	$q_{est} = 1.583 \pm 0.005$
Athens EQ (0-400)	3.31	$q = 1.599 \pm 0.002$	$q_{est} = 1.593 \pm 0.003$
Italy EQ (0-030)	1.55	$q = 1.681 \pm 0.003$	$q_{est} = 1.680 \pm 0.003$
Italy EQ (0-050)	1.55	$q = 1.670 \pm 0.003$	$q_{est} = 1.655 \pm 0.004$
Italy EQ (0-100)	1.55	$q = 1.656 \pm 0.003$	$q_{est} = 1.643 \pm 0.003$
Italy EQ (0-200)	1.55	$q = 1.644 \pm 0.002$	$q_{est} = 1.641 \pm 0.002$
Italy EQ (0-300)	1.55	$q = 1.655 \pm 0.002$	$q_{est} = 1.653 \pm 0.002$
Italy EQ (0-400)	1.55	$q = 1.694 \pm 0.003$	$q_{est} = 1.690 \pm 0.003$

As it is observed, the estimated (q_{est}) parameters are very close to those deriving from Eq. (2), indicating the appropriate approximation of the suggested formula. The latter evidence indicate that the suggested formula can adequately describe the nonextensive levels of the regional seismicity, as well as the nonextensive Eq. (2) which in turn uses the normalized

cumulative distribution of the magnitudes.

6.2.2 Applicability of the new formula to preseismic kHz EM emissions

Herein, a challenging issue would be to examine whether the latter formula can also describe the "fracto-electromagnetic earthquakes" (EM-EQS) contained in the preseismic kHz EM emissions observed prior large EQs. Focusing on the case of Athens EQ, in Fig. 6.14, the analysis of the 10kHz NS component is examined in terms of Eq. (6.7), for the two epochs of EQ dynamics that were mentioned in Chapter 2. Specifically, the depicted red parts refer to those epochs. The estimated q-parameters were found: $q_{est} = 1.748 \pm 0.004$ and $q_{est} = 1.8472 \pm 0.0044$ respectively. The green lines refer to the cut-off completeness threshold used for achieving the optimal estimation of q_{est}: $M_c = 5.0$ and $M_c = 6.0$, respectively.

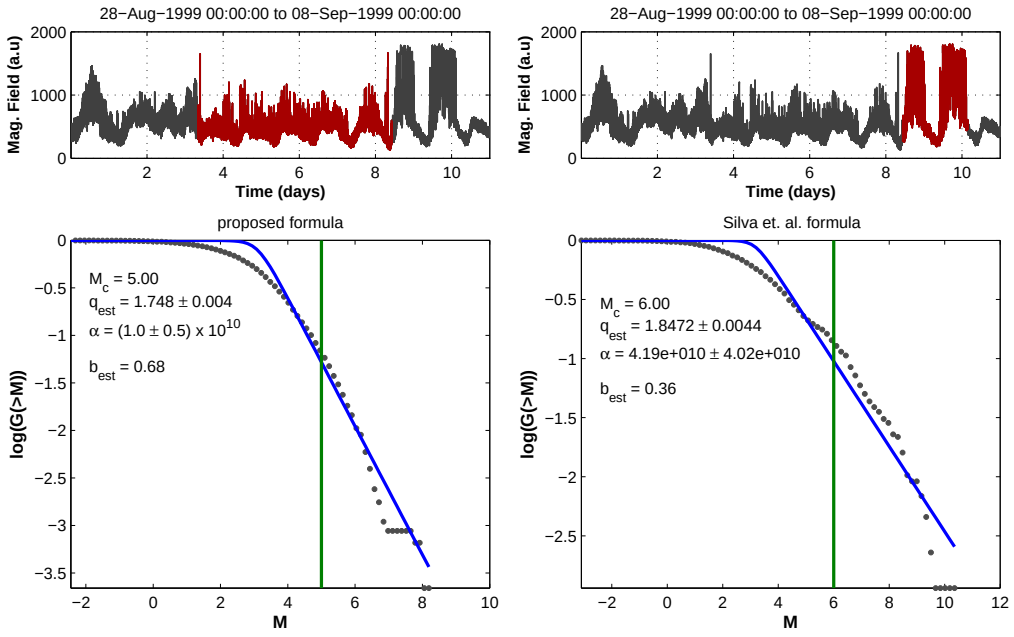

(a) Epoch 1, Athens EQ (b) Epoch 2, Athens EQ

Figure 6.14: (a,b) depict the fitting of Eq. (2) on the experimental data for a given q_{est} parameter as derives from Eq. (6.7). The data concern the preseismic kHz EM emissions observed prior to Athens EQ, analysed in Chapter 2

It should be noted that the selection of the threshold was considered to be relative high since it is not clear whether the lower magnitudes are related to the eligible signal or the background ionospheric activity-noise. However, the estimated q-parameters in terms of Eq. (2) obtained in Chapter 2, were found: $q = 1.748 \pm 0.004$ and $q = 1.834 \pm 0.001$ for the corresponding epochs verifying the consistency of the results.

The same analysis was also applied for the strong EM burst observed a few days prior to the case of L'Aquila EQ ($M = 6.3$) occurred on 06-Apr-2009 in Italy as shown in Fig. 6.15. Recent

studies have shown that this burst has been characterized by higher degree of organization, higher persistent behaviour and fractal properties [55, 56]. Herein, the q_est-parameter has been found $q_{est} = 1.847 \pm 0.004$ which is also similar to the q-parameter calculated by means of Eq. (2) ($q = 1.803 \pm 0.004$).

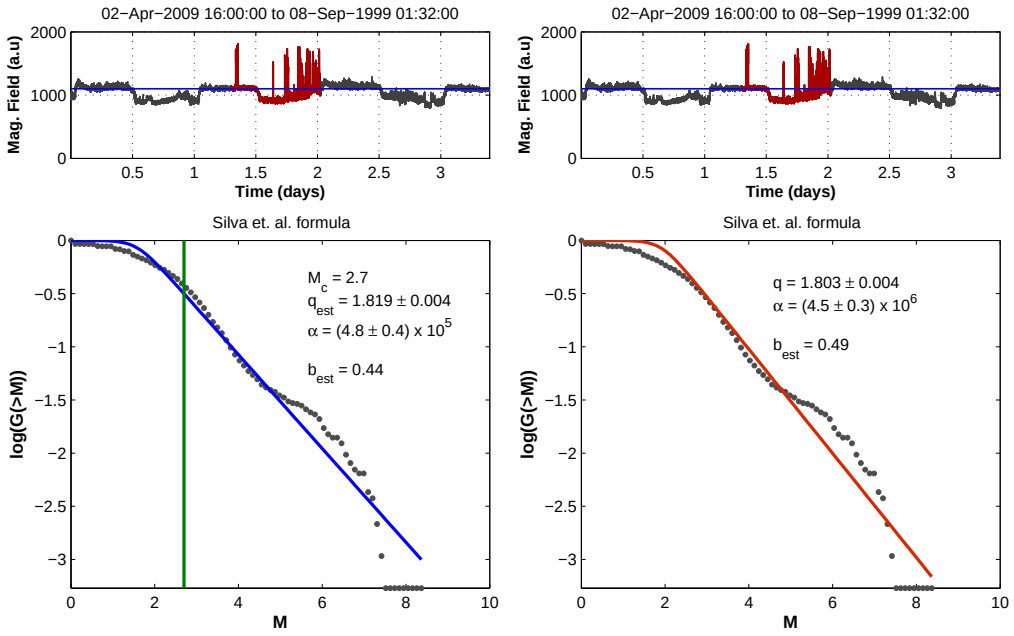

(a) L'aquila EQ (b) L'aquila EQ

Figure 6.15: (a) depict the fitting of Eq. (2) on the experimental data for a given q_{est} parameter as derives from Eq. (6.7). (b) the original fitting of Eq. (2). The data concern the preseismic kHz EM emissions observed prior to L'Aquila EQ.

It should be stressed out that a weakness of the proposed formula is the appropriate estimation of the magnitude cut-off completeness threshold (M_c). A crucial condition that should be fulfilled in order to apply such formula is the Gutenberg and Richter Law, implying that the linear part of the distribution of experimental data should not be violated. This violation is also observed in part Fig. 6.14b and has been justified in previous chapters. Specifically it has been shown that this inconsistence is due to the increased threshold used for distinguishing the eligible signal from the background EM activity, since for lower thresholds it is not clear whether the data refer to the generation process of the EQ. However, the obtained evidence indicate that the suggested formula can adequately describe the preseismic kHz EM emissions observed prior to large EQs, as well as the traditional nonextensive formula.

6.2.3 Applicability of the new formula to epileptic seizure recordings

Following latter evidence it would be challenging to examine whether the proposed Eq. (6.7) can also be applied to the distribution of electric events of the EEG recordings under study.

Thus, focusing on the first intracranial EEG recording, Fig. 6.16a depicts the fitting of Eq. (2) on the experimental data for a given q_{est} parameter as derives from Eq. (6.7). The green line refers to the cut-off completeness threshold used for achieving the optimal fitting-estimation of q_{est}. Since the intracranial EEG recordings are characterized by significant lower levels of noise, this threshold was found to be $M_c = 3.5$. Fig. 6.16b, depicts the fitting in terms of the original Eq. (2).

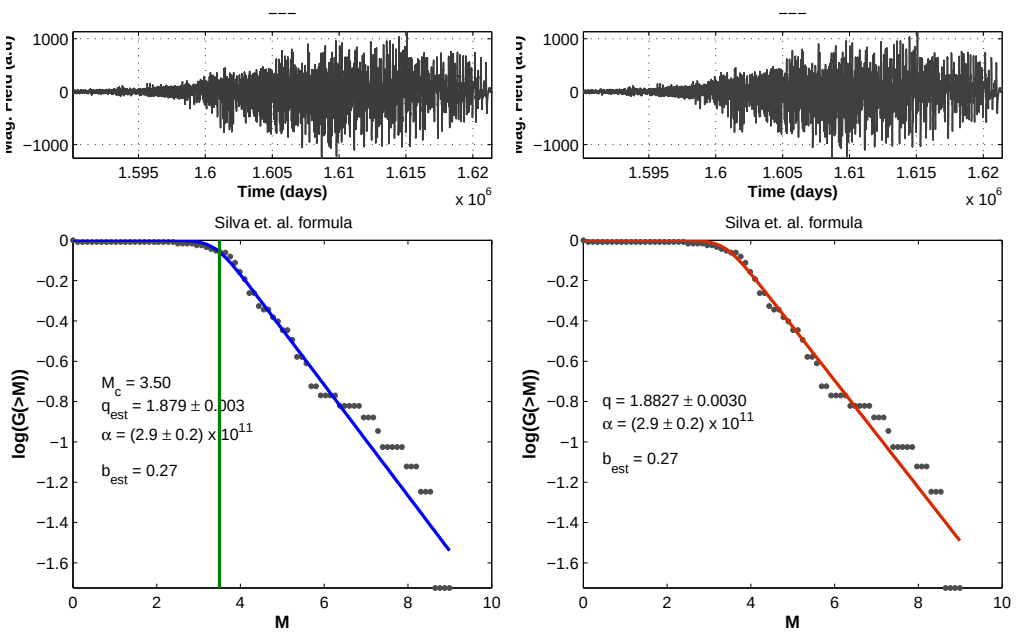

(a) Proposed formula (b) Silva et al. formula

Figure 6.16: (a) depict the fitting of Eq. (2) on the experimental data for a given q_{est} parameter as derives from Eq. (6.7). (b) depict the original fitting in terms of Eq. (2)

The same analysis was also applied for the second intracranial EEG recording as shown in Figs. 6.17a and 6.17b correspondingly. As observed from both analysed electrodes the q-parameters are very similar with those obtained from the original nonextensive Eq. (2). More precisely, for the first EEG recording we get $q_{est} = 1.879 \pm 0.003$ and $q = 1.8827 \pm 0.003$, while for the second EEG recording we get $q_{est} = 1.862 \pm 0.003$ and $q = 1.847 \pm 0.004$. In addition, the observed estimated s_{est} parameters obtained through Sarlis et. al. equation, are also similar yielding: $b_{est} = 0.27$ and $b_{est} = 0.27$ for the first electrode, $b_{est} = 0.32$ and $b_{est} = 0.36$ for the second electrode, correspondingly. In effect to this evidence it seems that the proposed Eq. (6.7) provides an appropriate framework to study the nonextensivity of complex systems by means of the mean magnitude contained in the sample under study.

Summarizing at this point of analysis, it should be noted that in a recent study, Telesca (2012) [231], also motivated to find an alternative mathematical relation for the estimation of nonextensive parameters q and α included in the nonextensive formula (6.6). Using the

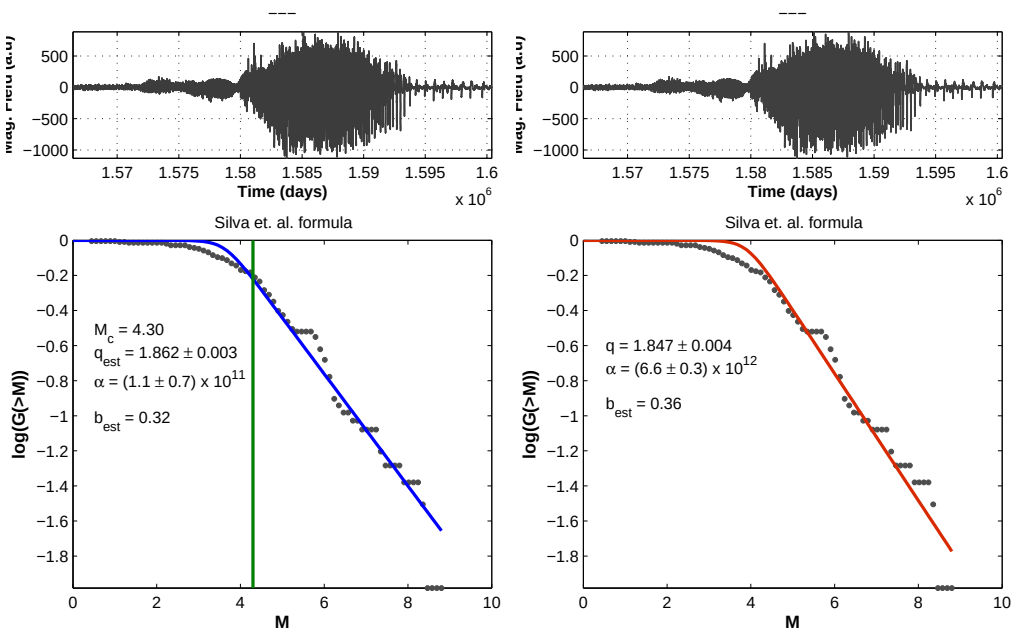

(a) Proposed formula (b) Silva et al. formula

Figure 6.17: (a) depict the fitting of Eq. (2) on the experimental data for a given q_{est} parameter as derives from Eq. (6.7). (b) depict the original fitting in terms of Eq. (2)

technique of Lagrange multipliers he proposed a slightly different equation, which leads to the Maximum Likelihood Estimation (MLE) of the parameters of the nonextensive magnitude distribution as proposed by Aki [3]. His proposed approach uses the term 10^M instead of the term 10^{2M} included in Eq. (2) suggesting that the G-R b-value is related to the nonextensive parameter q by means of $b = \frac{2-q}{q-1}$, which is in contrast with Sarlis Eq. (6.6). However, although the present study draws from the Sarlis Eq. (6.6) the estimated q parameters seem to be consistent with those obtained from Eq. (2). Moreover, the applicability of the proposed formula on three different kinds of data sources, approves its validity one hand and provides further evidence of the dynamical analogy between biological and geophysical shocks.

On these grounds the proposed formula seems to be superior to Eq. (2), since it incorporates the benefits of Utsu's formulation for the study of various catastrophic phenomena [257, 258]. Specifically, the benefits of this formulation read as follows: (i) The new formula does not require an fitting process. This in effect reduces the complexity of the estimation of p parameter. (ii) Depending on the distribution of experimental points, Eq. (2) may give too heavy weight to the points for large magnitudes. Extending this type of research, in the following section a new formula is proposed based on a statistical significance test between two populations.

6.3 A new formula for measuring the statistical significance between two populations

Utsu (1966) [254] proposed a statistical significance test of the difference in b-value between two earthquake groups. More precisely, he showed that the probability that two samples may come from the same population, given their b-values and the number of EQs N, is given by:

$$P \approx exp[-(dA/2) - 2], \tag{6.8}$$

where

$$dA = -2N\ln N + 2N_1 \ln\left[N_1 + N_2\left(\frac{b_1}{b_2}\right)\right] + 2N_2 \ln\left[N_1\left(\frac{b_2}{b_1}\right) + N_2\right] - 2 \tag{6.9}$$

Lower values of P indicate the higher statistical significant difference between two samples under study, or equivalently these two samples do not come from the same population. Herein, a challenging issue would be to examine whether the latter formula can be described through the nonextensive q-parameter q instead of the b-value. Indeed, combining equations (6.8) and (6.6), results to the following approach of the term dA included in Eq. (6.8):

$$P \approx exp[-(dS/2) - 2], \tag{6.10}$$

where

$$dS = -2N\ln N + 2N_1 \ln\left[N_1 + N_2\left(\frac{(2\text{-}q_1)(q_2 - 1)}{(q_1\text{-}1)(2\text{-}q_2)}\right)\right] + \tag{6.11}$$

$$2N_2 \ln\left[N_1\left(\frac{(2\text{-}q_2)(q_1 - 1)}{(q_2\text{-}1)(2\text{-}q_1)}\right) + N_2\right] - 2, \tag{6.12}$$

where $q1$ and $q2$ are the estimated parameters deriving from the proposed Eq. (6.7).

It should be noticed that according to Utsu proposed methodology, when studying two groups of EQs with different b-values obtained, they should obey the G-R law in order to be examined for their statistical difference. However, the latter approach is mainly based on the nonextensive q-parameter which is connected with the increased correlations developed within a system under study while the b-value is connected with the accumulated stresses developed. These two physical quantities are different in the sense that they have different natural explanation. The question here naturally concentrates on whether the difference of nonextensivity between two samples can adequately express the underlying statistical difference between two samples of EQs. Thus in order to test the latter approach, 10000 random pairs of data were first created with magnitude rates ranging between $0 \sim 10$, where each pair of data contained 100 EQs. For each one of these pairs, Eq. (6.8) and (6.10) were applied. Note that

although these random-based data do not necessary obey the G-R law, since they are random, this approach could give a first indication on whether the two equations are consistent beyond their natural meaning. Indeed, Fig. 6.3 depicts the scatter plot of this analysis showing the linear relation between the estimated probabilities indicating the underlying consistency.

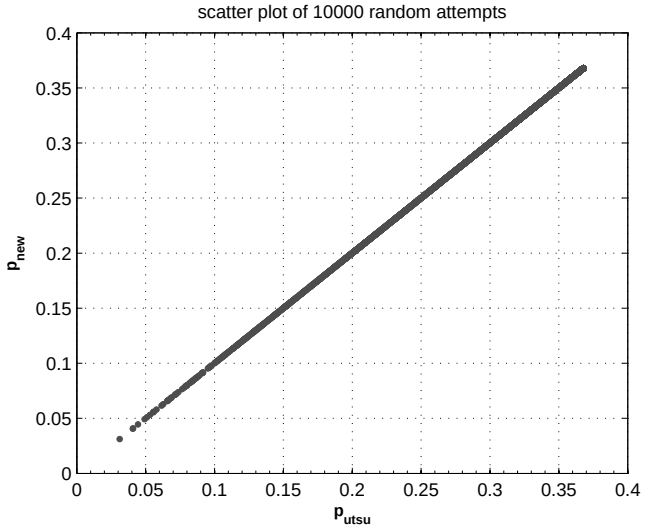

Figure 6.18: Scatter plot of the estimated probabilities obtained from Eq. (6.8), using a combination of Eq. 6.5 and (6.7), respectively.

6.3.1 Testing the formula on seismicity

Beyond the latter results, the most appropriate way to examine the latter proposed formula would be to compare its results by calculating the q-parameters used or the term dS, through Eq. (2) instead of Eq. (6.7). However such analysis requires real data sources that obey the G-R law. Thus analysis is first focuses on the regional seismicity prior to L'Aquila EQ, Central Italy, occurred on 6 April 2009 at 01:32:39 UTC with magnitude $M = 6.3$. According to the literature, Papadopoulos et al. [174], reported that from the beginning of 2006 up to the end of October 2008 no particular earthquake activation was noted in that seismogenic area. On the contrary, from 28-October-2008 up to 27-March-2009 the seismicity was in the state of weak foreshock activity, and dramatically increased 10 days prior the main event (from $\approx$ 26-Mar-2009) [174]. Herein, the updated Italian EQ catalogue was used, which is available on the website of the *Istituto Nazionale di Geofisica e Vulcanologia* (INGV: `http://bollettinosismico.rm.ingv.it`). Fig. 6.19 depicts the cumulative distribution of EQs 30 km around the epicenter of the main event for the period between 01-Jan-2008 00:00:00 up to 6 April 2009 01:32:39. The cut-off completeness threshold for that period was found $M_c = 1.55$, which was first estimated through the distribution of the experimental data that

refer to the linear part of the Gutenberg & Richter frequency-magnitude relation. As observed from the cumulative distribution of EQs, the period from the beginning of 2008 up to the end of 28-Oct-2008 has been considered as the background (BG) seismicity period [174]. The period from 28-Oct-2008 00:00:00 up to 18-Jan-2009 00:00:00 (E1) has been considered as the first time-frame of interest followed by a period of weak foreshock activity from 18-Jan-2009 00:00:00 up to 30-Mar-2009 12:00:00 (E2). The period from 30-Mar-2009 12:00:00 up to 6 April 2009 01:32:39 (E3) has been considered as the strong foreshock activity observed prior to the main event [174].

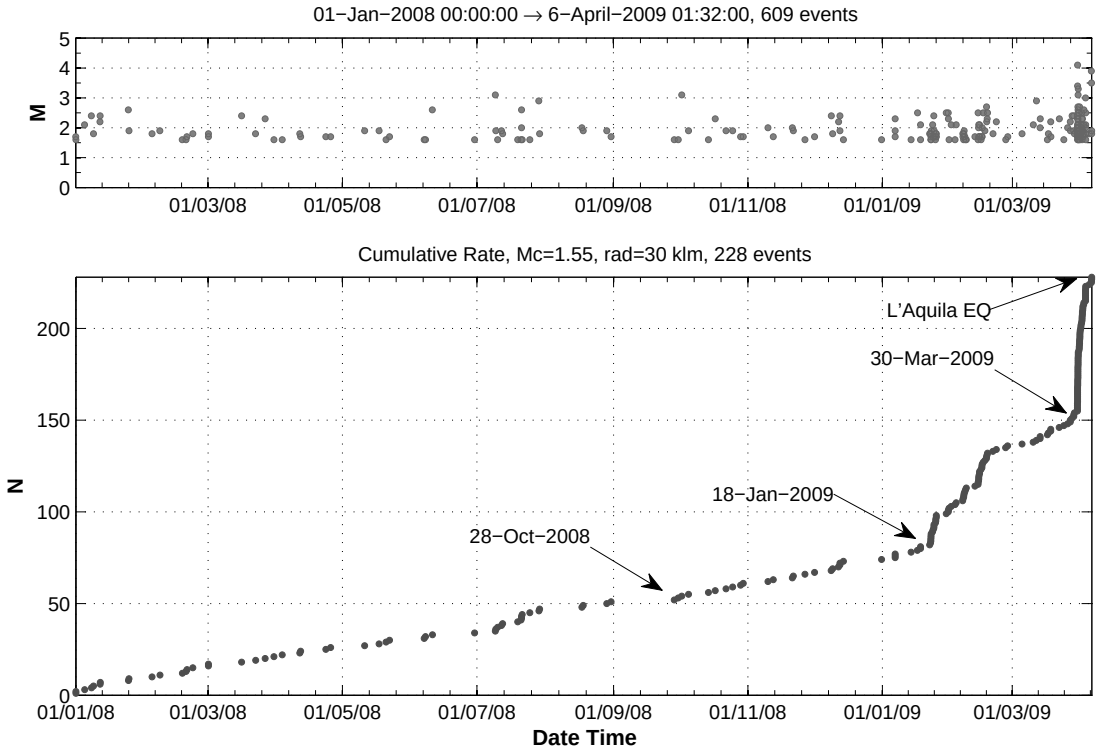

Figure 6.19: The top chart depicts the distribution of EQs 30 km around the epicenter of L'Aquila EQ, concerning the period between 01-Jan-2008 00:00:00 up to 6 April 2009 01:32:39. The bottom chart depicts the cumulative distribution of EQs for that period

Each one of the periods E1,E2 and E3 mentioned above, were examined in contrast to the background seismicity (BG), using three different approaches: (i) the Utsu original approach which uses the b-values calculated through Eq. (6.5) (ii) the new proposed Eq. (6.10) and (iii) the new proposed Eq. (6.10) in which the q-parameters derive from Eq. (2), instead of Eq. (6.7). Fig. 6.20, depicts these three approaches. It is observed that the first two comparisons provide identical results revealing the same behaviour with that of the 10000 random pairs analysed in this section. Additionally, the probability that the samples E1,E2,E3 under study may come from the same population is decreased as approaching to the occurrence of the

main event. This means that these three populations refer to a regional seismicity related to the activated fault and not to the BG seismicity of the area under study, which are compared with. Additionally, similar results were obtained due to the statistical significance tests applied through the use of the nonextensive Eq. (2) (see third chart in Fig. 6.20).

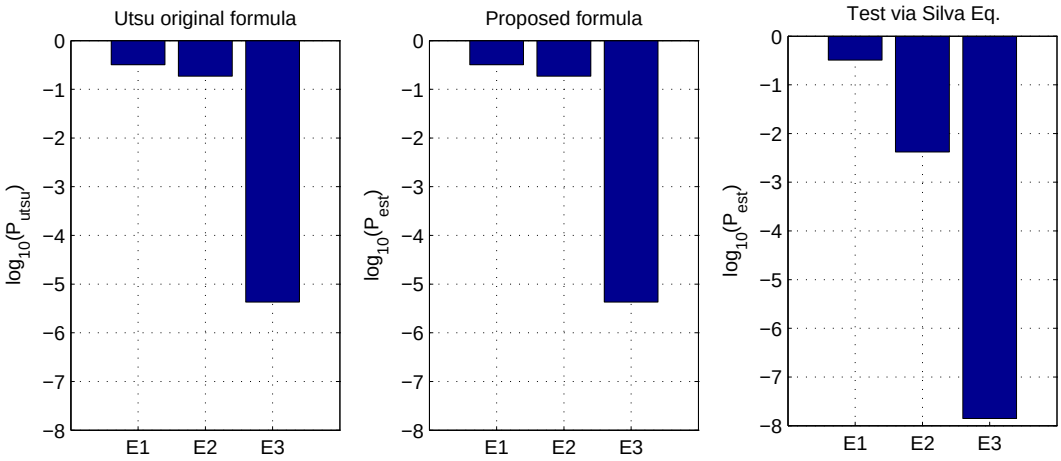

Figure 6.20: The probability estimations for the three periods of foreshock activity (E1,E2,E3) versus the background seismicity, 30 km around the epicenter of L'Aquila EQ. From left to right Eq. (6.8) is examined using three different approaches: (i) the Utsu original approach which uses the b-values calculated through Eq. (6.5) (ii) the proposed Eq. (6.10) and (iii) the proposed Eq. (6.10) which uses the q-parameters that derive from Eq. (2).

On these grounds, bypassing the impact of b-value included in the G-R formula, the new proposed equation shows that the underlying statistical significance can also be determined in terms of the nonextensive q-parameter. A significant benefit on this point of view is that the long-range correlated behaviour within a system under study is directly related to the stresses developed, indicating the coexistence of these two regimes due to the generation process of an EQ.

6.3.2 Testing the formula on preseismic kHz EM emissions

Herein an interesting issue would be to examine whether Eq. (6.8) and (6.10) can be applied to the EM-EQs contained in the preseismic kHz EM emissions observed prior to Athens EQ. The Athens EQ is a particular case of interest since two different epochs were identified during the last stage of its generation process, as shown in Fig. 6.21. Specifically, analysis in Chapter 2, revealed that the first epoch refers to the fracture of fragments intervening between the two anomalous surfaces of the fault that contributes to the hindering of their relative motion. The second epoch of the preseismic kHz electromagnetic emission which contains two strong EM bursts, refers to the reflection of collision and breakup of large and strong teeth (asperities) of

the irregular surfaces. Herein, the notion of the background seismicity is absent since there is not any preseismic EM emission during the daily background activity of these signals. Thus, it would be therefore interesting to examine whether Eq. (6.8) can distinguish these two epochs which refer to different fracture mechanisms.

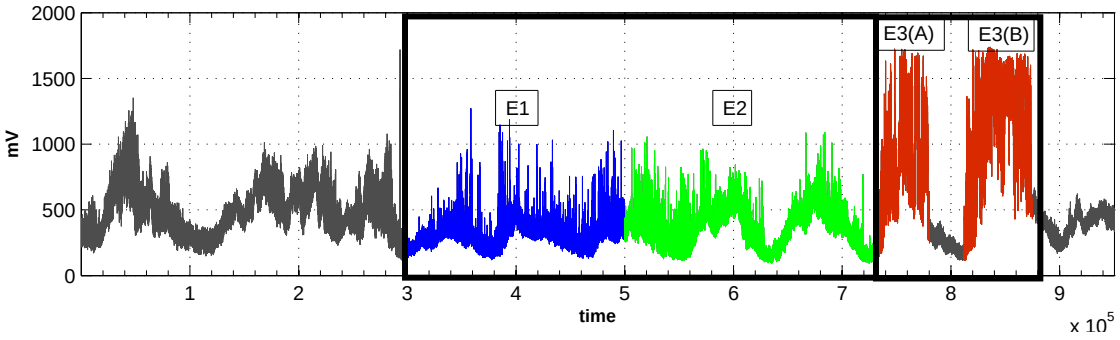

Figure 6.21: The 10 kHz EW component recorded prior to Athens 1999 EQ. Epoch 1 refers to the blue and green parts of the signal, while epoch 2 refers to the red part.

Figs. 6.22a , 6.22b and 6.22c, depict the probability tests by means of the three previous mentioned approaches. For the needs of the analysis, Epoch 1 was split in two separate epochs where its first part (depicted with blue color), was considered as the reference epoch to be compared with each one of the rest. Therefore, the results indicate that each one of the examined epochs, present gradually statistically significant difference in relation to the first one. This characteristic behaviour can be observed at all the three different approaches, indicating the consistency of the results on one hand, revealing the gradually state changing of the fault mechanism that governs the system on the other hand.

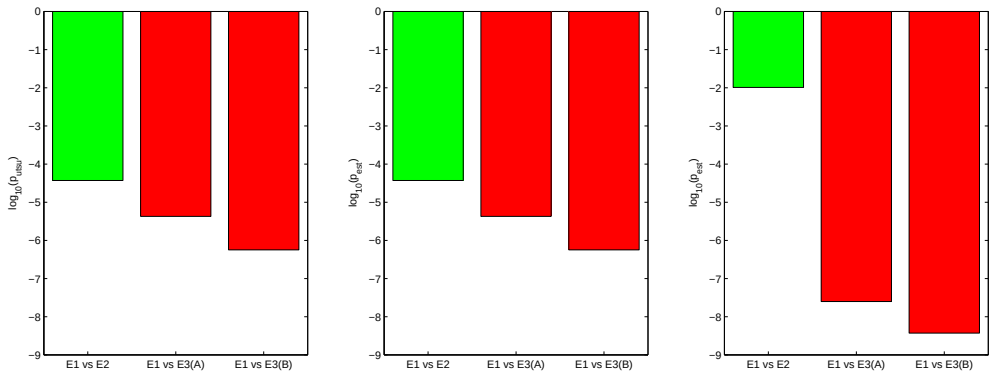

(a) Utsu formula (b) New formula (c) New formula (SCP)

Figure 6.22: (a,b) show the probability estimations calculated through Eq. (6.8) and Eq. (6.10) respectively. (c) refers to Eq. (6.10) using the q-parameters that derive from Eq. (2).

The latter observed behaviour, verifies the results of section 6.1, suggesting that as we

approaching to the final break up, the residual between the fault planes is reduced resulting to the increase of the mean magnitude in the sample. This process increases the levels of the volumetric energy density required for the fracturing, leading to a state changing of the fault mechanism that governs the system: namely from a negative to a positive feedback mechanism as shown in Chapter 2. However in order to further verify this suggestion, the overall statistical significant difference between the two underlying epochs was calculated by means of the three aforementioned approaches. The results were positive, indicating that the probability that these two epochs may come from the same population is significant low: $p_{utsu} = 3.097192 \times 10^{-6}$, $p_{est} = 3.097192 \times 10^{-6}$ and $p_{est_silva} = 2.051542 \times 10^{-6}$. In other words, this means that they belong to different regimes of fracture.

Summarizing at this point of analysis, the latter results revel that the nonextensive q-parameter can adequately express whether two samples may come from the same population, through Eq. (6.10). This relevance was an expected result since the relation between the b-value and the q-parameter is mathematically expressed through Sarlis et al. Eq. (6.6), where the only unknown parameter included in the formula is the q-parameter. This suggestion is also justified by the linear relation between the two probability estimations as shown in Fig. 6.18, indicating that the expected results should be identical.

6.4 Discussion & further arguments

Drawing from a model for EQ dynamics which is routed on a nonextensive Tsallis framework, in this study a spatial analysis of seismicity catalogues deriving from three different regions of the globe, was applied. A linear relation was found between the average magnitude (M_{av}) of the sample and the logarithmic expression of volumetric energy density α (see Eq. 6.2). The latter formula does not claim any inconsistence of the previous two equations mentioned above, but just verifies a simple relation that has been empirically found in terms of a nonextensive model for EQ dynamics. However, the similarity on results between the three seismic catalogues, provides a relative framework for understanding the toughness-size of the geological ingredients that sustain these areas. It is recalled that according to the fragment-asperity model, the energy is proportional to the size r of the fragment: $\varepsilon \propto r^3$ [208]. Thus it is reasonable to assume that regions which provide higher volumetric energy density α, are mainly refer to an interaction of stronger and larger fragments-asperities. The linear relation that was found in this study between the mean magnitude and the logarithmic expression of the volumetric energy density, indicates that as the residual between the fault planes is gradually reduced, due to the interference between the fragments-asperities, the mean size of the remaining residual is

increased. This phenomenon results to an increase of the energy-strain needed for the breakage of these fragments-asperities entities which in turn leads to an increase of the mean magnitude of EQs contained in the area under study. This process continues until the maximum magnitude in the sample exceeds some magnitude threshold, which in our case was empirically found: $M_c \gtrsim 4.7$, where the situation changes. The larger fractures contribute to the development of smaller fragments which in turn reduce the mean size of fragments and therefore the levels of energy. However the small fractures along with the corresponding redistribution of stresses significantly contributes to the increment of the correlation length, maintaining the system at higher levels of nonextensivity [214, and references therein]. On these grounds it is reasonable to assume that regions which provide high nonextensive behaviour and high volumetric energy density are mainly refer to an interaction of stronger and larger fragments-asperities. On the contrary, regions which provide high nonextensive behaviour and lower volumetric energy density, are those that have been experienced with relative strong fractures that have canceled the accumulation process of stresses. The observed high q-parameters for both cases reveal that the nonextensivity in the underlying fracture mechanisms remains high.

The aforementioned scenario was also verified due to the spatial analysis of the brain activity related to a single epileptic seizure (ES). Specifically it was found that the two regimes mentioned above, coexist under a single regional ES brain activity. Analogous coexistence has been also justified from the study of Osorio et al. [169], who mentioned that increases in inter-neuronal excitatory coupling generate characteristic scale seizures regimes that coexist in space-time with scale-free ones. In this study both mentioned regimes are governed by scale-free laws related to the energy distribution of events and further express the fractal nature of the systems under study [203, 249, 200, 118, 30]. The similarity of the behaviour with seismicity, provides preliminary indication that verifies the existence of two different scale-free regimes, indicating that further consideration should be given on the common-universal character of such complex phenomena in terms of energy and nonextensivity. The same features were found in Chapter 2 due to the temporal analysis of the two identified epochs included in the preseismic kHz EM activity observed prior to large EQs, revealing the richness and complexity of both biological and geophysical dynamics.

Extending this type of research along with the prospect to link the long-range correlated behaviour of the fracture process with the mean magnitude of the sample, in sections 6.2 and 6.3, two more equations have been proposed: Eq. (6.7) and Eq. (6.10). Focusing on the first one, it has been shown that the entropic q-parameter that derives from the nonextensine Tsallis statistical mechanics framework [245] can also be expressed by the mean magnitude

of the sample under study through Eq. (6.7). The latter formula was applied to seismicities generated at different regions of the globe, providing similar results with those obtained from the nonextensive model for EQ dynamics. In addition similar results were also obtained from the analysis of both the preseismic kHz EM emissions related to Athens EQ and the intracranial EEG recordings related to epileptic seizures. In effect, this observation indicates that complex systems which develop long-range correlations, this behaviour can be also be expressed by the mean magnitude of the sample. This suggestion has been also justified in part by Telesca (2012) [231], who proposed an alternative method based on the maximum likelihood estimation of the parameters q and α. Focusing on the second proposed approach, it has been shown that the entropic index q can also distinguish through Eq.(6.10), whether two samples under study may come from the same population, namely different regimes of fracture process. This was verified from both the analysis of regional seismicity and preseismic kHz EM emissions observed prior to large EQs.

Against this evidence the present study suggests that further consideration should be taken in this direction in order to have an overall view for the relation between the energy, the entropic index q and the average magnitude of the sample. Characteristically, Kanamori (1983) [106] mentioned that the physical process that is associated to earthquakes is much more complex to be described with a few parameters while the use of these parameters should be made very carefully.

6.5 Conclusion

In this chapter the underlying nonextensive model for EQ dynamics has been further extended by elucidating the link between the entropic index q, the average magnitude of the sample, the fragment-asperity size, and the volumetric energy density. Within this framework of analysis, two regimes of fracture process have been identified, which refer to different populations: (i) those that refer to an interaction of stronger and larger fragments-asperities and (ii) those that have been experienced with stronger fractures that have canceled the accumulation process of stresses. In this direction, two more equations have been proposed that link the long-range correlated behaviour of the fracture process with the mean magnitude of the sample, providing an alternative way for the study of such phenomena that adopts the advantages and features of Utsu formulation. Another strength of the proposed equations is that under controlled conditions they do not require any fitting process. Finally, the underlying framework of analysis has further verified the sesmogenic origin and the predictive capability of preseismic kHz EM emissions.

Chapter 7

Discussion & Conclusions

Focusing on the generation process of catastrophic events, this study has intended to promote our understanding of the spatio-temporal behaviour of earthquake dynamics and the dynamics of regional brain activity. Drawing on recently introduced models and methods for EQ dynamics, that involve issues such as complexity, self-affinity, universality, organization and fractal structures, two general directions of analysis have been considered in this study, subjected in two crucial questions: *(i) whether the generation process of an extreme event has more than one facets prior to its final appearance, and (ii) whether there is a unified approach for the study of catastrophic phenomena*. Conformed with such questions, the present work focused on the analysis of two diverse extreme phenomena: (i) large catastrophic EQs and their relation with preseismic kHz EM emissions, and (ii) epileptic seizures (ESs), in the prospect to identify common mechanisms that may explain both the nature and the generation process of such phenomena. In the following sections the key findings and areas of contribution of this work are presented within the above mentioned framework.

7.1 Does the generation process of an extreme event have more than one facets prior to its final appearance?

Although this question has been partly answered from recent cross-disciplinary literature [260, 191, 170, 195, 54], the present work contributes to the long-standing debate on the possible precursory phenomena observed prior to catastrophic events. From the EQs viewpoint, recent cross-disciplinary literature has reported evidence of precursory phenomena observed prior to large EQs. Specifically, studies related to Seismic Electric Signals (SES) [260], electromagnetic (EM) precursors rooted in Lithosphere-Atmosphere-Ionosphere (LAI) coupling [191], and precursors related with other disciplines such as: Seismology, Infrared Remote Sensing [170], Synthetic Aperture Radars Interferometry [195], have provided evidence that support

the seismogenic origin of such precursory observations. Among these precursors, preseismic electromagnetic (EM) emissions have been also reported by the literature, suggesting that the science of EQ prediction should be from the start multidisciplinary [123, 36, 172, 55, 56]. However, the study of precursory phenomena in terms of preseismic EM emissions is still questionable, from a significant part of the scientific community, since they have not been adequately accepted as real physical quantities [259, 179]. On these grounds, the present study extended the focus of inquiry to the study of kHz EM emissions, in the prospect to examine whether there are preseismic EM precursors. Should this case exists, such a multidisciplinary analysis could possible answer on the underlying question. The results were positive.

7.1.1 The seismogenic origin of kHz EM emissions: key findings

A recently well documented two-stage model [123, 36, 40, 172, 59, 65] that links an individual EM precursor with a distinctive stage of the EQ preparation has provided an initial framework for the analysis and classification of these kHz-MHz EM anomalies. More precisely, the MHz EM emission refers to the fracture of the highly heterogeneous system that surrounds the fault while the kHz EM emission is rooted in the final stage of EQ generation, reflected to the fracture of entities sustaining the system. According to the literature, the appearance of MHz EM emission does not signify that the EQ is unavoidable [123, 36]. The MHz EM time series have been characterized by anti-persistent behaviour and multi-fractal properties [123, 36], reflecting to a set of fluctuations tending to induce stability within the system under study: for example, a nonlinear negative feedback mechanism which kicks-off the opening cracks away from extremes [54]. The system heterogeneity could account for the appearance of a stationary-like behavior in the antipersistent MHz part of the prefracture EM time series and thus enable the fracture in highly heterogeneous systems to be described via an analogy with thermal continuous phase transition of second order [54].

Based on the latter theoretical approach, the first attempt of this study was to further examine the link between the observed kHz EM emissions and EQ dynamics, building on two more theoretical models. Specifically, the first self-affine asperity model [47], states that the EQ is due to the slipping of two rough and rigid Brownian profiles one over the other in which an individual EQ occurs when there is an intersection between them. The second model [218, 208], which is routed in a nonextensive Tsallis [245] framework starting from first principles, concerns two rough profiles interacting via fragments filling the gap, in which the mechanism of triggering EQ is established through the interaction of their irregularities and the fragments included between them. Analysis in Chaprer 2, has provided evidence that the

two models for EQ dynamics mentioned above, supplement each other, in a sense that both are mirrored in two qualitative different epochs of the preseismic kHz EM emission observed prior to large EQs. It is argued that the profile of first epoch of the emerged precursory activity follows the nonextensive model for EQ dynamics, reflected to the fracture of fragments filling the gap between the two rough planes of the activated fault. The second epoch refers to the emerged precursory activity that contains the abruptly emerged strong impulsive EM bursts which in turn follow the self-affine asperity model.

On these grounds, the following scenario is suggested, which in turn extends the theoretical approach of the kHz EM activity: the first epoch refers to the fracture of fragments intervening between the two anomalous surfaces of the fault that contributes to the hindering of their relative motion. Once the fracture of one fragment has occurred, there is a reformation of fragments followed by a redistribution of stresses. This process practically results to a relative displacement of the fault planes (fault slip). The next "fracto-electromagnetic earthquake" (EM-EQ), will emerge when a new fragment breaks under the impact of the increased tensions. This process is consistent with the antipersistent character of the first epoch. As the fragments are broken, the two rough planes of the fault approaches each other. The abruptly emerged second epoch of large EM-EQs is the reflection of collision and breakup of large and strong teeth of the irregular surfaces. The persistent behaviour, the increased degree of organization, the corresponding higher magnitudes M and energy density α, are footprints that support this scenario.

It is recalled that the nonextensive model for EQ dynamics was considered to be the most appropriate framework to study the relevance of preseismic kHz EM emissions: it includes both the entropic content and complexity issues that derive from the nonextensive Tsallis theoretical framework [245] and further involves a profile of EQ dynamics that includes the interference between fragments that comprise the residual between two fault planes. Thus, the link between kHz EM emissions and seismicity was further verified in Chapter 3, by applying a combined spatiotemporal analysis on the regional seismicity observed prior to large EQs. Analysis focused on the case of Athens (Greece) EQ occurred on 09-Sep-1999, a few weeks after the major Turkish event occurred on 17-Aug-1999 near the Izmit area. It was found that the sequence of electromagnetic EQs (EM-EQs) contained in the preseismic kHz EM signal emitted before the impending EQ, also follows the theoretical approach of the nonextensive model for EQ dynamics, providing similar results with those derived from seismicity. Furthermore, it was found that before the major Turkish event, the seismicity in the wider Greek area presented increased nonextensivity centered on central and western Greece. On the contrary, after the

Turkish event, the higher nonextensivity was shifted towards the central Greece around the metropolitan area of Athens, with even higher levels of nonextensivity. The latter results were further verified in terms of Fisher information [157, 75, 69] and the Hurst exponent [109, 110] applied to inter-event times of EQs, revealing that higher levels of organization and higher persistent behaviour were mainly developed around the ensuing EQ epicenter. This work also provided a first indication in terms of nonextensive statistical approach that the transient stresses of the seismic waves of a major EQ can trigger a considerably distant significant EQ.

Building on the self-affine nature of fracture and faulting theory in terms of the nonextensive model for EQ dynamics, analysis in Chapter 4 focused on two well documented cases of EQs, where kHz EM anomalies have been observed: the case of L'Aquila EQ occurred on 06-Apr-2009 and the case of Athens EQ. Applying a combined spatial analysis, it was found that the population of: (i) the EQs that precede of a significant event and occur around its the epicentre, and (ii) the "fracto-electromagnetic earthquakes" that emerge during the fracture of strong entities distributed along the activated single fault sustaining the system follow the same statistics, namely, the relative cumulative number of earthquakes against magnitude. In effect, since the preseismic kHz EM emissions refer to the activation of a single fault [172], it is reasonable to assume that the activation of a single fault is a reduced self-affine image of regional seismicity. The results were further supported from recent studies in terms of the traditional Gutenberg-Richter law [203, 249, 200, 118, 30] providing evidence that enhance the physical background of the underlying self-affinity in terms of nonextensivity. This work further supports the hypothesis that the statistics of regional seismicity is a macroscopic reflection of the physical processes in the earthquake source, as has been initially suggested by Huang and Turcotte [108].

Expanding on the relevance of preseismic kHz EM emissions to the study of EQs, their seismogenic origin was further supported in Chapter 6 by means of two equations, given by the literature, which are based on Utsu [253, 254] formulation. In this direction, two more equations have been proposed that link the individual long-range correlated behaviour of the fracture process with the mean magnitude of the sample under study. All the formulas mentioned above were applied to seismicities generated at different regions of the globe and preseismic kHz EM emissions related to Athens EQ, providing similar results with those obtained from the nonextensive model for EQ dynamics. Specifically, focusing on the two identified epochs of the kHz EM emissions observed prior to Athens EQ, it was found that as approaching to the final break up, the residual between the fault planes is reduced resulting to the increase of the mean magnitude in the sample. Each one of the examined epochs, presented gradually

statistically significant difference in relation to the first one. Additionally, the probability that these two epochs may come from the same population was found to be significant low, verifying the argument that they are mirrored in two different fracture mechanisms. The latter results were further verified by means of the two proposed equations deriving from the nonextensive model for EQ dynamics, showing that the entropic index q can also be used as a parameter for distinguishing whether two samples under study may come from the same population.

7.1.2 Identifying the preseismic kHz EM emissions: further discussion and arguments

Motivated by the plurality of findings in this work, a key concern was to find a suitable framework which links the observed seismicity with the phenomenology of kHz EM precursors, without violating the laws of physics and without leaving any potential inconsistencies. This framework has been mainly subjected in the following crucial questions:

Q1. How can we identify a kHz EM anomaly as a preseismic one? As has been stated by the literature, since the seismicity is a critical phenomenon [213, 263], it is expected that significant changes in the statistical pattern of the temporal kHz EM time series should reflect to the deviation of the normal behaviour, revealing in effect the presence of a preseismic EM precursor [54]. This suggestion has been well documented from previous studies on preseismic kHz EM emissions in terms of information theory (entropic metrics) [117, 125, 124, 117, 55, 56], showing that these precursors are characterized by significantly higher organization (or lower complexity) in respect to the noise and the ionospheric background activity contained in these recorded signals. Additional fractal spectra analysis has revealed that these emissions are also characterized by strong persistency [123, 36]. However analysis in Chapter 2 revealed that this combination of footprints is mainly rooted in the second epoch of kHz EM activity that refers to fracture of the asperities and follows the persistent fBm temporal fractal profile with a "roughness" index represented by the Hurst exponent by the value $H \sim 0.7$. The first identified epoch which refers to the fragment-asperity interaction, is characterised by lower organization and antipersistent behaviour in contrast to the second epoch (or equivalently higher organization and antipersistent behaviour in contrast to the background).

Q2. Are the kHz EM signals consistent with the self-affine nature of faulting? Beginning with the pioneer work of Maslov et al. (1994) [154], the authors have formally established the relationship between spatial fractal behavior and long-range temporal correlations for a broad range of critical phenomena. They showed that both the temporal and spatial activity can be described as different cuts in the same underlying fractal. In addition, from the early work of

Mandelbrot (1982) [149], much effort has been put to statistically characterise the resulting fractal surfaces in fracture processes focusing on two crucial theoretical ingredients:

- *Fracture surfaces have been found to be self-affine following the fractional Brownian motion (fBm) model over a wide range of length scales [47, 93, 31, 32].*

- *The spatial roughness of fracture surfaces has been interpreted as a universal indicator of surface fracture, weakly dependent on the nature of the material and on the failure mode [146, 94, 186, 162, 272].*

Analysis in Chapters 2, 3 has shown that the kHz fracto-EM-precursor rooted in the activation of a single fault is consistent with the above mentioned incredients. In effect this finding predicts that the activation of a single fault is a reduced-magnified image of the regional (and laboratory) seismicity [108]. Moreover in Chapter 4 it has been shown by means of traditional Gutenberg-Richter power-law, as well as in terms of a nonextensive formulation that the populations of (i) EM EQs included in an observed EM precursor associated with the activation of a single fault, (ii) EQs included in different radius around the epicenter of a significant seismic event (foreshock activity), follow the same statistics, namely the relationship between frequency and event magnitude.

7.1.3 The spatiotemporal complexity of earthquake and fault structures

A critical-controversial issue facing the scientific community involved with materials science, is the interpretation of scaling laws, on material strength, that concentrates on whether the spatial and temporal complexity of EQ and fault structures emerges from geometry or from the chaotic behaviour inherent to the nonlinear equations governing the dynamics of these phenomena. Rundle et al. (2003) [198] suggested that such processes can be regarded as a type of generalized phase transition, similar to the nucleation and critical phenomena that are observed in thermal and magnetic systems. In contrast to this argument, Carpinteri and Pugno (2005) [30], purely based on geometry, stated that *"as happened for relativity, geometry could again hold an unexpected and fundamental role."*.

Against these arguments the study of preseismic EM emissions provides a relevant framework for examining the nature of the spatiotemporal complexity and fault structures emerged by such phenomena. According to the literature, the preceding seismicity of a significant EQ has been defined as a critical phenomenon that can be attributed to a phase transition of second order, while empirical evidence have shown that main shocks occur a few days up to one week after the appearance of criticality [263, 262, 261, 250]. Regarding the two stage model, it has been shown in terns of preseismic MHz EM emissions that the scaling laws associated

with the fracture of highly heterogeneous component that surrounds the family of asperities can be attributed to a phase transition of second order. The MHz EM emissions also emerge at the same time from approximately one week up to a few hours before the EQ occurrence [36].

The link between seismicity and preseismic kHz EM emissions has been further justified in this work showing that these emissions refer to the to the fragment-asperity interaction process. This has been justified by both spatial and temporal analysis. Therefore the existence-acceptance of preseismic kHz EM emissions, suggests that geometry holds a fundamental role in phenomena associated with the fracture of asperities. Specifically, the scaling laws associated with the fracture of the backbone of asperities of a single fault (also justified in terms of the kHz EM emissions) could be a product of the fractal scaling of asperities. Moreover, the persistent behaviour of kHz EM emission, which is emerged in the tail of the preseismic preseismic EM activity, refers to an nonequilibrium process without any footprint of an equilibrium thermal phase transition. In contrast to the MHz EM activity, this process indicates that the system develops a self-regulating character and to a great degree the property of irreversibility, which in turn is one of the important components of predictive capability [54].

7.2 Is there a unified approach for the study of catastrophic phenomena?

Analysis in Chapters 2 - 4 has provided strong evidence for the seismogenic origin of preseismic kHz EM emissions observed prior to large EQs. In summary, it was found that the corresponding time series are governed by: memory effects, gradually increment of the correlation length between the nonlinear domination of the neighbor units, transition from a negative to a positive feedback mechanism, development of fractal structures, gradual improvement of quality of the fractal structure and its transition at larger spatial scales with maintaining self-similarity. Of crucial importance is that these dynamics of complex systems have been also founded on universal principles that may used to describe disparate problems [20, 180, 45, 131, 214, 2, 76, 176]. Specifically, Kossobokov et al. (2000) [131], reported similarities of multiple fracturing on a neutron star and on Earth, by examining the power-law energy distributions, clustering, and the symptoms of transition to a major rupture. The authors suggest that such similarities may reflect a scenario of a critical transition, common for a broader class of nonlinear systems. Fukuda et al. (2003) [76] reported quantitative similarities between the statistical properties of healthy heart rate variability and non-congested Internet traffic, and diseased heart rate variability and congested Internet traffic. The authors suggest that the understanding of the mechanisms underlying the "human-made" Internet could provide a relevant framework to

understand the "natural" network that controls the heart. de Arcangelis et al. (2006) [45], who analyzed available experimental catalogs of solar and earthquake activity, showed that these apparently different phenomena exhibit the same distributions of sizes, inter-occurrence times and the same temporal clustering, revealing a universal character. The authors suggest a common approach to the interpretation of both phenomena in terms of the same driving physical mechanism. Picoli et al. (2007) [180] reported similarities between the dynamics of geomagnetic signal and heartbeat intervals suggesting that their findings are consistent with the concept of universality in complex systems. Moreover, Balasis et al. (2011) [16], reported universality in solar flare, magnetic storm and earthquake dynamics in the framework of Tsallis statistical mechanics theory.

Contributing to the underlying cross-disciplinary literature and also motivated by a recent study of Osorio et al. (2010) [169], in which the authors have shown that a dynamical analogy exists between epileptic seizures and earthquakes, analysis in Chapter 5, endeavored to provide further evidence for the underlying dynamical analogy in terms of preseismic kHz EM emissions. Specifically, it was shown that the same "scale-free" statistics govern not only the populations of EQs occurred in different faults and ESs occurred in different patients [169], but also the populations of: (i) fracto-electromagnetic pulses rooted in the fracture of the backbone of strong entities distributed along a single fault sustaining the system, and (ii) the electric pulses included in a single ES. Moreover, the present study extended the focus of inquiry for the applicability of models for earthquake dynamics to examine both scalp-recorded and intracranial electroencephalogram recordings related to epileptic seizures. By introducing an updated definition of the electric event in terms of magnitude the study was focused on the underlying model for earthquake dynamics, routed in a nonextensive Tsallis framework and leading to a Gutenberg & Richter type formula that expresses the frequency distribution of earthquakes against magnitude. It was further shown that the nonextensive formula can adequately describe the sequences of electric events included in both types of electroencephalogram recordings related to epileptic seizures. The results were further verified using the traditional Gutenberg & Richter law and an combined with and alternative method for the magnitude-frequency relation for earthquakes [252, 3]. Finally, using a specific method that applies different thresholds of magnitudes, similar behavior was observed for the parameters included in the nonextensive formula with that obtained from the corresponding analysis of earthquakes, indicating the underlying dynamical analogy. The underlying similarities were also observed for both types of electroencephalogram recordings under study, providing preliminary evidence of self-affinity of the regional electroencephalogram-epileptic-seizure activity.

The underlying analysis suggests that further consideration should be taken for the analysis of both biological and geophysical shocks, within a unified framework that utilizes transferable ideas and methods.

7.3 Summarizing the key findings: contribution to theory

This thesis has intended to promote our understanding of the spatiotemporal behavior of regional seismicity and the generation mechanisms that govern large and strong earthquakes, employing a broad multi-disciplinary perspective for the interpretation of catastrophic events. The study has focused on recently introduced models and methods for EQ dynamics that address issues such as: complexity, self-affinity, universality, nonextensive dynamics, self-organized and intermittent criticality, organization and fractal structures. The potential for applicability and transferability of these methods to the study of regional brain activity in epileptic seizures has also been partially examined. In summary, the key findings and areas of contribution of this work read as follows:

(i) Examination of the link between precursory kHz EM activity and EQ dynamics lead to the identification of an intermediate epoch of preseismic kHz EM activity. This finding provides the possibility to discriminate whether a seismic shock is sourced in the fracture of fragments filling the gap between two rough profiles or in the fracture of "teeth" distributed across the fractional Brownian profiles that sustain the system. In effect this work extends the existing model for preseismic EM emissions contributing to the predictive capability of these precursors

(ii) The link between precursory kHz EM activity and seismicity has been further verified spatiotemporally, showing in geophysical scale that the transient stresses of the seismic waves of a major EQ can trigger a considerably distant significant EQ at a later time. In effect this work further elucidates the suggestion that a major EQ may trigger an ensuing EQ.

(iii) It has been shown that the population of EQs that precede a significant event and occur around its epicentre, and the population of "fracto-electromagnetic earthquakes" that emerge during the fracture of strong entities distributed along the activated single fault, follow the same statistics. This finding proves the self-affine nature of fracture and faulting.

(iv) Extending the focus of inquiry to the study of epileptic seizures, it has been shown that a dynamical analogy exists between ESs and EQs at the level of a single fault / seizure

activation. This verifies the common scale-free nature of such phenomena and provides preliminary indications for the self-affine nature of regional ES activity in the brain. In addition this unified approach further verifies that the study of catastrophic phenomena should be from the start cross-disciplinary.

(v) The underlying nonextensive model for EQ dynamics has been further extended, identifying two different regimes of fracture process that refer to different populations: (i) those that refer to an interaction of stronger and larger fragments-asperities and (ii) those that have been experienced with stronger fractures that have canceled the accumulation process of stresses. Finally, a set of new algorithms have been proposed, providing an alternative way for the study of catastrophic phenomena that adopts the advantages and features of Utsu formulation [257, 258]. In effect this study contributes to the understanding of the generation process of catastrophic phenomena.

7.4 Future work, contribution and perspectives

The key findings of this thesis and areas of contribution to theory and analytic methods, open up different directions for future research. First, the preseismic EM emissions examined in this study have been found to be a promising field of research that contributes to the predictive capability of prospective earthquakes. Moreover, analysis applied so far in terms of fault modelling, laboratory experiments, criticality, scaling similarities of multiple fracturing of solid materials, fractal electrodynamics and complexity, has provided sufficient evidence that validate the association of these precursors with the fracturing process in the pre-focal area. Thus, the need for designing and developing practical tools for managing, monitoring and predicting associated earthquakes in real-time basis in terms of preseismic EM emissions, has been now corroborated. Moreover, extending this type of research, the predictive capability of the earthquake location in terms of preseismic kHz EM emissions would be also an interesting issue. Thus the expansion of the available station network on locations that fulfill the needs for a proper electromagnetic recording could give the trigger for such a study in the future. The unified approach employed in this study provides a relevant framework for understanding of the propagation pathways of both epileptic and seismic networks, by cross-fertilizing the knowledge from the study of earthquake cycles with the study of epileptic seizure cycles. Second, the last decades, human activities related to the energy technology development have caused a number of lesser magnitude seismic events followed by small significant earthquakes. Those events have been felt by local residents, and have caused several damages in properties. Thus from the perspective of preseismic EM time series and the basic theoretical principles

studied in this thesis, an interesting issue could be to examine whether analogous observations can be obtained from such seismic processes. Such a study could contribute to the better understanding of induced seismicity on one hand, and will help to the development of better tools for managing and controlling the risks and induced hazards of such technologies. Common crucial questions that should be debated in future research may read as follows:

Does an extreme event beget another, in the case of earthquakes and epileptic seizures? Analogous to the earthquake cycles, after symptoms of seizure end, the remaining epileptic seizure activity in some cases may trigger a new one [97]. In certain cases, the post-crisis activity remains strong and the patient's life is in crucial state. Despite the critical significance of this question with respect to clinical implications, this remains a relatively under-explored area which the proposed project addresses in terms of examining the potential contribution of models and metrics for earthquake dynamics to the early detection and prevention of such failures in the brain.

Are there earthquake-swarms in the case of regional brain activity? In seismology, swarms are considered to be those earthquake sequences striking in a relatively short period of time and that do not eventually lead to a large event. Recently, the discrimination between foreshocks and swarms as a diagnostic tool of forthcoming strong mainshock in real-time conditions has attracted evolving interest [85]. Although previous works have reached indefinite findings in both fields of study, it would be interesting to shed light on this topic through the study of epileptic seizure recordings. Note that the role of propagating stress waves between two major EQs has been corroborated in this study both in terms of regional seismicity and preseismic EM emissions. Of crucial interest could be to examine whether in the case of brain activity potential "EEG-swarms" or even seizures may give preliminary indications for ensuing (or not) epileptic seizures and whether results obtained can feed back into the study of earthquakes.

Are the neighborhood regions of the focal epileptogenic zone organized to prevent seizure? This is a crucial question under debate and it is strongly related with the concept of localization of the brain region that triggers an epileptic seizure. Towards the generation of catastrophic phenomena, the corresponding time series are usually governed by: memory effects, gradually increment of the correlation length between the nonlinear domination of the neighbor units, transition from a negative to a positive feedback mechanism, development of fractal structures, gradual improvement of quality of the fractal structure and its transition at larger spatial scales with maintaining self-similarity. These dynamics of complex systems are also founded on universal principles [220, 221, 222, 265, 266], that may used to describe disparate problems. The later features have also verified in the present study both directly and indirectly. On these

grounds the main concept is whether the avalanches observed in EEG epileptic seizure cycle are mostly a result of the neighborhood (healthy part) and not of the focal epileptogenic zone. In this direction it would be very interesting to compare the behavior of neighborhood and focal areas in epileptic seizure-related brain activity with those obtained from the study of earthquakes and vise versa. This approach is expected to contribute to the localization methods and metrics for hazard analysis and potentially enhance theoretical work on the generation process of complex phenomena.

Ultimately, in line with the preceding questions, a future study could involve the development of new algorithms and optimized computational models for early warning and detection, contributing to an integrated risk assessment approach in both clinical and seismological fields. This could also include new algorithms developed in the context on the present research.

Bibliography

[1] S. Abe and G. B. Bagci. Necessity of q-expectation value in nonextensive statistical mechanics. Phys. Rev. E, 71:016139, January 28 2005. [cited at p. 22, 40]

[2] S. Abe and N. Suzuki. Statistical similarities between internetquakes and earthquakes. Physica D, 193:310–314, 2004. [cited at p. 25, 27, 109, 112, 137, 177]

[3] K. Aki. Maximum likelihood estimates of b in the folmula $logn = a - bm$ and its confidence limits. Bulletin of the Earthquake Research Institute, University of Tokyo, 43:237–239, 1965. [cited at p. 134, 147, 156, 162, 178, 205]

[4] D. Alexeev and P. Egorov. Persistent cracks accumulation under loading of rocks and concentration criterion of failure. Reports of RAS, 6(333):769Ű770, 1993. in Russian. [cited at p. 68]

[5] D. Alexeev, P. Egorov, and V. Ivanov. Hurst statistics of time dependence of electromagnetic emission under rocks loading. Physical-Technical problems of exploitation of treasures of the soil, 5:27–30, 1993. [cited at p. 68]

[6] C Allegre, J. L. Mouel, and A Provost. Scaling riles in rock fracture and possible implications for earthquake predictions. Nature, 297:47, 1982. [cited at p. 92]

[7] J. Andersen, D. Sornette, and K. Leung. Tricritical behavior in rupture induced by disorder. Phys. Rev. Lett., 78:2140–2143, 1997. [cited at p. 92]

[8] R. Andrzejak, K. Lehnertz, F. Mormann, C. Rieke, P. David, and C. Elger. Indications of nonlinear deterministic and finite-dimensional structures in time series of brain electrical activity: Dependence on recording region and brain state. Phys. ReV. E., 64(061907), 2001. [cited at p. 116, 117, 127]

[9] G. Antonopoulos. Modeling the geoelectric structure of Zante island from MT measurements. PhD thesis, Phys. Dept., University of Athens, Greece, 1996. [cited at p. 31]

[10] K. Baddari, V. Frolov, A.D. Tourtchine, and F. Rahmoune. An integrated study of the dynamics of electromagnetic and acoustic regimes during failure of complex macrosystems using rock blocks. Rock Mech Rock Eng, 44:269–280, 2011. [cited at p. 25, 92]

[11] D. Bahat, A. Rabinovitch, and Vladimir F. Tensile Fracturing in Rocks. Tectonofractographic and Electromagnetic Radiations Method. Springer, Verlag Berlin Heidelberg, 2005. [cited at p. 15, 25, 35, 92]

[12] P. Bak and C. Tang. Earthquakes as a self-organized critical phenomenon. J. Geophys. Res., 94:15635–15637, 1989. [cited at p. 23]

[13] WH Bakun and AG Lindh. The Parkfield, California, Earthquake Prediction Experimen, volume 229 of 4714. Science, 1985. [cited at p. 148, 151]

[14] M. Balasco, V. Lapenna, M. Lovallo, G. Romano, A. Siniscalchi, and L. Telesca. Fisher information measure analysis of earth's apparent resistivity. Int. J. Nonlinear Sci., 5:230–236, 2008. [cited at p. 71, 73, 80]

[15] G. Balasis, P. A. Bedrosian, and K. Eftaxias. A magnetotelluric study of the sensitivity of an area to seismoelectric signals. Natural Hazards and Earth System Sciences, 5:931–946, 2005. [cited at p. 31]

[16] G. Balasis, I. Daglis, A. Anastasiadis, C. Papadimitriou, M. Mandea, and K. Eftaxias. Universality in solar flare, magnetic storm and earthquake dynamics using Tsallis statistical mechanics. Physica A, 390:341–346, 2011. [cited at p. 178]

[17] G. Balasis, I. Daglis, C. Papadimitriou, M. Kalimeri, A. Anastasiadis, and K. Eftaxias. Dynamical complexity in Dst time series using non-extensive Tsallis entropy. Geophysical Research Letters, 35(L14102), 2008. [cited at p. 110]

[18] G. Balasis, I. Daglis, C. Papadimitriou, M. Kalimeri, A. Anastasiadis, and K. Eftaxias. Investigating dynamical complexity in the magnetosphere using various entropy measures. Journal of Geophysical Research, 114,(A00D06), 2009. [cited at p. 110]

[19] Georgios Balasis, Ioannis A. Daglis, Constantinos Papadimitriou, Anastasios Anastasiadis, Ingmar Sandberg, and Konstantinos Eftaxias. Quantifying dynamical complexity of magnetic storms and solar flares via nonextensive tsallis entropy. Entropy, 13(10):1865–1881, 2011. [cited at p. 54]

[20] Y. Bar-Yam. Dynamics of complex systems. Addison-Wesley, Reading, Massachusetts, 1997. [cited at p. 25, 27, 109, 110, 111, 137, 177]

[21] B. Barriere and D. L. Turcotte. A scale-invariant cellular automata model for distribited seismicity. Geophys. Res. Lett., 18:2011–2014, 1991. [cited at p. 43]

[22] D.M. Bates and D.G. Watts. Nonlinear Regression Analysis and Its Applications. Wiley, New York, 1988. [cited at p. 49]

[23] J. M. Beggs and D. and Plenz. Neuronal Avalanches in Neocortical Circuits. The Journal of Neuroscience, 23:11167–11177, 2003. [cited at p. 111]

[24] M. Bouchon. The state of stress on some faults of the San Andreas system as inferred from near-field strong motion data. J. Geophys. Res., 102:731Ű–744, 1997. [cited at p. 42]

[25] D. Bowman and J. King, G. Accelerating seismicity and stress accumulation before large earthquakes. Geophys. Res. Lett., 28(21):4039–4042, 2001. [cited at p. 23]

[26] D. D. Bowman, G. Ouillon, C. G. Sammis, A. Sornette, and D. Sornette. An observational test of the critical earthquake concept. J. Geophys. Res., 103(NB10):24359–24372, 1998. [cited at p. 23]

[27] D. D. BOWMAN and C. G. SAMMIS. Intermittent Criticality and the Gutenberg-Richter distribution. Pure appl. geophys., 161:1945–1956, 2004. [cited at p. 23]

[28] E. E. Brodsky, V. Karakostas, and H. Kanamori. A new observation of dynamically triggered regional seismicity: Earthquakes in Greece following the August, 1999 Izmit, Turkey earthquake. Geophysical Research Letters, 27:2741–2744, SEPTEMBER 1 2000. [cited at p. 71, 100]

[29] C. Bufe and D. Varnes. Predictive modeling of the seismic cycle 1 of the greater San Francisco Bay region. 1993, 98 (B6):9871–9883, J. Geophys. Res. [cited at p. 23, 141]

[30] A. Carpinteri and N. Pugno. Are scaling laws on strength of solids related to mechanics or to geometry. Nature Materials, 4:421–423, 2005. [cited at p. 26, 49, 69, 94, 111, 132, 137, 138, 141, 169, 174, 176]

[31] B. Chakrabarti and L. Benguigui. Statistical Physics of Fracture and Breakdown in Disordered Systems. Oxford University Press, oxford 1998 edition, 1998. [cited at p. 176]

[32] B. Chakrabarti and R. Stinchocombe. Stick-slip statistics for two fractal surfaces: a model for earthquakes. Physica A, 270:27–34, 1999. [cited at p. 43, 176]

[33] T Chelidze. Percolation and fracture. Phys. Earth Planet. Inter., 28:93, 1982. [cited at p. 92]

[34] Chien Chih Chena, Ya Ting Lee, and Young Fo Chang. A relationship between hurst exponents of slip and waiting time data of earthquakes. Physica A, 387:4643–4648, 2008. [cited at p. 81]

[35] Judith S Chester, Frederick M Chester, and Andreas K Kronenberg. Fracture surface energy of the punchbowl fault, san andreas system. Nature, 437(7055):133–136, 2005. [cited at p. 54]

[36] P. Contoyiannis, Kapiris and K. Eftaxias. A monitoring of a pre-seismic phase from its electromagnetic precursors. Physical Review E, 71:061123–1 – 061123–14, 2005. [cited at p. 14, 16, 17, 18, 19, 25, 36, 43, 44, 51, 72, 83, 84, 87, 92, 104, 105, 115, 172, 175, 177]

[37] Y. Contoyiannis and F. Diakonos. Criticality and intermittency in the order parameter space. Phys. Lett. A, 268:286–272, 2000. [cited at p. 18]

[38] Y. Contoyiannis, F. Diakonos, P. Kapiris, A. Peratzakis, and K. Eftaxias. Intermittent dynamics of critical pre-seismic electromagnetic fluctuations. Physics and Chemistry of the Earth, 29:397–408, 2004. [cited at p. 16, 18]

[39] Y. Contoyiannis, F. Diakonos, and A. Malakis. Intermittent dynamics of critical fluctuations. Phys. Rev. Lett., 89:35701–35704, 2002. [cited at p. 18]

[40] Y. Contoyiannis and K. Eftaxias. Tsallis and Levy statistics in the preparation of an earthquake. Nonlinear Processes in Geophysics, 15:379–388, 2008. [cited at p. 16, 17, 18, 36, 43, 44, 72, 83, 84, 92, 93, 104, 105, 172]

[41] Y. Contoyiannis, C. Nomicos, J. Kopanas, G. Antonopoulos, L. Contoyiannis, and K. Eftaxias. Critical features in electromagnetic anomalies detected prior to the L'Aquila earthquake. Physica A, 389:499–508, 2010. [cited at p. 18]

[42] A.M. Correig, M. Urquizu, J. Vila, and J. Marti. Analysis of temporal occurrence of seismicity at deception island (Antarctica): a nonlinear approach. Pure and Applied Geophysics, 149:553–574, 1997. [cited at p. 81]

[43] P.A. Cowie, D. Sornette, and C. Vanneste. Multifractal scaling properties of an organising fault population. Geophys. J. Int., 122:457–469, 1995. [cited at p. 119]

[44] P.A. Cowie, C. Vanneste, and D. Sornette. Statistical physics model for the spatio-temporal evolution of faults. J. Geophys. Res., 98:21809–21822, 1993. [cited at p. 119]

[45] L. de Arcangelis, C. Godano, E. Lippiello, and M. Nicodemi. Universality in solar flare and earthquake occurrence. Phys. Rev. Lett., 96:051102, Feb 2006. [cited at p. 16, 25, 27, 109, 112, 137, 177, 178]

[46] L. De Arcangelis, A. Hansen, and H. Herrmann. Scaling laws in fracture. Phys. Rev. B, 40:877–880, 1989. [cited at p. 61]

[47] V. De Rubeis, R. Hallgas, V. Loreto, G. Paladin, L. Pietronero, and P. Tosi. Self-affine asperity model for earthquakes. Phys. Rev. Lett., 76(14):2599–2602, 1996. [cited at p. 13, 36, 41, 56, 57, 59, 62, 66, 172, 176]

[48] J. Dickinson, S. Langford, L. Jensen, G. McVay, J. Kelso, and C. Pantano. Fractoemission from fused silica sodium silicate glasses. J. Vac. Sci. Technol. A, 6:1084–1089, 1988. [cited at p. 15]

[49] W. Ebeling. Prediction and entropy of nonlinear dynamical systems and symbolic sequences with LRO. Physica D, 109:42–52, 1997. [cited at p. 19]

[50] W. Ebeling. Entropies and predictability of nonlinear processes and time series, volume 2331 of LNCS. Springer Berlin Heidelberg, computational science Ů iccs 2002 edition, 2002. [cited at p. 19]

[51] W. Ebeling and G. Nicolis. Word frequency and entropy of symbolic sequences: A dynamical perspective. Chaos, Solitons & Fractals, 2:635–650, 1992. [cited at p. 19]

[52] W. Ebeling, R. Steuer, and M. Titchener. Partition-based entropies of deterministic and stochastic maps. Stochastics and Dynamics, 1:45–61, 2001. [cited at p. 19, 207]

[53] K. Eftaxias. Footprints of nonextensive Tsallis statistics, self-affinity and universality in the preparation of the L'Aquila earthquake hidden in a pre-seismic em emission. Physica A, 389:133–140, 2010. [cited at p. 92, 93, 110]

[54] K Eftaxias. Are there pre-seismic electromagnetic precursors? A multidisciplinary approach. In Sebastiano D'Amico, editor, Earthquake Research and Analysis - Statistical Studies, Observations and Planning, pages 217–246. InTech, 2012. ISBN: 978-953-51-0134-5. [cited at p. 13, 14, 17, 18, 19, 21, 23, 25, 26, 27, 35, 88, 155, 171, 172, 175, 177]

[55] K. Eftaxias, L. Athanasopoulou, G. Balasis, M. Kalimeri, S. Nikolopoulos, Y. Contoyiannis, J. Kopanas, G. Antonopoulos, and C. Nomicos. Unfolding the procedure of characterizing recorded ultra low frequency, kHz and MHz electromagnetic anomalies prior to the L'Aquila earthquake as pre-seismic ones. Part I. Natural Hazards and Earth System Sciences, 9:1953–Ű1971, 2009. [cited at p. 14, 16, 18, 19, 22, 25, 36, 44, 51, 56, 92, 97, 99, 121, 160, 172, 175]

[56] K. Eftaxias, G. Balasis, Y. Contoyiannis, C. Papadimitriou, M. Kalimeri, J. Kopanas, G. Antonopoulos, and C. Nomicos. Unfolding the procedure of characterizing recorded ultra low frequency, khz and mhz electromagnetic anomalies prior to the L'Aquila earthquake as pre-seismic ones. Part II. Natural Hazards and Earth System Sciences, 10:275–294, 2010. [cited at p. 18, 19, 22, 25, 51, 92, 97, 99, 121, 160, 172, 175]

[57] K. Eftaxias, Y. Contoyiannis, G. Balasis, K. Karamanos, J. Kopanas, G. Antonopoulos, G. Koulouras, and C. Nomicos. Evidence of fractional-brownian-motion-type asperity model for earthquake generation in candidate pre-seismic electromagnetic emissions. Natural Hazards and Earth System Science, 8(4):657–669, 2008. [cited at p. 19, 56, 57]

[58] K. Eftaxias, P. Frangos, P. Kapiris, J. Polygiannakis, J. Kopanas, A. Peratzakis, P. Skountzos, and D. Jaggard. Review-model of pre-seismic electromagnetic emissions in terms of fractal-electrodynamics. Fractals, 12:243–273, 2004. [cited at p. 16, 23, 25, 36, 87, 88, 92, 93, 118]

[59] K. Eftaxias, P. Kapiris, G. Balasis, A. Peratzakis, K. Karamanos, J. Kopanas, and K. Antonopoulos, G.and Nomicos. A unified approach to catastrophic events: From the normal state to geological or biological shock in terms of spectral fractal and nonlinear analysis. Natural Hazards and Earth System Sciences, 6:205–228, 2006. [cited at p. 15, 16, 17, 92, 110, 172]

[60] K. Eftaxias, P. Kapiris, E. Dologlou, J. Kopanas, N. Bogris, G. Antonopoulos, A. Peratzakis, and V. Hadjicontis. Em anomalies before the kozani earthquake: A study of their behaviour through laboratory experiments. Geophys. Res. Lett., 29:69/1–69/4, 2002. [cited at p. 16, 36, 92, 93]

[61] K. Eftaxias, P. Kapiris, J. Polygiannakis, N. Bogris, J. Kopanas, G. Antonopoulos, A. Peratzakis, and V. Hadjicontis. Signatures of pending earthquake from electromagnetic anomalies. Geophys. Res. Let., 28:3321–3324, 2001. [cited at p. 16, 31, 44, 88, 92, 93, 115]

[62] K. Eftaxias, P. Kapiris, J. Polygiannakis, J. Kopanas, G. Antonopoulos, and D. Rigas. Experience of short term earthquake precursors with VLF-VHF electromagnetic emissions. Natural Hazards and Earth System Sciences, 3:217–228, 2003. [cited at p. 23, 87, 92]

[63] K. Eftaxias, J. Kopanas, N. Bogris, K. Kapiris, G. Antonopoulos, and Varotsos P. Detection of electromagnetic earthquake precursory signals in Greece. Proc. Japan Acad., 76(B):45–50, 2000. [cited at p. 14, 31, 44, 88, 92, 123]

[64] K Eftaxias, G Minadakis, S. M. Potirakis, and G Balasis. Dynamical analogy between epileptic seizures and seismogenic electromagnetic emissions by means of nonextensive statistical mechanics. Physica A, 392(3):497–509, 2012. [cited at p. 117, 133, 134, 137, 138]

[65] K. Eftaxias, V. Panin, and Deryugin Y. Evolution EM-signals before earthquake and during laboratory test of rocks. Tectonophysics, 431:273Ű–300, 2007. [cited at p. 16, 17, 93, 172]

[66] K. Eftaxias, V. Sgrigna, and T. Chelidze. (eds): Mechanical and electromagnetic phenomena accompanying preseismic deformation: from laboratory to geophysical scale. Tectonophysics, 431:1–301, 2007. [cited at p. 15, 92, 93, 115]

[67] Rafael Elul. Gaussian behavior of the electroencephalogram: Changes during performance of mental task. Science, 164(3877):328–331, 1969. [cited at p. 124]

[68] R. Englman, N. Rivier, and Z. Jaeger. Fragment-size distribution in disintegration by maximum-entropy formalism. Philos. Mag. B, 56(6):751, 1987. [cited at p. 40, 41]

[69] R. D. Fath and H. Cabezas. Exergy and Fisher Information as ecological indices. Ecol. Modelling, 174:25–35, 2004. [cited at p. 174]

[70] J. Feder. Fractals. Plenum Press, New York, 1988. [cited at p. 46]

[71] C. Filizzola, N. Pergola, C. Pietrapertosa, and V. Tramutoli. Robust satellite techniques for seismically active areas monitoring: a sensitivity analysis on September 7, 1999 Athens's earthquake. Physics and Chemistry of the Earth, 29:517–527, 2004. [cited at p. 14, 87]

[72] R. A. Fisher. Theory of statistical estimation. Mathematical Proceedings of the Cambridge Philosophical Society, 22:700–725, 1925. [cited at p. 80]

[73] F. T. Freund. Pre-earthquake signals Ű Part II: Flow of battery currents in the crust. Nat. Hazards Earth Syst. Sci., 7:543–548, 2007. [cited at p. 92]

[74] V. Frid, A. Rabinovitch, and D. Bahat. Fracture induced electromagnetic radiation. J. Phys. D. Appl. Phys., 36:1620–1628, 2003. [cited at p. 25, 35, 92]

[75] B. R. Frieden. Science from Fisher Information: A Unification. Cambridge University Press, Cambridge, UK, 2nd edition, 2004. [cited at p. 174]

[76] K. Fukuda, L. Nunes, and H. Stanley. Similarities between communication dynamics in the Internet and the automatic nervous system. Europhys. Lett., 62:189–195, 2003. [cited at p. 25, 27, 109, 112, 137, 177]

[77] K. Fukui, S. Okubo, and T. Terashima. Electromagnetic radiation from rock during uniaxial compression testing: the effects of rock characteristics and test conditions. Rock Mech. Rock Eng., 38:411Ű–423, 2005. [cited at p. 25, 35, 92]

[78] A.R. Gallant. Nonlinear regression. The American Statistician, 29:73–81, 1975. [cited at p. 49]

[79] R. Geller, D. Jackson, Y. Kagan, and F. Mulargia. Earthquakes cannot be predicted. Science, 275:1616–1617, 1997. [cited at p. 13]

[80] Lucas Girard, Jérôme Weiss, and David Amitrano. Damage-cluster distributions and size effect on strength in compressive failure. Phys. Rev. Lett., 108:225502, May 2012. [cited at p. 92]

[81] M. B. Gokhberg, V. A. Morgunov, T. Yoshino, and I. Tozawa. Experimental measurement of electromagnetic emissions possibly related to earthquakes in Japan. J. Geophys. Res., 87:7824Ű–7828, 1982. [cited at p. 92]

[82] M.B. Gokhberg, V.A. Morgounov, and O.A. Pokhotelov. Earthquake Prediction - Seismo-Electromagnetic Phenomena. Gordon and Breach Publishers, Singapore, 1995. [cited at p. 35, 92]

[83] A. Goldberger, L. Amaral, L. Glass, Hausdorff J., Ivanov P., R. Mark, J. Mietus, G. Moody, C-K Peng, and H. Stanley. Physiobank, physiotoolkit, and physionet: Components of a new research resource for complex physiologic signals. Circulation, 101:215–220, June 13 2000. [cited at p. 115, 116, 121, 122]

[84] A. Gonzalez and C. Pantano. Fractoemission during crack propagation in glass. Appl. Phys. Lett., 57:246Ű248, 1990. [cited at p. 15]

[85] Aladino Govoni, Luigi Passarelli, Thomas Braun, Francesco Maccaferri, Milena Moretti, Francesco Pio Lucente, Simone Rivalta, Eleonora andCesca, Sebastian Hainzl, Heiko Woith, Pasquale De Gori, Torsten Dahm, Claudio Chiarabba, and Lucia Margheriti. Investigating the origin of seismic swarms. Eos, Transactions American Geophysical Union, 94(41):361–362, 2013. [cited at p. 181]

[86] P. Grassberger and I. Procaccia. Characterization of strange attractors. Phys. Rev. Lett., 50:346–349, 1983. [cited at p. 19, 206]

[87] A. Gusev. On relation between earthquake population and asperity population on the fault. Tectonophysics, 211:85–98, 1992. [cited at p. 42]

[88] B. Gutenberg. The energy of earthquakes. Quarterly Journal of the Geological Society, 112:1–14, February 1956. [cited at p. 13, 141, 152, 153]

[89] B. Gutenberg and C. Richter. Seismicity of the Earth and Associated Phenomena. Princeton Univ. Press, Princeton, New Jersey, USA, 2 edition, 1954. [cited at p. 7, 39, 61, 117, 156, 205]

[90] B. Gutenberg and C. F. Richter. Earthquake magnitude, intensity, energy, and acceleration: (Second paper). Bulletin of the Seismological Society of America, 46:105–145, April 1956. [cited at p. 152]

[91] B. Gutenberg and C.F. Richter. Earthquake magnitude, intensity, energy and acceleration. Bull. Seismol. Soc. Amer., 32:163–191, 1942. [cited at p. 20, 152]

[92] S. Hainzl, G. Zoller, and F. Scherbaum. Earthquake clusters resulting from delayed rupture propagation in finite fault segments. J. Geophys. Res., 108:2013, 2003. [cited at p. 21, 132, 134]

[93] R. Hallgass, V. Loreto, O. Mazzella, G. Paladin, and L. Pietronero. Self-affine model of earthquakes. Phys. Rev. Lett., 76:2599–2562, 1997. [cited at p. 36, 41, 43, 56, 176]

[94] A. Hansen and J. Schmittbuhl. Origin of the universal roughness exponent of brittle fracture surfaces:stress-weighted percolation in the damage zone. Phys. Rev. Lett., 90:45504–45507, 2003. [cited at p. 56, 57, 81, 93, 176]

[95] B-L. Hao. Elementary symbolic dynamics and chaos in dissipative systems. World Scientific, page 476pp, 1989. [cited at p. 37]

[96] E. Hauksson, W. Yang, and P.M. Shearer. Waveform relocated earthquake catalog for southern California (1981 - 2011). Bull. Seismol. Soc. Am., 102(5):2239–2244, 2012. [cited at p. 142]

[97] W.A. Hauser and J.R. Lee. Do seizures beget seizures? Prog. Brain Res., 135:215, 2002. [cited at p. 181]

[98] M. Hayakawa. Atmospheric and ionospheric electromagnetic phenomena associated with earthquakes. Terrapub, Tokyo, page 997, 1999. [cited at p. 15, 92]

[99] M. Hayakawa and Y. Fujinawa. Electromagnetic phenomena related to earthquake prediction. Terrapub, Tokyo, 1994. [cited at p. 15, 92]

[100] M. Hayakawa and O. Molchanov, editors. Seismo Electromagnetics. Terrapub, Tokyo, 2002. [cited at p. 15, 92]

[101] Jasper HCC. Report of the committee on methods of clinical examination in electroencephalography: 1957. Electroencephalography and Clinical Neurophysiology, 10:370–375, 1958. [cited at p. 137]

[102] C. Heneghan and G. McDarby. Establishing the relation between detrended fluctuation analysis and power spectral density analysis for stochastic processes. Phys. Rev. E, 62:6103–6110, 2000. [cited at p. 19, 57, 59]

[103] H. J. Herrmann, G. Mantica, and D. Bessis. Space-filling bearings. Phys. Rev. Lett, 65:3223, 1990. [cited at p. 39]

[104] H. J. Herrmann and S. Roux. Statistical Physics for the Fracture of Disordered Media. North-Holland, Amsterdam, 1990. [cited at p. 18, 39, 92]

[105] A. Herz and J. Hopfield. Earthquake cycles and neural reverberations: Collective oscillations in systems with pulse-coupled threshold elements. Phys. Rev. Lett., 75:1222–1225, 1995. [cited at p. 27, 110, 111, 137]

[106] Kanamori Hiroo. Magnitude scale and quantification of earthquakes. Tectonophysics, 93:185–199, 1983. [cited at p. 152, 170]

[107] J. Hopfield. Neurons, dynamics and computation. Phys. Today, 40:40–46, 1994. [cited at p. 27, 110, 111, 137]

[108] J. Huang and D. Turcotte. Fractal distributions of stress and strength and variations of b-value. Earth and Planetary Science Letters, 91:223–230, 1988. [cited at p. 22, 27, 43, 72, 86, 89, 91, 94, 106, 174, 176]

[109] H. Hurst. Long term storage capacity of reservoirs. Trans. Am. Soc. Civ. Eng., 116:770–808, 1951. [cited at p. 19, 46, 81, 115, 138, 174]

[110] H.E. Hurst, R.P. Black, and Y.M. Simaika. Long-Term Storage: An Experimental Study. Constable, London, 1965. [cited at p. 19, 46, 71, 115, 174]

[111] M. Ishimoto and K. Iida. Observations surles seism enregistre par le microseismograph construite derniermen. Bull. Earthquake Res. Inst., Univ. Tokyo, 17:443–478, 1939. with Japanese summary. [cited at p. 20]

[112] D. Jaggard. On fractal electrodynamics. In H. Kritikos and D. Jaggard, editors, Recent Advances in Electromagnetic Theory, pages 183–224. Springer-Verlag, New York, 1990. [cited at p. 24]

[113] D. Jaggard and P. Frangos. Surfaces and superlattices. In D. Werner and R. Mittra, editors, Frontiers in Electrodynamics, pages 1–47. IEEE Press, 2000. [cited at p. 24]

[114] C. Jaume and L. R. Sykes. Evolving towards a critical point: A review of accelerating seismic moment/energy release prior to large and great earthquakes. Pure Appl. Geophys., 155:279, 1999. [cited at p. 23, 152]

[115] A. Jimenez, K. F. Tiampo, S. Levin, and A. M. Posadas. Testing the persistence in earthquake catalogs: The Iberian Peninsula. Europhysics Letters, 73 (2):171–177, 2006. [cited at p. 81]

[116] Y. Kagan and L. Knopoff. Spatial distribution of earthquakes: the two-point correlation function. Geophys. J. R. Astr. Soc., 62:303Ű–320, 1980. [cited at p. 43]

[117] M. Kalimeri, K. Papadimitriou, G. Balasis, and K. Eftaxias. Dynamical complexity detection in pre-seismic emissions using nonadditive Tsallis entropy. Physica A, 387:1161–1172, 2008. [cited at p. 16, 18, 19, 22, 36, 43, 44, 52, 72, 80, 87, 92, 93, 114, 115, 116, 121, 175]

[118] E Kaminski and C Jaupart. The size distribution of pyroclasts and the fragmentation sequence in explosive volcanic eruptions. Journal of Geophysical Research, 103:29759–29779, 1998. [cited at p. 69, 94, 111, 132, 137, 138, 141, 169, 174]

[119] H. Kanamori. The energy release in great earthquakes. J. Geophys. Res., 82(20):2981–298, 1977. [cited at p. 141, 152, 153]

[120] Hiroo Kanamori. Quantification of earthquakes. Nature, 271:411–414, 02 February 1978. [cited at p. 13, 145]

[121] P. Kapiris, G. Balasis, J. Kopanas, G. Antonopoulos, A. Peratzakis, and K. Eftaxias. Scaling similarities of multiple fracturing of solid materials. Nonlinear Processes in Geophysics, 11:137–151, 2004. [cited at p. 16, 18, 20, 51, 118]

[122] P. Kapiris, J. Polygiannakis, X. Yao, and K. Eftaxias. Similarities in precursory features in seismic shocks and epileptic seizures. Europhysics Letters, 69:657–663, 2005. [cited at p. 16, 27, 88, 113, 115, 137]

[123] P. G. Kapiris, K. A. Eftaxias, and T. L. Chelidze. Electromagnetic signature of prefracture criticality in heterogeneous media. Phys. Rev. Lett., 92:065702, Feb 2004. [cited at p. 14, 16, 17, 19, 21, 23, 25, 36, 43, 44, 51, 72, 83, 84, 87, 88, 92, 93, 104, 105, 115, 134, 172, 175]

[124] K. Karamanos, D. Dakopoulos, K. Aloupis, A. Peratzakis, L. Athanasopoulou, S. Nikolopoulos, P. Kapiris, and K. Eftaxias. Pre-seismic electromagnetic signals in terms of complexity. Physical Review E, 74(016104):1–21, 2006. [cited at p. 19, 22, 25, 43, 44, 92, 93, 110, 115, 123, 175]

[125] K. Karamanos, A. Peratzakis, P. Kapiris, S. Nikolopoulos, J. Kopanas, and K. Eftaxias. Extracting preseismic electromagnetic signatures in terms of symbolic dynamics. Nonlin. Processes Geophys., 12:835–848, 2005. [cited at p. 19, 22, 43, 93, 175]

[126] Y. Khan and J. Gotman. Wavelet based automatic seizure detection in intracerebral electroencephalogram. Clin Neurophysiol, 114(5):898–908, 2003. [cited at p. 126]

[127] M. Kikuchi and H. Kanamori. Inversion of complex body waves - III. Bull. Seism. Soc. Am., 81:2335–2350, 1990. [cited at p. 88]

[128] L. Knopoff. The magnitude distribution of declustered earthquakes in Southern California. Proc. Natl. Acad. Sci. U.S.A., 97(22):11880–11884, 2000. [cited at p. 132, 134]

[129] C. Kontoes, P. Elias, O. Sycioti, P. Briole, D. Remy, M. Sachpazi, G. Veis, and I. Kotsis. Displacement field and fault model for the September 7, Athens earthquake inferred from the ERS2 satellite radar interferometry. Geophys. Res. Lett., 27:3989Ű–3992, 2000. [cited at p. 88]

[130] V. Kossobokov. Testing earthquake prediction methods: the West Pacific short-term forecast of earthquakes with magnitude MwHRV ¿ 5.8. Tectonophysics, 413:25–31, 2006. [cited at p. 13]

[131] V. Kossobokov, V. Keillis-Borok, and B. Cheng. Similarities of multiple fracturing on a neutron star and on Earth. Phys. Rev. E, 61:3529–3533, 2000. [cited at p. 16, 25, 27, 109, 112, 137, 177]

[132] G. Koulouras, K. Kontakos, I. Stavrakas, J. Stonham, and C. Nomicos. Embedded compact flashŹ Ű a new data storage system designed for a data acquisition system. IEEE Circuits and Devices Magazin, 21(4):27–34, 2005. [cited at p. 28]

[133] Gregory Koulouras. A versatile data acquisition system for capturing electromagnetic emissions in VHF band. PhD thesis, Brunel University School of Engineering and Design, 2007. [cited at p. 28, 29]

[134] L. C. Krysac and J. D. Maynard. Evidence for the role of propagating stress waves during fracture. Phys. Rev. Lett., 81:4428–4431, 1998. [cited at p. 72, 89]

[135] G. Lacidogna, A. Carpinteri, A. Manuello, G. Durin, A. Sciavi, G. Niccolini, and A. Agosto. Acoustic and electromagnetic emissions as precursor phenomena in failure processes. Strain, 47:1–9, 2011. [cited at p. 25, 92]

[136] G. Lacidogna, A. Carpinteri, A. Manuello, G. Durin, A. Sciavi, G. Niccolini, and A. Agosto. Acoustic and electromagnetic emissions as precursor phenomena in failure processes. Strain, 47:1–9, 2011. [cited at p. 35]

[137] L. Lamaignere, F. Carmona, and D. Sornette. Experimental realization of critical thermal fuses rupture. Phys. Rev. Lett., 77:2738–2741, 1996. [cited at p. 92]

[138] S. Langford, J. Dickinson, and L. Jensen. Simultaneous measurements of the electron and photon emission accompanying fracture of single-crystal mgo. J. Appl. Phys., 62:1437–1449, 1987. [cited at p. 15]

[139] X. Lei, K. Masuda, O. Nishizawa, L. Jouniaux, L. Liu, W. Ma, T. Satoh, and K. Kusunose. Detailed analysis of acoustic emission activity during catastrophic fracture of faults in rock. Journal of Structural Geology, 26:247–258, 2004. [cited at p. 68]

[140] X. Lei, O. Nishizawa, K. Kusunose, A. Cho, T. Satoh, and O. Nishizawa. Compressive failure of mudstone samples containing quartz veins using rapid a monitoring: the role of asperities. Tectonophysics, 328:329Ű–340, 2000. [cited at p. 68]

[141] X. Lei and T. Satoh. Indicators of critical point behavior prior to rock failure inferred from pre-failure damage. Tectonophysics, 431:97Ű111, 2007. [cited at p. 21]

[142] K. Levenberg. A method for the solution of certain non-linear problems in least squares. The Quarterly of Applied Mathematics, 2:164–168, 1944. [cited at p. 49, 74, 96, 126, 144, 157]

[143] X. Li, J. Polygiannakis, P. Kapiris, A. Peratzakis, K. Eftaxias, and X. Yao. Fractal spectral analysis of pre-epileptic seizures in terms of criticality. Journal of Neural Engineering, 2:1–6, 2005. [cited at p. 113, 152]

[144] T. Lolajicek and J. Sikula. Acoustic emission and electromagnetic effects in rocks. In T. Kishi, Y. Mori, H. Higo, and M. Enoki, editors, Progress in Acoustic Emission VIII, Proceedings of the 13th International Acoustic Emission Symposium, pages 311–314, Nara, Japan, 30 November 1996. Japanese Society for NDI. [cited at p. 25, 35, 92]

[145] C. Lomnitz. Fundamentals of Earthquake Prediction. John Wiley & Sons, Inc., New York, 1994. [cited at p. 81]

[146] J. Lopez and J. Schmittbuhl. Anomalous scaling of fracture surfaces. Phys. Rev. E, 57:6405–6408, 1998. [cited at p. 56, 57, 81, 93, 176]

[147] M. Lovallo and L. Telesca. Complexity measures and information planes of X-ray astrophysical sources. J. Stat. Mech., page P03029, J. Stat. Mech. 2011. [cited at p. 73, 111]

[148] J. Makris, N. Bogris, and K. Eftaxias. A new approach in the determination of characteristic directions of the geoelectric structure using mohr circles. Earth Planets Space, 51:1059–1065, 1999. [cited at p. 31]

[149] B. Mandelbrot. The Fractal Geometry of Nature. WH Freeman, New York, 1 edition, 1982. [cited at p. 56, 91, 176]

[150] B. B. Mandelbrot. Self-affine fractals and fractal dimension. Physica Scripta, 32(4):257, 1985. [cited at p. 50]

[151] B.B. Mandelbrot and J.R. Wallis. Noah, Joseph, and Operational Hydrology. Water Resour. Res., 4:909–918, 1968. [cited at p. 46]

[152] D.W. Marquardt. An algorithm for least-squares estimation of nonlinear parameters. Journal of the Society for Industrial and Applied Mathematics, 11(2):431–441, 1963. [cited at p. 49, 74, 96, 126, 144, 157]

[153] M. T. Martin, F. Pennini, and A. Plastino. Fisher's information and the analysis of complex signals. Phys. Lett. A, 256:173–180, 1999. [cited at p. 73]

[154] S. Maslov, M. Paczuski, and P. Bak. Avalanches and 1/f noise in evolution and growth models. Phys. Rev. Lett., 73:2162–2165, 1994. [cited at p. 56, 175]

[155] T. Matcharashvili, T. Chelidze, Z. Javakhishvili, N. Jorjiashvili, and U. FraPaleo. Non-extensive statistical analysis of seismicity in the area of Javakheti, Georgia. Computers and Geosciences, 37(10):1627–1632, 2011. [cited at p. 49, 50, 84, 103, 106, 121, 142]

[156] C. Mavromatou, V. Hadjicontis, D. Ninos, D. Mastroyiannis, E. Hadjicontis, and K. Eftaxias. Understanding the fracture phenomena in inhomogeneous rock samples and ionic crystals, by monitoring the electromagnetic emission during the deformation. Physics and Chemistry of the Earth, 29:353–357, 2004. [cited at p. 15, 25, 35, 92]

[157] A. L. Mayer, C. W. Pawlowski, and H. Cabezas. Fisher Information and dynamic regime changes in ecological systems. Ecol. Modelling, 195:72–82, 2006. [cited at p. 174]

[158] G. Minadakis, S. M. Potirakis, C. Nomicos, and K. Eftaxias. Linking electromagnetic precursors with earthquake dynamics: an approach based on nonextensive fragment and self-affine asperity models. Physica A, 391(6):2232–2244, 2012. [cited at p. 106, 123, 138]

[159] G. Minadakis, S. M. Potirakis, J. Stonham, C. Nomicos, and K. Eftaxias. The role of propagating stress waves in geophysical scale: evidence in terms of nonextensivity. Physica A, 391(22):5648–5657, 2012. [cited at p. 138]

[160] T. Miura and K. Nakayama. Spectral analysis of photons emitted during scratching of an insulator surface by a diamond in air. Appl. Physics J., 88:5444–5447, 2000. [cited at p. 15]

[161] V.A. Morgounov. A multiple fracture model of pre-seismic electromagnetic phenomena. Tectonophysics, 431:61–72, 2007. [cited at p. 92]

[162] G. Mourot, S. Morel, E. Bouchaud, and G. Valentin. Scaling properties of mortar fracture surfaces. Int. J. of Fracture, 140:39–54, 2006. [cited at p. 56, 57, 81, 93, 176]

[163] J. Muto, H. Nagahama, T. Miura, and I. Arakawa. Frictional discharge at fault asperities: origin of fractal seismoelectromagnetic radiation. Tectonophysics, 431:113–122, 2007. [cited at p. 91]

[164] T. Nagao, Y. Enomoto, and Y. Fujinawa. Electromagnetic anomalies associated with 1995 Kobe earthquake. J. Geodyn., 33:401–411, 2002. [cited at p. 92]

[165] T. Ogawa, K. Oike, and T. Miura. Electromagnetic radiation from rocks. J. Geophys. Res., 90:6245Ű6249, 1985. [cited at p. 25, 35, 92]

[166] S. G. Okeefe and D. V. Thiel. A mechanism for the production of electromagnetic radiation during fracture of brittle materials. Phys. Earth Plant. Inter., 89:127–135, 1995. [cited at p. 25, 35, 92]

[167] Z. OLAMI, H. J. S. FEDER, and K. CHRISTENSEN. Self-organized criticality in a continuous, nonconservative cellular automaton modeling earthquakes. Phys. Rev. Lett., 68:1244–1247, 1992. [cited at p. 23, 42]

[168] I. Osorio, M. G. Frei, D. Sornette, and J. Milton. Pharmaco-resistant seizures: self-triggering capacity, scale-free properties and predictability? European Journal of Neuroscience, 30:1554–1558, 2009. [cited at p. 137, 138, 141]

[169] Ivan Osorio, Mark G. Frei, Didier Sornette, John Milton, and Ying-Cheng Lai. Epileptic seizures: Quakes of the brain? Phys. Rev. E, 82:021919, Aug 2010. [cited at p. 25, 27, 111, 112, 113, 117, 118, 119, 122, 128, 137, 154, 155, 169, 178]

[170] D. Ouzounov and F. Freund. Mid-infrared emission prior to strong earthquakes analyzed by remote sensing data. Advances in Space Research, 33:268–273, 2004. [cited at p. 17, 171]

[171] V. Panin, Ye. Deryugin, V. Hadjicontis, C. Mavromatou, and K. Eftaxias. Scale levels of strain localization and fracture mechanism of LiF single crystals under compression. Physical Mesomechanics, 4:21–32, 2001. [cited at p. 25, 35, 92]

[172] K. Papadimitriou, M. Kalimeri, and K. Eftaxias. Nonextensivity and universality in the earthquake preparation process. Physical Review E, 77(36101), 2008. [cited at p. 14, 16, 17, 18, 20, 21, 22, 26, 27, 36, 43, 44, 51, 54, 72, 83, 84, 88, 92, 93, 104, 105, 106, 115, 121, 123, 130, 132, 133, 134, 172, 174]

[173] G. A. Papadopoulos. The Athens, Greece, earthquake (ms 5.9) of 7 September 1999: An event triggered by the Izmit, Turkey, 17 august 1999 earthquake? Bulletin of the Seismological Society of America, 92:312–321, February 2002. [cited at p. 13, 17, 87, 151]

[174] G. A. Papadopoulos, M. Charalampakis, A. Fokaefs, and G. Minadakis. Strong foreshock signal preceding the L'aquila (Italy) earthquake (m_w 6.3) of 6 april 2009. Natural Hazards and Earth System Science, 10(1):19–24, 2010. [cited at p. 13, 95, 134, 151, 164, 165]

[175] G. A. Papadopoulos and A. Kijko. Maximum likelihood estimation of earthquake hazard parametersin the aegean area from mixed data. Tectonophysics, 185:277–294, 1991. [cited at p. 21]

[176] Ole Peters, Christopher Hertlein, and Kim Christensen. A complexity view of rainfall. Phys. Rev. Lett., 88:018701, Dec 2001. [cited at p. 25, 27, 109, 112, 137, 177]

[177] A. Petri, G. Paparo, A. Vespignani, A. Alippi, and M. Constantini. Experimental evidence for critical dynamics in microfracturing processes. Phys. Rev. Let, 73:3423–3426, 1994. [cited at p. 119]

[178] S. Peyrat, K. Olsen, and R. Madariaga. Dynamic modeling of the 1992 landers earthquake. J. Geophys. Res., 106:467Ű482, 2001. [cited at p. 42]

[179] V. N. Pham and R. J. Geller. Comment on "signature of pending earthquake from electromagnetic anomalies" by K. Eftaxias et al. Geophys. Res. Lett., 29(18):1871, 2002. [cited at p. 14, 16, 35, 172]

[180] S. Picoli, R. Mendes, L. Malacarne, and A. Papa. Similarities between the dynamics of geomagnetic signal and heartbeat intervals. Europhysics Letters, 80:50006, 2007. [cited at p. 25, 27, 109, 112, 137, 177, 178]

[181] S. Pincus. Approximate entropy as a measure of system complexity. Proc. Nati. Acad. Sci. USA, 88(6):2297–2301, 1991. [cited at p. 19, 206, 207]

[182] S. Pincus and A. Goldberger. Physiological time-series analysis: what does regularity quantify? Am. J. Physiol, 266(H1643), 1994. [cited at p. 116]

[183] S. Pincus and B. Singer. Randomness and degrees of irregularity. Proc. Natl. Acad. Sci. U.S.A., 93(5):2083–2088, 1996. [cited at p. 116, 207]

[184] D. Plenz. When inhibition goes incognito: feedback interaction between spiny projection neurons in striatal function. TRENDS in Neurosciences, 26(8):436–443, 2003. [cited at p. 110]

[185] A. Ponomarev, A. Zavyalov, V. Smirnov, and D. Lockner. Physical modelling of the formation and evolution of seismically active fault zones. Tectonophysics, 277:57–81, 1997. [cited at p. 21, 68]

[186] L. Ponson, D. Bonamy, and E. Bouchaud. Two-dimensional scaling properties of experimental fracture surfaces. Phys. Rev. Lett., 96:35506–1/4, 2006. [cited at p. 56, 57, 81, 93, 176]

[187] S.M. Potirakis, G. Minadakis, and K. Eftaxias. Analysis of electromagnetic pre-seismic emissions using Fisher Information and Tsallis entropy. Physica A, 391:300–306, 2012. [cited at p. 73, 93]

[188] S.M. Potirakis, G. Minadakis, C. Nomicos, and K. Eftaxias. A multidisciplinary analysis for traces of the last state of earthquake generation in preseismic electromagnetic emissions. Natural Hazards and Earth System Sciences, 11:2859–2879, 2011. [cited at p. 80]

[189] W. L. Power, T. E. Tullis, S. R. Brown, G. N. Boitnott, and C. H. Scholz. Roughness of natural fault surfaces. Geophys. Res. Lett., 1:14, 1987. [cited at p. 42]

[190] W.H. Press, S.A. Teukosky, W.T. Vetterling, and B.P. Flannery. Numerical Recipes in C. Cambridge University Press, second edition, 1992. [cited at p. 49]

[191] S. Pulinets and K. Boyarchuk. Ionospheric Precursors of Earthquakes. Springer, 2004. [cited at p. 17, 92, 171]

[192] A. Rabinovitch, V. Frid, and D. Bahat. Gutenberg-Richter-type relation for laboratory fracture-induced electromagnetic radiation. Phys. Rev. E, 65:11 401/1–11 401/4, 2001. [cited at p. 21, 35, 119, 133, 134]

[193] F. Renard, C. Voisin, D. Marsan, and J. Schmittbuhl. High resolution 3D laser scanner measurements of a strike-slip fault quantity its morphological anisotropy at all scales. Geophys. Res. Lett., 33:L04305, 2006. [cited at p. 57]

[194] C.F. Richter. An instrumental magnitude scale. Bull. Seismol. Soc. Amer., 25:1–32, 1935. [cited at p. 20]

[195] P. Rosen, S. Hensley, I. Joughin, F. Li, S. Madsen, E. Rodriguez, and R. Goldstein. Aperture Radar Interferometry: Synthetic. Proceedings of the IEEE, 88:333–382, 2000. [cited at p. 17, 171]

[196] J. Rundle, W. Klein, S. Gross, and D. Turcotte. Boltzmann fluctuations in numerical simulations of nonequilibrium lattice threshold systems. Phys. Rev. Lett., 75:1658–1661, 1995. [cited at p. 110]

[197] J. Rundle, K. Tiampo, W. Klein, and J. Sa Martins. Selforganization in leaky threshold systems: the influence of near mean field dynamics and its implications for eqs, neurology, and forecasting. PNAS, 99:2514–2521, 2002. [cited at p. 27, 111, 137]

[198] J. Rundle, D. Turcotte, R. Shcherbakov, W. Klein, and C. Sammis. Statistical physics approach to understanding the multiscale dynamics of earthquake fault systems. Rev. Geophys., 41(4):5–15–30, 2003. [cited at p. 26, 176]

[199] M. Sahimi. Flow phenomena in rocks: from continuum models to fractals, percolation, cellular automata, and simulated annealing. Rev. Mod. Phys., 65:1393–1534, 1993. [cited at p. 23, 24, 43]

[200] G. Sammis, H. Osborne, L. Anderson, M. Banerdt, and P. White. Self-similar cataclasis in the formation of fault gauge. Pure Appl. Geophys., 123:53–78, 1986. [cited at p. 69, 94, 111, 132, 137, 138, 141, 169, 174]

[201] S. G. Sammis and D. Sornette. Positive feedback, memory, and the predictability of earthquakes. Proc. Natl. Acad. Sci. U.S.A., 99:2501–2508, 2002. [cited at p. 68]

[202] N. Sarlis, E. Scordas, and P. Varotsos. Nonextensivity and natural time: The case of seismicity. Phys. Rev. E, 82:021110, 2010. [cited at p. 7, 41, 69, 79, 94, 113, 121, 131, 135, 156, 158, 205]

[203] N. Sator and H Hietala. Damage in impact fragmentation. Int J. Fract., 163:101–108, 2010. [cited at p. 69, 94, 111, 132, 137, 138, 141, 169, 174]

[204] C. H. Scholz and B. Mandelbrot, editors. Fractals in Geophysics. Birkhauser Verlag, Berlin, 1989. [cited at p. 51, 69, 94]

[205] C. E. Shannon. A mathematical theory of communication. The Bell System Tech. J., 27:379–423, 623–656, 1948. [cited at p. 19, 38]

[206] E. Sharon and J. Fineberg. Microbranching instability and the dynamic fracture of brittle material. Phys. Rev. B, 54(10):712–7139, 1996. [cited at p. 15]

[207] E. Sharon and J. Fineberg. Conforming the continuum theory of dynamic brittle fracture for fast cracks. Nature, 397:333–335, 1999. [cited at p. 15]

[208] R. Silva, G. Franca, C. Vilar, and J. Alcaniz. Nonextensive models for earthquakes. Phys. Rev. E, 73(0026102):1–5, 2006. [cited at p. 7, 22, 28, 40, 41, 50, 54, 69, 72, 83, 84, 91, 94, 106, 121, 126, 130, 142, 168, 172]

[209] A. SORNETTE and D. SORNETTE. Self-organized criticality and earthquakes. Europhys Lett., 9:197, 1989. [cited at p. 23]

[210] A. Sornette and D. Sornette. Earthquake rupture as a critical point : Consequences for telluric precursors. Tectonophysics, 179:327–334, 1990. [cited at p. 92]

[211] D. Sornette. Self-organized criticality in plate tectonics. In T. Riste and D. Sherrington, editors, Spontaneous Formation of Space-Time Sructures and Criticality, pages 57–106. Kluwer Academic Publishers, 1991. [cited at p. 24]

[212] D. Sornette. Predictability of catastrophic events: Material rupture, earthquakes, turbulence, financial crashes, and human birth. Proc. Natl. Acad. Sci., 99:2522–2529, 2002. [cited at p. 41]

[213] D. Sornette. Critical phenomena in natural sciences, in: Chaos, Fractals, Self-Organization and Disorder. Springer, Heidelberg, 2 edition, 2004. [cited at p. 18, 23, 25, 91, 92, 175]

[214] D. Sornette and A. Helmstetter. Occurrence of finite-time singularities in epidemic models of rupture, earthquakes, and starquakes. Phys. Rev. Lett., 89:158501, Sep 2002. [cited at p. 23, 25, 27, 53, 54, 103, 106, 109, 110, 111, 112, 126, 129, 130, 137, 169, 177]

[215] D. SORNETTE, P. MILTENBERGER, and C. VANNESTE. Statistical physics of fault patterns self-organised by repeated earthquakes. Pure Appl. Geophysics, 142:491–527, 1994. [cited at p. 119]

[216] D. Sornette and C Sammis. Complex critical exponents from renormalization group theory of earthquakes: Implications for earthquake predictions. J. Phys. I. France, 5:607–619, 1995. [cited at p. 23]

[217] D. Sornette and C. Vanneste. Dynamics and memory effects in rupture of thermal fuse networks. Phys. Rev. Lett., 68:612–615, 1992. [cited at p. 23, 92]

[218] Oscar Sotolongo-Costa and A. Posadas. Fragment-asperity interaction model for earthquakes. Phys. Rev. Lett., 92:048501, Jan 2004. [cited at p. 7, 21, 22, 36, 39, 41, 50, 68, 71, 72, 73, 91, 94, 106, 112, 120, 121, 130, 141, 142, 172]

[219] E. J. Speckmann and C.E. Elger. Electroencephalography, Basic Principles, Clinical Applicatios, and Related Fields, chapter Introduction to the Nuerophysiological Basis of the EEG and DC Potentials, pages 17–29. Williams and Wilkins, Baltimore, 4 edition, 1999. [cited at p. 124]

[220] H. Stanley. Scaling, universality, and renormalization: Three pillars of modern critical phenomena. Rev. Mod. Phys., 71:358–366, 1999. [cited at p. 27, 109, 111, 137, 181]

[221] H. Stanley. Exotic statistical physics: Applications to biology, medicine, and economics. Physica A, 285:1–17, 2000. [cited at p. 27, 109, 111, 137, 181]

[222] H. E. Stanley, L. Amaral, P. Gopikrishnan, P. Ivanov, T. Keitt, and V. Plerou. Scale invariance and universality: Organizing principles in complex systems. Physica A, 281:60–68, 2000. [cited at p. 109, 181]

[223] L.R. Sykes and S. Jaume. Seismic activity on neighbouring faults as a long-term precursor to large earthquakes in the San Francisco Bay area. Nature, 348:595–599, 1990. [cited at p. 23]

[224] A. Takeuchi and H. Nagahama. Scaling laws between seismoelectric/magnetic fields and eq magnitude. Terra Nova, 16:152–156, 2004. [cited at p. 15]

[225] L. Telesca. Quantifying the time-clustering in SGR 1806-20 Bursts. Fluctuation Noise Lett., 5:L417–L422, 2005. [cited at p. 112]

[226] L. Telesca. Identifying time-clustering structures in the sequence of solar flare hard X-ray bursts. Physica A, 384:516–521, 2007. [cited at p. 112]

[227] L. Telesca. Analysis of Italian seismicity by using a nonextensive approach. Tectonophysics, 494:155–162, 2010. [cited at p. 94, 121, 142]

[228] L. Telesca. A non-extensive approach in investigating the seismicity of L' Aquila area (central Italy), struck by the 6 april 2009 earthquake (ml $= 5.8$). Terra Nova, 22:87–93, 2010. [cited at p. 84, 106, 121, 129, 138]

[229] L. Telesca. Nonextensive analysis of seismic sequences. Physica A, 389:1911–1914, 2010. [cited at p. 22, 41, 50, 84, 106, 121]

[230] L. Telesca. Tsallis-based nonextensive analysis of the Southern California seismicity. Entropy, 13(7):1267–1280, 2011. [cited at p. 22, 41, 50, 84, 106]

[231] L. Telesca. Maximum likelihood estimation of the nonextensive parameters of the earthquake cumulative magnitude distribution. Bulletin of the Seismological Society of America, 102:886–891, 2012. [cited at p. 94, 113, 161, 170]

[232] L. Telesca, M. Bernardi, and C. Rovelli. Intra-cluster and inter-cluster time correlations in lightning sequences. Physica A, 356:655–661, 2005. [cited at p. 112]

[233] L. Telesca and M. Lovallo. Are global terrorist attacks time-correlated? Physica A, 362:480–484, 2006. [cited at p. 112]

[234] L. Telesca and M. Lovallo. Nonrandom components in aircraft accidents time series. Physica A, 381:407–410, 2007. [cited at p. 112]

[235] L. Telesca and M. Lovallo. Non-uniform scaling features in central Italy seismicity: a non-linear approach in investigating seismic patterns and detection of possible earthquake precursors. Geophys. Res. Lett., 36:L01308, 2009. [cited at p. 112]

[236] L. Telesca and M. Lovallo. Analysis of time dynamics in wind records by means of multifractal detrended fluctuation analysis and fisher-shannon information plane. J. Stat. Mech., page P07001, 2011. [cited at p. 73]

[237] L. Telesca, M. Lovallo, A. E.-E. Amin Mohamed, M. ElGabry, S. El-hady, K. M. Abou Elenean, and R. E. Fat ElBary. Informational analysis of seismic sequences by applying the Fisher information measure and the Shannon entropy: An application to the 2004-2010 seismicity of Aswan area (Egypt). Physica A, 391:2889–2897, 2012. [cited at p. 80]

[238] L. Telesca, M. Lovallo, and R. Carniel. Time-dependent fisher information measure of volcanic tremor before 5 april 2003 paroxysm at stromboli volcano, italy. J. Volcanol. Geoterm. Res., 195:78–82, 2010. [cited at p. 73]

[239] L. Telesca, M. Lovallo, and R. Carniel. Time-dependent Fisher Information measure of volcanic tremor before the 5 April 2003 paroxysm at Stromboli volcano. J. Volcan. Geoth. Res., 195:78–82, 2010. [cited at p. 71, 73]

[240] L. Telesca, M. Lovallo, H.-L. Hsu, and C.-C. Chen. Analysis of dynamics in magnetotelluric data by using the Fisher-shannon method. Physica A, 390:1350–1355, 2011. [cited at p. 73]

[241] L. Telesca and W. Song. Time-scaling properties of city fires. Chaos Solit. & Fractals, 44:558–568, 2011. [cited at p. 112]

[242] K. Thurber, H. Zhang, F. Waldhauser, J. Hardebeck, A. Michael, and D. Eberhart-Phillips. Three-dimensional compressional wavespeed model, earthquake relocations, and focal mechanisms for the Parkfeld, California, region. Bulletin of the Seismological Society of America, 96(4B):S38ŰS49, 2006. [cited at p. 148, 151]

[243] M Titchener. T-entropy of EEG/EOG sensitive to sleep state. International Symposium on Nonlinear Theory and Applications, 2006. Paper submitted to the International Symposium on Nonlinear Theory and Applications (NOLTA) 2006. [cited at p. 116, 208]

[244] M. Titchener, R. Nicolescu, L. Staiger, A. Gulliver, and U. Speidel. Deterministic complexity and entropy. Fundamenta Informaticae, 64:443–461, 2005. [cited at p. 19, 44, 116, 137, 207, 208]

[245] C. Tsallis. Possible generalization of Boltzmann-Gibbs statistics. J. Stat. Phys., 52:479–487, 1988. [cited at p. 19, 21, 27, 28, 32, 36, 38, 40, 41, 72, 91, 111, 112, 113, 117, 137, 169, 172, 173]

[246] C. Tsallis. Nonextensive statistical mechanics and its applications. Lecture Notes in Physics, 560:3–98, 2001. [cited at p. 21, 36, 91]

[247] C. Tsallis. Introduction to Nonextensive Statistical Mechanics, Approaching a Complex World. Springer, New York, 2009. [cited at p. 21, 36, 41, 72, 91, 109, 111]

[248] D. Turcotte. Fractals and chaos in geology and geophysics. Cambridge University Press, United Kingdom, 2 edition, 1997. [cited at p. 56, 91]

[249] D.L. Turcotte. Fractals and fragmentation. Journal of Geophysical Research, 91:1921–1926, 1986. [cited at p. 69, 94, 111, 132, 137, 138, 141, 169, 174]

[250] D.L Turcotte. Seismicity and self-organized criticality. Physics of the Earth and Planetary Interiors, 111:275–293, 1999. [cited at p. 176]

[251] A. Tzanis and K. Makropoulos. Did the 7/9/ 1999 m5.9 Athens earthquake come with a warning? Natural Hazard, 27:85–103, 2002. [cited at p. 17, 87]

[252] T. Utsu. On the statistical formula showing the magnitude frequency relation of earthquakes. Kenshinjiho (Quart. J. Seism.), 28:79–88, 1964. in Japanese with English summary. [cited at p. 113, 133, 134, 147, 178]

[253] T. Utsu. A method for determining the value of b in a formula log N = a-bM showing the magnitude-frequency relation for earthquakes. Geophys. Bull. Hokkaido Univ., 13:99–103, 1965. in Japanese. [cited at p. 133, 134, 147, 156, 174, 205]

[254] T. Utsu. A statistical significance test of the difference in b-value between two earthquake groups. J. Phys. Earth., 14:37–40, 1966. [cited at p. 134, 156, 163, 174, 205, 206]

[255] T. Utsu. Some problems of the frequency distribution of earthquakes in respect to magnitude (i). Geophys. Bull. Hokkaido Dniv., 18:53–69, 1967. in Japanese with English summary. [cited at p. 13, 133, 134]

[256] T. Utsu. Some problems of the frequency distribution of earthquakes in respect to magnitude (ii). Geophys. Bull. Hokkaido Dniv., 17:85–112, 1967. in Japanese with English summary. [cited at p. 133, 134]

[257] T Utsu. Aftershocks and earthquake statistics(1) : Some parameters which characterize an aftershock sequence and their interrelations. Geophys. Bull. Hokkaido Univ., 3(4):129–195, 1970. [cited at p. 162, 180]

[258] T Utsu. Aftershocks and earthquake statistics (3) : Analyses of the distribution of earthquakes in magnitude, time and space with special consideration to clustering characteristics of earthquake occurrence(1). Geophys. Bull. Hokkaido Univ., 3(5):379–441, 1972. [cited at p. 133, 134, 162, 180]

[259] S. Uyeda, T. Nagao, and M. Kamogawa. Short-term earthquake prediction: Current status of seismo-electromagnetics. Tectonophysics, 470:205–213, 2009. [cited at p. 14, 15, 16, 35, 172]

[260] P. Varotsos. The Physics of Seismic Electric Signals. TerraPub, Tokyo, 2005. [cited at p. 17, 171]

[261] P. Varotsos, K. Eftaxias, V. Hadjicontis, N. Bogris, E. Skordas, P. Kapiris, and M. Lazaridou. Three notes on the extent of the SES sensitive area around Lamia (LAM), Greece. Acta Geophys. Polonika, XLVII:435–443, 1999. [cited at p. 14, 87, 176]

[262] P. Varotsos, K. Eftaxias, V. Hadjicontis, N. Bogris, E. Skordas, P. Kapiris, and M. Lazaridou. Three notes on the extent of the SES sensitive area around Lamia (LAM), Greece. Acta Geophys. Polonika, XLVII:435–443, 1999. [cited at p. 176]

[263] P. Varotsos, N. Sarlis, E. Skordas, S. Uyeda, , and M. Kamogawa. Natural time analysis of critical phenomena. PNAS, 108:11361–11364, 2011. [cited at p. 175, 176]

[264] A. Vespignani, A. Petri, A. Alippi, G. Paparo, and M. Costantini. Long range correlation properties of aftershock relaxation signals. Fractals, 3:839, 1995. [cited at p. 119]

[265] T. Vicsek. A question of scale. Nature, 411:421, 2001. [cited at p. 27, 109, 111, 137, 181]

[266] T. Vicsek. The bigger picture. Nature, 418:131 pp., 2002. [cited at p. 27, 28, 109, 110, 111, 137, 181]

[267] C.S. Vilar, G.S. Franca, R. Silva, and J.S. Alcaniz. Nonextensivity in geological faults? Physica A, 377:285–290, 2007. [cited at p. 22, 40, 41, 50, 84, 116]

[268] A. Voss, J. Kurths, H. Kleiner, A. Witt, N. Wessel, N. Saparin, K. Osterziel, R. Schurath, and R. Dietz. The application of methods of non-linear dynamics for the improved and predictive recognition of patients threatened by sudden cardiac ceath. Cardiovascular Research, 31(3):419–433, 1996. [cited at p. 37]

[269] J. W. Warwick, C. Stoker, and T. R. Meyer. Radio emission associated with rock fracture: possible application to the great Cjilean earthquake of May 22, 1960. J. Geophys. Res., 87:2851–2859, 1982. [cited at p. 92]

[270] L. Wu, Y. Wu, S. Liu, G. Li, and Y. Li. Infrared radiation of rock impacted at low velocity. Rock Mechanics and Mining Sciences, 41:321–327, 2004. [cited at p. 15]

[271] Y. Xu and P. W. Burton. Time varying seismicity in Greece: Hurst's analysis and Monte Carlo simulation applied to a new earthquake catalogue for Greece. Tectonophysics, 423:125–136, 2006. [cited at p. 81]

[272] S. Zapperi, P. Kumar, V. Nukala, and S. Simunovic. Crack roughness and avalanche precursors in the random fuse model. Phys. Rev. E, 71:26106/1Ű10, 2005. [cited at p. 56, 57, 81, 93, 176]

Appendices

Appendix A

Appendix

A.1 List of proposed equations

A.1.1 A proposed formula for the calculation of nonextensivity

It is recalled that the frequency magnitude relationship for EQ dynamics is given by the Gutenberg & Richter formula [89], Eq. 1. Utsu on 1965 [253, 3, 254], proposed an alternative method for determining the b-value of the Gutenberg & Richter formula, showing that it is inversely proportional to the mean magnitude $\overline{M}$, given the minimum magnitude, M_{min}, of the EQ magnitudes. The final equation reads as follows, for the case where the magnitude frequency distribution of EQs obey the Gutenberg-Richter law:

$$b_{utsu} = \frac{\log_{10} e}{\overline{M} - (M_c - \frac{\Delta M}{2})} \tag{A.1}$$

where, ΔM, is the lowest binned magnitude in the sample and M_c is the smallest magnitude in the sample. Moreover Sarlis et al. (2010) [202], mentioned that the q-parameter included in the nonextensive formula (2) is associated with the b parameter of Gutenberg & Richter formula (Eq. (1)), above some magnitude threshold, by the relation:

$$b = 2 \times \left(\frac{2-q}{q-1} \right) \tag{A.2}$$

Combining equations (A.1) and (A.2), we get a new estimation of q-parameter based on the mean magnitude of the sample by simply replacing the estimated b parameter of Eq. (A.2) to Eq. (A.1). The mathematical solution reads as follows for $M_k = M_c - \frac{\Delta M}{2}$:

$$2 \times \left(\frac{2-q}{q-1} \right) = \frac{\log_{10} e}{\overline{M} - M_k} \Leftrightarrow \frac{4-2q}{q-1} = \frac{\log_{10} e}{\overline{M} - M_k} \tag{A.3}$$

The latter becomes:

$$4(\overline{M} - M_k) - 2q(\overline{M} - M_k) = q log_{10} e - log_{10} e \Leftrightarrow 4(\overline{M} - M_k) + log_{10} e = 2q(\overline{M} - M_k) + q log_{10} e \tag{A.4}$$

From A.4 we get:

$$q_{est} = \frac{\log_{10}e + 4(\overline{M} - M_k)}{\log_{10}e + 2(\overline{M} - M_k)} = \frac{\frac{4}{\log_{10}e}(\overline{M} - M_k) + 1}{\frac{2}{\log_{10}e}(\overline{M} - M_k) + 1} \simeq \frac{9.2103(\overline{M} - M_k) + 1}{4.6052(\overline{M} - M_k) + 1}, \tag{A.5}$$

where $M_k = M_c - \frac{\Delta M}{2}$, with M_c the smallest magnitude in the sample, and ΔM the lowest binned magnitude in the sample, respectively. The parameter $\overline{M}$ is the average magnitude of the sample.

A.1.2 A new formula for measuring the statistical significance between two populations

Utsu (1966) [254] proposed a statistical significance test of the difference in b-value between two earthquake groups. More precisely, he showed that the probability that two samples may come from the same population, given their b-values and the number of EQs N, is given by:

$$P \approx exp[-(dA/2) - 2], \tag{A.6}$$

where

$$dA = \; - \; 2\mathrm{N}\ \ln\ \mathrm{N} \; + \; 2\ \mathrm{N_1} \ln\ \left[\mathrm{N_1} + \mathrm{N_2}\left(\frac{\mathrm{b_1}}{\mathrm{b_2}}\right)\right] \; + \; 2\mathrm{N_2} \ln\ \left[\mathrm{N_1}\left(\frac{\mathrm{b_2}}{\mathrm{b_1}}\right) + \mathrm{N_2}\right] \; - 2 \tag{A.7}$$

Lower values of P indicate the higher statistical significant difference between two samples under study, or equivalently these two samples do not come from the same population. Herein, a challenging issue would be to examine whether the latter formula can be described through the nonextensive q-parameter q instead of the b-value. Indeed, combining equations (A.6) and (A.2), results to the following approach of the term dA included in Eq. (A.6):

$$P \approx exp[-(dS/2) - 2], \tag{A.8}$$

where

$$dS \;\; = \;\; - \; 2\mathrm{N}\ \ln\ \mathrm{N} \; + \; 2\ \mathrm{N_1} \ln\ \left[\mathrm{N_1} + \mathrm{N_2}\left(\frac{(2\text{-}\mathrm{q_1})(\mathrm{q_2} - 1)}{(\mathrm{q_1}\text{-}1)(2\text{-}\mathrm{q_2})}\right)\right] \; + \tag{A.9}$$

$$2\mathrm{N_2} \ln\ \left[\mathrm{N_1}\left(\frac{(2\text{-}\mathrm{q_2})(\mathrm{q_1} - 1)}{(\mathrm{q_2}\text{-}1)(2\text{-}\mathrm{q_1})}\right) + \mathrm{N_2}\right] \; - 2, \tag{A.10}$$

where $q1$ and $q2$ are the estimated parameters deriving from the proposed Eq. (A.5).

A.2 Approximate entropy

Approximate Entropy (ApEn) has been defined as a metric for measuring the degree of irregularity or randomness that exists within a data-series under study. ApEn is rooted in the theoretical framework of Grassberger and Procaccia [86] and has been introduced by [181] as a measure of system complexity. Specifically, ApEn is a "regularity" statistical method which that quantifies the unpredictability of fluctuations in a time series: it examines the presence of repetitive patterns of fluctuations contained in a time series in contrast to those that this patterns are absent. Small rates of ApEn indicate that

the time series under study contains many repetitive patterns. On the contrary, a less predictable process has a higher $ApEn$ expressing the higher complexity of the system. ApEn "statistics" draw from the negative logarithm of conditional probability that two similar sequences of m points remain similar within a tolerance r, for the next examined point. Smaller values of ApEn indicate that the examined set of data will be followed by a data set which is more likely to be conserved at the same state of regularity. On the contrary, higher levels of ApEn signify a lesser chance of similar data being repeated, indicating the irregular state of the system characterized by higher disorder, randomness, and complexity. Thus a low or high value of APEN reflects a high or low degree of regularity, respectively. Specifically, For a give sequence of data points $u(i), i = 1...N$, a vector of sequences $x(i)$ of length m is defined, consisting of consecutive $u(i)$ series in the form:

$$x(i) = (u[i], u[i+1], ..., u[i+m-1]) \tag{A.11}$$

For the estimation of the frequency that vectors $x(i)$ repeat themselves within a tolerance r, the maximum difference between the scalar components $x(i)$,$x(j)$ is estimated: $d(x[i], x[j])$. The latter two vectors are considered "similar" within a tolerance r, if the difference between any two values for $u(i)$ and $u(j)$ within runs of length m are less than r: $d(x[i], x[j]) \leq r$. For example, given the k point we calculate: $|u(i+k) - u(j+k)| \leq r, 0 \leq k \leq m$. Therefor, the frequency of occurrence of similar runs m within the tolerance r, reads as follows:

$$C_i^m(r) = \frac{\text{number of j such that } d(x[i], x[j]) \leq r}{N - M - 1}, \text{ where } j \leq (N - M - 1) \tag{A.12}$$

The measure of the prevalence of repetitive patterns of length m within the filter r, is given by the natural algorithm of Eq. A.12 as follows:

$$\Phi^m(r) = \frac{\sum_i^{N-m-1} \ln C_i^m(r)}{N - m - 1} \tag{A.13}$$

Finally, the approximate entropy for $APEN(m, r, N)$, is defined as the natural logarithm of the relative prevalence of repetitive patterns of length m as compared with those of length $m + 1$:

$$ApEn(m, r, N) = \Phi^m(r) - \Phi^{m+1}(r) \tag{A.14}$$

For a more comprehensive description of APEN please refer to the works of Pincus, Pincus et al. (1991,1996) in[181, 183].

A.3 T-entropy of a string

T-entropy is a novel grammar-based complexity / information measure defined for finite strings of symbols [52, 244]. It is a weighted count of the number of production steps required to construct a string from its alphabet. Specifically, it is based on the intellectual economy one makes when rewriting a string according to some rules that derive from the corresponding T-complexity measure. T-complexity is basically measured using a recursive hierarchical pattern copying algorithm (RHPC) which in turn

computes the effective number of T-augmentation steps required to generate the string. Specifically, a given alphabet set $x(n), n > 1$, is parsed to derive constituent substring patterns of $p_i \in A^+$ that have not been seen previously and further account for the associated copy exponents $k_i \in N^+, i = 1, 2, ..., q$ with $q \in N^+$. The decomposition derived for a string $x(n)$ is of the form:

$$x = p_q^{k_q} p_{q-1}^{k_{q-1}} ... p_i^{k_i} ... p_1^{k1} \alpha_0, \ \alpha_0 \in A^+ \tag{A.15}$$

Each pattern p_i is further constrained, requiring each sub-pattern to have the form:

$$p_i = p_{i-1}^{m_{i,i-1}} p_{i-2}^{m_{i,i-2}} . p_i^{m_{i,j}} . p_1^{m_{i,1}} \alpha_i, \ \alpha_i \in A^+ \text{ and } 0 \leq m_{i,j} \leq k_j \tag{A.16}$$

The T-complexity or $RHPC$-complexity $C_T\left(x\left(n\right)\right)$ of the string in terms of the copy exponent k_i, is therefore given by:

$$C_T\left(x\left(n\right)\right) = \sum_i^q \ln(k_i + 1) \tag{A.17}$$

The T-augmentation process may be applied systematically to produce strings that for a given length n have a maximum vocabulary k and therefore complexity k. In practice, for a binary alphabet, the string is parsed repeatedly from left to right but selection of patterns is from right to left. In effect to this, it has been possible to empirically derive an expression for the upper bound estimation as follows:

$$C_T\left(x\left(n\right)\right) \leq li(\ln 2 \ln(\#\mathsf{A}^{\mathsf{n}})), \tag{A.18}$$

where $li(z) = \int_z^0 du/\ln u$is the logarithmic integral function. The T-information of a string is the given by the inverse logarithmic integral of the fraction of T-complexity divided by the scaling constant $ln2$, implicitly giving to the T-information the units of "nats", as follows:

$$I_T\left(x(n)\right) = li^{-1}\left(\frac{C_T\left(x(n)\right)}{\ln 2}\right) \tag{A.19}$$

The average T-information rate per symbol, referred to here as the average T-entropy of $x(n)$ is therefore given by the following relation:

$$h_T(x(n)) = \frac{I_T(x(n))}{n}(nats/symbol) \tag{A.20}$$

For further information on T-Entropy please refer to the works of Titchener (2005,2006) in[244, 243] that includes a comprehensive representation and relevant examples.